2016-08-02

# Fabric Reinforced Cementitious Matrix (FRCM) Composites as a Repair System for Transportation Infrastructure

Vanessa A. Pino
*University of Miami*, v.pino40@umiami.edu

UNIVERSITY OF MIAMI

# FABRIC REINFORCED CEMENTITIOUS MATRIX (FRCM) COMPOSITES AS A REPAIR SYSTEM FOR TRANSPORTATION INFRASTRUCTURE

By

Vanessa A. Pino

A DISSERTATION

Submitted to the Faculty
of the University of Miami
in partial fulfillment of the requirements for
the degree of Doctor of Philosophy

Coral Gables, Florida

August 2016

UNIVERSITY OF MIAMI

A dissertation submitted in partial fulfillment of
the requirements for the degree of
Doctor of Philosophy

# FABRIC REINFORCED CEMENTITIOUS MATRIX (FRCM) COMPOSITES AS A REPAIR SYSTEM FOR TRANSPORATION INFRASTRUCTURE

Vanessa A. Pino

Approved:

| | |
|---|---|
| _____<br>Antonio Nanni, Ph.D.<br>Professor of Civil, Architectural,<br>and Environmental Engineering | _____<br>Francisco De Caso y Basalo, Ph.D.<br>Research Assistant Professor of<br>Civil, Architectural, and<br>Environmental Engineering |
| _____<br>Wimal Suaris, Ph.D.<br>Associate Professor of Civil,<br>Architectural, and Environmental<br>Engineering | _____<br>Guillermo Prado, Ph.D.<br>Dean of the Graduate School |
| _____<br>Thomas Cousins, Ph.D.<br>Professor of Civil Engineering<br>Clemson University | |

PINO, VANESSA A. (Ph.D., Civil Engineering)

Fabric Reinforced Cementitious Matrix (FRCM) Composites as a Repair System for Transporation Infrastructure. (August 2016)

Abstract of a dissertation at the University of Miami.

Dissertation supervised by Professor Antonio Nanni.
No. of pages in text. (231)

The use of composite materials in the strengthening, rehabilitation, and repair industry has been gaining popularity due to their ability to promote the safety and sustainability of civil infrastructure. Fabric reinforced cementitious matrix (FRCM) systems have recently emerged as a viable repair alternative for restoring the integrity of damaged or structurally deficient reinforced concrete (RC) short of replacing it. The success of FRCM has been driven by its proven structural performance, inherent heat resistance and excellent compatibility with the concrete substrate. Due to the novelty of FRCM technology, the full potential of FRCM has yet to be experimentally validated and as a result, technical literature is limited. Accordingly, the experimental and numerical evaluation of a polyparaphenylene benzobisoxazole (PBO) fabric based FRCM system was undertaken and presented through three interrelated studies, where an introductory chapter presents a detailed review of FRCM systems. The first study investigates the effect of multiple layers on FRCM material properties and performance, by means of conducting direct tension and bond tests. The study also investigates the early-age bond strength of a system applied to concrete, over a 28-day period. The second study entails the analysis and experimental investigation of impact-damaged prestressed concrete (PC) bridge girders strengthened with FRCM and was also expanded to include FRP as a repair system. The third study

investigates the experimental performance of FRCM strengthened RC beams subjected to static and fatigue loading where parameters such as ultimate strength, applied stress range, fatigue life, failure modes, and residual strength were observed. The global objective is to experimentally and numerically validate FRCM's potential as a repair system for transportation infrastructure as a means to expand the current knowledge of FRCM systems. Overall, the PBO-FRCM exhibited favorable mechanical behavior and structural performance. Through the use of effective methods of technology transfer, the results and observations serve to bridge the gap between applied research, design literature and structural application in order to promote the use of sustainable repair materials.

*To my husband and my parents,*

*Without God this would not be possible.*

**ACKNOWLEDGEMENTS**

I would like to express my sincerest gratitude and appreciation to my advisor Dr. Nanni, whom I have the utmost respect and admiration. Without his patience, guidance, support, and encouragement this would not have been possible as he has truly inspired me to be a better engineer and individual.

I am extremely grateful and thankful for the mentorship, knowledge, and guidance provided by my committee members, Dr. Francisco De Caso, Dr. Wimal Suaris, and Dr. Thomas Cousins.

Thank you to my best-friend and sister, Talia, for your love and support when I needed it most.

I would like to especially thank my friends Karina, Nicole, Guillermo, Diana, Keith, Omid, Houman, Zahra, and Maria. This journey would not have been possible without their support, encouragement, and positivity.

I gratefully acknowledge the University Transportation Center (UTC) RE-CAST, the Virginia Transportation Research Council via a subcontract with Virginia Tech, the CAIT Tier I UTC Consortium, the Qatar National Research Fund (a member of Qatar Foundation), and the NSF Industry/University Center for Integration of Composites into Infrastructure (CICI) at the University of Miami with its industrial member Ruredil S.pA for the support provided.

**TABLE OF CONTENTS**

## LIST OF FIGURES

## LIST OF TABLES

## LIST OF ABBREVIATIONS

AASHTO American Association of State Highway and Transportation Officials

AC Acceptance Criteria

ACI American Concrete Institute

ACMBS Advanced Composite Materials in Bridges and Structures

ASCE American Society of Civil Engineers

ASTM American Standards for Testing and Materials

DOT Department of Transportation

CEB-FIP Comite Euro-International du Beton-International Federation for Prestressing

CICI Center for Integration of Composites into Infrastructure

COV Coefficient of Variability

FHWA Federal Highway Administration

FRC Fiber Reinforced Concrete

FRCM Fabric Reinforced Cementitious Matrix

FRP Fiber Reinforced Polymer

IAB Industrial Advisory Board

IBC International Building Code

ICC-ES International Code Council Evaluation Services

LVDT Linear Variable Differential Transducer

NCHRP National Cooperative Highway Research Program

NSF National Science Foundation

PBO Polyparaphenylene Benzobisoxazole

PC Prestressed Concrete

PSY Percent of the Static Yield

RC Reinforced Concrete

S-N Stress vs. Number of Cycles Curve

SCMT Sustainable Construction Materials and Technologies

TRC Textile Reinforced Concrete/Cement

TRM Textile Reinforced Mortar

UTC University Transportation Center

# CHAPTER 1

## Introduction

In the last thirty years, there have been significant developments in composite materials used for the repair, retrofit, and rehabilitation of civil infrastructure. A composite system consists of two or more materials that possess different properties, but when combined they form a material that exhibits properties superior to its individual components. In many cases, a composite is comprised of a matrix and a reinforcing fiber. Composite materials used for structural application have been developed in an attempt to promote the safety and sustainability of civil structures. In the life of a structure, there may come a time when repair or demolition is required. The latter of which is typically the least attractive option due to cost and inconvenience. Among the many composite systems used specifically for the repair of reinforced concrete (RC) and masonry, fabric reinforced cementitious matrix (FRCM) and fiber reinforced polymer (FRP) have shown promising research based performance and are considered viable strengthening alternatives to traditional methods such as steel plates and post-tensioning.

FRP is comprised of fibers embedded into a polymeric resin matrix. The great success of FRP composites is driven by their high strength-to-weight ratio (lightweight), high tensile strength, and non-corrosive properties. The use of FRP in the repair industry has had an increasing momentum due to the many studies that have been conducted and reported, in order to understand the properties of FRP systems and their optimal uses. Despite all of these advantages, FRP has some limitations: poor behavior at increased temperatures, inability to bond to a wet surface, lack of vapor permeability, and UV

degradation. And while the use of FRP is more established, a recently emerged FRCM system is gaining the "spotlight" in the area of composites for structural application. FRCM recognizes the shortcomings of FRP and compensates for these drawbacks with its inherent heat resistance and excellent compatibility with the concrete substrate. FRCM consists of an inorganic cement-based matrix reinforced with a continuous arrangement of fibers commonly known as a fabric. FRCM is a system that combines novel (fabric) and traditional (cement) materials, where the use of cementitious materials dates back to the Roman era and continues to be one of the most widely used materials in construction (i.e., concrete).

There have been many advances in the mechanical characterization and structural evaluation of FRCM. FRCM systems exhibit favorable tensile behavior, bond properties, and durability performance, which are essential for the success of a repair system. Technical literature reports significant improvement in the flexural, shear, and axial behavior of RC and masonry components strengthened with FRCM (De Caso y Basalo et al. 2012, Babaeidarabad et al. 2014, Al-Salloum et al. 2012). There is no doubt that FRCM systems have proven mechanical and structural performance. However, due to the variety of fibers (from low to high modulus) and fabric weights (low to high equivalent thickness) in addition to the ability of having multi-fabric construction, there is still a large demand for experimental and theoretical research to validate mechanical effectiveness (Nanni 2012). FRCM has undeniable potential as a repair system, but because it is a relatively new material, its full potential has yet to be validated. In particular, FRCM has abundant capabilities in the area of RC repair/rehabilitation of transportation infrastructures, which is a recurring challenge in civil engineering. Traditional repair methods have proven to be

partially satisfactory in restoring and/or improving ultimate strength to damaged or under-designed bridge components, while FRP materials have shown great success in this area and in a sense have "paved the way" for the deployment of FRCM (Di Ludovico et al. 2006). FRCM systems have shown excellent performance in terms of increasing flexural strength of RC beams in small-scale application (Triantafillou 2007, D'Ambrisi and Focacci 2011, Babaeidarabad et al. 2014), but no literature has reported on the investigation of FRCM applied to full-scale bridge elements. Furthermore, it is crucial that a repair system used for bridge structures exhibit favorable long-term performance during the remaining service-life of a structure. A repair method may be effective in restoring capacity, but if the material does not exhibit favorable long-term performance, the repair itself will be short-lived. Accordingly, FRP has shown excellent long-term behavior when subjected to repetitive loading typically seen in bridges due to vehicular traffic (Kim and Heffernan 2008, Barnes and Mayes 1999, Dawood et al. 2007, Ekenel 2006). And while little to no studies on the long-term performance of FRCM-strengthened RC have been reported, the great success of FRP suggests that FRCM will follow in its path.

The objective of this dissertation is to expand the existing knowledge of FRCM and to investigate its un-discovered potential as a strengthening technique for transportation infrastructure. The investigation is divided into three interrelated studies: the aim of the first study is to experimentally investigate the material properties of a synthetic fabric-based polyparaphenylene benzobisoxazole (PBO) FRCM system used for RC strengthening. In this study, experimental tests are performed in accordance with established acceptance criteria to investigate the effect of multiple fabric layers on FRCM material performance. The following parameters are investigated: direct tension, FRCM-

concrete bond, and matrix mortar compression strength. Understanding the influence of multiple plies (layers) on material behavior is necessary for the design of FRCM systems as it is very likely that multiple layers of reinforcement will be used for structural application. In addition, this study will experimentally investigate the early age FRCM-concrete bond strength development. For bridge-type structures undergoing structural repair, the strength development versus time relationship is an important parameter that can be used to reduce traffic closure time that is typically associated with the FRCM curing period (28 days). The second study entails the analysis and experimental investigation of impact-damaged prestressed concrete (PC) bridge girders strengthened with FRCM. This study was also expanded to include FRP as a repair system in order to provide a better validation of the FRCM technology. Material properties from the first study were used in conjunction with design literature to determine theoretical capacities observed in the experimental tests. A separate analysis was performed using the same literature to determine design capacities using nominal material properties. The analytical, experimental, and design values obtained in this study aim to validate structural performance and ultimately increase the number of tools available for emergency repairs. Finally, the third study aims to investigate the long-term performance of FRCM strengthened RC beams. RC specimens are subjected to both static and cyclic (fatigue) loading where the following parameters are investigated and discussed: amount of supplemental reinforcement, ultimate strength, applied stress range, fatigue life, failure modes, and residual strength. Results are used to develop a stress ratio vs. number of cycles (S-N) curve with the objective of defining the endurance limit of the FRCM strengthened beams that can be used for design.

The results and observations from the aforementioned studies confirm FRCM's ability to optimize the performance of RC specifically for transportation infrastructure. Given the limited amount of FRCM literature reported to date, a successful attempt has been made to establish preliminary design guidelines that best reflect the behavior of FRCM systems. However, the progression of such design guidelines is at the mercy of the quantity and quality of available research. Accordingly, this work is intended to enhance the amount of FRCM literature, which subsequently can be used to expand and fine-tune the design criteria established by government organizations such as The American Concrete Institute (ACI), Department of Transportation (DOT's), American Association of State Highway and Transportation Officials (AASHTO) that are used by practicing design professionals.

**Technology Transfer**

It is not uncommon for engineers in practice to exhibit a sense of uncertainty when faced with the design of a new material system such as FRCM. Ironically, this reluctance inhibits the evolution of the repair industry which has a consistent demand for sustainable materials used for structural repair. The work presented herein is intended to bridge the gap between applied research, design literature, and structural application, which is achieved through the use of effective methods of technology transfer. Technology transfer in the form of presentations, conference proceedings, technical papers and reports, promotes the growth and evolution of the repair industry. The following literature has been submitted to expand the knowledge of material and structural performance of FRCM composites:

*Technical Papers and Reports*

- "Performance of FRCM Strengthened RC Beams Subject to Fatigue" – Paper submitted for review to the ASCE Journal of Composites for Construction.

- "Repair of Damaged PC Girder with FRCM and FRP Composites," Publication No. 00042134-04, Grant No. DTRT13-G-UTC45, USDOT RE-CAST University Transportation Center, 88, 2015.
- "Evaluation of Repair Techniques for Impact Damaged Prestressed Girders," FHWA/VTRC Report, June 2015.
- "Repair of Damaged Prestressed Concrete Girders with FRP and FRCM Composites" – Paper submitted for review to the ASCE Journal of Composites for Construction.

*Conference Proceedings*

- Long Term Performance of FRCM Strengthened RC Beams Subject to Fatigue" - Paper accepted for presentation at the Sustainable Construction Materials and Technologies (SCMT4) Convention in Las Vegas, NV, August 2016.
- "Repair of Damaged Prestressed Concrete Girders with FRP and FRCM Composites" – Paper accepted for presentation at the International Conference on Advanced Composite Materials in Bridges and Structures (ACMBS) in Vancouver, British Columbia, Canada, August 2016.

*Presentations*

- "Material Characterization of FRP and FRCM Systems for the Strengthening of Prestressed Concrete Girders" – Paper accepted for presentation at the International Conference on Advanced Composite Materials in Bridges and Structures (ACMBS) in Vancouver, British Columbia, Canada, August 2016.
- "Long Term Performance of FRCM Strengthened Beams Subject to Fatigue" Presentation given to the Center for Integration of Composites into Infrastructure (CICI) Industrial Advisory Board (IAB) Meeting in Miami, FL, February 2016.

- "Long Term Performance of FRCM Strengthened Beams Subject to Fatigue" – Abstract submitted and presentation given to the American Concrete Institute (ACI) Concrete Convention and Exposition in Milwaukee, WI, April 2016.

**Background**

In current literature, there are several terms used to describe FRCM composites. These terms include textile reinforced mortar (TRM) and textile reinforced concrete (TRC), mineral based composites, or fiber reinforced cement (FRC) which are a subset of a larger category of cement-based composites called ferrocement. Ferrocement is comprised of a cementitious matrix and a reinforcement, where the bond between the two materials is what determines the effectiveness of the composite. The American Concrete Institute defines ferrocement as "*a type of thin wall reinforced concrete commonly constructed of hydraulic cement mortar reinforced with closely spaced layers of continuous and relatively small size wire mesh. The mesh may be made of metallic or other suitable materials*". The use of ferrocement dates back to the 1960's where woven steel wire mesh was originally used as the reinforcement mechanism. During this time, a valid attempt was made to incorporate other types of reinforcement such as natural and polymeric meshes, but their success was short lived due to their low elastic modulus compared to steel. In the mid-1980's the development of polymeric meshes using high performance fibers such as carbon, glass, and Kevlar were available for ferrocement applications (Namaan 2012). The use of these high strength, high modulus materials expanded and optimized the performance of ferrocement in structural application. It was also discovered that the cementitious matrix properties can be enhanced with the addition of discontinuous fibers. The added fibers

increase the tensile and compressive strength of the matrix while also improving interlaminar and vertical shear resistance.

**Fabric Reinforced Cementitious Matrix (FRCM)**

FRCM systems consist of one or more layers of dry fabrics made of carbon, glass, aramid, or polyparaphenylene benzobisoxazole (PBO) fabrics (Figure 1) that are sandwiched between layers of cementitious mortars. FRCM is typically externally bonded to the tension face of a concrete member (Figure 2) and acts as supplemental reinforcement.

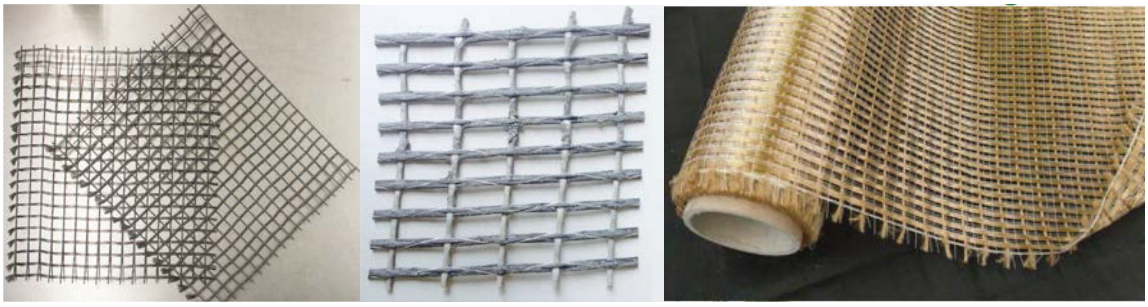

**Figure 1 – Types of FRCM Fabric: AR-Glass (left), Carbon (middle), PBO (right)**

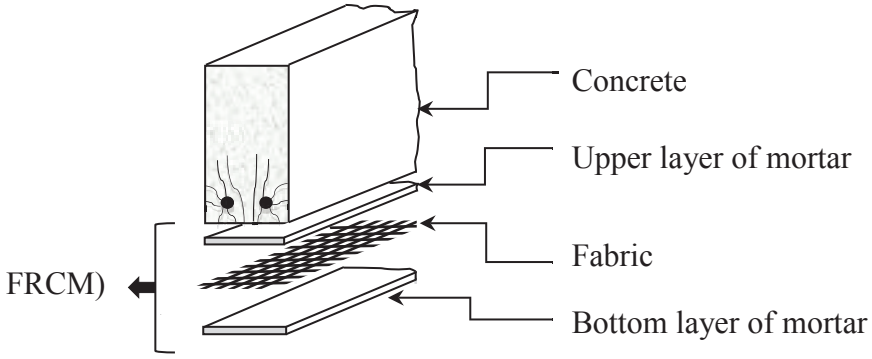


**Figure 2 – Schematic Representation of FRCM for Concrete Strengthening**

The fabrics are comprised of fibers that are bundled into yarns or rovings, that can be woven, knitted or bonded as shown in Figure 3. Fabrics are typically comprised of dry fibers that are coated with a polymeric resin, but are not bonded together or impregnated by such resin. The term “dry fibers” implies that the fibers are not fully impregnated by the

matrix, contrary to FRP systems. The cementitious matrix is typically Portland cement based and contains less than 5% by weight of dry polymers. The matrix which exhibits high compressive strength but low tensile strength, protects and transfers the load to the

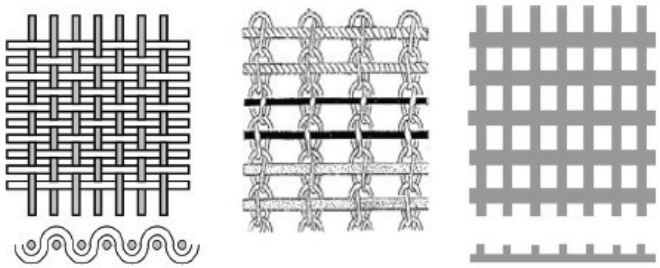

**Figure 3 – Different Types of Fabric: woven (left), kitted (middle), bonded (right)**

fabric. Therefore,the fabric is the primary tensile load carrying mechanism. The properties of a fabric can be described according to the direction of the yarns and fiber density. The warp direction is defined as the primary fabric direction along the length of the fabric that carries the tensile load, while the weft direction describes the yarns that (typically) run perpendicular to the warp. A balanced fabric network indicates that the fiber density in both the warp and weft directions are equal. An unbalanced network indicates different fiber densities, where the warp direction contains a higher density. An example of an un-balanced fabric network is given in Figure 4. FRCM's replace the organic binder seen in FRP, with an inorganic cementitious binder that possesses favorable material properties

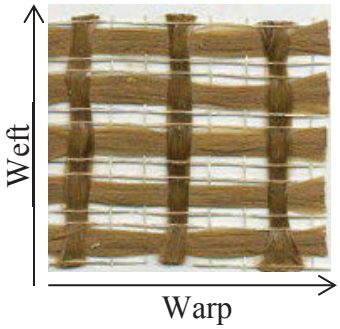


**Figure 4 – Un-balanced PBO Fabric**

including: inherent resistance to heat and excellent compatibility with the concrete substrate (i.e., can be applied on a wet surface and allow vapor permeability). Other advantages include excellent durability performance, ease of installation, and ease of reversibility (can be removed without damaging the structure). The behavior of FRCM is determined by a variety of different factors including: material properties of the fibers and mortar, layers of fabric, fabric-matrix bond, fabric orientation, and mortar penetration between mesh openings. A brief review of FRCM materials is presented in the following subchapters.

**FRCM Material Compliance and Design Literature**

FRCM systems are specifically designed by a manufacturer to provide a unique combination of fabric and matrix that exhibits optimal workability, (chemical/mechanical) bond and performance. FRCM systems should not be produced by randomly selecting and mixing commercially available materials. In order to validate the material system and provide accurate and safe design guidelines, the mechanical properties of the composite, the bond resistance to substrate, and understanding durability performance of the material is needed (Carozzi and Poggi 2015). When a FRCM system is developed, it must undergo various tests and meet certain criteria in order to be considered for structural application. The ICC Evaluation Services (ICC-ES) created a document titled “Acceptance Criteria for Masonry and Concrete Strengthening Using Fabric-reinforced Cementitious Matrix (FRCM) Composite Systems (AC434)” which defines the test methods and establishes acceptance criteria to be performed by an accredited laboratory in order to produce a product research report (Figure 5). The International Building Code (IBC) (Section 104.11.1) requires a product research report stating that FRCM evaluation and

characterization is compliant with AC434 guidelines in order for the system to be used in structural design. The following parameters are evaluated: material properties, axial, flexural and shear capacity, durability (environmental exposure) performance, fire performance, and structural design procedures. In particular, AC434 Annex A outlines the


**Figure 5 – AC434 (Left) and ACI 549.4R-13 (Right)**

test procedure and data analysis which yields the tensile material properties of FRCM. The tensile testing of FRCM is a critical component of this research; therefore, Annex A of AC434 is included in Appendix B of this dissertation.

Another useful tool, which was developed for the use of licensed design professionals, is a document titled: ACI 549.4R-13 "Guide to Design and Construction of Externally Bonded Fabric Reinforced Cementitious Matrix (FRCM) Systems for Repair and Strengthening Concrete and Masonry Structures" (ACI 549.4R 2013). This document was developed by the American Concrete Institute (ACI), and contains all necessary tools for the effective design and construction of FRCM system (Figure 5). It covers the many aspects of FRCM including: background information, installation guidelines, field applications, material properties for different systems, system qualifications, design guidelines (axial, flexural, and shear capacities), reinforcement details, and design

examples. The material properties determined from AC434 are used in accordance with ACI 549.4R-13 to effectively design externally bonded FRCM systems for strengthening RC and masonry structures. Furthermore, the design methodology provided in ACI 549.4R is fundamental for study 2 and study 3 of this dissertation where FRCM systems are designed for the strengthening of RC beams and PC bridge girders.

**FRCM Installation**

ACI 549.4R-13 outlines the provisions for a suitable FRCM installation to concrete and masonry. FRCM installation shall be performed by a licensed contractor that has received training from the manufacturer or an authorized training agent. It is important for the concrete surface to be properly prepared in order to avoid possible stress concentrations, debonding, or delamination. Surface preparation can vary depending on the FRCM system, but common preparation methods include: sandblasting, roughening, grinding, or hydrojetting. Putty fillers and mortars can also be used, per manufacturers' recommendations, to fill any voids or discontinuities in the substrate material. The substrate surface should be continuous, clean from dust and debris, and any corners should be rounded to a radius of at least 12.7 mm in order to avoid possible stress concentrations. The ideal temperature range for FRCM application is between 6°C and 35°C. Temperatures greater than 35°C may affect the workability of the mortar while temperatures less than 6°C may retard the setting time. Prior to installation, the concrete substrate shall be maintained saturated-surface-dry. The mortar matrix is normally mixed and prepared in accordance with the manufacturer's instructions where the mortar shall be applied during its plastic life state. A thin layer of mortar is applied uniformly and directly to the strengthened member, normally using a trowel (Figure 6a). The dry fabric is then gently

pressed onto the matrix, with the trowel (Figure 6b), where the primary direction of the fabric is specified by a license design profession and is typically orientated in the direction of the tensile loading. A final layer of mortar is applied over the fabric in order to create the "sandwich" (Figure 6b). Successive layers of mesh and mortar are applied to achieve a multiple layer configuration (Figure 7). The fiber shall be placed in order to maintain straightness and avoid bends, kinks, or folds.

a) b) c)

**Figure 6 – Specimen Preparation a) First Layer of Mortar b) Placing Mesh c) Layer of Mortar (Sandwich)**

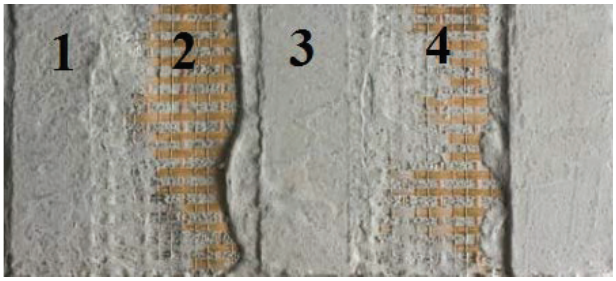


**Figure 7 – Multiple Layers of FRCM**

The placement of FRCM is dependent on the type of structural member that requires repair. For beams and slabs that require flexural strengthening, the system is typically externally bonded to the tension face where the primary fabric direction is in the direction of applied tensile stresses. Shear strengthening of RC beams is achieved by a U-wrap configuration or by completely wrapping the beam at shear-critical locations where

additional capacity is warranted. Whereas confined columns require helical wrapping around the member in order to resist the radial stresses associated with axial loading. And masonry walls that require the use of a balanced fabric network placed on one or both wall faces depending on the loading type (in-plane or out of plane).

**Mechanical Behavior of FRCM**

The structural design of FRCM requires an understanding of its mechanical behavior (Arboleda et al. 2015). Due to the fact that FRCM is typically applied to the tension face of reinforced concrete, the tensile behavior is an important parameter that is determined through experimental tests. Many have performed uniaxial tensile tests to evaluate the stress-strain behavior of different FRCM systems, where tensile behavior is influenced by several factors including: load transfer mechanism, strain measurement instrumentation and specimen preparation (Arboleda et al. 2015). The most common load transfer mechanisms reported in literature are the clamping grip and the clevis grip. The clamping grip consists of utilizing compressive stress to clamp the two extreme ends of a rectangular specimen (Figure 8 left), where the lower grip allows for torsional rotation of the specimen.

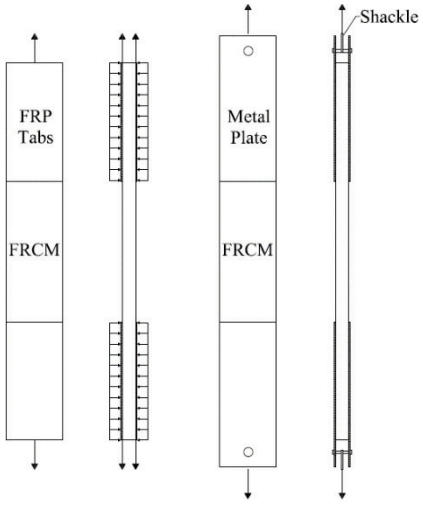


**Figure 8 – Different Test Setups: Clamping Grips (left), Clevis Grips (right)**

FRP tabs are applied to the end of each specimen in order to ensure a more homogeneous stress distribution (Carozzi and Poggi 2015). The latter load transfer mechanism, a clevis grip, consists of two steel plates that are adhesively bonded to each end of the tensile coupon. The tensile load is transferred as a shear stress by the adhesive bond between steel plates glued to the specimen ends (Figure 8 right). A pin is threaded through the ends of the bonded plates, where a shackle engages the pin and applies a tensile load.

A typical tensile stress-strain behavior for a clamping test setup can be represented as a tri-linear curve as shown by Arboleda et al. 2015 in Figure 9. The initial part of the curve

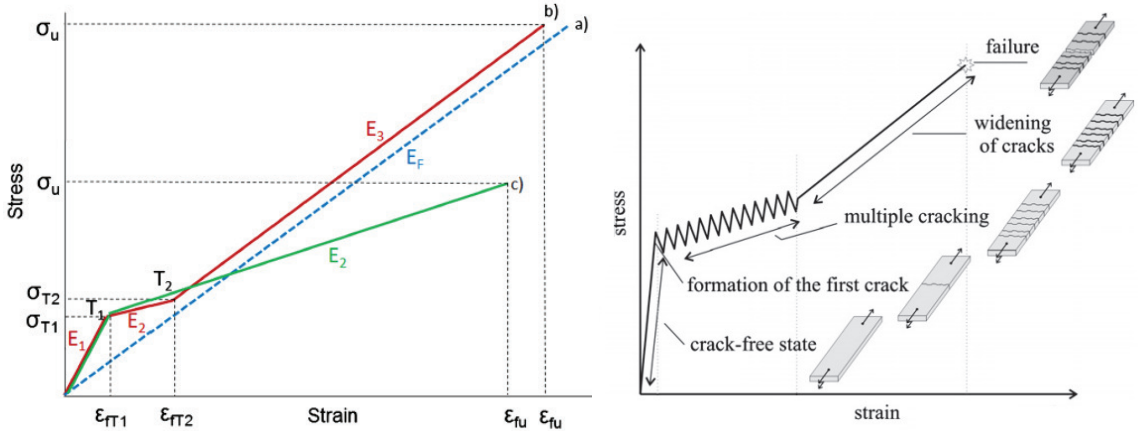


**Figure 9 – Typical Stress Strain Curve for FRCM (Arboleda et al. 2015), Left; Typical TRC Response (Mechtcherine 2013), Right**

corresponds to the uncracked linear elastic behavior of the specimen where the stiffness of the system is approximately equal to the stiffness of the cementitious matrix and is slightly enahanced by the presence of the reinforcing fibers. In the second phase, the curve exhibits a significant loss of stiffness due to matrix crack initiation and formation, described by relatively fine cracks, where the length of this portion is dependent on the quality of the matrix-fabric bond and the number of fabric layers of the specimen. The third portion is defined as the crack-widening region, where existing cracks continue to widen and

eventually failure occurs due to tensile rupture of the fabric or slipping of the fabric within the matrix, or a combination of the two modes. In the third phase, the matrix contributes very little to the tensile resistance which is provided mainly by the fabric. This concept is reflected in the stress-strain curve of where the slope runs parallel to the slope of a stand-alone fabric. Note that the transition from one phase to another is known as the transition zone, T. Mechtcherine 2013 beautifully illustrates the tensile behavior of a TRC specimen with respect to the idealized stress-strain curve previously described. The combined microcracking and cracking mechanisms observed in the tensile specimens results in an advantageous pseudo-ductility. Accordingly, for a clevis-type test setup, the slope of the third stage is almost indistinguishable from the second stage and a bilinear curve best represents the stress-strain behavior as shown in curve c) of Figure 9 (Arboleda et al. 2015). A detailed summary and description of uniaxial tensile behavior can be found in Arboleda et al. 2015.

AC434 Annex A recommends that a clevis-type connection be used to ensure the load is transmitted directly from the matrix to the fabric which simulates actual conditions in the field. As opposed to the clamping grip mechanism that causes the fibers to be constrained and experience compressive concentrations at the ends, which does not simulate field conditions (Arboleda 2014). In addition, flexural tests performed on RC beams strengthened with externally bonded FRCM indicate that the tensile capacity of the fibers is never reached and failure occurs due to slipping of the fabric within the matrix, FRCM delamination, or any combination of the two modes (D'Ambrisi and Focacci 2011; Babaeidarabad et al. 2014). This further justifies the use of a clevis-type mechanism. While there are many forms of technology that allow for the observation of specimen deformation

(strain gauges, extensometers, LVDT's), an extensometer having a minimum gauge length of atleast 50 mm is typically used to ensure inclusion of at least one crack within the gauge length (AC434).

AC434 Annex A outlines the tensile testing procedure for FRCM specimens and defines the stress-strain behavior as a bilinear curve as shown in Figure 10, which also describes curve c) Figure 9. According to AC434, the tensile test results shall be analyzed to determine material properties necessary for material specification and structural analysis

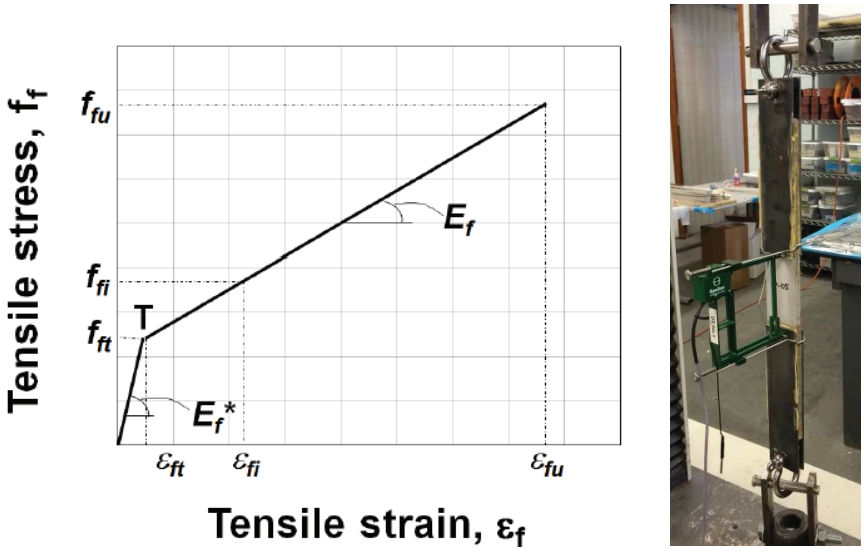


**Figure 10 – Typical Stress Strain Curve for a FRCM Tensile Specimen (AC434 Annex A), Left; Tensile Test with Clevis Grips, Right**

and design (ICC-ES 2013), where the following material properties are obtained: tensile modulus of elasticity of the uncracked specimen, $E_f$*, transition stress, $f_{ft}$, and transition strain, $\varepsilon_{ft}$, corresponding to the transition point, $T$, between the uncracked and cracked state, tensile modulus of elasticity of the cracked specimen, $E_f$, ultimate tensile stress, $f_{fu}$, and ultimate tensile strain, $\varepsilon_{fu}$. A detailed description of the methodology and equations used

to determine these properties is presented in AC434 Annex A, which has been included as a part of this dissertation in Appendix B.

**FRCM Bond**

The fact that FRCM incorporates a "dry fabric" combined with the granularity of the mortar, prevents the matrix from fully impregnating and bonding to each individual fiber (Ombres 2010). The bond between matrix and fibers occur only along the external perimeter fibers directly in contact with the matrix (D'Ambrisi et al. 2012) which makes the material susceptible to slipping and debonding. This concept can be modeled as a yarn bundle containing a sleeve and a core as shown in Figure 11. The bond between the mortar

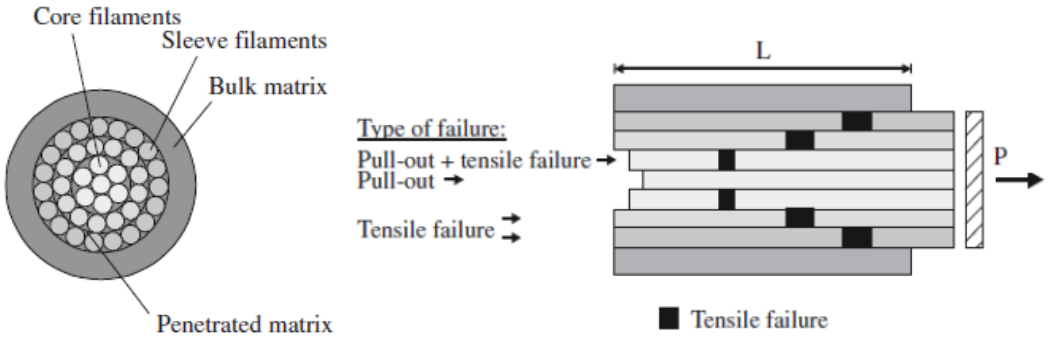


**Figure 11 – Illustrative Model of a Fabric Bundle Failure (Brameshuber 2006)**

and the external yarns (sleeve) as well as the frictional bond between the internal fibers (core) greatly influences the behavior of FRCM where two types of mechanisms are observed: slippage between the fibers and the mortar (debonding) or slippage between the internal core fibers. Fiber-mortar slipping (debonding) is associated with the mortar's lack of ability to completely impregnate the fibers, debonding at the fiber-mortar interface, or chemical incompatibility and occurs as a fracture mode. Slipping within the internal fibers is attributed to a telescopic slipping mode caused by the low friction between the fibers as

well as the bond between the external and internal fibers as shown in Figure 11 (Arboleda et al. 2015).

Published technical literature reporting on the material characterization and experimental analyses of RC strengthened with FRCM observed two critical failure modes: fabric slippage within the matrix and FRCM delamination, or a combination of the two modes (Figure 12). Fabric slipping within the matrix is described as the combination of

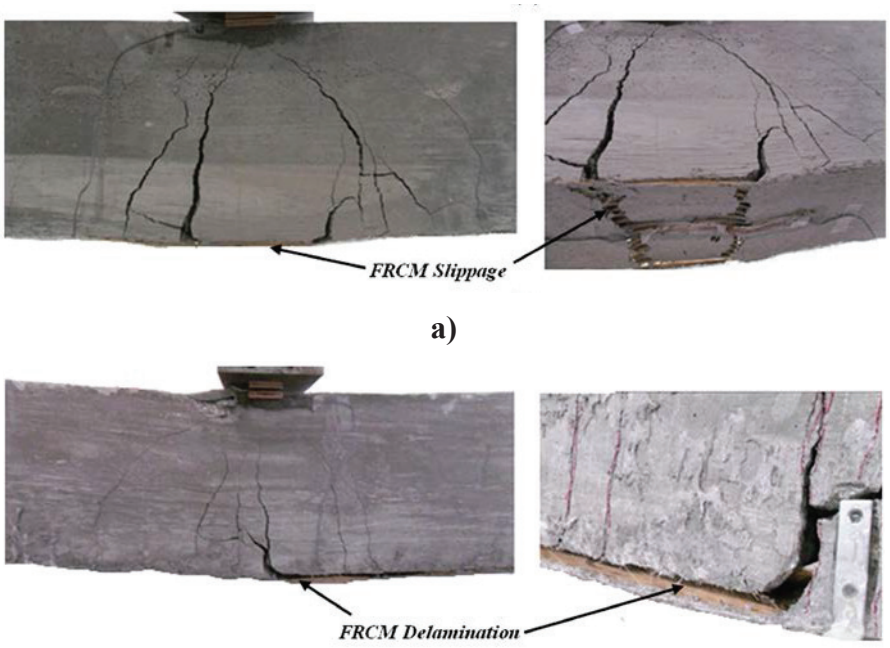


**Figure 12 – FRCM Failure Modes: a) Fabric Slipping b) Delamination (Babaeidarabad et al. 2014)**

gradual fiber-mortar slipping and slipping within the internal fibers. While FRCM (interlaminar) delamination consists of a more sudden fiber-mortar slipping mechanism with little to no slipping within the internal fibers. The term FRCM delamination is described as the debonding of one material from another. Two types of FRCM

delamination can occur: interlaminar delamination and surface delamination. Interlaminar delamination consists of FRCM fabric debonding from the matrix mortar which was described previously, while surface delamination is described as the debonding of the FRCM from the concrete substrate. Surface delamination occurs when the bond capacity between the concrete and FRCM matrix is reached and fracture occurs at the concrete-mortar interface. Typically a combination of both surface and interlaminar delamination is observed.

It is well-established that the bond behavior of FRCM is largely dependent on the load transfer mechanism occurring at the concrete-matrix interface as well as within the FRCM material at the fabric-matrix interface and within the internal fibers (Ombres 2015). Other factors affecting FRCM bond include: material properties of the fibers and the mortar, volume fraction, and fabric roving orientation respective to the direction of loading. Another bond mechanism that has yet to be investigated experimentally is the bond performance of FRCM systems subjected to fatigue loading due to the limited amount of research available on the fatigue behavior of FRCM applied to concrete members.

**FRCM Structural Performance**

The effectiveness of FRCM systems as supplemental reinforcement to RC members has been evaluated with several studies performed to investigate confined columns (Triantafillou 2007, De Caso y Basalo et al. 2012, Di Ludovico et al. 2010), and beams tested in both flexure ( D'Ambrisi and Focacci 2011, Babaeidarabad et al. 2014) and shear (Triantafilloui and Papanicolaou 2006, Al-Salloum et al. 2012). Results from experimental analyses indicate that the structural performance of RC strengthened with FRCM is largely dependent on the matrix and fabric design. FRCM confined columns exhibited an increase

in compressive strength and deformation where failure occurred due to fiber fracture or debonding. For FRCM strengthened RC subjected to flexure, literature consistently reports a significant increase in load-carrying capacity and deformation, with an observed pseudo-ductility. Reported failure modes include: concrete cover delamination, fabric slippage within the matrix, surface delamination at the concrete-matrix interface, and interlaminar delamination, or any combination of these mechanisms. Failure was observed in the area of maximum moment which typically occurred at or near midspan for three and four-point bending tests. RC Beams tested in shear also exhibit a noticeable increase in strength and ductility with similar FRCM failure modes. For all axial, flexural, and shear tests, there is an observed increase in strength associated with added number of reinforcement layers. However, when increasing the number of FRCM layers, it is essential to ensure that the resulting change in stiffness of the system does not adversely affect the load sharing which can result in premature delamination. In this event, mechanical anchorages have been shown to reduce the occurrence of premature delamination (Al-Salloum et al. 2012).

**Durability**

In addition to FRCM performance under certain loading conditions, it is required for the system to demonstrate good durability performance when exposed to extreme conditions including: weathering action, repeated loading, chemical attack, abrasion, or any other process of deterioration. The material must resist the affects of these conditions and maintain it's original physical and structural integrity throughout its lifetime. The durability of FRCM is related to the quality, design, and manufacturing process of its constituents as well as material application, service environment, and service loading (Arboleda 2013). AC434 provides guidelines for the evaluation of FRCM performance

under accelerated environmental exposures including: freezing and thawing, water vapor, alkali, saltwater, and fuel exposure. Arboleda 2013 performed a durability study on two FRCM systems from the same manufacturer, each consisting of PBO fabric and Carbon fabric mesh. Specimens were subjected to the aforementioned environmental exposures where no significant degradation in strength was observed. However, other types of fabrics such as those comprised of glass fibers may exhibit material properties that are susceptible to long-term durability effects. The use of alkali-resistant glass fibers with cementitious mortars has been successfully implemented provided they are designed to account for any long-term changes in material properties. In general, FRCM systems demonstrate good durability performance. Nevertheless, the durability performance of one FRCM system does not reflect the characteristics of another system with different or even similar constituent. Therefore, every FRCM system should be evaluated separately and independently.

**Field Application**

There have been a number of commercial projects involving the strengthening/repair of concrete and masonry structures with FRCM systems which demonstrate its potential. A RC tunnel located along the Egnatia Odos Mortorway in Greece was strengthened with FRCM in a successful attempt to repair a structural deficiency (Figure 13a). The base support of a trestle railway bridge located in New York was wrapped with FRCM to provide confinement to the member which was severely cracked and deteriorated (Figure 13b). This application required the use of a porous material that allows for vapor permeability to the substrate material. Additionally, several RC bridge piers located in Novosibirsk, Russia exhibited excessive cracking where epoxy injections proved to be

partially satisfactory in preventing crack propagation. Thus, FRCM strengthening was chosen to strengthen and prevent further crack formation. The strengthening of masonry structures has also been conducted. A school located in Karystos, Greece contained shear-deficient masonry walls and RC slabs with steel reinforcement that was severely corroded.

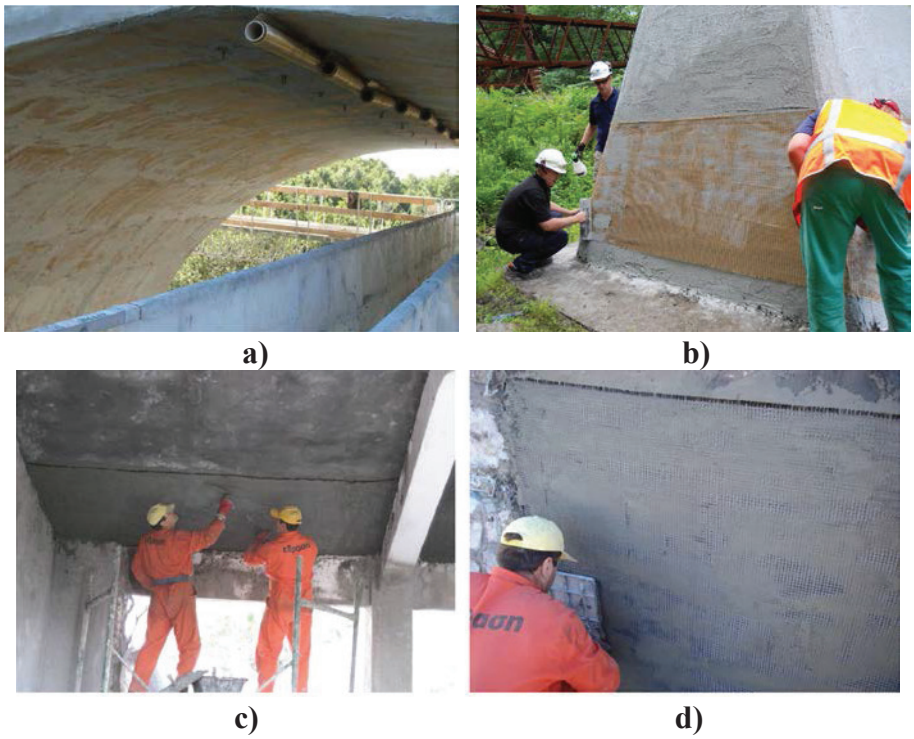

**a)** **b)**

**c)** **d)**

**Figure 13 – FRCM Strengthening of a) RC Tunnel Lining and b) Bridge Base Confinement c) R Slab d) Masonry Wall (ACI 549.4R-13)**

FRCM was used to increase flexural capacity in the RC slabs and shear capacity in the unreinforced masonry walls (Figure c&d). Additional examples of successful FRCM field applications can also be found in ACI 549.4R-13.

A detailed review of FRCM's mechanical behavior, design and testing criteria, system installation, structural performance, and field application has been presented. This was done to give the reader a general prerequisite to the material, experimental and design parameters that are presented in the following three chapters.

# CHAPTER 2

## Study 1 – FRCM MATERIAL CHARACTERIZATION: INVESTIGATION OF MULTI-PLY BEHAVIOR

The use of FRCM materials is gaining momentum in the repair, retrofit and rehabilitation industry where its success is dependent on various factors including optimal structural design, service performance, and strength and durability. FRCM is distinguishable from FRP systems with its inherent heat resistance, compatibility with the substrate, vapor permeability, and workability. FRCM composites are also considered to be a sustainable repair alternative for transportation infrastructures because they are easy to install and can extend the structure's service life. While technical literature reports that FRCM systems have proven mechanical, bond, and durability performance (Arboleda et al. 2015, Carozzi and Poggi 2015, Ombres 2015), experimental and theoretical research is still needed to fully characterize FRCM and quantify its mechanical effectiveness.

The work conducted in this study aims to investigate the effect of multi-ply behavior on the mechanical performance of a polyparaphenylene benzobisoxazole (PBO)-FRCM system. Material characterization tests specified in AC434 were performed for FRCM specimens with several fabric layers. These tests include direct tension and bond pull-off tests. Direct tension tests investigate FRCM load-deformation behavior when subjected to tensile stresses and bond tests investigate FRCM bond performance.

The FRCM system under evaluation has been previously investigated by Arboleda (2014) following AC434 provisions for a one layer fabric configuration. Results determined the mechanical properties and durability performance with no significant degradation in strength. Results from this previous study were used to certify the material

system which has been successfully implemented as a RC repair method. In addition, the material properties were included in ACI 549.4R-13 as a tool for the design of PBO-FRCM systems.

Accordingly, this study intends to build on the previous work and develop an understanding of how the FRCM system behaves when the fabric plies were increased to yield multiple layer configurations. To date, there have been little to no studies investigating the effect of multiple fabric layers on FRCM mechanical performance, which is critical considering the likelihood of multiple layers used for structural application. Another important parameter in RC repair specifically for transportation structures is the curing time required to develop substantial FRCM bond strength. Typically, bridge operations are ceased for in-service bridges needing repair/rehabilitation due to the repair time and associated curing times. As a result, this study also investigates the early age FRCM bond strength development within hours of installation throughout a 28-day period. Results from this study can be used by government organizations such as Departments of Transportation (DOTs) to estimate bridge closure time when structural repairs are warranted.

**FRCM Material System**

The FRCM system under evaluation consists of two main elements, a stabilized inorganic cementitious mortar that is Portland cement based and contains a low dosage of dry polymers (less than 5%), and a polyparaphenylene benzobisoxazole (PBO) fiber fabric. PBO fibers exhibit great impact tolerance, creep and fire resistance, energy absorption capacity, and chemical compatibility with the cementitious mortar matrix (Ombres 2015). The PBO fabric is an unbalanced network made of 10 and 20 mm spaced fiber rovings.

The free space between the rovings is roughly 5 and 15 mm, respectively, and the nominal thickness in the two fibers directions is 0.046 mm in the primary direction and 0.01 mm in the secondary direction (Figure 14d). The area per unit width in the primary and secondary direction is 45.72 and 12.95 $mm^2/m$, respectively. The cementitious matrix contains short disperse fibers, protects and transfers the load to the fabric. The FRCM system is typically used for concrete flexural and shearing stress reinforcement. Figure 14 illustrates the FRCM constituent materials and geometric properties. The fabric, fiber, and matrix material properties as reported by the manufacturer are given in Appendix A. Two types of FRCM test specimens were prepared: rectangular coupons and bond specimens. Rectangular tensile coupons were prepared for the direct tension tests and the bond

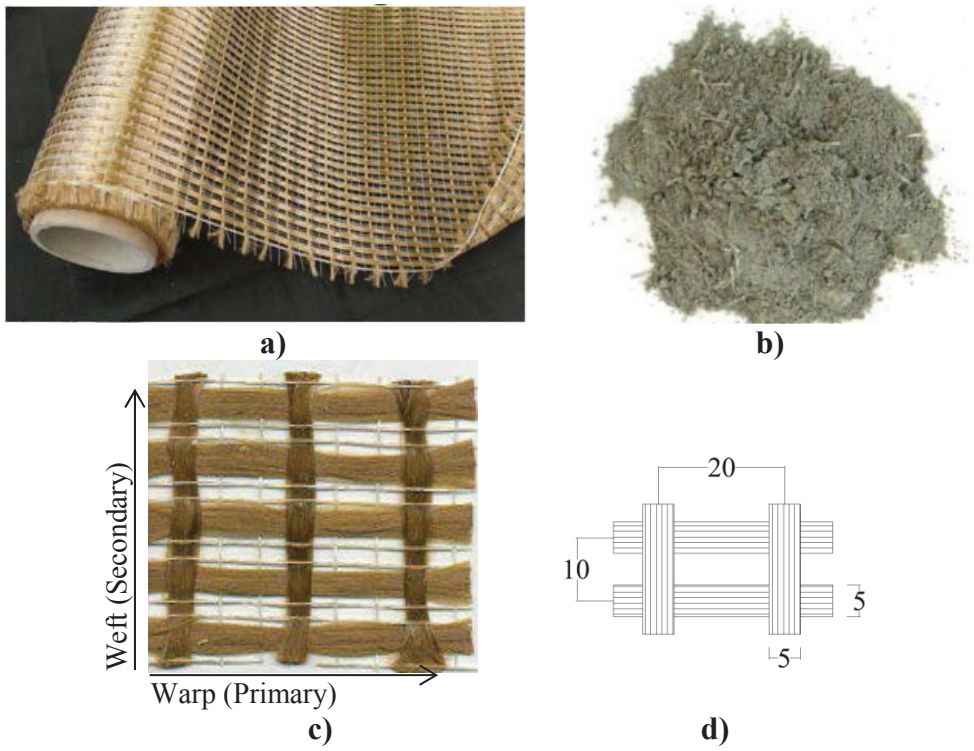


**Figure 14 – FRCM Material System a) Fabric Roll b) Matrix c) Fabric Grid d) Fabric Geometry**

specimens were prepared by means of applying FRCM to RC slabs. Table 1 shows the test matrix outlining the test type, number of FRCM layers, and number of replicates.

**Table 1 – Test Matrix for Direct Tension and FRCM Bond Tests**

| Test | Layers | Replicates |
|---|---|---|
| FRCM Direct Tension | One | 5 |
| | Two | 5 |
| | Three | 5 |
| | Four | 5 |
| FRCM Bond | One | 5 |
| | Two | 5 |
| | Four | 5 |

**Specimen Preparation**

Preparation of FRCM samples begins with the preparation of the inorganic matrix mortar by mechanical mixing. The preparation initiates by adding the dry cementitious powder to 90% of the water needed, and mixing until a homogeneous paste was attained. The remaining 10% water was then mixed with the homogeneous paste. Once the matrix was formed, a first layer of matrix was applied with a trowel onto the substrate or panel with a thickness of 3 to 4 mm (Figure 15a). The precut fabric was placed on top of the matrix layer with the appropriate fiber orientation and pressed with the bottom of the trowel to embed the fabric in the matrix (Figure 15b). A second layer of matrix was

**a)** **b)** **c)**

**Figure 15 – FRCM Specimen Preparation a) First Layer of Mortar b) Placing Fabric c) Layer of Mortar**

applied with the trowel to cover the fabric with a thickness of 3 to 4 mm (Figure 15c). For multiple layers, an additional layer of fabric and matrix layer was added until the desired numberof layers is reached. The direct tension specimens were cut from rectangular FRCM panels shown in Figure 15. The panels were made using a flat mold with a non-adhesive surface surrounded by rectangular aluminum rods to control the overall thickness of the panel. The bond test specimens were prepared by applying FRCM to a RC concrete slab as shown in Figure 16. Prior to FRCM application, the concrete slab surface was cleaned

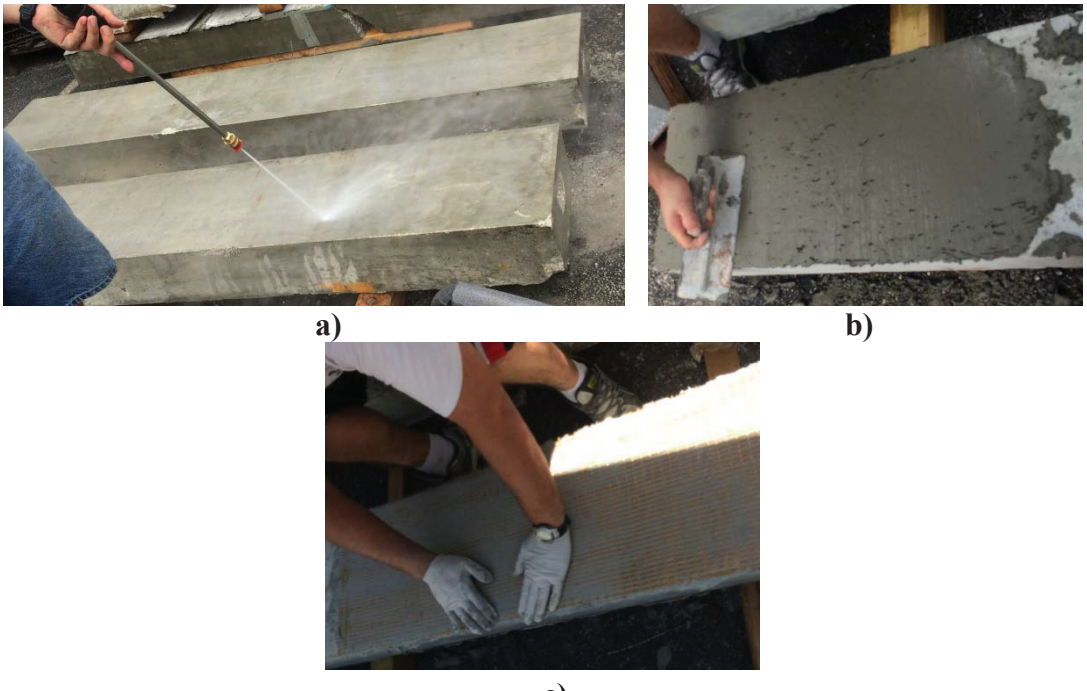

**a)** **b)**

**c)**

**Figure 16 – FRCM Application to Concrete Substrate b) Surface Preparation a) First Layer of Mortar c) Mesh Impregnation**

with high pressure water where the substrate was maintained saturated surface dry. The early age bond specimens were prepared in a more complex manner which will be described in the respective sub-chapter. Specimens were prepared in an environment with a temperature range between 5 and 35 ºC. All concrete specimens were conditioned prior

to testing under laboratory ambient conditions at room temperature 23 ± 3°C and 60 ±5% relative humidity, for at least 28 days.

**FRCM Direct Tension**

FRCM panels were cut with a circular diamond blade saw to prepare rectangular coupons as shown in Figure 17. Continuous two, three, and four layer specimens were cut with 410 x 560 mm (length x width) dimensions and had nominal thicknesses of 11, 12, and 13 mm, respectively. Fiber alignment was set in the 0° direction along the length of

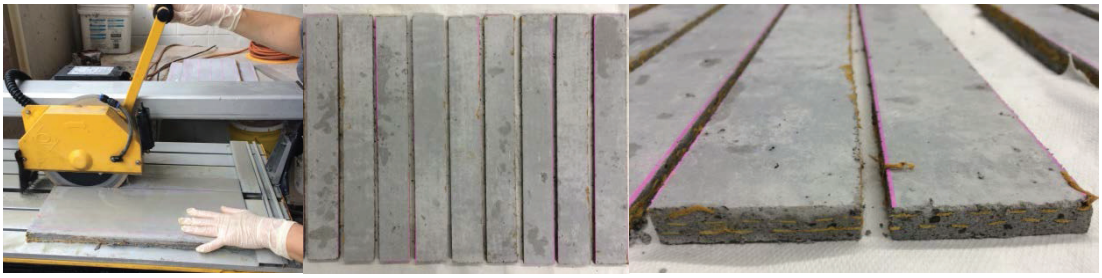

**Figure 17 – FRCM Coupon Saw Cutting (left), Cut Coupons (Middle and Right)**

the coupon. Steel metal tabs with clevis openings were bonded to each end of the specimen with bonded tab lengths of 150-mm (Figure 18). The tensile load is transferred as a shear

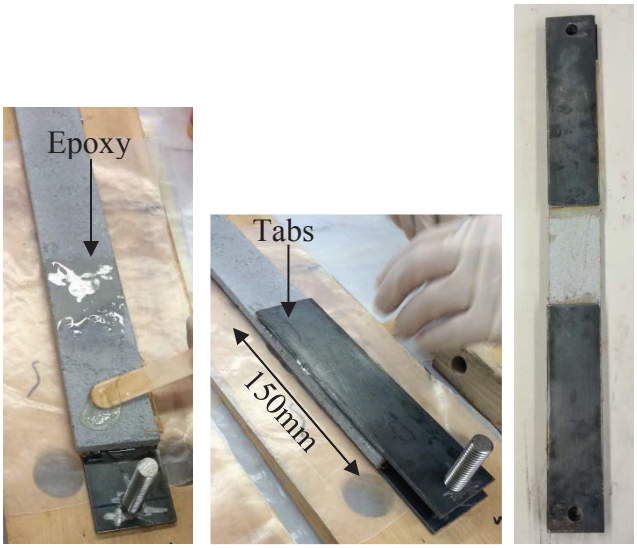


**Figure 18 – Tab Installation**

stress by the adhesive bond between steel plates glued to the specimen ends. Tensile coupons were tested according to AC434 Section 4.2.3 for Tensile Strength and Annex A Tensile Testing of FRCM Composite Specimens (AC434 2013), which is included in Appendix B of this document. Uniaxial tension load was applied to the tensile coupons. Testing was performed using a screw driven Universal Test Frame with a maximum capacity of 130 kN. Axial deformation was measured using a clip on extensometer with a 100 mm gauge length, placed mid-length of the specimen. The gripping mechanism used was a double clevis connection (Figure 19), giving maximum degrees of freedom and allowing the fabric to slip within the matrix. This gripping mechanism most accurately represents boundary conditions exhibited in field applications. All data was gathered using Instron's Bluehill software and data acquisition system. The test was performed under displacement control at a rate of 0.25 mm/minute. An initial pre-tension load of 0.10 kN, less than 5% of the anticipated failure load, was applied to engage the specimen and clevis grip setup. The applied load and extensometer strain was recorded. The stress was

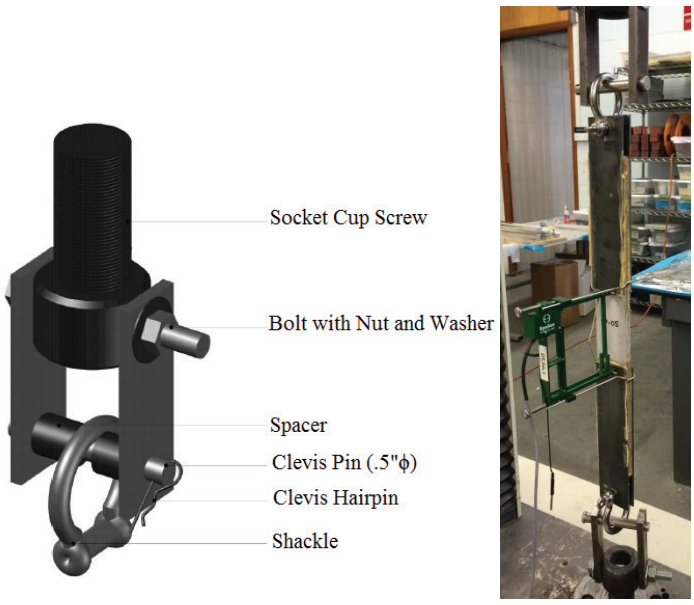


**Figure 19 – Specimen Test Set-Up with Clevis Grip and Extensometer**

determined by dividing the load by the cross sectional fabric area and a stress vs. strain curve was developed for each specimen. As per AC434 Annex A, the stress-strain behavior is expected to be bi-linear (Figure 20). The initial branch of the curve corresponds to the un-cracked state, followed by a second branch with a reduced slope, corresponding to the cracked specimen. The intersection point of the two branches is the known as the transition point, *T*. The ultimate stress, $f_{fu}$, is the maximum stress carried before failure. To determine

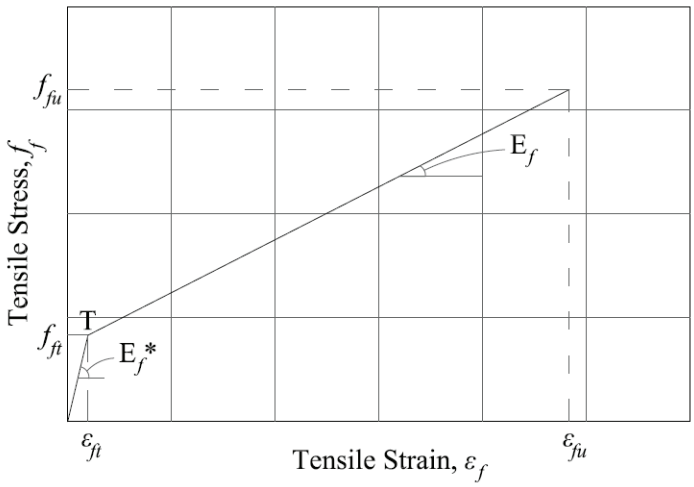


**Figure 20 – Expected Stress vs. Strain Curve**

the modulus of elasticity of the *cracked* specimen, $E_f$, attention is given to the segment of the response curve corresponding to cracked behavior after the transition as defined in AC434 A7.2. Two points are selected on the experimental curve at a stress level equal to $0.90f_{fu}$ and $0.60f_{fu}$ where the slope of the line that connects these two points represents the cracked modulus:

$$E_f = \frac{\Delta f}{\Delta \varepsilon} = \frac{0.90 f_{fu} - 0.60 f_{fu}}{\varepsilon_{f@0.90 ffu} - \varepsilon_{f@0.60 ffu}}$$

The strain values $\varepsilon_{f@0.90ffu}$ and $\varepsilon_{f@0.60ffu}$ are taken as the strain values that correspond to $0.90f_{fu}$ and $0.60f_{fu}$ on the curve. The y-intercept of the line that defines $E_f$ is determined as

$$y_{\text{int}} = 0.60 f_{fu} - E_f \varepsilon_{f@0.60 ffu}$$

Determination of the modulus of elasticity of the *uncracked* specimen, $E_f *$, is achieved by selecting two points from the uncracked linear segment of the curve. These points must form a line that closely follows the trend and slope of the curve in the uncracked region (AC 434 Annex A). The transition point (*T*) is then determined to be the stress and strain corresponding to the intersection between the initial and secondary branch of the response curve.

**Direct Tension Test Results**

Five replicates of two, three, and five ply (15 total) specimens were tested in direct tension and exhibited a bilinear stress vs. strain behavior as predicted. In addition, the results from tests conducted for one ply coupons by Arboleda (2014) are presented for comparison purposes which also demonstrate an equivalent bilinear trend. The initial linear phase represents the specimens in the un-cracked state which is controlled by the cementitious matrix properties. During this phase, the coupons were loaded until the tensile strength of the matrix mortar was reached and the first crack occurred. The specimens then experienced a loss of stiffness due to further crack formation and propagation which denotes the start of the second phase (line). With each new crack, the load is redistributed within the system. Micro-cracks result in low levels of load distribution. Macro-cracks release larger amounts of energy which is immediately transferred to the fabric bridging the cracks, and is then redistributed to the system. The large amount of energy released by macro-cracks can result in stress concentrations in other parts of the specimen, which in turn causes further macro-cracking, fabric-matrix debonding, and fiber slipping within the fabric bundles. The curve resumes linearity during the second stage as crack propagation

ceases. Crack widening initiates, and the resistance is provided primarily by the fabric-matrix bond and the friction between the internal fibers. As the load is increased, progressive fabric-matrix debonding, internal fiber slippage, and fiber breakage occur which results in specimen failure due to a loss in strength from slipping of the fabric within the matrix and/or interlaminar delamination.

For one ply specimens, Arboleda (2014) observed a typical failure mode to be slipping of the fabric within the matrix after multiple cracking. The crack patterns spanned the entire width of the specimen and propagated completely through the thickness along with fabric slippage (Figure 21a). The two ply specimens exhibited a failure mode consisting of interlaminar delamination and fabric-matrix slipping with a different damage progression mechanism (Figure 21b). Cracks initially spanned the entire width on each side of the specimen and attempted to propagate through the specimen thickness. Upon reaching the next fabric layer, the cracks changed direction and propagated along the fabric-matrix interface, parallel to the length of the specimen as interlaminar delamination occurs. As a result, the length over which the load is transferred is reduced and the cracks then shifted inward in the thickness direction and converge towards each other where fabric slippage occurs resulting in specimen failure. This phenomenon suggests that the load is transferred from the outer most layers towards the inner layers. The two ply specimens exhibited a failure more from fabric slippage than interlaminar delamination. Accordingly, there was a noticeable transition between the two versus three and four ply failure modes. Specimens with three and four plies exhibited a failure mode due to interlaminar delamination with minimal fabric slippage (Figure 21c/d). There were considerably less visible cracks in comparison to the behavior observed for the one, two and three ply tests. Initially the cracks

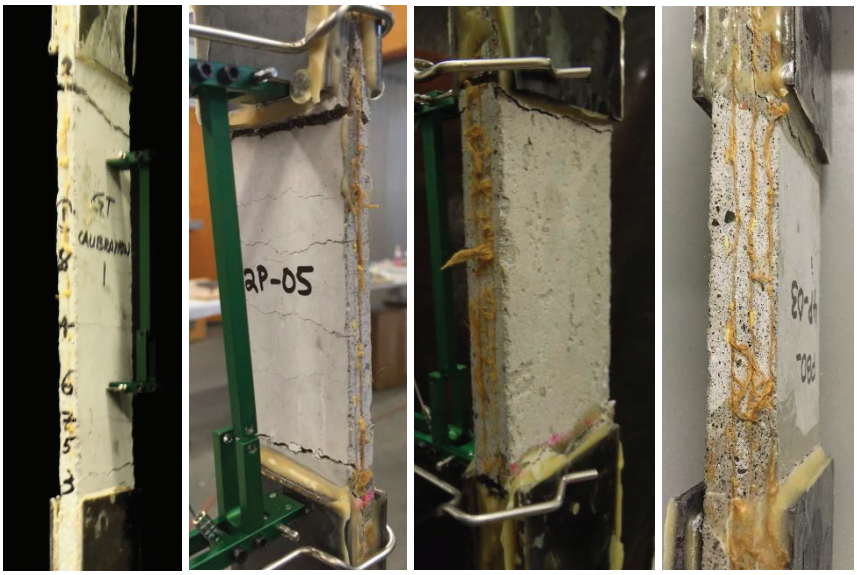

a) b) c) d)

**Figure 21 – Typical Failure Modes for a) One b) Two c) Three d) Four Ply Specimens**

formed on the outer surface of the specimen and propagated inward. Once the next fabric layer was reached, the cracks changed direction and propagated either along the fabric-matrix interface or in a diagonal direction along the thickness as progressive interlaminar delamination occurred within one or multiple layers. Crack propagation continued along this interface(s) until the effective bond length was reduced at which point failure occurred due to a sudden interlaminar delamination. The effective bond length is defined as the minimum bonded length required to sustain the maximum load in the system. These results indicate that an increase in fabric layers causes a shift in crack propagation as well as a shift in failure mode. One ply failure was defined by fabric-matrix slipping and three and four ply failure was caused by interlaminar delamination, while two plies exhibit a hybrid combination of both failure types. Figure 23 demonstrates the crack propagation modes based on number of fabric layers for the direct tension specimens.

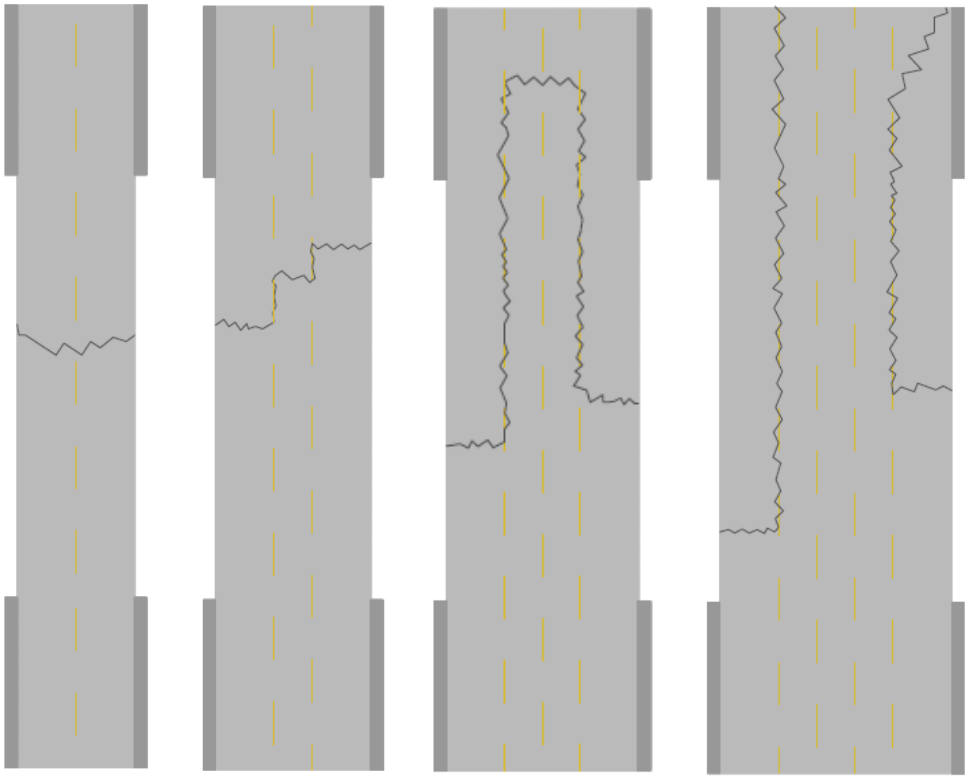

**a)** **b)** **c)** **d)**

**Figure 22 – Typical Crack Propagation Modes for a) One b) Two c) Three d) Four Ply Specimens**

The stress- strain curves for one, two, three, and four ply specimens are shown in Figure 23, Figure 24, Figure 25, and Figure 26, respectively. For each specimen, the stress-strain data was analyzed per AC434 Annex A.The un-cracked and crack modulus of elasticity ($E_f$*,$E_f$), ultimate tensile stress and strain ($f_{fu}$,$\varepsilon_{fu}$), and the transition point ($f_{ft}$,$\varepsilon_{ft}$) were determined. Table 2, Table 3, Table 4, and Table 5 contain the summarized tabulated values for each fabric ply and Appendix C presents the values determined for each specimen.

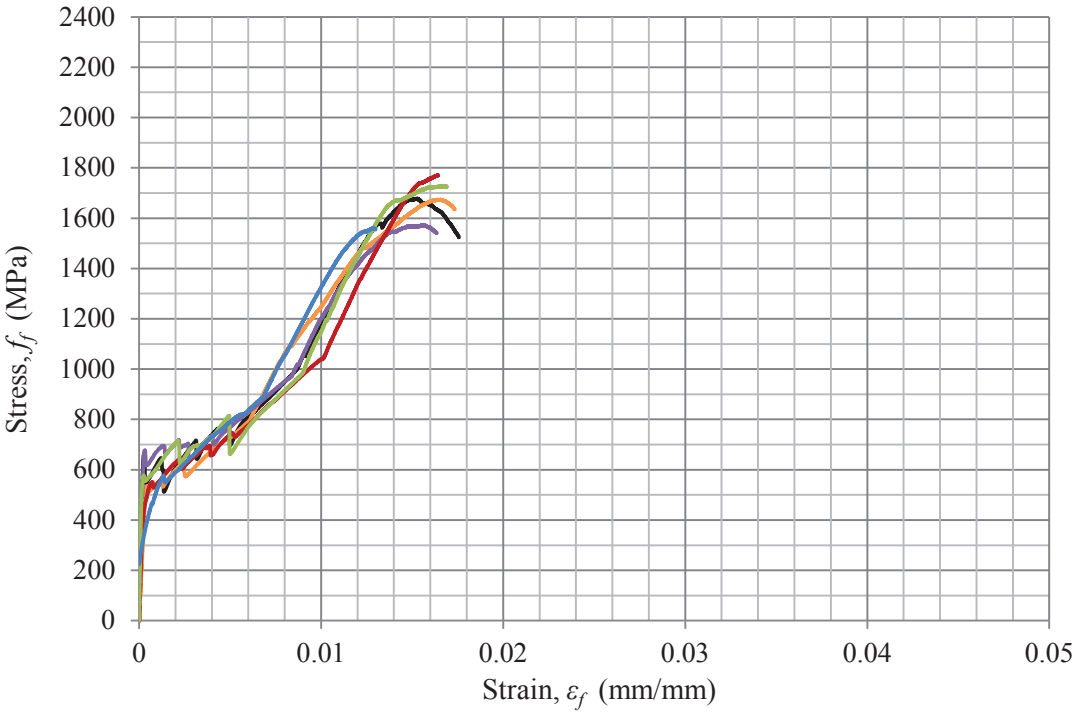


**Figure 23 – Stress vs. Strain Behavior for 1 Ply Direct Tension Tests (Arboleda 2014)**

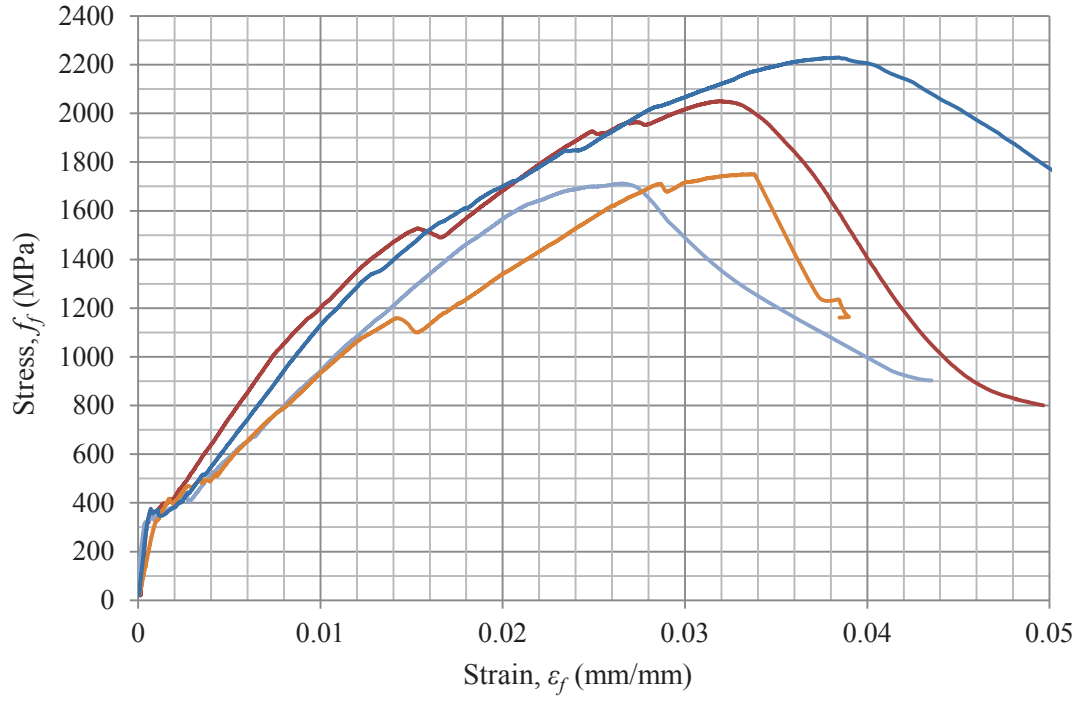


**Figure 24 – Stress vs. Strain Behavior for 2 Ply Direct Tension Tests**

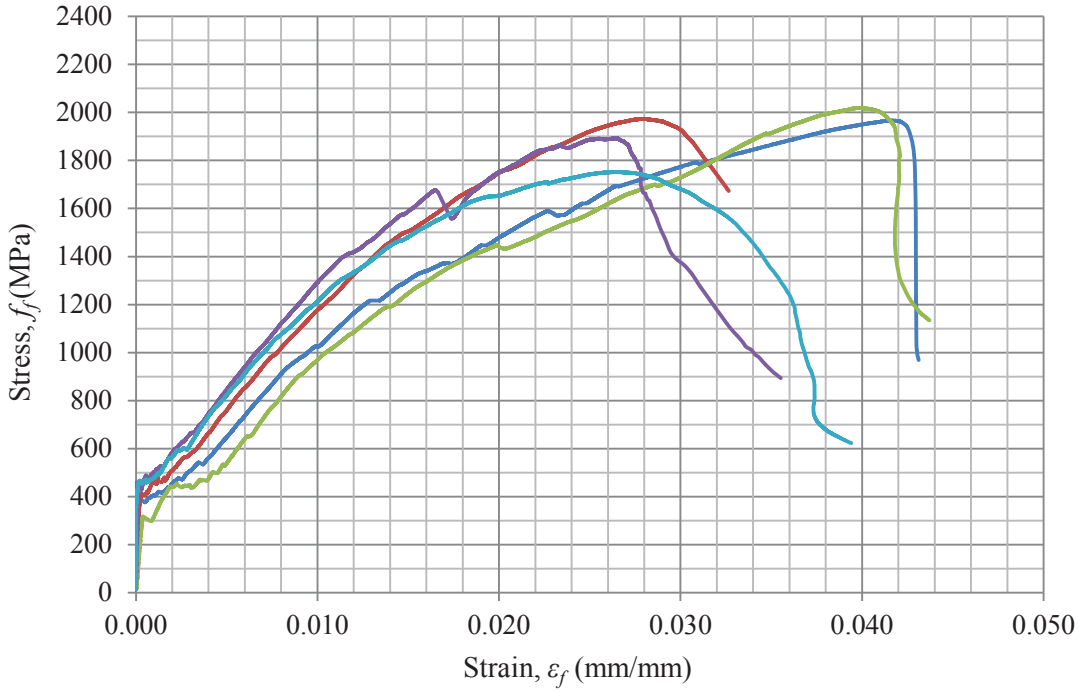


**Figure 25 – Stress vs. Strain Behavior for 3 Ply Direct Tension Tests**

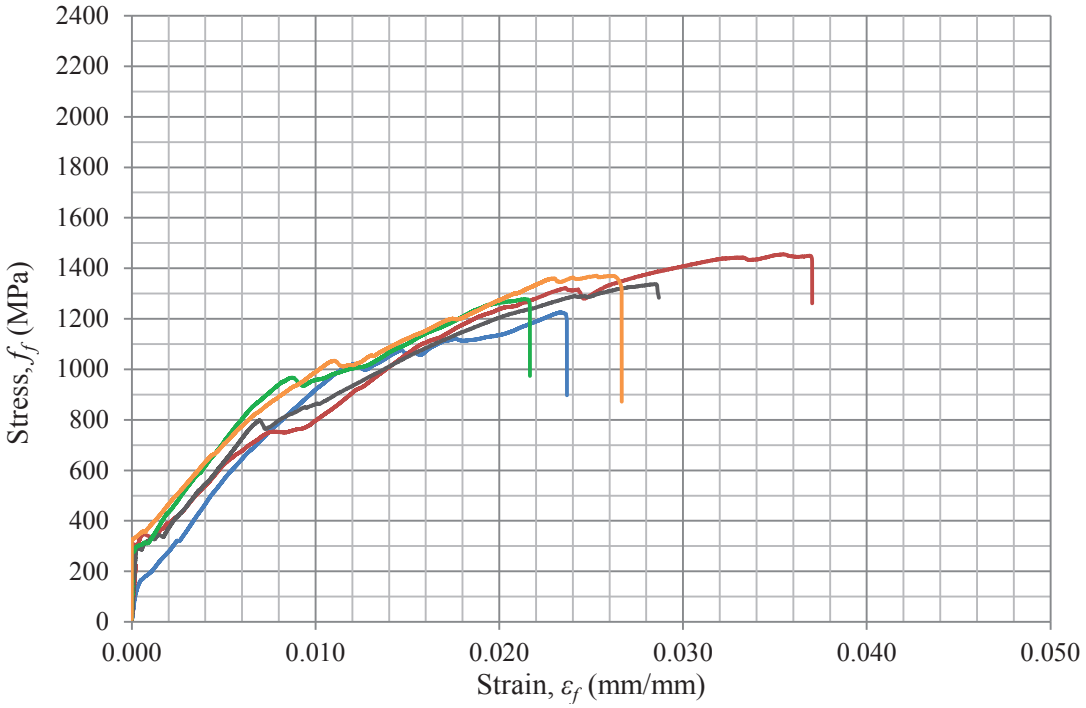


**Figure 26 – Stress vs. Strain Behavior for 4 Ply Direct Tension Tests**

**Table 2 – Summarized Tensile Strength Results for 1 Ply Coupons (Arboleda 2014)**

| Description | Symbol | Units | Mean | STD | COV |
|---|---|---|---|---|---|
| Modulus of elasticity of the uncracked specimen | $E_f$* | GPa | 1,806 | 452 | |
| Modulus of elasticity of the cracked specimen | $E_f$ | GPa | 128 | 15 | 12% |
| Tensile stress corresponding to the transition point | $f_{ft}$ | MPa | 375 | 82 | |
| Tensile strain corresponding to the transition point | $\varepsilon_{ft}$ | mm/mm | 0.00017 | 0.00004 | |
| Ultimate tensile strength | $f_{fu}$ | MPa | 1,664 | 77 | 5% |
| Ultimate tensile strain | $\varepsilon_{fu}$ | mm/mm | 0.0176 | 0.0013 | 8% |

**Table 3 – Summarized Tensile Strength Results for 2 Ply Coupons**

| Description | Symbol | Units | Mean | STD | COV |
|---|---|---|---|---|---|
| Modulus of elasticity of the uncracked specimen | $E_f$* | GPa | 621* | 208 | |
| Modulus of elasticity of the cracked specimen | $E_f$ | GPa | 49 | 8 | 16% |
| Tensile stress corresponding to the transition point | $f_{ft}$ | Mpa | 726 | 226 | |
| Tensile strain corresponding to the transition point | $\varepsilon_{ft}$ | mm/mm | 0.0027 | 0.00348 | |
| Ultimate tensile strength | $f_{fu}$ | Mpa | 1,933 | 215 | 11% |
| Ultimate tensile strain | $\varepsilon_{fu}$ | mm/mm | 0.0277 | 0.0039 | 14% |

*One specimen was omitted for the calculation of this value

**Table 4 – Summarized Tensile Strength Results for 3 Ply Coupons**

| Description | Symbol | Units | Mean | STD | COV |
|---|---|---|---|---|---|
| Modulus of elasticity of the uncracked specimen | $E_f$* | GPa | 1,613 | 770 | |
| Modulus of elasticity of the cracked specimen | $E_f$ | GPa | 46 | 11 | 5% |
| Tensile stress corresponding to the transition point | $f_{ft}$ | MPa | 717 | 52 | |
| Tensile strain corresponding to the transition point | $\varepsilon_{ft}$ | % | 0.0005 | 0.00022 | |
| Ultimate tensile strength | $f_{fu}$ | MPa | 1,921 | 105 | 5% |
| Ultimate tensile strain | $\varepsilon_{fu}$ | % | 0.0283 | 0.008 | 28% |

**Table 5 – Summarized Tensile Strength Results for 4 Ply Coupons**

| Description | Symbol | Units | Mean | STD | COV |
|---|---|---|---|---|---|
| Modulus of elasticity of the uncracked specimen | $E_f$* | GPa | 1,282 | 1,660 | |
| Modulus of elasticity of the cracked specimen | $E_f$ | GPa | 36 | 4 | 11% |
| Tensile stress corresponding to the transition point | $f_{ft}$ | MPa | 568 | 149 | |
| Tensile strain corresponding to the transition point | $\varepsilon_{ft}$ | mm/mm | 0.0018 | 0.0029 | |
| Ultimate tensile strength | $f_{fu}$ | MPa | 1,315 | 91 | 7% |
| Ultimate tensile strain | $\varepsilon_{fu}$ | mm/mm | 0.0228 | 0.0039 | 17% |

The uncracked modulus of elasticity is an important value that reinforces the initial phase of the bilinear stress-strain behavior. This value is significantly affected by coupon geometry, small load eccentricities, and initial imperfections such as micro-cracking during specimen preparation. The point at which the first crack occurs denotes the end of the initial

phase and also indicates that the specimen is fully engaged. Typically, FRCM systems are designed to resist stress and strain values corresponding to the second phase in the cracked state. Therefore, the properties associated with the cracked and ultimate states are be discussed in detail. Figure 27 contains a typical stress vs. strain curve for each fabric ply where the differences in deformation behavior can be observed. The cracked modulus, ultimate stress, and ultimate strain characteristics were compared. The cracked modulus exhibits a decreasing trend with increasing number of plies (Figure 28). In addition, the transition of failure mode can also be observed in the tail end of each curve. After reach a maximum stress, the one and two plies show a gradual decrease in stress (fabric slipping) while the three and four plies demonstrate a sudden decrease in stress (interlaminar delamination). One ply specimens show the largest $E_f$ followed by decreasing values in the two, three and four plies. Two and three plies exhibited similar as well as the largest values of ultimate stress followed by one and four plies (Figure 29).

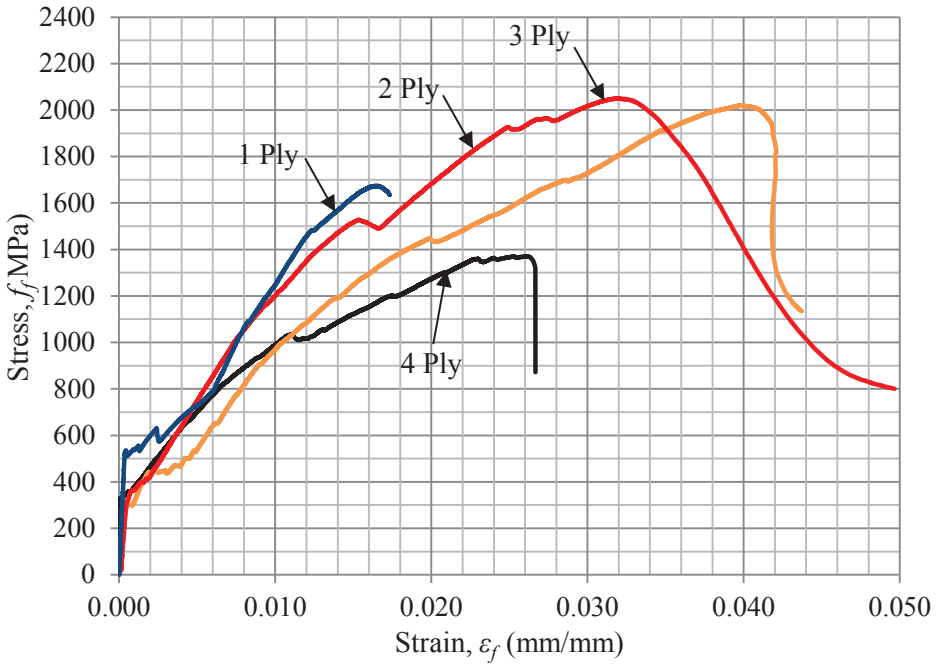


**Figure 27 – Typical Stress vs. Strain Curves for each Fabric Ply**

Similarly, two and three plies showed close values as well as the largest values of ultimate strain followed by four and one layer(s) (Figure 29). Material properties indicate that for FRCM optimal performance, a two or three layer strengthening configuration should be used.

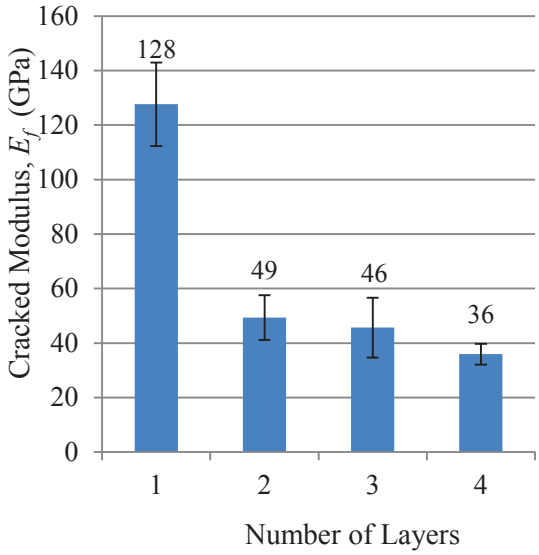


**Figure 28 – Cracked Modulus of Elasticity Based on Fabric Ply**

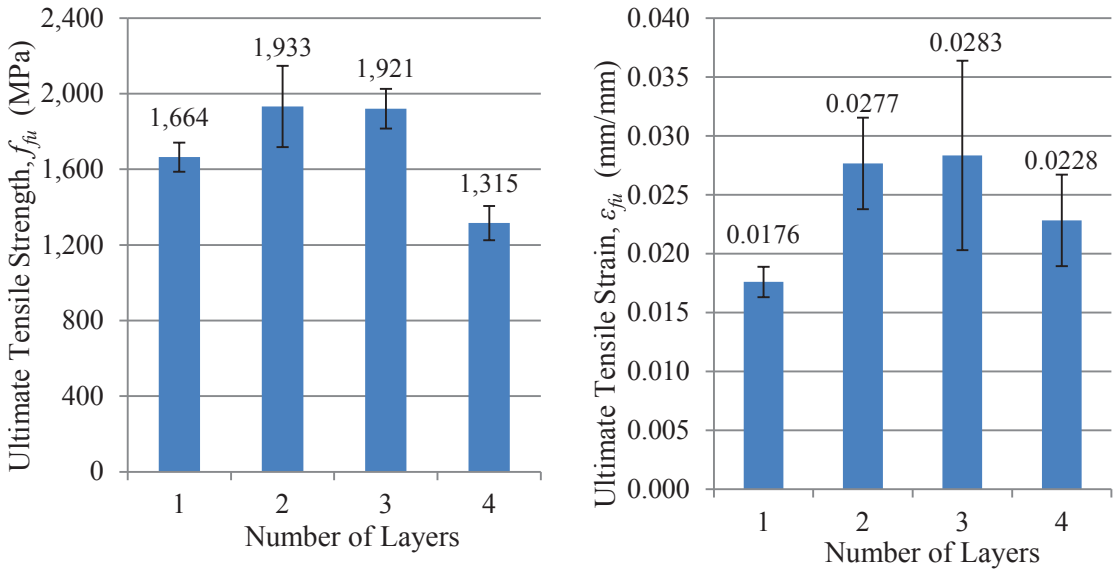


**Figure 29 – Ultimate Stress and Strain Based on Fabric Ply**

**Implications for Design**

Results from the direct tension tests are used to determine theoretical ultimate behavior for RC beams strengthened with the PBO-FRCM system. The RC beam design, material properties, and theoretical and design analysis are discussed in detail in Study 3 of this document. The theoretical and design capacities ($P_{u,\,Th}$, $\phi P_n$) were determined for RC beams strengthened with one and three plies of FRCM where theoretical values are determined using FRCM direct tension properties without any strain limitation. Results from the one ply direct tension tests given in Table 9 were used to determine $P_{u,\,Th}$ and $\phi P_n$ for the one ply strengthened RC beam. But when multiple FRCM layers are used for strengthening, many will argue as to which material properties should be used to accurately reflect the experimental behavior. Results from the direct tension tests demonstrate how the FRCM system behaves independently. The one ply specimens exhibited a larger cracked modulus, and lower ultimate stress and strain values compared to the three ply specimens, which exhibited a lower cracked modulus, but higher ultimate stress and strain. Thus in an attempt to determine which properties should be used, two different values of theoretical and design capacities were computed using the one ply and three ply direct tension results given in Table 2 and Table 4, respectively, for the RC beam strengthened with 3 layers. All theoretical values were compared to the experimental test results from static tests performed on RC beams strengthened with one and three FRCM layers. A detailed discussion of the static test procedure and experimental results is presented in Study 3.

Table 6 contains a summary of all theoretical, experimental, design, and enhancement values. The enhancement ratios are defined as the ratio of the strengthened RC element to

the control RC member. The theoretical and design capacities for the RC beam with 3 FRCM layers indicates a larger strength enhancement when using the one ply direct tension properties than when using the three ply properties. Similarly, when compared to the

**Table 6 – Summary of Theoretical and Experimental Ultimate Load Values**

| External Reinf. | FRCM Material Properties | Theoretical (no ε limit) | | Experimental | | Design | | Experim./ Theoretical |
|---|---|---|---|---|---|---|---|---|
| | | Load $P_{u,\,Th}$ (kN) | Enhancement $P_{u,Th,strength}/P_{u,Th,control}$ | Load $P_{u,\,avg}$ (kN) | Enhancement $P_{u,strength}/P_{u,control}$ | Load $\phi P_n$ (kN) | Enhancement $\phi P_{n,strengthened}/\phi P_{n,control}$ | $P_{u,avg}/P_{u,Th}$ |
| None | - | 89.5 | 1 | 97.1 | 1 | 54.7 | 1 | 1.08 |
| 1 Layer | 1 Ply (Table 1) | 90 | 1.01 | 107 | 1.1 | 59 | 1.08 | 1.19 |
| 3 Layers | 1 Ply (Table 1) | 112 | 1.25 | 125.7 | 1.29 | 72.8 | 1.33 | 1.12 |
| 3 Layers | 3 Ply (Table 3) | 104 | 1.16 | | | 59.8 | 1.09 | 1.21 |

experimental values, the one ply direct tension properties result in a theoretical load that is much closer to the experimental than the value computed with three ply direct tension results. Therefore, if the analysis is performed based on the direct tension results for multiple plies, the outcome is lower than if one ply material properties are used. However, the capacities determined from the one ply properties (Table 2) represent a more realistic prediction of beam behavior while maintaining a safe design, and thus will be used for theoretical and design analysis in the subsequent studies.

**FRCM Bond**

A critical parameter in the success of an externally bonded composite lies in the system's bond performance. For FRCM, the load is transferred from the substrate to the composite through the concrete-matrix bond interface and is then distributed within the composite through the fabric-matrix interfaces. Several bond tests were conducted to investigate FRCM bond behavior per AC434 Section 4.8 for one, two and four ply

specimens. Specimens were prepared by applying FRCM to a RC concrete slab as previously shown in Figure 16 and were left to cure for a 28-day period. Bond tests were performed following ASTM C1583/C1583M 13. A 51-mm diameter circular cut was made on the cured FRCM system using a core drill, to a depth of 12.7 mm into the substrate (Figure 30a/b). A steel disk was attached with the epoxy to the FRCM surface as a means to pull off the circular area (Figure 30c). The adhesive was left to cure for 24 hours before performing the pull off test.

(a) (b) (c)

**Figure 30 – Bond Test a) Drilling Instrument b) Circular Cut c) Bonded Steel Disk**

Uniaxial tensile load was applied perpendicular to the test surface using a pull-off test machine known as a James Bond Tester (NDT James Instruments, Inc., 2016). The load was applied manually using the screw system of the test machine connected to a hydraulic piston. Figure 31 shows the test set up. The test was performed under load control at a

(a) (b)

**Figure 31 – Pull off Test Instrumentation a) James Bond Test b) Test Configuration**

constant rate so that the tensile stress increased at a rate of 35 ± 15 kPa/s, and the ultimate load was recorded using an integrated dial gauge in the test machine. The different types of failure modes given in ASTM C1583 include: failure in the substrate, failure at the concrete-FRCM interface, failure within the FRCM, or adhesive failure in the epoxy used to attach the steel disk. An illustration of each mode is shown in Figure 32. The ultimate bond strength was calculated based on the type of failure, following the guidelines provided by AC434 by dividing the recorded tensile load at failure by the net area (failure type A or B) or the matrix area (type C failure). The net area is defined as total area under the disk

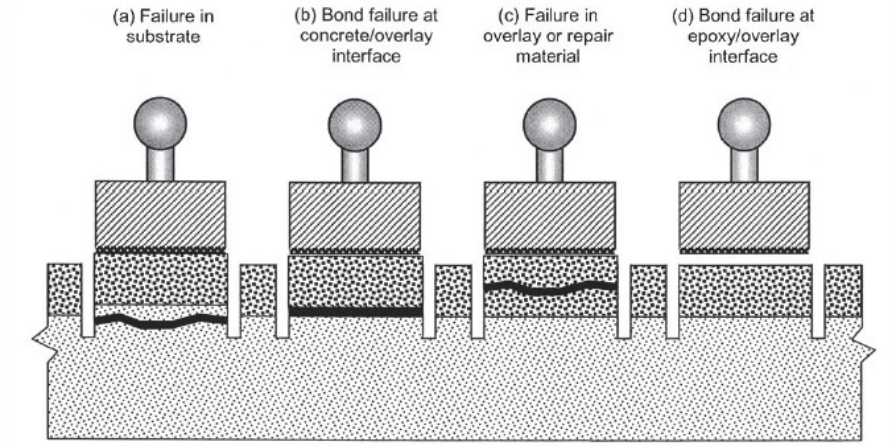


**Figure 32 – Bond Test Failure Mode Types (ASTM C1583)**

minus the area covered by the fabric. Five replicates of one, two and four ply specimens (15 total) were tested. The average bond strengths and respective failure modes are given in Table 7. All specimens exhibited a type C failure mode where failure occurred at the

**Table 7 – Summarized Bond Strength Tests**

| Number of Layers | Ultimate Stress (MPa) | C.O.V. (%) | Failure Mode |
|---|---|---|---|
| 1 | 3.89 | 15 | C |
| 2 | 1.78 | 29 | C |
| 4 | 1.39 | 38 | C |

fabric-matrix interface as shown in Figure 33. The area used to determine ultimate stress values was taken as 707 $mm^2$ which describes the net matrix area. Failure typically occurred within the first fabric layer and propagated away from the substrate further into the other FRCM layers. Each test specimen contained a layer of mortar completely attached

**Figure 33 – Type "C" Failure Modes for 2 Plies (Left) and 4 Plies (Right)**

to the concrete substrate. For a failure occurring at the fabric- matrix interface, AC434 Section 4.8.2 states the minimum bond strength shall be at least 2.76 MPa. One ply specimens satisfy this criteria, while the two and four ply results did not meet the expected threshold. This suggests that additional bond tests should be performed using different types of FRCM systems with multiple fabric layers in order to re-evaluate the fittingness of AC434's threshold.

Results indicate that the fabric-matrix bond is weaker than the concrete-matrix bond. This type of failure was predicted due to the fact that the matrix does not completely impregnate the fabric fibers thus acting as a bond breaker. Accordingly, the bond strengths exhibit a decreasing trend with an increasing number of layers (Figure 34) due to the reduction of net area caused by each additional layer. Contrary to the direct tension test results, an increase in fabric plies does not necessarily guarantee an increase in bond strength. Accordingly, the ambient (no durability exposure) strength of FRCM applied to RC can best be described as a combination of tensile (direct tension) and bond strength.

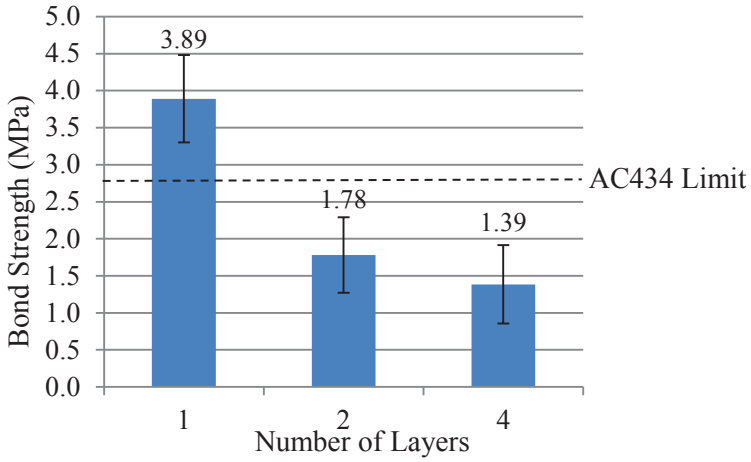


**Figure 34 – Bond Strength Based on Fabric Plies**

Increasing the number of layers enhances tensile performance (up to 3 plies) but diminishes bond strength. As a result, it is crucial to select a fabric ply configuration that yields an optimum balance between tensile and bond performance.

**FRCM Early Age Bond Development**

When concrete is cast, the most crucial period is the time immediately following placement, which is when significant material strength is developed. This time is defined as the curing period. Similarly for FRCM, the cementitious mortar requires a curing period where it undergoes hydration and develops strength. In the previous tests, all FRCM specimens were given a minimum curing period of 28 days which is a standard value used for concrete. While 28 days is a conservative time period, it may be considered overly conservative for RC structures such as bridges and parking garages in need of FRCM repair which remain closed during installation and curing times. In an attempt to ensure minimal closure times while ensuring adequate FRCM strength and to determine a practical curing period for the PBO-FRCM system, the early age performance was investigated. The compressive strength of the matrix mortar and the bond strength were measured within the

early hours following FRCM installation throughout a 28-day time period. The matrix mortar compressive strength was determined by preparing and testing cube specimens per ASTM C109/C109M13. The FRCM system was applied to small concrete beams with dimensions of 10 cm x 10 cm x 35 cm in a similar manner to the previous sub-chapter. The concrete beams used for bond tests performed within 24 hours of application were pre-drilled prior to FRCM application because previous attempts to drill holes in the FRCM system during this time period resulted in damaged inflicted to the composite system. Inflicted damaged was caused by the wet cementitious mortar that was unable to hold the fabric in lace during drilling. In addition, due to the state of the cementitious mortar, the compressive tests of the mortar cubes were not performed within 24 hours of specimen preparation. FRCM installation for the pre-drilled beams consisted of pre-cutting 51-mm diameter circular shaped pieces of fabric and applying them individually to the pre-drilled holes. All stages prior to and during application can be seen in Figure 35 for one FRCM

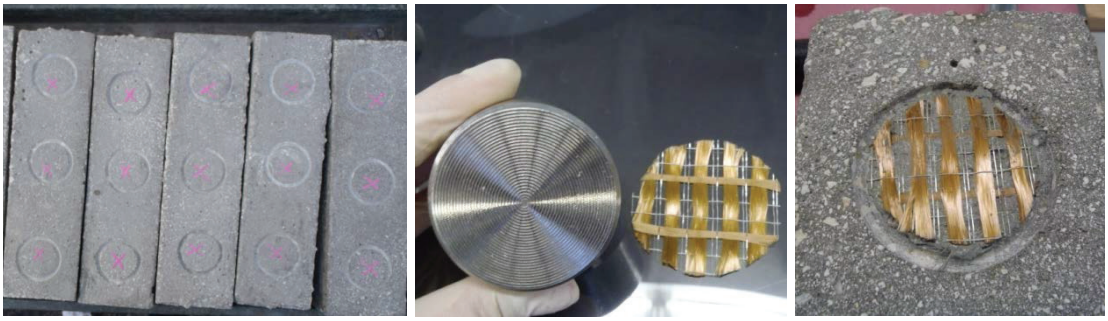

**a)** **b)** **c)**

**Figure 35 – FRCM Application a) Pre-Drilled Beams b) Pre-Cut Fabric c) FRCM Application**

layer. The remaining concrete beams were also strengthened with one continuous layer of FRCM. The final installation for both application types is shown in Figure 36. Bond tests were conducted after each respective time increment per ASTM C1583/C1583M 13

following the same test preparation, instrumentation and procedure presented in the previous subchapter.

a) b)

**Figure 36 – FRCM Application to a) Regular Beams b) Pre-Drilled Beams**

All matrix mortar cubes were prepared and tested per ASTM C109/C109M13. Uniaxial compression load was applied to the cube specimens using a screw type universal test frame. The test was performed under displacement control at a rate 0.635 mm/min. Table 8 summarizes the time increments, number of replicates, and results for the average bond and compressive strengths. For the bond tests, the primary failure mode occurred within

**Table 8 – Early Age Test Matrix and Summary of Results for One Ply**

| Time | Number of Replicates | | Average Stress | |
|---|---|---|---|---|
| | Bond Test | Compression of Mortar Cubes | Bond Strength (MPa) | Mortar Compressive Stress (Ma) |
| 3 hours | 5 | - | 0.05 | - |
| 7 hours | 5 | - | 0.08 | - |
| 10 hours | 5 | - | 0.14 | - |
| 1 day | 5 | 5 | 0.74 | 10.8 |
| 2 days | 5 | 5 | 0.75 | 15.3 |
| 3 days | 5 | 5 | 2.59 | 15.7 |
| 7 days | 5 | 5 | 2.97 | 21.7 |
| 14 days | 5 | 5 | 2.59 | 20.8 |
| 21 days | 5 | 5 | 3.19 | 19.5 |
| 28 days | 5 | 5 | 3.18 | 24.1 |

the FRCM composite system, at the interface between the FRCM mortar and fabric, herein referred to as failure type “C” (Figure 37). For the compression of matrix mortar, a typical test specimen and failure mode is shown in Figure 38.

**Figure 37 – Bond Strength Typical Failure Mode**

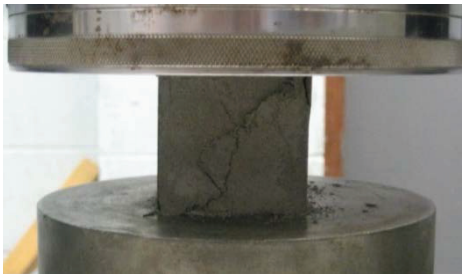

**Figure 38 – Typical Failure Mode for Compression of Matrix Mortar**

The early age strength development curves for both bond strength and mortar compressive strength are shown in Figure 39. Based on these results, a significant amount of strength develops after 3 days and almost full strength was developed after 7 days. The bond tests exceed the AC343 threshold of 2.76 MPa after a 7-day curing period. And in addition, the mortar compressive strengths exceed AC434 requirements of having strengths greater than 17 MPa and 24 MPa at 7 days and 28 days, respectively.

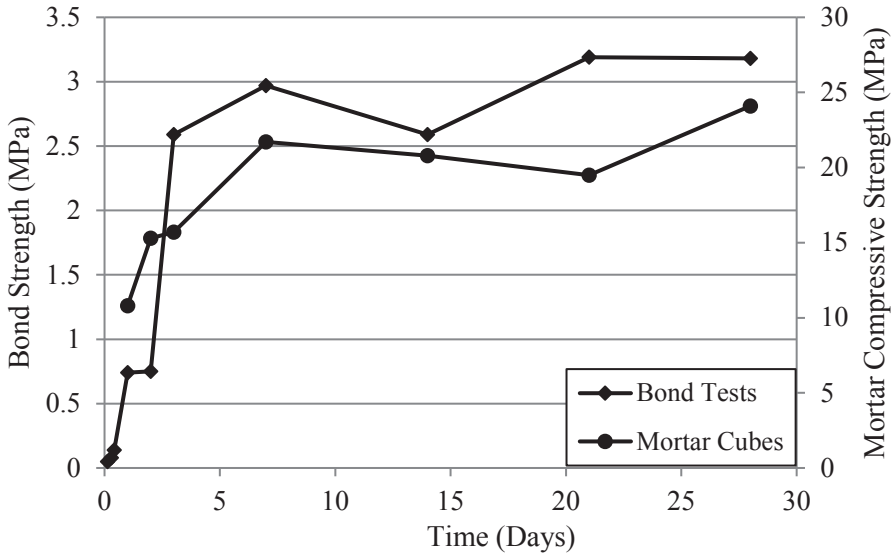


**Figure 39 – Early Age Bond and Compressive Strength Development Curves for One Ply**

## Concluding Remarks

The objective of this study was to investigate the effect of FRCM multiple fabric layers on the direct tension and bond strength behavior. The material system consisted of a PBO fabric mesh and Portland cement based mortar matrix that is typically used for the shear and flexural strengthening of RC. In addition, the early age bond development for the same system was investigated within the early hours of FRCM application throughout a 28-day time period. The experimental findings are summarized as follows:

- Increasing fabric plies results in a decreased crack modulus of elasticity, $E_{f.}$ and a decreased bond strength.
- Two and three ply direct tension specimens exhibited the largest values of ultimate stress and ultimate strain followed by one and four plies.
- Increase in fabric plies causes a shift in crack path as well as a change in failure mode where one ply failure is defined by fabric-matrix slipping (Arboleda 2014)

and four ply failure is caused by interlaminar delamination, while two and three plies exhibit a hybrid combination of both failure types.

- FRCM behavior when applied to RC is influenced by both the tensile and bond characteristics for a specific fabric ply. For this PBO-FRCM system, a two or three layer configuration is considered ideal to ensure optimum FRCM performance when applied to RC.
- Significant early age bond and matrix compressive strength development occurs within 3 days and full strength is nearly developed after 7 days of FRCM installation.

Results from direct tension tests were used to determine theoretical ultimate capacities of RC beams strengthened with one and three FRCM layers. Suitably, the material properties determined from the one ply direct tension tests were used to design the RC beam strengthened with one FRCM layer. The theoretical capacity for the RC beam strengthened with three FRCM layers was computed twice using material properties from the one and three ply direct tension tests. Results indicate that the one ply direct tension properties result in a larger theoretical load that is closest in value to the experimental result, thus yielding a more realistic prediction of ultimate behavior. Therefore, the one ply material properties given in Table 9 are used for all theoretical and design calculations in the subsequent studies.

# CHAPTER 3

## Study 2 – REPAIR OF DAMAGED PRESTRESSED CONCRETE GIRDERS WITH FRCM AND FRP COMPOSITES

Traditional methods used to repair prestressed concrete (PC) girders subjected to impact damage due to over-height vehicles include strand splicing and external post tensioning. These methods have proven to be partially satisfactory in restoring the damaged girder's ultimate strength. The use of composite materials in the strengthening, rehabilitation, and repair industry has been gaining popularity due to their excellent material behavior and ease of application. Composites such as fiber reinforced polymer (FRP) and fabric reinforced cementitious matrix (FRCM) systems are presently available alternatives for restoring the integrity of a damaged girder short of replacing it. Many studies and field applications have been conducted using externally bonded FRP systems but there is currently very limited research on damage assessment and repair of full-scale PC bridge girders specifically subject to vehicular impact (Di Ludovico 2005, Nanni 1997). Di Ludovico et al. 2005 conducted an experimental investigation of full-scale damaged PC girders with externally bonded CFRP laminates. One benchmark girder and two intentionally damaged girders, cutting two and four strands respectively, were strengthened with CFRP laminates and subjected to flexural tests. All strands were damaged on one side of the girder to simulate a vehicular impact. The repaired girders exhibited a loss of ductility, partly due to the primary failure mode which consisted of a sudden CRFP delamination. In addition, all experimental ultimate moment capacities were greater than or within 0.5% of the theoretical experimental values.

FRCM composites represent an alternative material to FRP for structural retrofit/rehabilitation. Currently, no studies or field applications have been conducted using externally bonded FRCM systems applied to damaged PC girders but based on previous research, there are very clear indications that prove FRCM to be an excellent alternative. The objective of this study is to evaluate both experimentally and numerically the effectiveness of FRCM and FRP as repair systems to impact-damaged precast, PC girders. This study was conducted as a joint partnership with Virginia Tech and the Virginia Department of Transportation (VDOT). The material characterization of FRP and FRCM systems and the girder strengthening design using both composite systems was performed by University of Miami students and faculty, while the material testing of the girder properties and the experimental investigation was performed by Virginia Tech students and faculty. The FRP and FRCM installation and application to the PC girders was performed by a licensed contractor that specializes in structural repair using composite materials.

The girder specimens consisted of three AASHTO Type III PC bridge girders retrieved from a bridge after 55 years of service. One specimen was load tested undamaged and used as a benchmark. The other two were damaged (four cut strands) and repaired with FRP and FRCM prior to being load tested. Numerical analysis was performed to theoretically predict strength and behavior of all specimens using AASHTO LRFD Bridge Design Specifications, ACI 440.2R, FRPS-1, and ACI 549.4R. Theoretical values were compared to experimental values and the effectiveness of the strengthening methods and respective design approaches were evaluated.

**ASHTO Type III Girders**

A bridge spanning over Interstate 81 near Arcadia, VA was comprised of AASHTO Type III girders spaced at 2.2 m on center. The bridge was built between 1957-1960 and was recently demolished, where three girders were extracted. A typical girder has a span of 18.3 meters, with an overall height of 1.14 m and is reinforced with 50 - 9.53-mm diameter seven-wire stress-relieved strands. During demolition, one girder was broken into two pieces and the overall remaining length of the girder was about 13.4 m. Excessive spalling occurred at the bottom flange of this girder, leaving only about 10.9 m of undamaged girder. Upon extracting the girders, another separate girder contained residual saw cuts in the top deck from demolition. These saw cuts spanned the entire width of the deck and were located along the length of the girder (Figure 40). The geometry and


**Figure 40 – Saw Cut Gaps in Concrete Deck of Girder D**

prestressing strand orientation is shown in Figure 41. Prestressing steel consists of two straight strands in the top flange, 40 straight strands in the bottom flange, and eight harped strands where harping points are located at 7.3 m from each end (Jones et al. 2015). Shear reinforcement consists of two No. 5 single leg stirrups with variable spacing from 229 mm

near the ends to 533 mm near midspan. Prior to demolition, the girders were individually removed by saw cutting the top deck on each side of the girder flange. This resulted in a narrow section of deck that remained attached to the top of the girders and did not

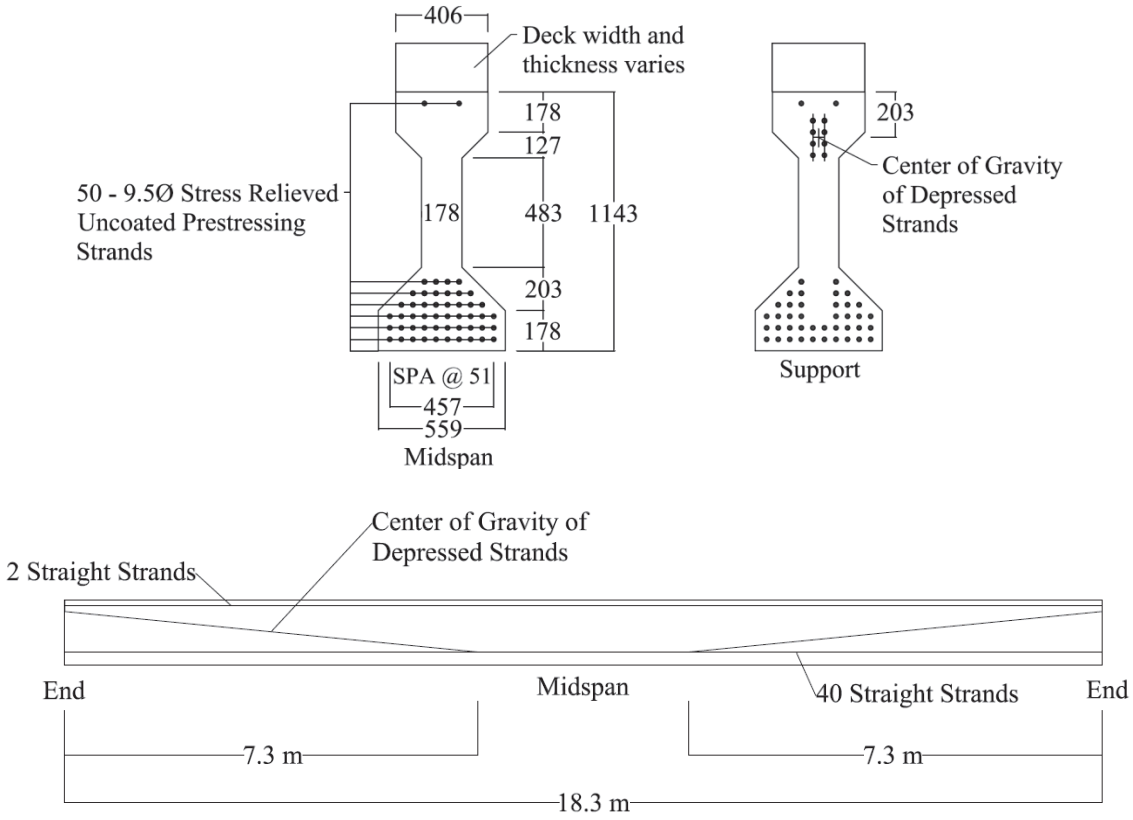


**Figure 41 – AASHTO Type III Girder Dimensions and Prestressing Details (dimensions in mm)**

accurately represent the larger deck width that would be seen in the field. Saw cutting of the deck resulted in slightly different deck widths for each girder (Figure 42). The nominal material properties for the concrete slab, PC girder, and prestressing steel given in the construction documents are shown in Table 9.

Three PC girders were extracted and consist of one control girder (Girder A) that was chosen to be the shorter girder broken during demolition, one FRP strengthened girder (Girder C) and one FRCM strengthened girder (Girder D) that was chosen to be the girder

with several saw cuts in the top deck. In an attempt to avoid confusion and maintain consistent cross-referencing with Jones et al. (2015) and Pino et al. (2015), the same girder nomenclature given in the aforementioned documents is used herein. Results from the testing of Girder B (Jones et al. 2015) strengthened with a separate repair method is not included in this study.

Due to the limited number of girders, it was decided to damage, repair, and test girder C and girder D at two locations in order to maximize the amount of experimental results. For girder C, one damaged location was repaired with FRP and the other location was repaired using strand splicing (Jones et al. 2015). Girder D was repaired with FRCM at one damaged area while the other repair consisted of combined strand splicing and FRCM (Jones et al. 2015). Figure 42 shows the girder type and repair method used for each damaged location.

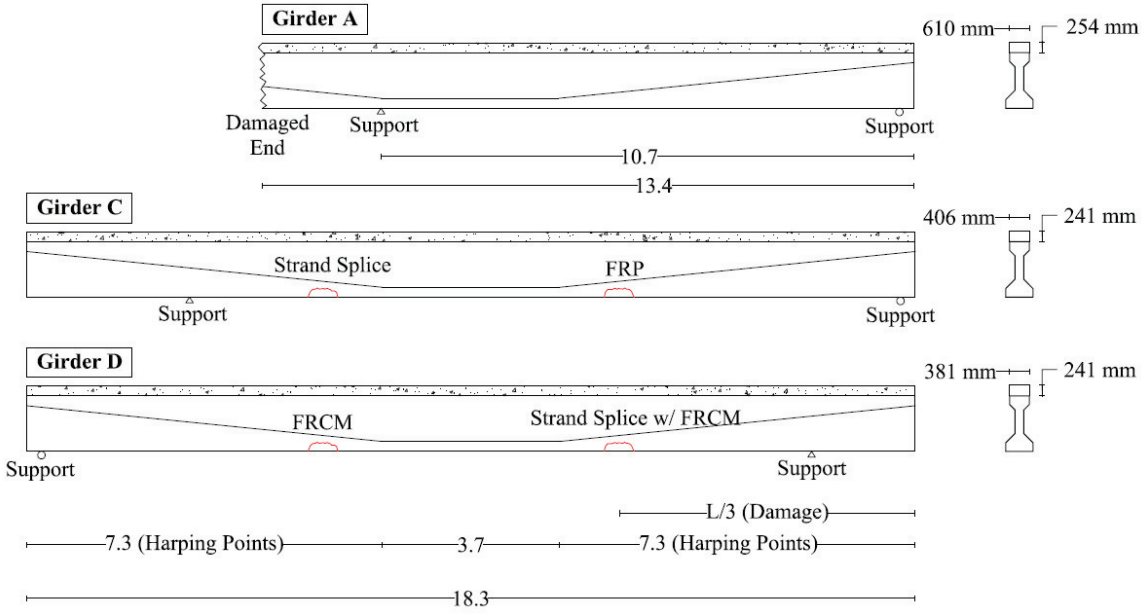


**Figure 42 – AASHTO Type III Girder Dimensions and Prestressing Details (dimensions in m)**

**PC Girder and Deck Material Properties**

The nominal material properties specified in the original construction documents are given in Table 9. Similarly, the prediction of experimental values can best be determined using accurate material properties. Concrete samples were taken from the deck and girder

**Table 9 – Girder Nominal Properties (From Construction Documents)**

| Property | Symbol | Value |
|---|---|---|
| *Slab* | | |
| Compressive Stress | $f'_c$ | 27.6 MPa |
| *Girder* | | |
| Compressive Stress | $f'_c$ | 34.5 MPa |
| *Prestressing Steel* | | |
| Ultimate Stress | $f_{pu}$ | 1.72 GPa |
| Yield Stress | $f_{py}$ | 1.42 GPa |
| Modulus of Elasticity | $E_s$ | 186.16 GPa |
| Initial Prestressing | $P_i$ | 62.28 kN |

and prestressing strands samples were extracted. Cylindrical concrete samples were attained using a concrete core drill, from an unused section of a girder. Two samples from the deck and two samples from the girder were tested for compressive strength (Table 10). The average compressive strength of the girder and deck are close to the design compressive strength values of 34.5 and 27.6 MPa, respectively. Two prestressing strand samples were extracted from the same unused section and tested in tension. The bridge construction documents required the steel to have a minimum ultimate tensile strength of

**Table 10 – Concrete Web and Deck Samples Test Results**

| Specimen | Diameter (mm) | Failure Load (kN) | Compressive Strength (MPa) |
|---|---|---|---|
| Web #1 | 69.9 | 173 | 45.3 |
| Web #2 | 69.9 | 178 | 46.4 |
| Average | | 175.7 | 45.9 |
| Deck #1 | 69.9 | 156 | 40.6 |
| Deck #2 | 69.9 | 162 | 42.4 |
| Average | | 159 | 41.5 |

1.72 GPa and a minimum yield strength of 1.42 GPa. Experimental results exceed the design requirements with an average 1.81 GPa ultimate strength and 1.48 GPa yield strength (Table 11). Tests were also performed to determine the effective prestress force

**Table 11 – Prestressing Strand Samples Tests Results**

| Strand # | Load (kN) | Area ($in^2$) | Yield (GPa) | Average Yield (Gpa) | Strength (GPa) | Average Strength (Gpa) |
|---|---|---|---|---|---|---|
| 1 | 91.2 | 51.6 | 1.50 | 1.48 | 1.77 | 1.81 |
| 2 | 95.2 | 51.6 | 1.45 | | 1.84 | |

by severing six strands with an electric grinder. An extensometer was used to measure the change in length of the strand when cut. The average effective prestress force was determined to be 910 MPa (50.3% of ultimate from Table 11).

**FRP and FRCM Materials**

The FRP system consisted of two types: C200H and C400H. Each contain high strength unidirectional carbon fiber sheets with a minimum nominal fiber density of 600 and 1350 $gm^2$, respectively (Figure 43). The matrix consists of a two parts epoxy. A complete material characterization is reported in Pino et al. (2015) following the test criteria specified by AC125 (ICC-ES 2014) which is the established acceptance criteria for

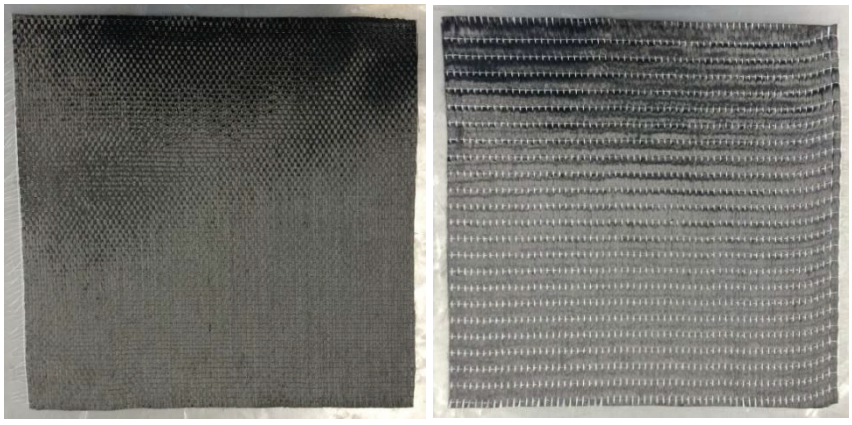

**Figure 43 – FRP Material Systems C200H (Left) and C400H (Right)**

externally bonded FRP systems. Results indicate that both systems exhibit excellent mechanical and durability performance exceeding AC125 requirements. It is shown that direct tension tests best represent the composite's stress-strain behavior when subjected to tensile forces. One-layer and two-layer specimens were prepared and tested according to ASTM D3039/D3039M where load was applied in displacement control. The extension (elongation) of the specimen was measured using a 50-mm gauge length extensometer, placed at mid-length of the coupon specimen (Figure 44). The mode of failure was by fiber rupture and the behavior was linear until failure as shown in Figure 44 compared to the bi-linear behavior seen in FRCM coupons. Table 12 contains direct tension test results

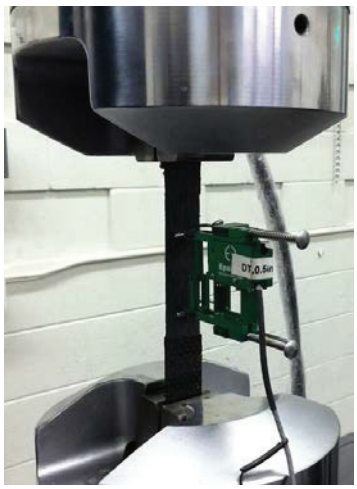

**Figure 44 – FRP Tensile Test Setup**

**Table 12 – Material Properties of FRP C200H and C400H Direct Tension Tests**

| Description | Symbol | Units | C200H 1 Ply | C200H 2 Ply | C400H 1 Ply | C400H 2 Ply |
|---|---|---|---|---|---|---|
| Ultimate Strength | $\overline{f_{fu}}$ | GPa | 1,328 | 1,347 | 1,294 | 935 |
| Ultimate Stength St. Dev | $\sigma_{f_{fu}}$ | GPa | 79.6 | 31.5 | 45.5 | 24.5 |
| Modulus of Elasticity | $\overline{E_f}$ | GPa | 75.7 | 95.67 | 76.11 | 83.53 |
| Ultimate Strain | $\overline{\varepsilon_{fu}}$ | mm/mm | 0.0175 | 0.0141 | 0.017 | 0.0112 |
| Ultimate Strain St. Dev | $\sigma_{\varepsilon_{fu}}$ | mm/mm | 0.0004 | 0.0011 | 0.0007 | 0.0001 |

including ultimate strength and strain, respective coefficient of variation, and modulus of elasticity for each CFRP laminate according to the respective number of plies. The C200H one-and two-ply coupons have an average ultimate stress of 1,328 MPa and 1,347 MPa, respectively. The C400H one-and two-ply coupons had an average ultimate stress of 1,294 MPa and 935 MPa, respectively.

**FRCM Materials**

The FRCM system consists of a PBO fabric with an unbalanced network that is identical to the system evaluated in Study 1 of this dissertation. A detailed description of the geometry, test methods performed, and material properties can be found in Chapter 2. The material properties specifically used for this study are the 1 ply specimens given in Chapter 2, Table 2.

**Simulated Impact Damage**

Four prestressing strands were cut at 1/3 points from the girder ends (Figure 42). Two strands were cut from the bottom row, one strand from the second and third rows each (Figure 45). The damage was performed by placing the girder on its side and striking it with a hydraulic hammer attached to a backhoe (Figure 45). After the strands were cut, the repair area was saw cut 254 mm deep in order to create a well-defined edge. The loose and or weakened concrete was chipped from around the exposed strands and the repair area was sandblasted and pressure washed in order to allow for a repair mortar to penetrate between and around the strands. Wood formwork was placed around the repair area and the repair mortar restored the original shape of the girder (Figure 46). A hammer tap test was then performed to ensure sufficient bond between repair mortar and the girder concrete prior to the application of the composites. The hammer test involves tapping the FRP

surface with a hammer and if a change in frequency is observed, this change indicates the location of a possible void or delamination between the FRP and concrete substrate. Table 13 and Figure 42 summarize each girder test, repair type, and method of strengthening.

**Figure 45 – Prestressing Strand Damage**

**Figure 46 – a) Concrete Repair Formwork b) Repaired Area**

**Table 13 – Description of Damages and Repair Types**

| Girder | Test No. | Repair Type | Strands Cut | Girder Length m | Damage Location | Damage Length m |
|---|---|---|---|---|---|---|
| A | 1 | None | 0 | 13.4 | - | - |
| C | 3 | FRP | 4 | 18.3 | 1/3 Point | 1.22 |
| D | 5 | FRCM | 4 | 18.3 | 1/3 Point | 1.22 |

In some instances, experimental challenges were encountered that resulted from equipment malfunction and unintentional damage to other repaired areas which required for some tests to be repeated. In this paper only tests 1, 3, and 5 which consist of the control girder and two girders strengthened with FRP and FRCM, respectively, are reported. The other tests 2, 4, and 6 consist of separate repair methods and are not included (Jones et al. 2015).

**Analysis of PC Girders**

In the United States, all bridges under federal funding must meet the requirements and design guidelines given in the American Association of State Highway and Transportation Officials (AAASHTO) LRFD Bridge Design Specifications (AASHTO 2010). Mandated by the Federal Highway Administration (FHWA), this document is considered the "law of the land" for bridge evaluation, design, and rehabilitation. As the development of composite materials has successfully evolved into design and construction applications, a guideline to assist in the evaluation of the severity of the damage, and to recommend composite repair techniques appropriate for various levels of damage is needed to consistently, efficiently and economically address impact damage.

The current design guidelines established for externally bonded FRP and FRCM materials for repair of RC are ACI 440.2R-08 and ACI549.4R-13, respectively, where ACI 440.2R-08 is the "Guide for the Design and Construction of Externally Bonded FRP

Systems for Strengthening Concrete Structures" (ACI 440.2R 2008). Accordingly, a theoretical analysis for each girder was performed using the aforementioned design literature. Each girder was analyzed per AASHTO LRFD 2010 for the damaged and un-damaged states. The strengthened capacities were determined for Girder C repaired with FRP and Girder D repaired with FRCM using AASHTO LRFD guidelines in combination with the corresponding ACI guidelines for each composite system. All theoretical analyses for each girder in its un-damaged, damaged, and strengthened configuration was performed using a program developed in Mathcad. An example of a Mathcad program analyzing girder D strengthened with FRCM is included in Appendix D.

As per the assumptions specified in AASHTO LRFD Section 5.7.2, ACI549.4R-13 and ACI 440.2R-08, LRFD the following assumptions were made: material properties from Table 2, Table 10, Table 11, and Table 12 are used, reduction factors are omitted, linear strain distribution exists along the depth of the section, force equilibrium is satisfied, strain compatibility is used to determine strains in the external reinforcement, perfect bond exists between prestressing steel and concrete, perfect bond exists between the composite reinforcement and concrete, maximum usable compressive strain in the concrete is 0.003, and concrete tensile strength is negligible. The stress distribution throughout the girder cross section during various stages of loading is illustrated in Figure 47 showing the axial, bending, dead, and live load force effects. The non-composite, composite, non-transformed, and transformed section properties including: area, moment of inertia, section modulus, prestressing steel, eccentricity, and dead loads were determined. Dead loads include the self weight of the girder and weight of deck. Prestressing losses were determined based on the measured effective prestress value of 910 MPa. In most cases the

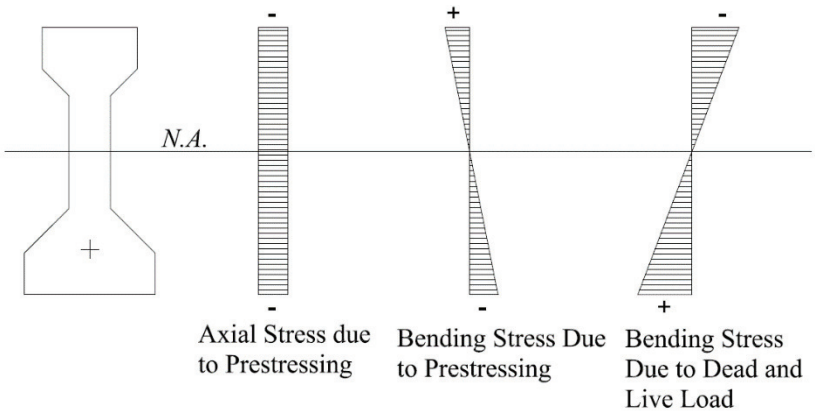


**Figure 47 – Stresses Applied to Girder Cross-Section**

effective prestress force cannot be measured and can be estimated using AASHTO LRFD Section 5.9.5.3 Approximate Estimate of Time Dependent Losses Method, but for this study an effective prestress of 910 MPa was used. The corresponding strain behavior in the cross section due to each stage of load application until failure is shown in Figure 48, where $P_e$ is the effective prestressing force.

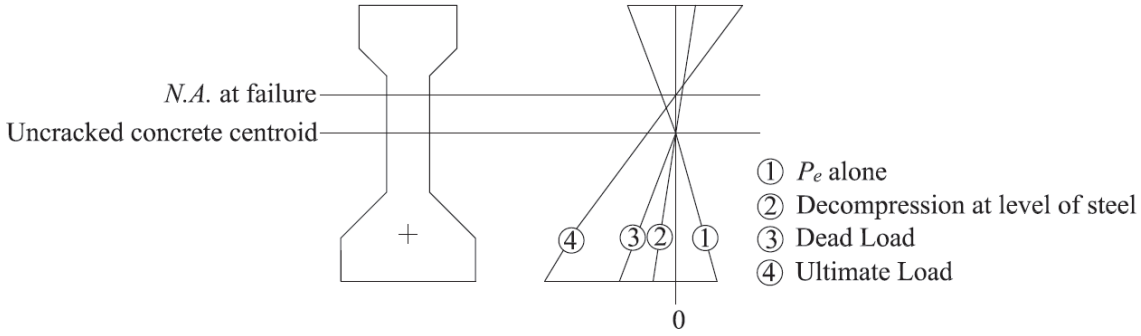


**Figure 48 – Strain Applied to Girder Cross-Section**

**Un-damaged and Damaged States**

The analysis of each girder in the un-damaged and damaged states was performed in accordance with LRFD Section 5.7.3 by satisfying force equilibrium (Figure 49) where the following equation is satisfied:

$$F_p - C_c = 0$$

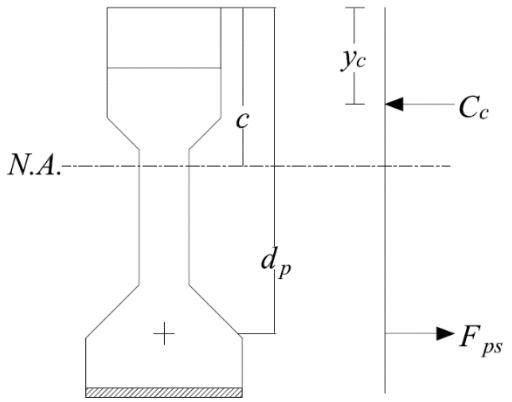


**Figure 49 – Force Equilibrium for PC Cross Section**

Where $F_p$ is the tensile force in the Prestressing steel and $C_c$ is the compressive force in the concrete. All prestressing strands (top and bottom) were considered when determining $F_p$. The tensile force in the prestressing steel, $F_{ps}$, is defined as $F_p = A_{ps}f_{ps}$ where $f_{ps}$is the stress in the prestressing steel determined using AASHTO's formula:

$$f_{ps} = f_{pu}\left(1 - k\frac{c}{d_p}\right)$$

$A_p$ is the area of Prestressing, $c$ is the distance from extreme compression fiber to the neutral axis, $k$ is a factor that accounts for the assumption that the tensile reinforcement is lumped at the location of prestressing centroid and defined as $k = 2\left(1.04 - \frac{f_{py}}{f_{pu}}\right)$, $d_p$ is the distance from extreme compression fiber to the centroid of prestressing steel, $f_{py}$ is the yield stress in the prestressing steel, and $f_{pu}$ is the ultimate stress in the prestressing steel. The compressive force in the concrete, $C_c$, is defined as $C_c = \alpha_1 f'_c A_c$ for $\varepsilon_c = 0.003$ where $\alpha_1$ is taken as .85, $f'_c$ is the 28 day concrete compressive strength, $A_c$ is the area of concrete in compression, and $\varepsilon_c$ is the strain in the concrete at the extreme compression fiber. If the strain in the concrete is less than 0.003, then Todeschini's stress-strain model

is used which allows for a more accurate prediction of concrete stress-strain behavior and is defined as $\sigma_c(\varepsilon_c) = \frac{2(0.9f'_c)\frac{\varepsilon_c}{\varepsilon_{c0}}}{1+\left(\frac{\varepsilon_c}{\varepsilon_{c0}}\right)^2}$ where $\varepsilon_{c0} = \frac{1.71f'_c}{E_c}$ and the compressive force in the concrete is then $C_c = b\int_0^c \frac{2(0.9f'_c)\frac{\varepsilon_c}{\varepsilon_{c0}}}{1+\left(\frac{\varepsilon_c}{\varepsilon_{c0}}\right)^2} dy$, and $E_c$ is the modulus of elasticity of the concrete. The ultimate flexural capacity is determined as:

$$M_u = F_{ps}(d_p - y_c)$$

where $y_c$ is the distance from extreme compression fiber to the centroid of the concrete compression force.

When the girder is damaged due to four (4) cut prestressing strands, the girder cross section experiences a reduction of prestressing force and therefore, a reduction in flexural capacity. The same properties and assumptions previously discussed are used to determine the damaged capacity, except for the number of prestressing strands which is reduced to 46 strands. This strand reduction corresponds to a tensile force equal and opposite to the initially applied prestressing. This tensile force is applied at the centroid of the cut strands which results in an added stress and strain distribution in the cross section, thus affecting the initial stress and strain conditions when the FRP or FRCM systems are applied. In addition, when the four strands were cut, the center of prestressing shifted both laterally and vertically, resulting in an unsymmetrical eccentricity with respect to the girder centerline. Only the vertical change in eccentricity is considered in this paper in order to simplify the analysis of each damaged girder. The theoretical undamaged and damaged flexural capacities were determined for each girder and are given in Table 14. In comparing the damaged and undamaged values, the loss of strength due to the cutting of the strands represents the level of strengthening required by the FRP and FRCM systems. Each girder

was analyzed separately and different theoretical capacities were determined due to the varying deck widths shown in Figure 42.

**Table 14 – Theoretical Ultimate Flexural Capacities**

| Girder | Test No. | Repair Type | Un-damaged (kN-m) | Damaged (kN-m) |
|---|---|---|---|---|
| A | 1 | None | 4540 | - |
| C | 3 | FRP | 4170 | 3870 |
| D | 5 | FRCM | 4110 | 3810 |

**Girder C Strengthened with FRP**

The same analysis approach given in the previous sub-chapter is used for the computation of damaged girder C strengthened with FRP. There is an additional tensile force provided by the FRP system that provides flexural resistance to the cross section as shown in Figure 50. Following the design methodology stated in ACI 440.2R-08, this additional force is introduced into the cross sectional analysis and a new equilibrium equation and moment and moment equation is developed. The force equilibrium equation now becomes:

$$F_{ps} + F_{frp} - C_c = 0$$

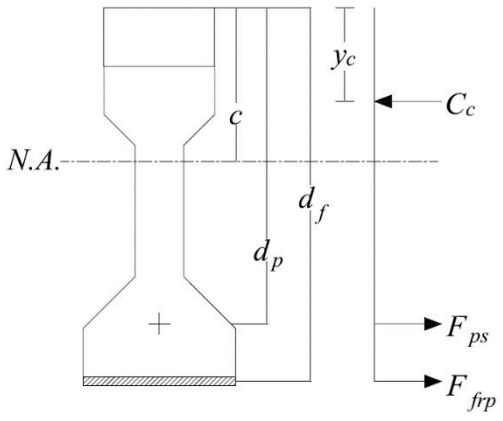


**Figure 50 – Force Equilibrium for PC Cross Section with FRP**

Where the tensile force in the FRCM, $F_{frp}$, is defined as $F_{frp} = A_f f_{frp}$ where $A_f$ is the effective area of FRP define as $A_f = nt_f b$, $f_{frp}$ is the stress in the FRP defined as $f_{frp} = E_f \varepsilon_{frp}$ , and $\varepsilon_{frp}$ is the strain in the FRP which is dependent on the controlling mode of failure where the following modes were checked: concrete crushing, steel rupture, and FRP failure (FRP rupture and/or FRP debonding). The FRP strain is defined as:

$$\varepsilon_{frp} = \begin{cases} \varepsilon_{fd} \leq \overline{\varepsilon_{fu}} & \text{for FRP failure} \\ \varepsilon_{cu}\left(\dfrac{d_f - c}{c}\right) - \varepsilon_{bi} \leq \varepsilon_{fd} & \text{for concrete crushing} \\ \left(0.035 - \varepsilon_{pi}\right)\left(\dfrac{d_f - c}{d_p - c}\right) - \varepsilon_{bi} \leq \varepsilon_{fd} & \text{for tendon rupture} \end{cases}$$

Where $d_f$ is the distance from extreme compression fiber to the centroid of FRCM reinforcement, $\varepsilon_{bi}$ is the initial strain in the concrete substrate at the time of FRP application and $\varepsilon_{pi}$ is the initial strain in the prestressing steel. All other variables are defined in Table 15 and are determined by the material characterization direct tension tests for C400H 1 ply specimens given in Table 12.

**Table 15 – FRP Material Properties Used for Analysis**

| Description | Symbol | Value | Units |
|---|---|---|---|
| Modulus of Elasticity from Characterization | $\overline{E_f}$ | 1,328 | Gpa |
| Ultimate Tensile Strain from Characterization | $\overline{\varepsilon_{fu}}$ | 0.0175 | mm/mm |
| Ultimate Tensile Stress from Characterization | $\overline{f_{fu}}$ | 75.7 | Gpa |
| FRP debonding strain | $\varepsilon_{fd}$ | $.083\sqrt{\frac{f'_c}{n\overline{E_f}t_f}}$ | mm/mm |
| Number of Plies | $n$ | 2 | - |
| Thickness of FRP | $t_f$ | 0.08 | in |

The ultimate flexural capacity is determined as:

$$M_u = F_{ps}(d_p - y_c) + F_{frp}(d_f - y_c)$$

Results for girder C strengthened with FRP are given in Table 16 where the un-damaged damaged, and repaired values are compared. The strengthening configuration was chosen

**Table 16 – Theoretical Capacities for Girder C**

| Girder | Un-Damaged (kN-M) | Damaged (kN-M) | Repaired (kN-M) | Repaired/ Un-Damaged |
|---|---|---|---|---|
| C | 4170 | 3870 | 4690 | 1.125 |

to be two longitudinal C400H layers and one transverse C200H layer which served as confinement to the two longitudinal layers. The repaired theoretical ultimate capacity is predicted to successfully restore and exceed the girders original strength by 520 kN-m (12.5%).

**Girder D Strengthened with FRCM**

Similarly, the design approach used for girder C is also used to theoretically predict the ultimate flexural capacity of girder D strengthened with FRCM. The additional tensile force is provided by the FRCM system as shown in Figure 51 and the design methodology specified in ACI 549.4R-13 is used for the cross sectional analysis.

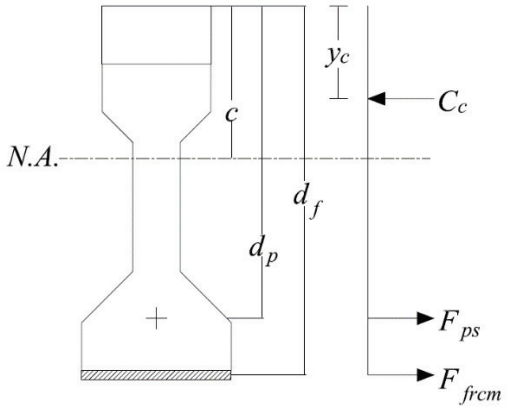


**Figure 51 – Force Equilibrium for PC Cross Section with FRCM**

The force equilibrium equation now becomes:

$$F_{ps} + F_{frcm} - C_c = 0$$

Where the tensile force in the FRCM, $F_{frcm}$, is defined as $F_{frcm} = A_f f_{frcm}$ where $A_f$ is the effective area of FRCM define as $A_f = nA_{funit}b$. $b$ is the width of the girder soffit, $f_{frcm}$ is the stress in the FRCM defined as $f_{frcm} = E_f \varepsilon_{frcm}$ , and $\varepsilon_{frcm}$ is the strain in the FRCM that is defined based on the controlling failure mode:

$$\varepsilon_{frcm} = \begin{cases} \varepsilon_{fu.max} & \text{for FRCM failure} \\ \varepsilon_{cu}\left(\dfrac{d_f - c}{c}\right) - \varepsilon_{bi} \le \varepsilon_{fu.max} & \text{for concrete crushing} \\ \left(0.035 - \varepsilon_{pi}\right)\left(\dfrac{d_f - c}{d_p - c}\right) - \varepsilon_{bi} \le \varepsilon_{fu.max} & \text{for tendon rupture} \end{cases}$$

All other variables are defined in

Table 17 and are determined by the material characterization direct tension tests for 1 ply specimens given in Table 2 of Chapter 2. The ultimate flexural capacity is determined as:

$$M_u = F_{ps}(d_p - y_c) + F_{frcm}(d_f - y_c)$$

**Table 17 – FRCM Properties Used for Analysis**

| Description | Symbol | Value | Units |
|---|---|---|---|
| Modulus of elasticity from characterization | $E_f$ | 128 | GPa |
| Ultimate tensile strain from characterization | $\varepsilon_{fu}$ | 0.01757 | mm/mm |
| Ultimate tensile strength from characterization | $f_{fu}$ | 1,664 | MPa |
| Number of Plies | $n$ | 4 | - |
| FRCM maximum permissible tensile strain | $\varepsilon_{fu.max}$ | $min\left(\varepsilon_{fu}, \frac{f_{fu}}{E_f}\right)$ | mm/mm |
| Area of FRCM by unit weight | $A_{f.unit}$ | 0.04572 | $mm^2/mm$ |

Results for the analysis of girder D are given in Table 18 where the strengthened flexural (moment) capacity is compared to the damaged and un-damaged capacities. the same FRCM system demonstrates that for a 4 ply configuration, the failure mode of the system is due to FRCM delamination from the concrete (Babaeidarabad et al. 2014). Therefore, a maximum of four plies was selected. The FRCM restores the damaged girder with an increase of about 210 kN-m,and with about 90 kN-m (2.2% of target value) remaining in

**Table 18 – Theoretical Capacities for Girder D**

| Girder | Un-Damaged (kN-M) | Damaged (kN-M) | Repaired (kN-M) | Repaired/ Un-Damaged |
|---|---|---|---|---|
| D | 4110 | 3810 | 4020 | 0.978 |

order to restore to its original strength. The Mathcad program written and used to determine FRCM flexural capacity is provided in Appendix D. Table 19 summarizes the theoretical ultimate capacities for all girders in the un-damaged, damaged, and repaired configurations.

**Table 19 – Summary of Theoretical Girder Capacities**

| Girder | Repair Type | Un-Damaged (kN-M) | Damaged (kN-M) | Repaired (kN-M) | Repaired/ Un-Damaged |
|---|---|---|---|---|---|
| A | None | 4540 | - | - | - |
| C | FRP | 4170 | 3870 | 4690 | 1.125 |
| D | FRCM | 4110 | 3810 | 4020 | 0.978 |

**FRCM and FRP Strengthening Configurations**

The FRCM and FRP systems are intended to provide an increase in flexural strength that restores the damaged girders to their original ultimate capacity. The total length of each repair is equivalent to two times the development length of a prestressing strand plus the damaged length and the FRCM/FRP development length and results in roughly 4.6 m along the length of the girder. One damaged location on girder C was strengthened with two layers of C400H FRP in the longitudinal direction (fibers are oriented parallel to the length of the girder) and one layer of C200H in the transverse direction (Figure 52). The


**Figure 52 – Girder C FRP Strengthening Configuration**

transverse layer served to confine and prevent the delamination of the longitudinal C400H layers. Surface preparation consisted of rounding sharp corners to a 127 mm radius in order to prevent stress concentration in the fabric and voids between the FRP and concrete substrate. The surface was mechanically roughened to the aggregate level using a grinder in order to ensure good bond to the substrate by eliminating any loose material or geometric inconsistencies. A two part epoxy resin was then mixed and applied as a surface primer to the concrete substrate where all voids were filled to minimize surface discontinuity and create a good bond between concrete and composite. CFRP sheets were run through a saturator to ensure proper fiber impregnation while removing excess resin. The 4.6 m long impregnated sheet was then applied to the repair area where a ribbed roller was pressed to help bond the fabric to the epoxy. Another layer of epoxy was then applied where a second ply was impregnated and applied over the first ply. A third layer of epoxy was applied and the transverse sheets were installed followed by a final layer of epoxy for a smooth finished surface. The application procedure is shown in Figure 53.

**Figure 53 – FRP Application to Damaged PC Girder C**

One damaged location on girder D was strengthened with the equivalent of four layers of FRCM wrapped completely around the bulb of the girder (Figure 54). Surface preparation was performed identical to that of girder C with the exception that the surface

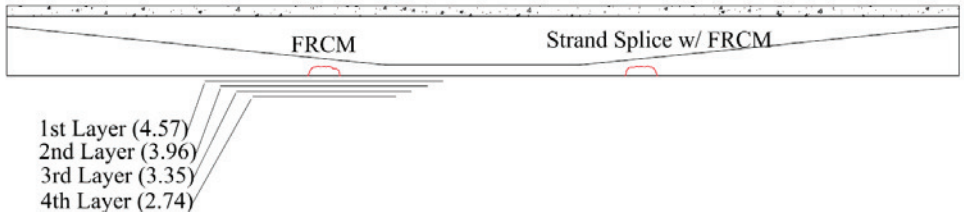


**Figure 54 – Girder D FRCM Strengthening Configuration**

of the concrete was maintained saturated surface dry prior to the application of the matrix mortar. The mortar was mixed and applied to the bottom bulb of the girder using a trowel. A 4.6 m long layer of fabric was placed and embedded into the mortar using a trowel. A second layer of mortar was applied using the trowel to create a sandwich around the fabric. This procedure was repeated until four layers were applied (Figure 55). Due to the geometry of the fabric, which was 1 meter in width, the four fabric layers were divided into

**Figure 55 – FRP Application to Damaged PC Girder C**

several strips and applied in a specific order, which in the end resembled a four fabric strengthening configuration as shown in Figure 56. In order to prevent the delamination of FRCM from the concrete at the repair ends, each layer of FRCM was of a different length, resulting in a tapered configuration from the center of damage to the repair ends (Figure

54). The first, second, third, and fourth layers were 4.6, 3.9, 3.3, and 2.7 m long, respectively. Figure 56 shows the cross sectional strengthening configuration for girder C with FRP and girder D with FRCM, respectively.

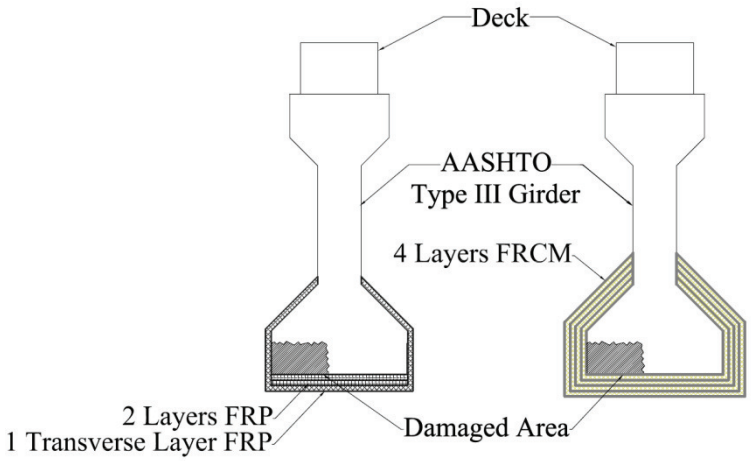


**Figure 56 – Strengthening Configuration for Girder C (left) and Girder D (right)**

**Test program**

All girders were tested using a four point bending, simple span configuration with a pin and roller support at each end. The pin and roller supports were in turn supported by W21x101 steel cross sections. This simple span configuration was chosen to induce a flexural failure in the girders rather than a shear failure. A 1780 kN load actuator was used to apply the loading where a spreader beam equally distributed the load from the actuator to rubber pads located 1.2 m apart. All loads were applied in 89 kN increments. In order to prevent movement or tipping of the girder, two horizontal steel members were used as bracing frames along the length of the girder. Figure 57 shows the instrumentation layout including: wire potentiometers to measure horizontal and vertical deflection, linear variable differential transformers (LVDT's) to measure the slipping between repair system and concrete substrate as well as the longitudinal girder deformation and strain transducers to

measure the longitudinal strain in the concrete throughout the depth of the girder (Jones et al. 2015). Table 20 and Figure 58 describe the test set-up and repair type for each girder.

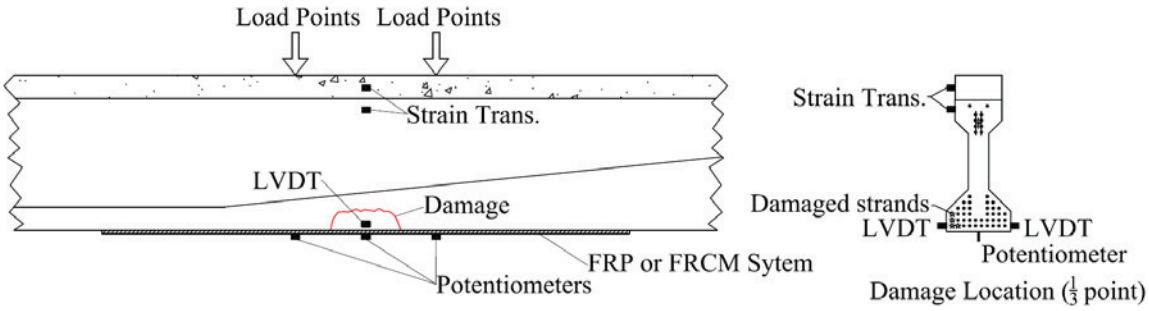


**Figure 57 – Typical Test Instrumentation Layout**

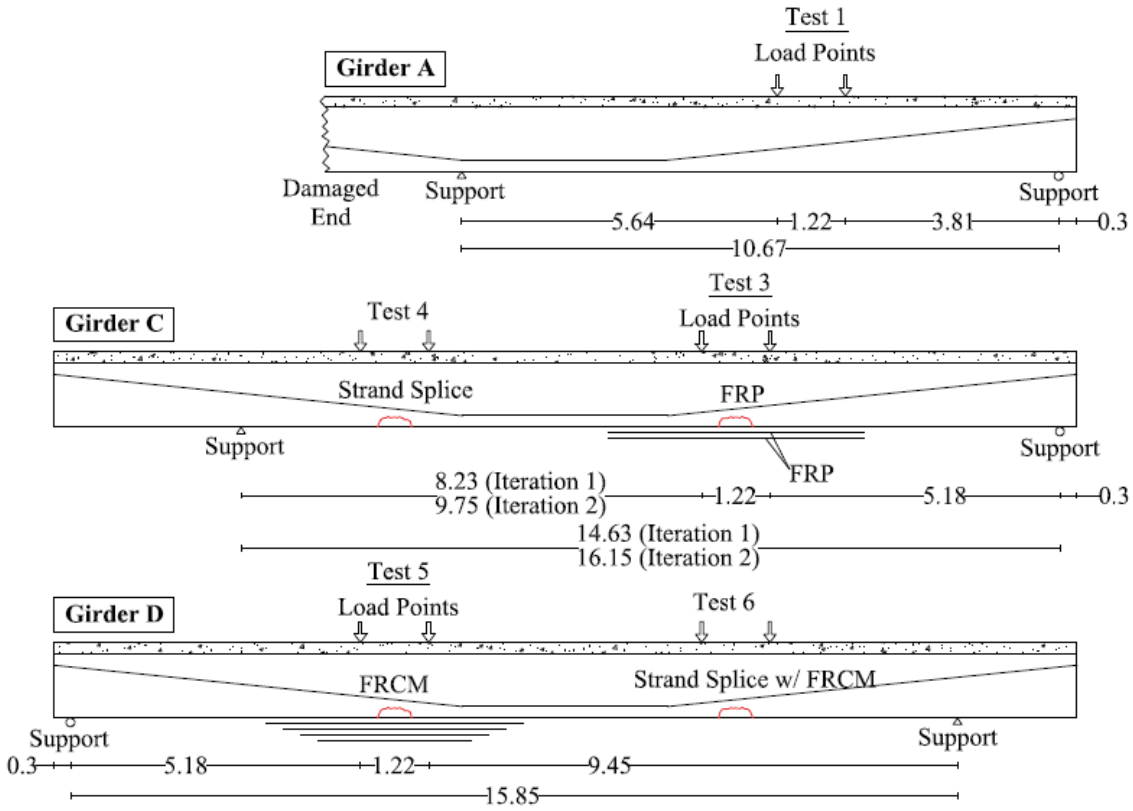


**Figure 58 – Girder Test Set-Up (all dimensions in m)**

**Table 20 – Test Set-Up and Girder Properties**

| Girder | Length (m) | Test No. | # of Strands Cut | Description of Repair Type | Test Span Length (m) | Deck Thickness (mm) | Deck Width (mm) |
|---|---|---|---|---|---|---|---|
| A | 13.4 | 1, Iteration 1<br>1, Iteration 2 | 0 | None | 10.7 | 254 | 610 |
| B* | 18.3 | 2 | 8 | Strand Splicing | 17.7 | 241 | 406 |
| C | 18.3 | 3, Iteration 1<br>3, Iteration 2 | 4 | FRP | 14.6<br>16.2 | 241 | 406 |
| C* | 18.3 | 4, Iteration 1<br>4, Iteration 2 | 4 | Strand Splicing | 17.7<br>15.24 | 235 | 406 |
| D | 18.3 | 5 | 4 | FRCM | 15.9 | 241 | 381 |
| D* | 18.3 | 6 | 4 | Strand Splicing w/ FRCM | 15.9 | 241 | 381 |

* Not covered in this paper

## Test Results and Discussion

*Test 1 - Control Girder A*

Girder A – Test 1 served as the control test to compare with successive tests where two test iterations were performed with a span of 10.7 m. During the first attempt, cracking occurred at 1188 kN which corresponds to a cracking moment of 2940 kN-m. Unfortunately, a hydraulic malfunction occurred when the girder reached a maximum moment of 3830 kN-m and 36.4 mm deflection and the test was stopped. The pump was replaced and a re-test was then performed. The second test iteration reached the the actuator limit of 1780 kN, which was equivalent to a maximum moment of 4320 kN-m and deflection of 47 mm in the girder. Upon reaching the actuator's capacity the test was stopped and the girder was not tested to failure. The second test iteration included a 3.3 mm residual deflection from the first iteration. Because the girder had already been cracked, the girder showed an initial loss in stiffness during loading. Although the girder was not tested to failure, careful observation of the crack patterns indicated an impending flexural failure. Figure 59 shows flexural cracks in the bottom bulb of the girder. The

**Figure 59 – Test A-1, Iteration 2 Flexural Cracks in the Bottom Bulb**

predicted failure moment was 4540 kN-m which is slightly higher than the experimental value and proves to be a reasonable prediction considering the girder was close to failure. Figure 60 compares the theoretical predicted moment with the measured moment versus deflection behavior.

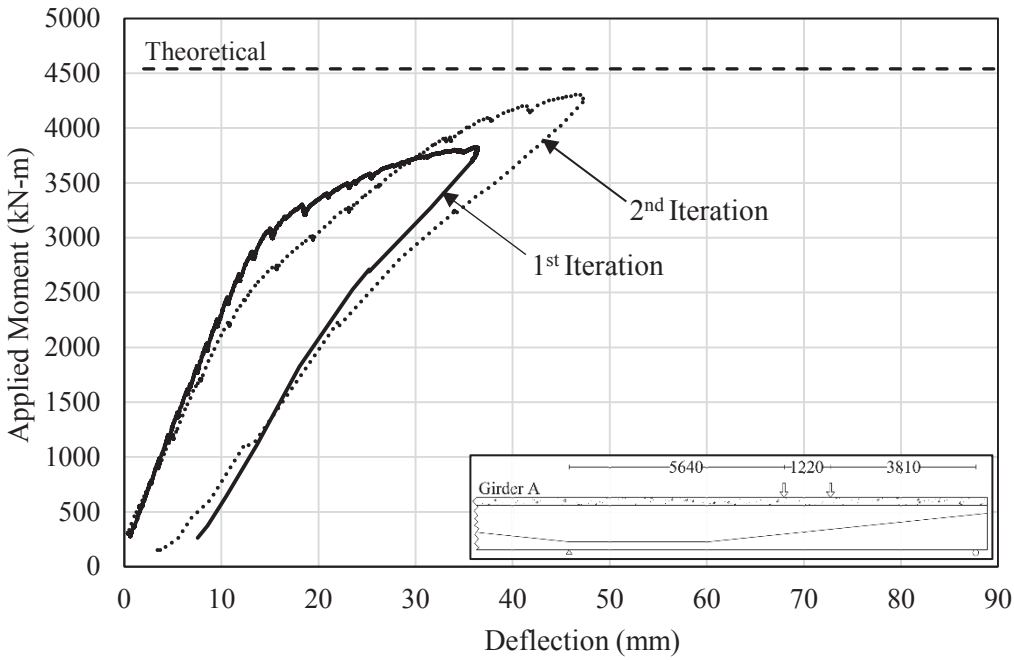


**Figure 60 – Test A-1 Moment vs. Deflection Behavior**

*Test 3 – FRP Strengthened Girder C*

Two iterations were performed for test 3, girder C strengthened with FRP. The first test iteration was performed with a span of 14.6 m. The applied cracking moment was 3360 kN-m and the maximum moment and deflection reached 4690 kN-m and 80 mm, respectively. The first crack was observed in the concrete above the FRP and was assumed to have propagated from behind the FRP (Figure 61a). This implies that the crack originated in the girder's bottom flange but was masked by the FRP cover (Jones et al. 2015). When the test reached 4690 kN-m, shear cracks formed in the girder web at

**a)** **b)**

**Figure 61 – Test C-3, Iteration 1 a) Crack Propagation b) Cracking Near Peak Load**

locations of minimal shear reinforcement (Figure 61b) and flexural cracks at the other repaired location (strand splicing) were observed which required the test to be stopped (Jones et. al., 2015). The other repair location was tested (Test C-4) and subsequently the second iteration was performed with a span of 16.2 m and a maximum moment of 4350 kN-m and deflection of 85 mm was attained. During this test, the actuator began to slip and a steel frame was introduced to prevent slippage. The test was stopped due to flexural compression cracks developed between the two loading points, in the area of constant moment, which were characteristic of a flexural compressive failure. No bond failure was

observed even though there were multiple cracks in the bottom bulb. The predicted moment capacity was 4690 kN-m and is consistent with the experimental maximum for the first test iteration. Also, the maximum moments measured in both test iterations exceeded the theoretical un-damaged capacity of 4170 kN-m. Because the first iteration demonstrated the maximum moment capacity, Figure 62 presents the moment versus deflection relationship only for C-3, Iteration 1.

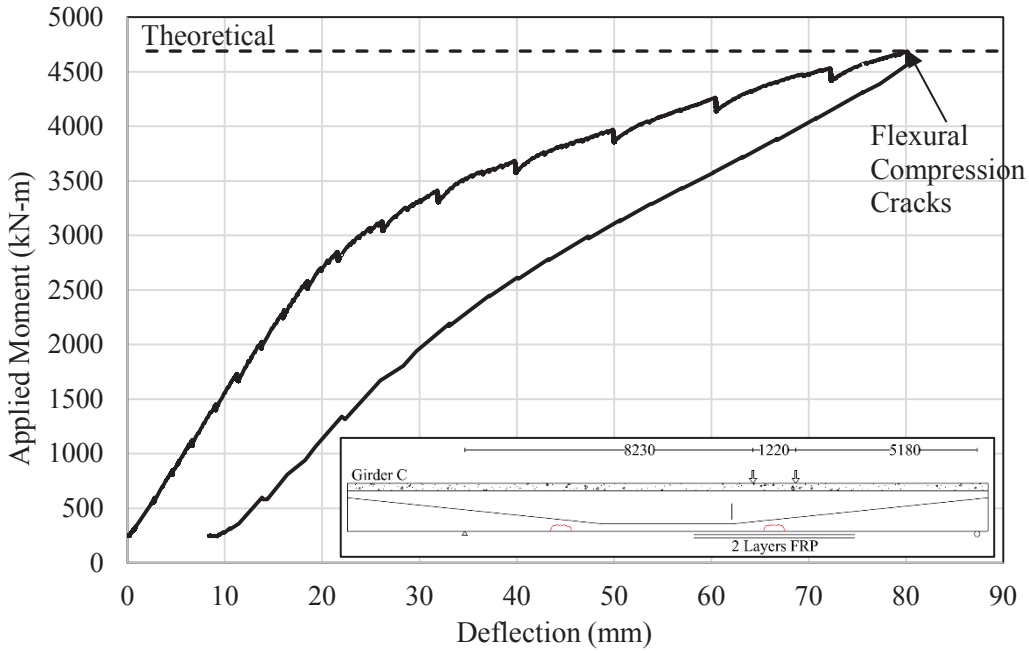


**Figure 62 – Test C-3, Iteration 1 Moment vs. Deflection Behavior**

*Test 5 – FRCM Strengthened Girder D*

Prior to testing, girder D was deemed defective due to the presence of saw cuts through the width of the deck at various locations along the length of the girder (Figure 40). The discontinuities caused the member to be divided into different lengths of composite section. Hence, test 5 was performed with a span of 15.9 m and the cracking moment was observed to be 3000 kN-m. During testing, the actuator malfunctioned and the test was paused. The test was resumed and the applied moment reached a maximum of 3630 kN-m with a 57

mm deflection (Figure 63). At this point, horizontal shear cracks were observed in the deck-to-top-flange interface and testing was completed. The presence of saw cut gaps reduced the shear strength and prevented full composite action between the deck and girder. As a result, horizontal shear cracking at the interface occurred between the gaps and separate cracks formed and propagated from the deck saw cuts into the girder's top flange (Figure 64). Failure consisted of sudden concrete crushing at the interface between the deck and

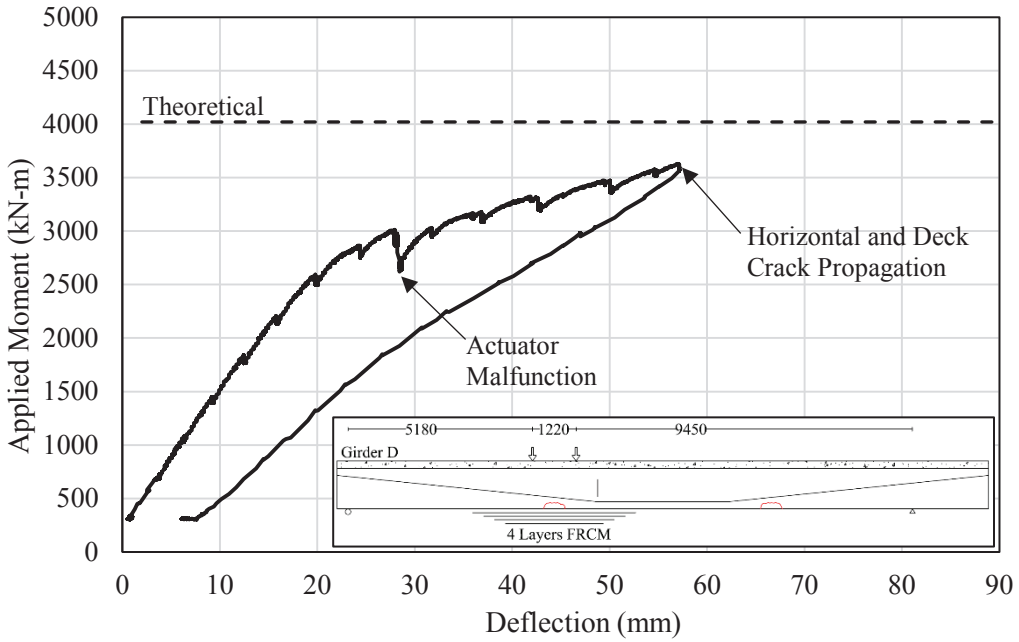


**Figure 63 – Test D-5, Moment vs. Deflection Behavior**


**Figure 64 – Test D-5, Horizontal Shear Cracks**

the girder. The predicted failure moment was 4020 kN-m and test results indicate that only 90% of this value was attained. Due to the presence of saw cuts, the girder could not be tested to its true maximum capacity as a composite section. This implies that if no saw cuts existed, it is very likely the girder could have reached the theoretical maximum. In addition, there were no signs of FRCM debonding from the substrate.

Table 21 shows a comparison of experimental and theoretical nominal flexural capacities for each girder. The control flexural capacity describes the girder strength with no damaged prestressing strands. The damaged values describe the flexural strength when the strands are cut, whereas the repaired values describe flexural capacity of the girders with the FRP and FRCM strengthening. Repaired and virgin capacities are compared to verify if the respective strengthening system is successful in restoring girder strength. Experimental and repaired values are compared to validate if the strengthened capacity was reached during testing and cracking moments were specified for each girder test.

**Table 21 – Predicted and Experimental Nominal Flexural Capacities**

| Girder | Test No. | Predicted | | | Experimental (kN-m) | $M_{repaired}/M_{virgin}$ | $M_{experimental}/M_{repaired}$ | $M_{crack}$ |
|---|---|---|---|---|---|---|---|---|
| | | Un-damaged (kN-m) | Damaged (kN-m) | Repaired (kN-m) | | | | |
| A | 1, Iteration 1 | 4540 | - | - | 3830 | - | 0.84 * | 2940 |
| | 1, Iteration 2 | | | | 4320 | | 0.95 * | - |
| C | 3, Iteration 1 | 4170 | 3870 | 4690 | 4690 | 1.12 | 1.00 | 3360 |
| | 3, Iteration 2 | | | | 4350 | | 0.93 | - |
| D | 5 | 4110 | 3810 | 4020 | 3630 | 0.98 | 0.90 | 3000 |

* $M_{repaired}$ is $M_{virgin}$ for girder A as it is a benchmark specimen

**Comparison with Existing Design Guidelines**

For this study, the design nominal flexural capacities are determined using the material properties given previously in Table 2, Table 9, and Table 12 and are summarized in the Table 22. The capacity of girder A was calculated according to AASHTO (2010). The nominal capacity of girder C strengthened with FRP is determined according to FRPS-1 is

a recently developed document, published by AASHTO, containing design guidelines for the strengthening of reinforced concrete structures and components using FRP Composites. This document is titled "Guide Specifications for Design of Bonded FRP Systems for Repair and Strengthening of Concrete Bridge Elements" and is built from ACI 440.2R-08.

**Table 22 – Nominal Material Properties**

| Material | Description | Design | St. Dev |
|---|---|---|---|
| Concrete Slab | 28-Day Strength | $f'_c$= 27.58 MPa | |
| Concrete Girder | 28-Day Strength | $f'_c$= 34.47 MPa | |
| Prestressing Steel | Yield Strength | $f_{py}$ = 1.42 GPa | - |
| | Ultimate Strength | $f_{pu}$= 1.72 GPa | |
| | Modulus of Elasticity | $E_s$=186.16 GPa | |
| | Initial Prestressing | $P_e$ = 62.28 kN | |
| FRCM | Ultimate Tensile Strength | $f_{fu}$= 1,352 MPa | $\sigma_{f_{fu}}$ = 77 Mpa |
| | Cracked Modulus of Elasticity | $E_f$ = 128 GPa | - |
| | Ultimate strain | $\varepsilon_{fu}$ = 0.0176 mm/mm | $\sigma_{\varepsilon_{fu}}$ = 0.0015 |
| FRP | Ultimate Tensile Strength | $\overline{f_{fu}}$= 1,294 MPa | $\sigma_{f_{fu}}$ = 45.5 Mpa |
| | Ultimate strain | $\overline{\varepsilon_{fu}}$ = 0.017 mm/mm | $\sigma_{\varepsilon_{fu}}$ = 0.0007 |

The significance of the AASHTO FRPS-1 document is of great importance and is a breakthrough for bridge strengthening and repair using composites. Finally, the capacity of girder D was calculated separately per AASHTO and ACI 549.4R. Because ACI 549.4R does not contain provisions to determine the stress in the prestressing steel, AASHTO's (2010) methodology was used. The design analysis includes all coefficients, reduction factors, and strain limitations specified by the aforementioned guides, which are established to promote an acceptable level of safety.

ACI 440.2R and ACI 549.4R limit the maximum allowable strain values in the composites in order to prevent failure due to FRP and FRCM debonding. ACI 440.4R-08 designates the FRP ultimate tensile stress to be $f_{fu} *= \overline{f_{fu}} - 3\sigma_{f_{fu}}$ and the ultimate tensile strain to be $\varepsilon_{fu} *= \overline{\varepsilon_{fu}} - 3\sigma_{\varepsilon_{fu}}$. The FRP design tensile stress is defined as $f_{fu} = C_E f_{fu} *$

and the design tensile strain is $\varepsilon_{fu} = C_E \varepsilon_{fu}*$, where $C_E$ is the environmental reduction factor. The modulus of elasticity is calculated to be $E_f = f_{fu}/\varepsilon_{fu}$ and the debonding strain is defined as $\varepsilon_{fd} = 0.083\sqrt{\frac{f'_c}{nE_f t_f}} \leq 0.9\overline{\varepsilon_{fu}}$. The maximum strain that is permitted in the reinforcement is dependent on the controlling failure mode (concrete crushing, tendon rupture or FRP delamination). This strain is defined as the effective tensile strain, $\varepsilon_{fe}$, and is determined as:

$$\varepsilon_{fe} = \begin{cases} \varepsilon_{fd} \text{ for FRP failure (debonding)} \\ \varepsilon_{cu}\left(\frac{d_f - c}{c}\right) - \varepsilon_{bi} \leq \varepsilon_{fd} \text{ for concrete crushing} \\ \left(0.035 - \varepsilon_{pi}\right)\left(\frac{d_f - c}{d_p - c}\right) - \varepsilon_{bi} \leq \varepsilon_{fd} \text{ for tendon rupture} \end{cases}$$

Where $\varepsilon_{cu}$ is equal to a maximum compressive concrete strain of 0.003, $\varepsilon_{pi}$ is the initial strain in the prestressing steel reinforcement, and $\varepsilon_{bi}$ is the strain level in the concrete substrate at the time of FRCM application.

ACI 549.4R-13 designates the FRCM design stress, $f_{fd}$, and design strain, $\varepsilon_{fd}$, to be $f_{fd} = f_{fu} - \sigma_{f_{fu}}$ and $\varepsilon_{fd} = \varepsilon_{fu} - \sigma_{\varepsilon_{fu}}$, respectively. Similar to FRP, the effective FRCM strain, $\varepsilon_{fe}$, is also dependent on the controlling failure mode which could be due to concrete crushing, tendon rupture or FRCM delamination. However, ACI 549.4R only designates the initial condition where concrete crushing controls the failure mode. The effective strain for the latter failure modes were determined based on the methodology given in ACI440.2R-08 for the repair of PC. Accordingly, the effective strain can be defined as:

$$\varepsilon_{fe} = \begin{cases} \varepsilon_{fd} \leq 0.012 \text{ for FRCM failure} \\ \varepsilon_{cu}\left(\frac{d_f - c}{c}\right) - \varepsilon_{bi} \leq min(\varepsilon_{fd}, 0.012) \text{ for concrete crushing} \\ \left(0.035 - \varepsilon_{pi}\right)\left(\frac{d_f - c}{d_p - c}\right) - \varepsilon_{bi} \leq min(\varepsilon_{fd}, 0.012) \text{ for tendon rupture} \end{cases}$$

In addition, AASHTO and ACI 440.2R specify different equations to determine the flexural strength contribution from the prestressing steel but yield relatively similar values, whereas ACI 549 does not contain such provisions. ACI 440.2R includes an additional factor, $\psi_f$, equal to 0.85 and the strength reduction factors ($\phi$) for all codes are computed differently as follows:

$$\phi_{AASHTO} = \begin{cases} 1.0 \text{ for} \varepsilon_{ps} \geq 0.005 \\ 0.583 - 0.25\left(\frac{d_p}{c} - 1\right) \text{ for } 0.002 < \varepsilon_{ps} < 0.005 \\ 0.75 \text{ for } \varepsilon_{ps} \leq 0.002 \end{cases}$$

$$\phi_{ACI549.4R} = \begin{cases} 0.9 \text{ for } \varepsilon_t \geq 0.005 \\ 0.65 - 0.25\left(\frac{\varepsilon_t - \varepsilon_{sy}}{0.005 - \varepsilon_{sy}}\right) \text{ for } \varepsilon_{sy} < \varepsilon_t < 0.005 \\ 0.65 \text{ for } \varepsilon_t \leq \varepsilon_{sy} \end{cases}$$

$$\phi_{ACI440.2R} = \begin{cases} 0.9 \text{ for } \varepsilon_{ps} \geq 0.013 \\ 0.65 - 0.25\left(\frac{\varepsilon_{ps} - 0.010}{0.013 - 0.010}\right) \text{ for } 0.010 < \varepsilon_{ps} < 0.013 \\ 0.65 \text{ for } \varepsilon_{ps} \leq 0.010 \end{cases}$$

Where $\varepsilon_t$ and $\varepsilon_{ps}$ are the net tensile strain, and the total tensile strain in the prestressing steel, respetively. The design nominal capacities are determined using the equations given in Table 23 and resultant design values are given in Table 24 which are compared with the experimental values from Table 21.

ACI 440.2R proves to have the most conservative estimate of design nominal flexural capacity ($\phi M_n$). The analysis predicts the failure to be in the FRP which results in a low level of strain in the pretressing steel. This strain then determines a low strength reduction factor ($\phi$) which reduces design capacity considerably. FRPS-1 combines AASHTO's PC girder design with ACI 440.2R's FRP design methodology and proves to be the most reasonable design prediction. This document includes the strength reduction factor ($\phi$)

from AASHTO for the PC analysis, as well as the FRP reduction factor, $\psi_f$, from ACI 440.4R. It is difficult to compare the girder D design values with the experimental due to the fact that the girder was not tested to its true ultimate capacity. However, if the deck section was free of the saw cuts, it is implicative that girder D would have reached a moment capacity exceeding 3630 kN-m. Based on this assumption, the AASHTO design prediction given in Table 23 proves to be a reasonable value in comparison to the experimental value. To date, there have been no provision established for the repair of PC with FRCM, but the design methodology used herein can be used to enhance these design limitations.

**Table 23 –Design Capacity Equations**

| Girder/Design Literature | $\phi M_n$ Equation |
|---|---|
| *Girder A* | |
| AASHTO | $\phi M_n = \phi_{AASHTO}\left[F_{ps}(d_p - y_c)\right]$ |
| *Girder C* | |
| AASHTO | $\phi M_n = \phi_{AASHTO}\left[F_{ps}(d_p - y_c)\right] + \phi_{ACI440.2R}\left[\psi_f F_{frp}(d_f - y_c)\right]$ |
| ACI 440.4R | $\phi M_n = \phi_{ACI440.2R}\left[F_{ps}(d_p - y_c) + \psi_f F_{frp}(d_f - y_c)\right]$ |
| FRPS-1 | $\phi M_n = \phi_{AASHTO}\left[F_{ps}(d_p - y_c)\right] + \psi_f F_{frp}(d_f - y_c)$ |
| *Girder C* | |
| AASHTO | $\phi M_n = \phi_{AASHTO}\left[F_{ps}(d_p - y_c)\right] + \phi_{ACI549.4R}\left[F_{frcm}(d_f - y_c)\right]$ |
| ACI 549.4R | $\phi M_n = \phi_{ACI549.4R}\left[F_{ps}(d_p - y_c) + F_{frcm}(d_f - y_c)\right]$ |

**Table 24 – Experimental versus Design Values**

| Girder Type | Experimental $M_{experimental}$ | AASHTO $\phi M_{nAASHTO}$ (kN-m) | ACI 440.2R $\phi M_{nACI440.2R}$ (kN-m) | FRPS-1 $\phi M_{nFRPS-1}$ (kN-m) | ACI 549.4R $\phi M_{nACI549.4R}$ (kN-m) | $\phi M_{nAASHTO}/M_{experimental}$ | $\phi M_{nACI440.2R}/M_{experimental}$ | $\phi M_{nFRPS-1}/M_{experimental}$ | $\phi M_{nACI549.4R}/M_{experimental}$ |
|---|---|---|---|---|---|---|---|---|---|
| Girder 1 | 4320 | 4200 | - | - | - | 1.03 | - | - | - |
| Girder 2 - FRP | 4690 | 3660 | 2840 | 3854 | - | 1.28 | 1.65 | 1.22 | - |
| Girder 3 - FRCM | 3630 | 3630 | - | - | 3280 | 1.00 | - | | 1.11 |

**Recommendations for ACI 440.2R-08**

The design nominal capacity determined by ACI 440.2R-08 demonstrates the most conservative value for girder C strengthened with FRP. The reason for such a low value is due to the reduction factor $\phi_{ACI440.2R}$ that greatly reduces the capacity as a result of the low level of strain in the prestressing steel. $\phi_{ACI440.2R}$ is established to reduced ultimate capacity based on the predicted ductility of the system. If the prestressing steel exhibits a high level of strain at failure, the system will behave more ductile. In contrast, if the level of strain in the prestressing steel is low, a more brittle failure will occur. The reduction factor in ACI 440.2R-08 accounts for this behavior and adjusts the girder strength accordingly. But the comparison of experimental and design values indicate that this is an overly conservative variable. If the $\phi M_n$ equation is revised to include the reduction factor given in AASHTO LRFD, the new equation would be:

$$\phi M_n = \phi_{AASHTO}\left[F_{ps}(d_p - y_c) + \psi_f F_{frp}(d_f - y_c)\right]$$

This equation would yield a new design capacity of 3918 kN-m which is about 84% of the experimental value. The increase in capacity from the original design value given in Table 24 is about 1,014 kN (roughly 21%). This is a more reasonable calculation of design capacity. Thus, the proposed reduction factor for ACI 440.2R Section 10.3.1.3 is recommended to be:

$$\phi = \phi_{AASHTO} = \begin{cases} 1.0 \text{ for } \varepsilon_{ps} \geq 0.005 \\ 0.583 - 0.25\left(\dfrac{d_p}{c} - 1\right) \text{ for } 0.002 < \varepsilon_{ps} < 0.005 \\ 0.75 \text{ for } \varepsilon_{ps} \leq 0.002 \end{cases}$$

**Recommendations for ACI 549.4R**

There are currently no design provisions for the repair of PC with FRCM given in ACI 549.4R. The design analysis performed herein incorporates the PC design methodology from AASHTO, the PC failure criteria specified in ACI 440.2R-08 that considers concrete crushing, prestressing steel rupture, and FRCM failure, and the FRCM design methodology from ACI 549.4R. Based on the experimental and analytical results, the following equations are recommended for the FRCM strengthening of PC to be included in ACI 549.4R design provisions:

$$\phi M_n = \phi_{AASHTO}\left[F_{ps}(d_p - y_c)\right] + \phi_{ACI549.4R}\left[F_{frcm}(d_f - y_c)\right]$$

Where $F_{ps} = A_{ps} f_{ps}$

$f_{ps} = f_{pu}\left(1 - k\frac{c}{d_p}\right)$ (LFRD Eq. 5.7.3.1.1-1)

$k = 2\left(1.04 - \frac{f_{py}}{f_{pu}}\right)$ (LFRD Eq. 5.7.3.1.1-1)

$F_{frcm} = nA_{f.unit} b E_f \varepsilon_{fe}$

$$\varepsilon_{fe} = \begin{cases} min\left(\varepsilon_{fu}, \frac{f_{fu}}{E_f}\right) \leq 0.012 \text{ for FRCM failure} \\ \varepsilon_{cu}\left(\frac{d_f - c}{c}\right) - \varepsilon_{bi} \leq min\left(\varepsilon_{fu}, \frac{f_{fu}}{E_f}, 0.012\right) \text{ for concrete crushing} \\ (0.035 - \varepsilon_{pi})\left(\frac{d_f - c}{d_p - c}\right) - \varepsilon_{bi} \leq min\left(\varepsilon_{fu}, \frac{f_{fu}}{E_f}, 0.012\right) \text{ for tendon rupture} \end{cases}$$

In addition, the PC member shall meet the provisions specified by AASHTO LRFD Article 5.7.3. The aforementioned recommendations can be used to determine the nominal flexural capacity at ultimate conditions, whereas the serviceability behavior has not been addressed in this research.

**Concluding Remarks**

In this study, the effectiveness of FRP and FRCM systems for the strengthening and repair of damaged PC girders is evaluated. Three prestressed concrete girders were tested: one control girder A, one girder strengthened with FRP (girder C) and one girder strengthened with FRCM (girder D). Experimental nominal flexural capacities were predicted using guidelines given in AASHTO (2010), ACI 440.2R (2008), and ACI 549.4R (2013). During testing, girder A reached a maximum moment of 4320 kN-m, yielding 95% of the theoretical ultimate capacity. Upon reaching the actuator's maximum load, the test was stopped and although failure was not attained, the girder exhibited crack patterns that were representative of a forthcoming flexural failure. For girder C, the predicted strengthened capacity was 4690 kN-m and the FRP strengthened girder reached this value which exceeds its original capacity (4170 kN-m). This work as well as previous studies, demonstrate that FRP as a strengthening technology successfully restores flexural strength to damaged PC girders. Finally, Girder D strengthened with FRCM was predicted to have an un-damaged capacity of 4110 kN-m. During testing, damage occurred prematurely due to deck defects from bridge demolition, at which point the test was stopped and the resulted maximum moment was 3630 kN-m. Without the presence of accidental saw cuts in the deck, it is likely the girder would have reached its predicted capacity.

Finally, design nominal capacities were determined using AASHTO 2010, ACI 440.2R, FRPS-1, and ACI 549.4R where each guide arrives at different nominal design values. Following ACI 440.2R proved to have a conservative estimate of design strengthened capacity, which is mainly due to the strength reduction factor for prestressing steel. ACI 549.4R only addresses the FRCM strengthening to reinforced concrete, but if

the same design approach from AASHTO and ACI 440.2R are used for the PC flexural contribution, it can also be applicable to ACI 549.4R for PC girders. The design recommendations provided herein for ACI 440.2R-08, FRPS-1, and ACI 549.4R-13 aim to fine-tune and strengthen the design literature specifically for FRP and FRCM composites for the repair and strengthening of PC girders.

# CHAPTER 4

## Study 3 – FATIGUE PERFORMANCE OF RC BEAMS STRENGTHENED WITH FRCM

In the previous study, FRCM technology was used to repair an impact-damaged PC girder. This girder was not tested to its full potential and failed due to horizontal and vertical shear cracking as a result of saw cuts that occurred during girder extraction. However, there was no observed failure due to the FRCM system which suggests that if the saw cuts were not present, the girder would have reached the theoretical ultimate capacity. This suggests that FRCM is a viable repair alternative to damaged PC girders which require additional flexural capacity. Aside from providing flexural strength, the FRCM system must also exhibit favorable long-term performance during the structure's service life. In addition to PC girders, other RC structures such as offshore structures, bridges, roads, airport pavements, parking structures, and railway structure are subjected to repeated loading that are caused by wave loads, wind loads, and/or vehicular loads. Over the service life of a structure, the number of repeated loads (number of cycles) can be very high. When subjected to repeated cyclic loads, the concrete, steel reinforcement, and FRCM experience fluctuating stresses that are typically less than the ultimate static and yield strengths. Stress concentrations at locations of material flaws and discontinuities result in the formation of cracks. Cracks propagate over time due to repeated loading and structural integrity is diminished resulting in structural failure. This concept is known as fatigue, or the progressive failure of a material under repeated stresses (Moore 1927).

Due to the novelty of FRCM technology, there is a lack of research regarding the fatigue performance of FRCM systems for RC strengthening. As a result, this study aims to experimentally investigate the parameters that most influence the flexural fatigue performance of PBO-FRCM strengthened RC beams. Although it seems appropriate to investigate the fatigue behavior of a PC girder strengthened with FRCM which is consistent with the previous study, it is first necessary to understand the performance of a plain RC member with FRCM subjected to fatigue. This is the reason for which the third study will focus on RC elements rather than PC elements, with the overall goal of providing a foundation for the future investigation of PC structures strengthened with FRCM composites subjected to fatigue. Accordingly, before the third study is presented, a general understanding of the fatigue performance of RC and its constituent materials is necessary. In the following subchapters, a summarized description of the fatigue behavior of concrete, steel, RC, and FRP strengthened RC beams is discussed.

**S-N Behavior**

Investigation of fatigue strength of a structure is typically accomplished by testing a system at different stress ranges. Results from these tests are used to determine a curve that relates stress range, $S_r$, and fatigue life, $N$, which is commonly known as an S-N curve. The stress range is defined as the algebraic difference between the maximum and minimum applied stress: $S_r = S_{max} - S_{min}$. A typical S-N curve is shown in Figure 65 and is divided into three parts: low cycle fatigue, finite-life region, and infinite life region. For the design of RC structures with long service lives, the area of interest is the fatigue characteristics associated with the finite and infinite life regions. It is important to know at what applied stress a material will experience fatigue failure and the corresponding fatigue life

associated with this value. In addition, it is also necessary to determine the maximum applied stress range that can be applied to a material without failure occurring. This property is known as the material's endurance limit which is an important characteristic of the infinite-life region as illustrated in Figure 65. The endurance limit is commonly associated with a stress range corresponding to a fatigue life of more than 2 million cycles (ACI 215R-97, Solani et al. 2012).

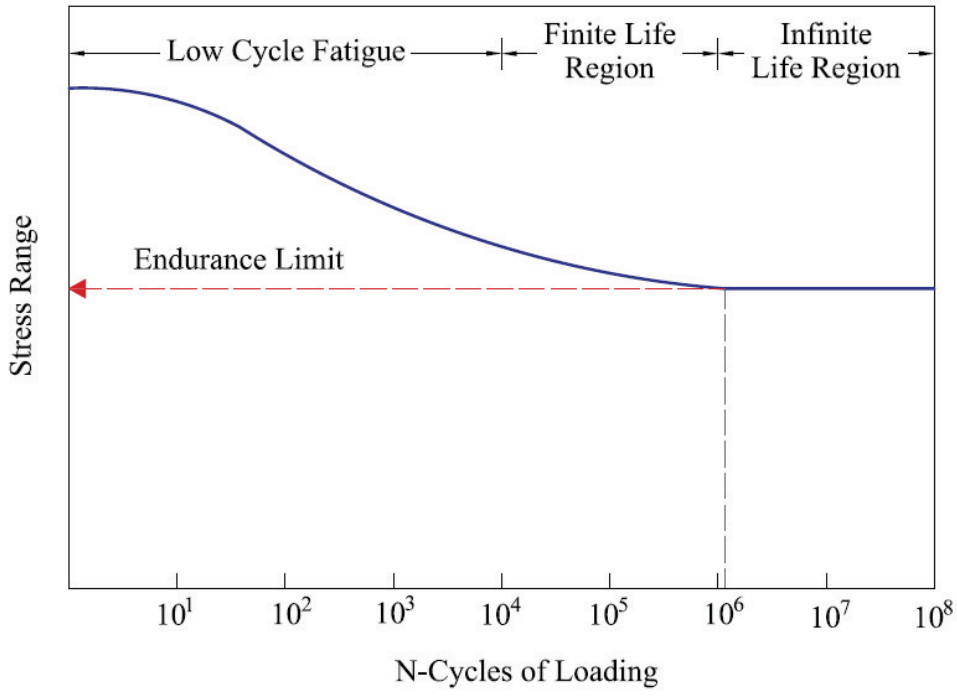


**Figure 65 – Typical Stress Range vs. Number of Cycles (S-N) Curve**

Much research has been conducted on the fatigue behavior and performance of reinforcing steel (Moore 1927, Kokubu, and Okamura 1965, MacGregor et al. 1971, Helgason et al. 1976, Tilly 1979, Abel and Zheng 1999, Soltani et al. 2012) while considerably less work has been done on concrete (Murdock and Kesler 1958, McCall 1958, Hilsdorf and Kesler 1960).

**Fatigue in Plain Concrete**

The fatigue behavior of plain concrete is determined by a number of factors including: material properties, load type, rate of loading, applied stress range, environmental conditions, age, and number of cycles of loading. Many studies have been performed to evaluate flexural fatigue behavior and in summary the response of plain concrete is described in three phases. Phase one consists of the initiation phase, where cracks initiate and deflection increase rapidly, but with a progressively decreasing rate as shown in Figure 66. Phase two represents a more stable condition as deflection increases almost linearly

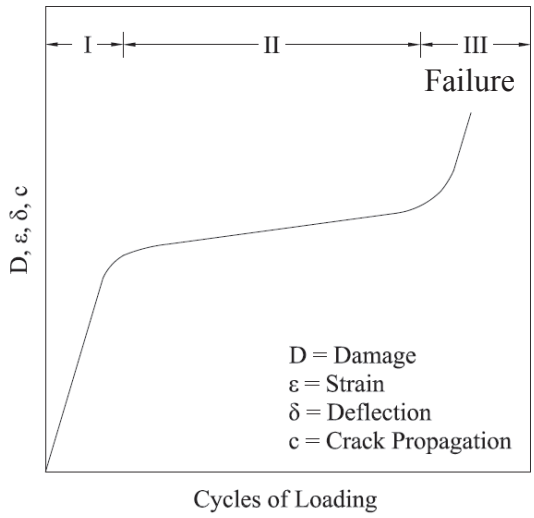


**Figure 66 – Typical Fatigue Behavior of Plain Concrete**

with the number of cycles. Phase three denotes instability, where deflections increase at a progressively increasing rate until fatigue failure occurs (Neville 1996). The three phases describe behavior in terms of deflection, but the same is also true for compressive strains, crack propagation, and is also inversely proportional to the change in modulus of elasticity with increasing number of cycles.

Fatigue damage can result from the formation of cracks in the aggregates, in the cement matrix, at the aggregate-cement interface or any combination of these modes. The actual mechanism that causes failure is not well established, but it is commonly agreed upon that progressive micro and macro cracking result in increasing strains and deflections, resulting in failure. Strains measured at fatigue failure are observed to be much larger than strains measuring at static failure, and specimens with larger fatigue lives tend to exhibit larger strains at failure, especially if the maximum stress is lower. To date, there is no established endurance limit at which infinite number of cycles can be applied without failure occurring in plain concrete. Many studies have determined a "fatigue limit" to be an applied stress range that results in a very high number of cycles ($10^7$ cycles). A fatigue limit of 55 percent of the static strength for 10 million cycles was determined for plain concrete. This limit is also true for tension and compression fatigue strengths (ACI 215R-97).

**Fatigue in Reinforcing Steel**

The fatigue behavior of reinforcing steel can be determined by performing axial tension tests on pieces of reinforcing steel or flexural tests on reinforced concrete beams. It is arguable as to which test method yields better results, but to maintain consistency with the tests performed herein, results from previous work performed on the flexural fatigue of RC beams will be discussed. It has been shown that fatigue behavior of steel reinforcing bars is largely dependent on bar diameter, bar geometry, existing corrosion, and applied stress range. Larger bar diameters generally have a greater likelihood of possessing more flaws compared to a smaller bar which results in a lower fatigue life. Bent bars have been shown to have shorter fatigue lives than straight bars due to the increase in stress concentrations

occurring at bend locations. And studies conclude that corroded bars experience a significant reduction in fatigue strength compared to non-corroded bars (Tilly 1979).

The use of steel reinforcement with deformations has proven to be an ideal mechanism for enhancing the bond between the concrete and steel. However, the presence of deformations produce stress concentrations at the rib root where fatigue cracks tend to initiate. Repeated cyclic stresses cause cracks to propagate within the bar cross section and, as a result, the effective cross section is reduced. Excessive reduction in area eventually results in a sudden brittle fracture of the section. Figure 67 is an example of a steel rebar that was embedded in concrete and subjected to flexural fatigue loading until failure occurred in the rebar. The smooth, dull surface on the right side of the cross section denotes the fatigue crack. The left side exhibits a rough jagged surface which represents the area where tensile fracture occurred due to the weakened cross section from fatigue crack propagation. This bar was located in the same orientation inside the concrete beam where the bottom of the bar was closest to the extreme tension fiber. An interesting observation is that the fatigue crack did not form at the bottom of the bar, but rather on the side of the

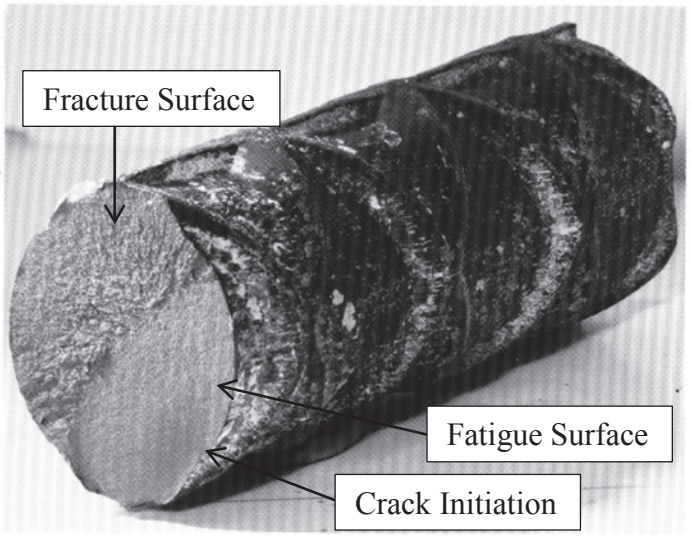


**Figure 67 – Fatigue Fracture of Steel Reinforcing Bar (NCHRP 1976)**

bar at a rib root, which is an area of high stress concentration. This type of crack initiation and propagation is typical of a fatigue failure in the steel reinforcement.

Unlike concrete, reinforcing steel does possess an endurance limit. A summary of available fatigue data for steel rebars tested in RC beams under flexure is given in ACI 215R-97, where all endurance limits are shown to be greater than or equal to 165 MPa (Figure 68). For a steel reinforcing bar with a yield strength, $f_y$, of 414 MPa, this lower bound endurance limit corresponds to 40% of $f_y$. The difference in each curve is due to the variation of minimum stress levels, bar size, steel grade, and bar deformation. There is one

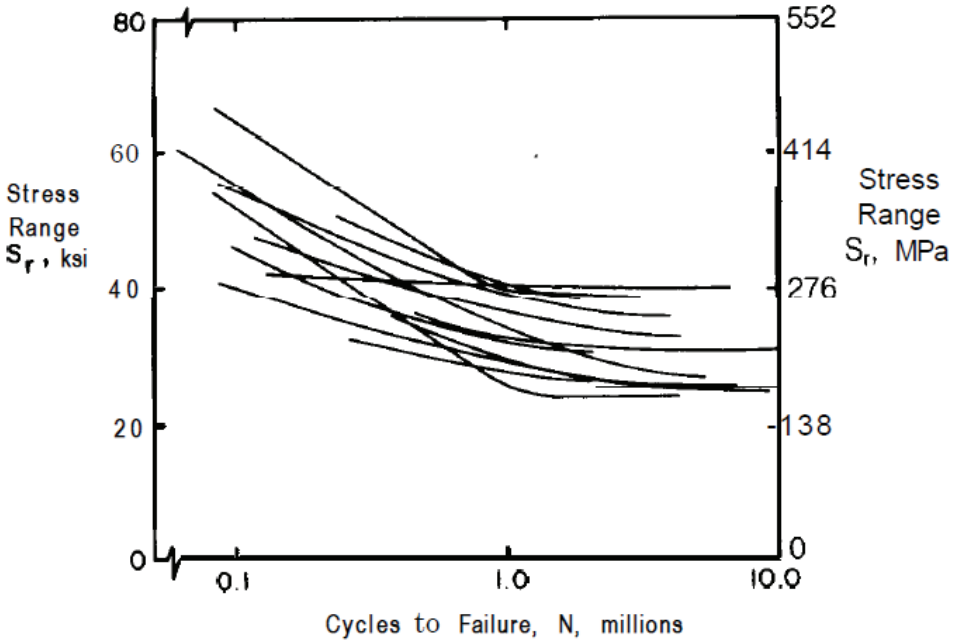


**Figure 68 – S-N Curves For Steel Reinforcing Bars (ACI 215R-97)**

occurrence of a fatigue failure occurring at an applied stress range of 145 MPa for a 35 mm diameter bar at 1.3 million cycles. However, this test was performed at a minimum stress level of 121 MPa and is only one occurrence out of the many other tests performed (ACI 215R-97).

Many have attempted to develop models that numerically define a relationship between stress range and number of cycles. These models are based on numerous repeated flexural tests on concrete beams with steel reinforcing bars. The CEB-FIP (Comite Euro-International du Beton-International Federation for Prestressing) Model Code is considered to be the most relevant in terms of developing equations depicting an S-N relationship for RC containing 15.9-mm diameter reinforcing bars and smaller (Soltani et al. 2012) with the following equations:

$$S_r^5 \times N = 4.08 \times 10^{17} \quad \text{(MPa)} \quad N < 100{,}000{,}000 \tag{1}$$

$$S_r^9 \times N = 7.71 \times 10^{26} \quad \text{(MPa)} \quad 1{,}000{,}000 < N < 100{,}000{,}000 \tag{2}$$

Moreover, there are no equations describing S-N behavior for steel reinforcement in concrete specified by any ACI or AASHTO design standard. The current fatigue provisions prescribed by ACI and AASHTO will be discussed in the following subchapters.

**Fatigue in Reinforced Concrete**

The fatigue performance of RC is a function of both the concrete and steel properties and can be described in three distinct phases. The first phase consists of an initial loss of stiffness due to the development of concrete cracks where local steel-concrete debonding occurs at crack locations. This is followed by a second stage of steady crack propagation, crack widening, and further deterioration of bond between steel and concrete, resulting in gradually increased strains and deflections. Within these two phases, a fatigue crack initiates in the reinforcing steel that steadily propagates within the cross section. After significant reduction in steel area, the RC member approaches the third stage where the rate of strength degradation drastically increases and is no longer steady. A brittle failure occurs in the steel reinforcement and failure of the RC member occurs. The fatigue failure

of RC is thus predominantly dependent on the steel reinforcement, and rarely controlled by concrete (Schläfli and Brühwiler 1998).

**Fatigue in RC Strengthened with FRP Composites**

Although FRP is a relatively new material, there have been a growing number of studies investigating the fatigue performance of externally bonded FRP materials applied to RC (Heffernan & Erki 2004, Ekenel et al. 2006, Dawood et al. 2007, Kim and Heffernan 2008). This is because FRP composites are proving to be a suitable alternative to the strengthening of RC members found in bridges and parking structures, and research on the application of FRP to these structures subjected to fatigue is necessary. A critical review was performed by Kim and Heffernan 2008, which summarizes published technical literature evaluating the fatigue behavior of FRP strengthened RC beams. Studies show that FRP applied to RC increases member stiffness and capacity, delays crack initiation and propagation, reduces crack widths, increases fatigue life and residual strength compared to unstrengthened members. A schematic representation of the improvement in S-N behavior due to FRP strengthening is shown in Figure 69. The enhanced fatigue performance occurs from the

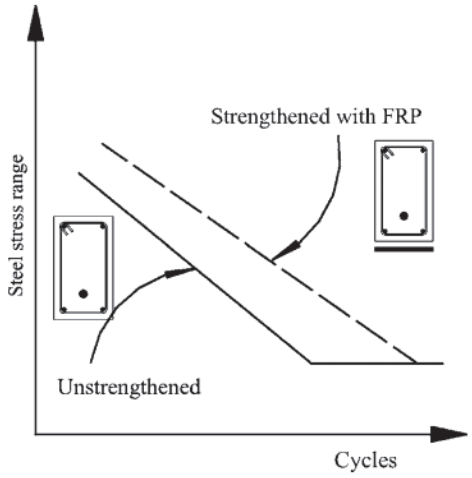


**Figure 69 – Representative S-N Curves for FRP Strengthened and Unstrenthened RC (Kim and Heffernan 2008)**

tendency of FRP to reduce the level of applied stress range in the steel reinforcement. FRP strengthened RC members exhibit a similar damage progression to that of traditional RC where significant damage occurs in the early load cycles followed by gradually accumulated damage, resulting in imminent failure.

Figure 70 illustrates the fatigue behavior of FRP strengthened RC beams with respect to number of cycles. The most common failure mode observed in literature is due to rupture of the steel reinforcement followed by secondary failure of FRP delamination. FRP delamination is described as the debonding of the FRP from the concrete substrate.

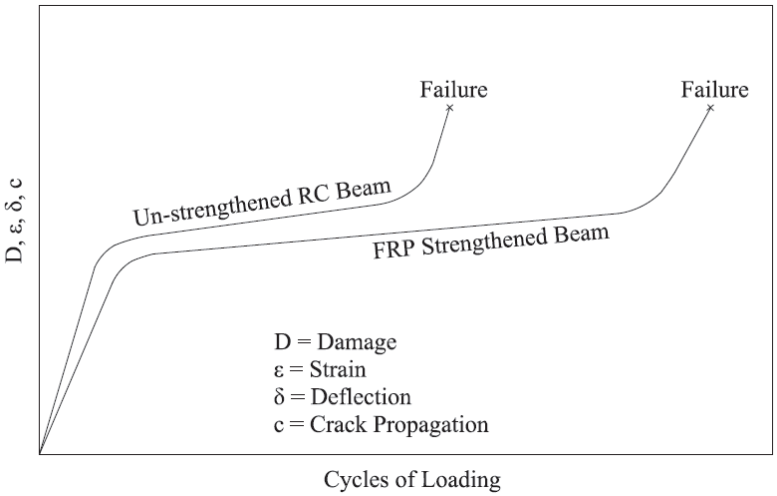


**Figure 70 – Typical Damage Progression for FRP Strengthened RC**

An illustrated sequence of the failure mechanisms observed in FRP strengthened RC beams is shown in Figure 71. Regardless of the reduced stress levels, the steel reinforcement is still more susceptible to fatigue failure than the FRP system and the applied stress range remains to be the critical parameter. Kim and Heffernan concluded that beams subjected to cyclic stress ranges between 30 and 50% of the steel yield stress did not exhibit fatigue failure up to 2 million cycles. To date, little to no studies on the

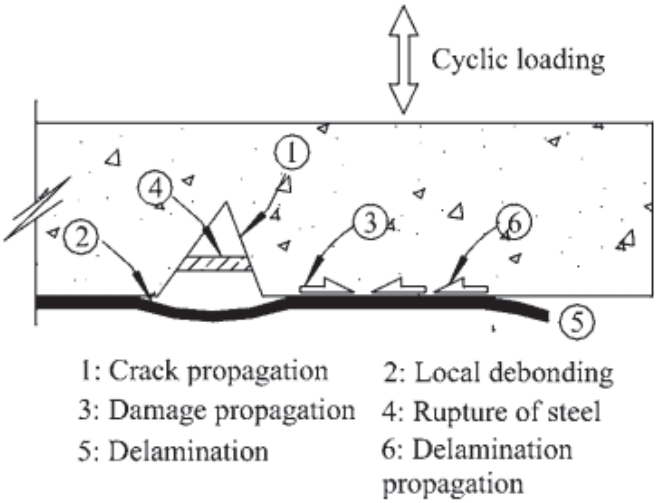


**Figure 71 – Typical Failure Mechanisms Observed in FRP Strengthened RC Beams (Kim and Heffernan 2008)**

fatigue performance of FRCM-strengthened RC have been reported. And while FRP and FRCM have significant differences in material properties, the test methods used to characterize their material properties are fairly similar. This suggests that the fatigue behavior of FRCM strengthened RC beams may be investigated following similar testing procedures given in the publications discussed in Kim and Heffernan 2008.

**Fatigue Design Guidelines**

ACI 215R-97 and AASHTO LRFD (2010) establish design guidelines that limit the applied stress range, $S_r$, to both concrete and steel, as a function of minimum applied stress values. The design specification for concrete specified by ACI 215R-97 states "*the stress range in concrete shall not exceed 40 percent of its compressive strength when the minimum stress is zero, or a linearly reduced stress range as the minimum stress is increased so that the permitted stress range is zero when the minimum stress is 0.75 $f'_c$*" (ACI 215R-97), where $f'_c$ is the 28-day concrete compressive strength. This value of $S_r$ is

based on a conservative prediction of the stress range corresponding to a fatigue life of 10 million cycles. A graphical representation of this relationship is given in Figure 72.

The allowable stress range, $S_r$, for straight deformed steel bars specified by ACI 215R-97 and AASHTO 2010 is determined using the following equations:

$$S_r = 161 - 0.33S_{min} \geq 138 \quad \text{(MPa)} \quad \text{(ACI 215R-97)} \tag{3}$$

$$S_r = 165 - 0.33S_{min} \quad \text{(MPa)} \quad \text{(AASHTO 2010)} \tag{4}$$

Where $S_{min}$ is the minimum applied stress. These equations are based on lower bound endurance limits determined from tests performed on RC beams reinforced with straight

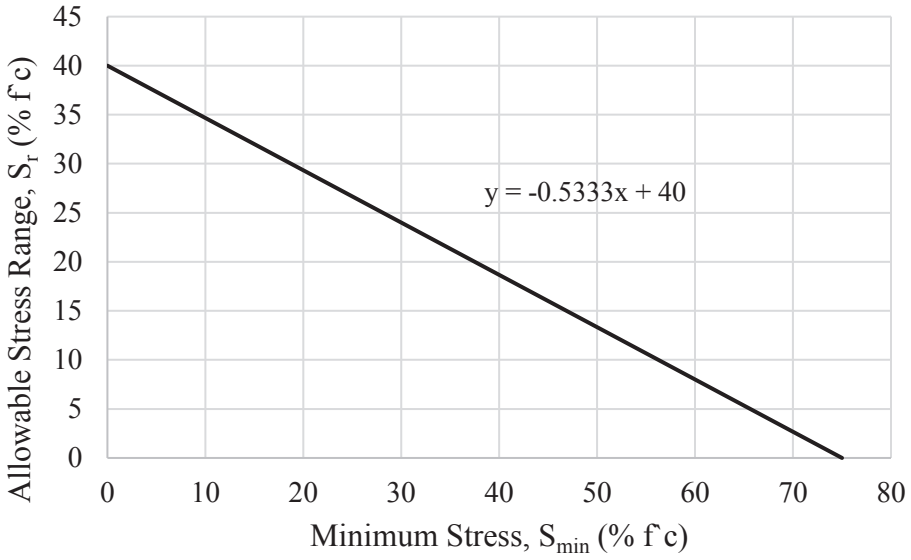


**Figure 72 – Allowable Stress Range Based on Minimum Stress Value for ACI 215R-97**

deformed bars. The fatigue provisions designated by ACI 549.4R-13 for externally bonded FRCM applied to RC state that the stress levels in the steel reinforcement shall not be greater than 80% of the yield strength, $f_y$, under service loading. Also, creep rupture and fatigue limitations are specified for FRCM systems depending on the fabric type, where $f_{fd}$ is the design tensile strength that is determined from ACI 549.4R-13 Section 11.1. Table

25 contains the design stress limits for creep rupture and fatigue for the respective fabric type where $f_{fd}$ is determined as the ultimate tensile strength, $f_{fu}$, taken from tests performed per AC 434 minus one standard deviation.

**Table 25 – Stress Limitations for Fatigue and Creep Rupture (ACI 549.4R-13)**

| AR Glass | Aramid | Basalt | Carbon | PBO |
|---|---|---|---|---|
| $0.20f_{fd}$ | $0.30f_{fd}$ | $0.20f_{fd}$ | $0.55f_{fd}$ | $0.30f_{fd}$ |

**FRCM Strengthened RC Beams Subjected to Fatigue**

A common denominator among the previously discussed topics is the damage progression seen throughout the fatigue life as well as the commonly reported failure mode of fracture in the reinforcing steel that is largely dependent on the applied stress range. The fatigue fracture mode of the steel reinforcement and damage progression behavior is illustrated in Figure 67 and Figure 70, respectively.

In particular, the strengthening of RC structures is a recurring challenge in the transportation infrastructure. When the strengthening of fatigue-prone structures is required, the repaired system needs to maintain a favorable long-term fatigue performance. Seeing as FRCM technology has proven to be a viable repair alternative to fatigue prone RC structures that may require repair, retrofit, and/or rehabilitation, it is critical to understand the fatigue behavior of FRCM. Accordingly, this study aims to investigate experimentally the fatigue performance of RC beams strengthened with FRCM. Beams are divided into two phases: Phase I consisting of static tests where specimens are loaded monotonically to failure, and Phase II comprised of beams subjected to cyclic (fatigue) loading. The experimental parameters that will be investigated include: amount of supplemental reinforcement, ultimate strength, static failure mode, applied stress range,

fatigue life, fatigue failure mode and residual strength. For members subject to cyclic loading, a stress ratio vs. number of cycles (S-N) curve is developed with the objective of defining the endurance limit for the strengthened beams.

**Beam Design and Specimen Preparation**

Fifteen RC beams were designed per ACI 318-14 to be under-reinforced while exceeding the minimum flexural steel requirements and all beams contain shear reinforcement (stirrups) in order to prevent a shear failure. Figure 73 shows the beam geometry and reinforcement details where not all specimens contained externally bonded FRCM materials. RC specimens were prepared by using wooden formwork to give the

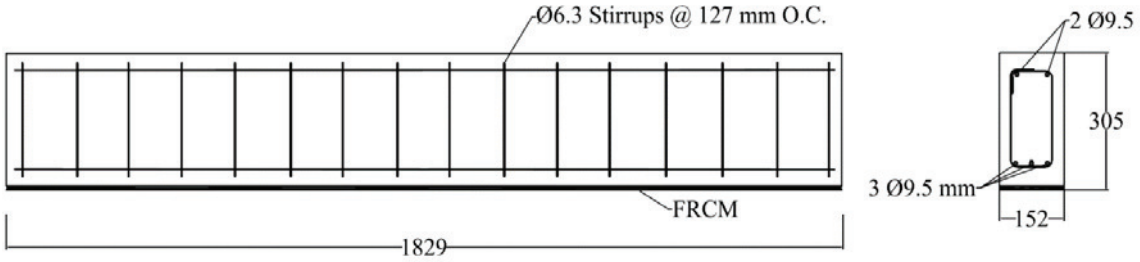


**Figure 73 – RC Beam Geometry and Detailing**

beams the designated concrete shape and finish. The straight deformed bars and stirrups were tied together using steel ties and the final assembly took the form of a steel cage (Figure 74). After the formwork was prepared, RC specimens and cylinder samples were casted following ASTM C192/C192M-07 using Type I Portland cement. The beams and cylinders were left to cure for at least 28 days prior to testing and/or FRCM application. Figure 74 shows the steel cage and formwork prior to and after concrete casting. RC beams were designed with a nominal 28-day concrete compressive strength of 48.3 MPa and design steel yield strength and elastic modulus of 413.7 MPa and 200 GPa, respectively, which are standard material properties specified by engineers in practice.

**Figure 74 – RC Beam Formwork Prior to and After Specimen Preparation**

## Material Characterization

Experimental tests were performed to determine the material properties for the concrete and steel reinforcement. Five concrete cylinder specimens were tested in compression to failure where the maximum loads and corresponding ultimate strengths are summarized in Table 26. After 28 days, the average compressive strength of five concrete cylinders was 52.5 MPa with a coefficient of variation (COV) of 2.65%. The typical failure mode for all concrete cylinders is shown in Figure 75. The steel reinforcing bars were tested in tension as per ASTM A370. A clip on extensometer with a 100-mm gauge length was placed at

**Table 26 – Summary of Concrete Cylinder Compression Tests**

| Specimen ID | Max Load (kN) | Ultimate Strength (MPa) |
|---|---|---|
| C-COMP-1 | 421.7 | 52.0 |
| C-COMP-2 | 443.7 | 54.7 |
| C-COMP-3 | 413.3 | 51.0 |
| C-COMP-4 | 432.3 | 53.3 |
| C-COMP-5 | 415.8 | 51.3 |
| Average | 425.4 | 52.5 |
| St. Dev. | 11.3 | 1.4 |
| COV | 2.65% | 2.65% |


**Figure 75 – Concrete Cylinders Before (left) and After (right) Compression Tests**

mid-length of the specimen to measure strain. Figure 76 represents a typical stress vs. strain curve for a reinforcing bar tested in tension. The yield strength was determined using the total extension under applied load procedure. Table 27 contains a summary of tensile test results for five randomly selected steel samples. The average yield strength of the steel was 471 MPa with a COV of 2.55%, and the average steel elastic modulus was 195 GPa with a COV of 2.23%.

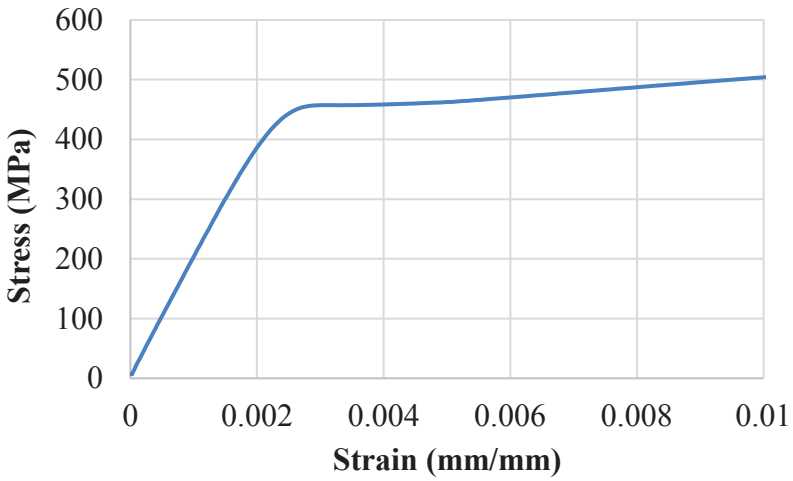


**Figure 76 – Typical Stress vs. Strain Curve for Steel Rebar Tension Tests**

**Table 27 – Summary of Steel Tension Tests**

| Specimen ID | Modulus Of Elasticity (MPa) | Yield Strength (MPa) |
|---|---|---|
| S-Rebar-01 | 188,440 | 459 |
| S-Rebar-02 | 193,584 | 493 |
| S-Rebar-03 | 194,639 | 475 |
| S-Rebar-04 | 198,590 | 463 |
| S-Rebar-05 | 201,127 | 467 |
| Average | 195,276 | 471 |
| St. Dev. | 4,364 | 12 |
| COV | 2.23% | 2.55% |

The FRCM used for application consists of a PBO fabric and (Portland cement based) cementitious matrix enriched with small synthetic fibers. The system is identical to the PBO-FRCM used in the previous studies and the geometric and material properties from can be found in Chapter 2 of this dissertation. Experimental results from 1 ply direct tension tests were used for this study and are summarized in Table 28. In some cases, the

**Table 28 – FRCM Direct Tension Test Results**

| Description | Symbol | Units | Value |
|---|---|---|---|
| Modulus of elasticity of the uncracked specimen | $E_f$* | GPa | 1,805.5 |
| Modulus of elasticity of the cracked specimen | $E_f$ | GPa | 127.7 |
| Ultimate tensile strength | $f_{fu}$ | MPa | 1,664 |
| St. Dev. Ultimate Strength | $\sigma_{f_{fu}}$ | MPa | 77 |
| Ultimate tensile strain | $\varepsilon_{fu}$ | mm/mm | 0.0176 |
| St. Dev. Ultimate Strain | $\sigma_{\varepsilon_{fu}}$ | mm/mm | 0.0015 |

design properties are used in lieu of experimental properties to perform structural calculations. In an attempt to avoid confusion, Table 29 was developed to clearly present anddistinguish between the design and experimental material properties. The effective FRCM tensile strain used for design, $\varepsilon_{fe}$, is defined as follows:

$$\varepsilon_{fe} = \begin{cases} \varepsilon_{fd} \leq 0.012 & \text{for FRCM failure} \\ \varepsilon_{cu}\left(\dfrac{d_f - c}{c}\right) - \varepsilon_{bi} \leq \min(\varepsilon_{fd}, 0.012) & \text{for concrete crushing} \end{cases}$$

**Table 29 – Summary of Design and Experimental Material Properties**

| Material | Description | Design | Experimental |
|---|---|---|---|
| Concrete | 28-Day Strength | $f'_c$= 48.3 MPa | $f'_c$ = 52.5 MPa |
| Steel | Yield Strength | $f_y$ = 413.7 MPa | $f_y$ = 471 MPa |
| Steel | Modulus of Elasticity | $E_s$=200 GPa | $E_s$=195 GPa |
| FRCM | Ultimate Tensile Strength | $f_{fe}$= 1,532 MPa | $f_{fu}$= 1,664 MPa |
| FRCM | Cracked Modulus | $E_f$ = 127.7 GPa | |
| FRCM | Ultimate strain | $\varepsilon_{fe}$ = 0.012 mm/mm | $\varepsilon_{fu}$ = 0.0176 mm/mm |

Where $\varepsilon_{fd}$ is the design FRCM strain defined as $\varepsilon_{fd} = \varepsilon_{fu} - \sigma_{\varepsilon_{fu}}$ which are determined from the experimental material properties given in Table 28 and $\varepsilon_{cu}$ is equal to a maximum compressive concrete strain of 0.003. The design effective tensile strength is then determined to be $f_{fe} = E_f \varepsilon_{fe}$, where $E_f$ is both the design and experimental modulus of elasticity taken from Table 28 with no reduction.

**FRCM Configuration**

For an optimal increase in flexural strength, the FRCM system is applied to the bottom soffit of each beam. As the RC beam cracks, the neutral axis shifts upward and any concrete material below the neutral axis provides little to no flexural resistance where the steel carries the tension component of the internal moment couple. Placing FRCM on the bottom soffit is ideal because the lever arm from the FRCM to the neutral axis is at its maximum and the FRCM ideally provides an increase in flexural strength. FRCM application consists of rotating the beam 180 degrees in order to apply FRCM to the bottom soffit. Once the beam was rotated, the compressive bars in turn became subjected to tensile stresses and successfully mitigated cracking due to self-weight. The *design* material properties were used in conjunction with ACI 549.4R-13 to determine theoretical design flexural capacities for various configurations of FRCM strengthening. The analysis was performed based on the given assumptions and possible failure modes specified in Section 11.1 of ACI 549.4R-

13. An example of the design calculations performed is given in Appendix E. Design capacities with the corresponding strength reduction factor ($\phi$) and enhancement ratios for several layers of FRCM strengthening are given in Table 30. The enhancement is the ratio of the strengthened member to the unstrengthened beam based on the material properties shown in Column 3 of Table 29. It is noteworthy to mention that ACI549.4R limits the increase in flexural strength to 50% of the un-strengthened member ($\phi P_{n,strengthened} \leq 1.5\phi P_{n,control}$). This limitation is applicable to an external reinforcement of five layers which exhibits a 58% design increase. The five layer reinforcement was the only FRCM configuration that was limited to this 50% increase constraint. Based on the results in Table 30, the enhancement ratios for one, three, and five FRCM layer(s) represent the lower (8%), middle (33%), and upper bound (50%) enhancement values, respectively. For this reason,

**Table 30 – Design Capacities**

| External Reinforcement | $\phi P_n$ (kN) | Enhancement $\phi P_{n,strengthened}/\phi P_{n,control}$ |
|---|---|---|
| None (Control) | 54.7 | 1.00 |
| 1 Layer | 59.0 | 1.08 |
| 2 Layers | 66.0 | 1.21 |
| 3 Layers | 72.8 | 1.33 |
| 4 Layers | 79.7 | 1.46 |
| 5 Layers | 82.1 | 1.50 |

one, three and five FRCM layers were applied to several RC beams. Two beams were strengthened with one FRCM layer, seven were strengthened with three layers of FRCM, two with five layers of FRCM, and the remaining four beams were left unstrengthened.

**FRCM Application**

The FRCM sequence of application is shown in Figure 77. The FRCM application consisted of pressure washing the bottom soffit of the concrete beams and removing any

loose particles using a high pressure water hose. The concrete substrate was maintained saturated-surface-dry prior to the application of the matrix mortar. The mortar was prepared and applied using a trowel with a thickness of 3 to 4 mm to the beam bottom face. A 1.83 m long pre-cut PBO fabric was placed and embedded into the mortar with the primary direction orientated along the longitudinal length of the beam. A trowel was used to embed the mesh into the matrix where a second layer of mortar of equal thickness was then applied to create a sandwich around the fabric. This procedure was repeated until the desired number of layers was applied. Beams with FRCM were left to cure for a minimum of 28 days prior to testing.

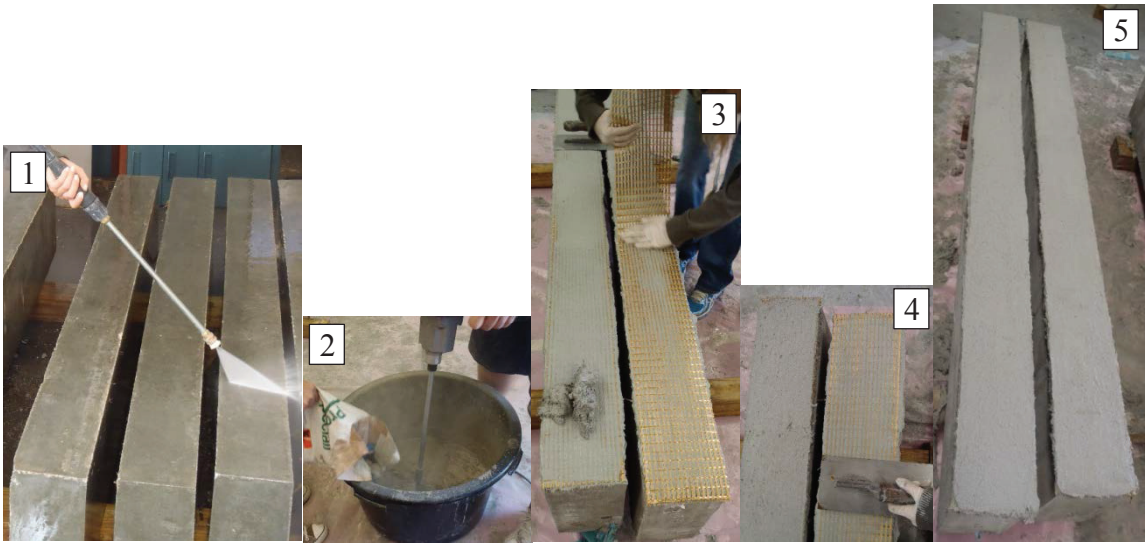


**Figure 77 – FRCM Sequence of Application 1) Water Pressure Cleaning 2) Mortar Mixing 3) Fabric Application 4) Fabric Impregnation 5) Finished Specimens**

### $\beta^f$ Factor

Seeing as the steel reinforcement and the PBO-FRCM system have different material and geometrical characteristics, it is necessary to speak in a language that is universal to

all types of material systems. Comparison between the two systems is performed by developing a stiffness-dependent factor, $\kappa$, for each material which is defined as:

$$\kappa^{\mathrm{s}} = \rho_s E_s \quad \text{(MPa) for Steel;}$$

$$\kappa^{\mathrm{f}} = \rho_f E_f \quad \text{(MPa) for FRCM;}$$

Where $E_s$ and $E_f$ are the design elastic moduli for steel and FRCM, respectively, found in column 3 of Table 29. The reinforcement ratios $\rho_s$ and $\rho_f$ are for steel and FRCM, respectively, which can be determined using the following equations:

$$\rho_s = \frac{A_s}{bd}$$

$$\rho_f = \frac{nA_{f.unit}}{bh}$$

Where $A_s$ is the effective area of steel, $b$ is the beam width, $d$ is the distance from the extreme compressive fiber to the steel reinforcement, $n$ is the number of FRCM layers, $A_{f.unit}$ is the effective area per unit width of FRCM, and $h$ is the beam height. All beams possess a tension steel reinforcement ratio of $\rho_s$= 0.55% which yields $\kappa^{\mathrm{s}}$ = 1054 MPa. The $\kappa^{\mathrm{f}}$ for FRCM varies depending on the number of layers used for strengthening. The contribution from each FRCM configuration (one, three, or five layers) is compared to that of the steel reinforcement using an expression, $\beta^{\mathrm{f}}$, which is determined as follows:

$$\beta^{\mathrm{f}} = \kappa^{\mathrm{f}}/\kappa^{\mathrm{s}}$$

Values of $\kappa^{\mathrm{f}}, \kappa^{\mathrm{s}}$, and $\beta^{\mathrm{f}}$ for various types of FRCM strengthening are given in Table 31. Given the plurality of fibers (from low to high modulus) and fabric weights (low to high equivalent thickness) in addition to having multi-fabric construction, the $\beta^{\mathrm{f}}$ parameter serves the function of allowing a designer to tailor the amount of FRCM to the strengthening requirements.

**Table 31 – Summary of Reinforcement Factors**

| External Reinforcement | $\kappa^s$ (Mpa) | $\kappa^f$ (Mpa) | $\beta^f = \kappa^f / \kappa^s$ (%) |
|---|---|---|---|
| None | 1054 | - | - |
| 1 Layer | | 19 | 1.7% |
| 3 Layers | | 56 | 5.1% |
| 5 Layers | | 93 | 8.5% |

**Theoretical Analysis**

For evaluation and differently from the design values determined previously, the *experimental* material properties from column 4 in Table 29 were used in accordance with the methodology given in ACI 549.4R to theoretically predict the *experimental* behavior of the beams at the level of yielding of the tension steel and at ultimate conditions. Only experimental values were used and no reduction values were incorporated. The analysis was based on the following assumptions: the concrete was modeled using Todeschini's relationship for stress-strain behavior, strain compatibility is satisfied, equilibrium of the section is satisfied, and perfect bond exists between FRCM and concrete as well as between concrete and steel. In addition, the following failure modes were checked to determine which of the following failure modes control at ultimate conditions: concrete crushing and FRCM failure (rupture and/or delamination). Appendix F contains an example of the detailed calculations used to determine the theoretical experimental capacities of both strengthened and un-strengthened members. A summary of the theoretical load values for both static yield and ultimate states with the corresponding enhancement ratios are given Table 32 where enhancement ratios are defined as the ratio of the strengthened RC element to the control RC member. The specimen ID is dependent on the type of test and will be

describe in the following sub-chapters. There is a significant difference between the theoretical design and theoretical experimental values. The former is determined by the

**Table 32 – Summary of Theoretical Experimental Values**

| Specimen ID | External Reinforcement | $\beta^f$ (%) | Yield | | Ultimate | |
|---|---|---|---|---|---|---|
| | | | $P_{y,Th}$ (kN) | Enhancement $P_{y,Th,strengthened}/P_{y,Th,control}$ | $P_{u,Th}$ (kN) | Enhancement $P_{u,Th,strengthened}/P_{u,Th,control}$ |
| S-CONa | None | - | 62.5 | 1.00 | 89.5 | 1.00 |
| S-FRCM-1P | 1 Layer | 1.7% | 64.5 | 1.03 | 90 | 1.01 |
| S-FRCM-3P | 3 Layers | 5.1% | 68.4 | 1.09 | 112 | 1.25 |
| S-FRCM-5P | 5 Layers | 8.5% | 72.3 | 1.16 | 134 | 1.50 |

engineer in practice which uses nominal material properties, stress and strain limitations as well as strength reductions factors, while the latter is determined to predict actual experimental behavior and uses experimental material properties with no limitations or reduction factors. Figure 78 shows both the design and experimental values plotted with

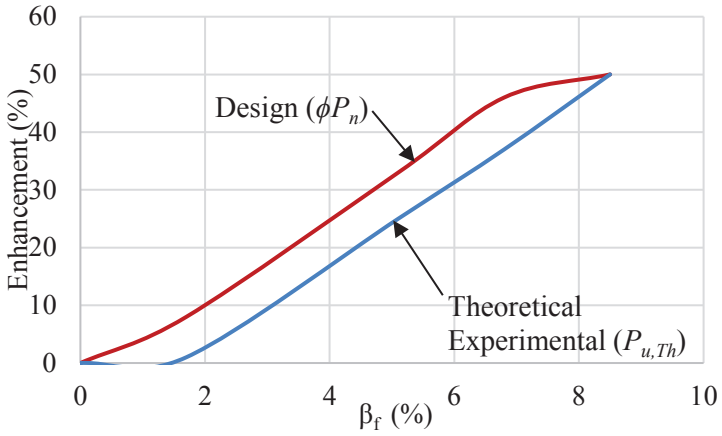


**Figure 78 – Design and Theoretical Experimental Enhancement for Values of $\beta^f$**

respect to the corresponding $\beta^f$ factor. Once validated experimentally, these curves will provide guidance for engineers in practice to choose a suitable amount of FRCM reinforcement for RC strengthening.

**Test Setup**

A three-point bending test configuration with a 1.54 m span was used for all specimens. Beams were instrumented with 6-mm and 60-mm strain gauges. Two 6-mm strain gauges applied to the center tension steel rebar measured tensile strain, two 60-mm gauges measured compressive strain in the concrete near midspan, and three 60-mm gauges measured tensile strain in the FRCM at midspan. In addition, three linear variable differential transducers (LVDTs) were placed at midspan and each support to measure deflection and settlement. To better simulate field conditions, a concrete grinder was used to cut the FRCM material adjacent to the supports so that the supports would not function as FRCM anchors. Figure 79 and Figure 80 show the test setup, instrumentation layout,

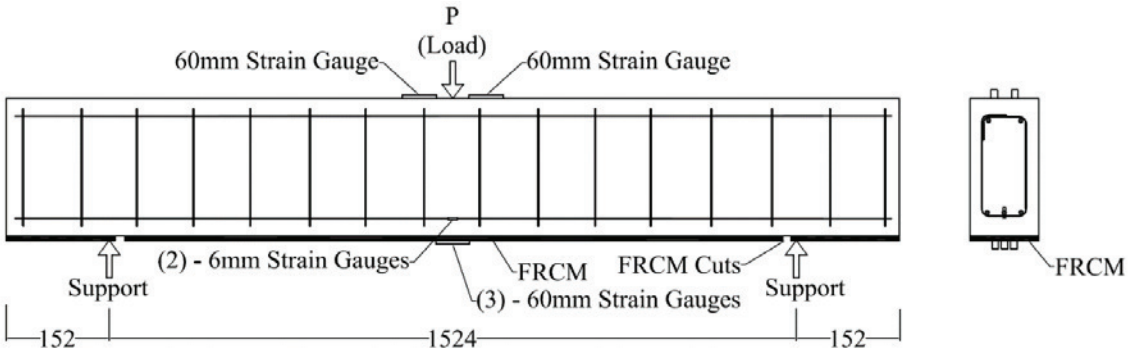


**Figure 79 – Load Configuration and Strain Gauge Instrumentation (dimensions in mm)**

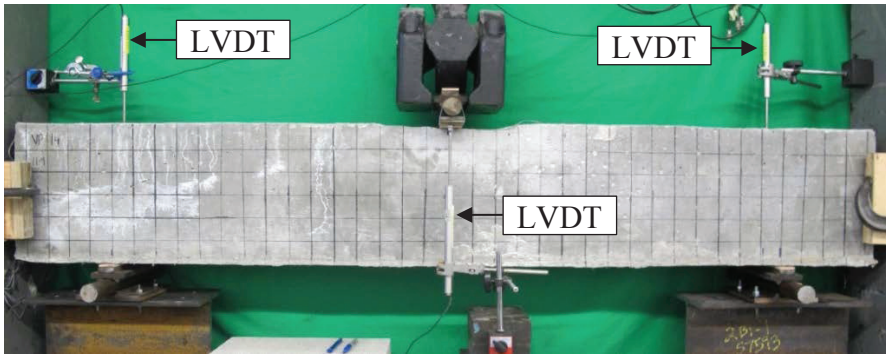


**Figure 80 – Load Configuration and LVDT Instrumentation**

and FRCM cut locations. Each specimen was tested with a 250-kN hydraulic actuator on a fatigue rated test frame. The applied load was measured using an internal force transducer connected to the actuator.

**Experimental Procedure**

The fifteen RC beams under evaluation were divided into two phases. In phase I, five specimens were tested monotonically to failure. Phase II consisted of ten beams subjected to fatigue loading. All loading procedures were determined based on the theoretical yield and ultimate capacities given in Table 32.

**Phase I**

Beams in the first phase were tested at a load controlled rate of 0.22 kN/sec with a total of 4 quasi-static loading and unloading cycles, followed by a final displacement-controlled load rate of 0.032 mm/sec up to failure. The maximum value for each loading cycle was determined to investigate beam performance before and after concrete cracking as well as before and after steel yielding. An illustrative example of the load steps are presented in Figure 81. Beams in Phase I consist of five beams total: two un-strengthened beams, and three RC beams each strengthened with one, three, and five layers of FRCM, respectively.

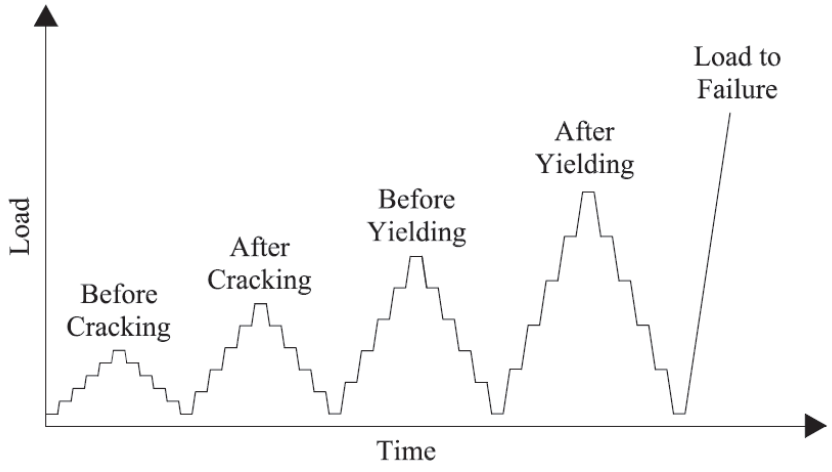


**Figure 81 – Typical Loading Cycles**

**Phase II**

Phase II consisted of initially pre-cracking each beam and then applying a cyclic fatigue loading resembling that of a sine wave at a load rate of 2 Hz (2 cycles/sec). The reference value used herein is the theoretical static load at which yielding of the reinforcing steel occurs in the beam, which has been previously discussed and can be found in Table 32. All cyclic (fatigue) loads are comprised of a maximum and minimum load, which are referred to a percentage of the static yield (PSY) load. Based on the simulation of a typical RC slab bridge designed according to AASHTO LFRD (2010), a minimum load value equivalent to 20 percent of the static yield (20 PSY) was used for all cyclic tests. Details of the simulated RC slab bridge can be found in Appendix G. Figure 82 illustrates the initial pre-cracking using 3 quasi-static load cycles followed by the cyclic loading and the maximum load in the 3rd quasi-static load cycle corresponds to the peak cyclic load value.

In previous studies, it has been shown that RC beams subjected to fatigue loads experience failure mainly due to fatigue rupture of the steel reinforcement and less

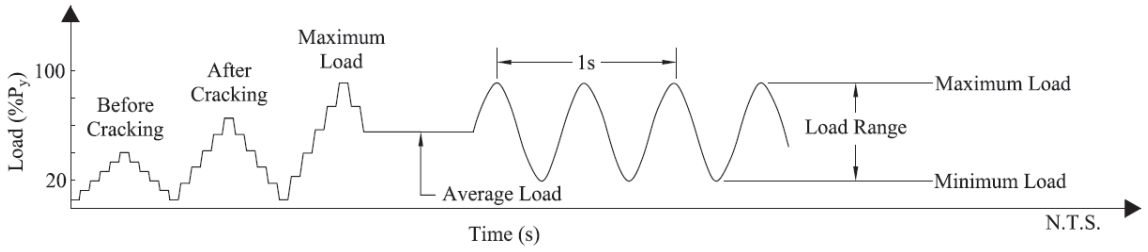


**Figure 82 – Pre-cracking and Cyclic Loading**

commonly by fatigue failure of the concrete. Therefore, it is necessary to address the fatigue limitations for steel provided by ACI 215R-97 and AASHTO LRFD (2010). For a minimum load of 20 PSY, a corresponding stress in the steel of 94 MPa is induced. Using equations (3) and (4), ACI 215R-97 and AASHTO LRFD (2010) specify an allowable

stress range of 138 MPa and 162 MPa, respectively. These values correspond to a peak of load of 50 PSY and 55 PSY. Thus, if the applied maximum load is less than 50 PSY, there should be no failure in the steel reinforcement up to 2 million cycles. But, if the maximum load is larger than 55 PSY, there is a significant likelihood that the steel will fail due to fatigue before reaching 2 million cycles. In addition, ACI 549.4R-13 limits the tensile stress in the steel reinforcement to be 80 PSY during service loading, but this number has yet to be experimentally verified. Seeing as the purpose of this study is to strengthen RC beams with FRCM and apply fatigue loads that will challenge the fatigue behavior in the steel, all maximum load values were chosen to be larger than the maximum permitted values specified by ACI 215R-97 (50 PSY), AASHTO LRFD 2010 (55 PSY), and ACI 549.4R-13 (80 PSY).

It is also necessary to ensure that concrete stresses do not exceed the fatigue provisions specified by ACI 215R-97. A minimum load of 20 PSY corresponds to a concrete stress of 4.9 MPa which yields 10% of the concrete compressive strength ($f`_c$) and according to Figure 72, the maximum allowable stress range in the concrete is 35% of $f'_c$. This corresponds to a maximum stress of 45% of $f'_c$. As a result, all maximum load values were chosen to induce concrete stresses less than the threshold of 45% of the concrete compressive strength ($f`_c$). Accordingly, the first peak load was set at 90 PSY corresponding to a theoretical maximum concrete compressive stress of 40% $f`_c$ and maximum FRCM stress of 335 MPa which is 23% of $f_{fd}$, as shown in Figure 83. Note that the stress in the FRCM satisfies the fatigue limit of 30% $f_{fd}$ provided by ACI 549.4R-13 in Table 25, which further predicts that failure will likely occur in the steel reinforcement. Based on the observed behavior from the first test, the following maximum load values

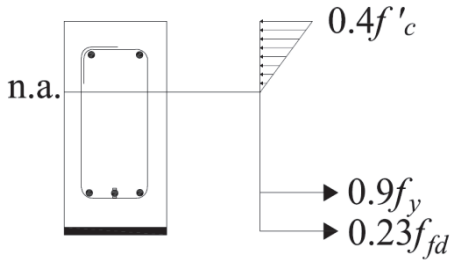


**Figure 83 – Stress Distribution for FRCM Strengthened Beam**

were selected for the subsequent beams subject to cyclic loading: 85 PSY, 80 PSY, and 75 PSY, as summarized in Table 33. All cyclic loads were applied until failure of the specimens or 2 million cycles, whichever occurred first. All beams that reached a fatigue life of 2 million cycles were tested statically to determine the post-fatigue residual strength. The same load procedure used for Phase I static tests was used for the Phase II residual static tests. Of the ten beams subjected to fatigue loads, six beams were strengthened with three layers of FRCM, which depicts the middle bound enhancement ratio and represents a realistic strengthening scheme that would be used by engineers in practice, resulting in a 33% nominal increase in design strength (from Table 30). Two RC beams were strengthened with one and five layers of FRCM, respectively, and the remaining two beams were left un-strengthened. Table 33 contains a description of each specimen in Phase I and II, which are labeled using the "*A–B–C-D*" format, where "*A*" represents the test type (F for Fatigue and S for Static), "*B*" represents the beam type (CON for control beams and FRCM for PBO strengthened beams), "*C*" denotes the number of FRCM layers applied (1P for one layer, 3P for three layers, and 5P for five layers), and "*D*" represents the maximum cyclic load value (75 for 75PSY, 80 for 80PSY, 85 for 85PSY and 90 for 90PSY) for fatigue tests.

Based on the maximum load levels, an additional step was taken to predict the number of cycles at which failure would occur in the steel reinforcement. This prediction

**Table 33 – Test Matrix for Specimens in Phase I and Phase II**

| Specimen | Load Type | External Reinforcement | Max Load (PSY) |
|---|---|---|---|
| S-CONa | Static | None | - |
| S-CONb | | | |
| S-FRCM-1P | | 1 Layer | |
| S-FRCM-3P | | 3 Layers | |
| S-FRCM-5P | | 5 Layers | |
| F-FRCM-3P-90 | Cyclic (Fatigue) | 3 Layers | 90 |
| F-FRCM-3P-85 | | | 85 |
| F-FRCM-3P-80a | | | 80 |
| F-FRCM-3P-80b | | | |
| F-FRCM-3P-75a | | | 75 |
| F-FRCM-3P-75b | | | |
| F-CON-0-75a | | None | 75 |
| F-CON-0-75b | | | |
| F-FRCM-1P-75 | | 1 Layer | 75 |
| F-FRCM-5P-75 | | 5 Layers | 75 |

is based on the previously discussed equations (1) and (2). Table 34 summarizes the maximum load values, equivalent stress range, and predicted fatigue life for each peak load. It is predicted that all maximum load values will result in fatigue failure prior to

**Table 34 – Fatigue Life Prediction Based on Maximum Load**

| Peak Load (PSY) | Stress Range ($S_r$) | Predicted Fatigue Life ($N$) |
|---|---|---|
| 90 | 330 | 104,827 |
| 85 | 306 | 251,843 |
| 80 | 283 | 226,572 |
| 75 | 259 | 350,065 |
| 70 | 235 | 563,783 |
| 65 | 212 | 894,715 |
| 61 | 194 | 2,000,000 |
| 60 | 188 | 2,582,601 |
| 55 | 165 | 8,589,835 |
| 50 | 141 | 34,395,839 |
| 48 | 132 | 63,999,255 |
| 47 | 127 | 88,781,672 |

2 million cycles. The maximum load corresponding to 2 million cycles is determined to be 60 PSY which is slightly larger than the conservative values specified by ACI 215R-97 (50 PSY) and AASHTO LRFD (2010) (55 PSY).

**Phase I Test Results**

All beams in Phase I were tested statically to failure. For each specimen, an experimental load vs. deflection envelope was plotted, which does not include unloading portions from the loading cycles described in the experimental program. Each load-deflection graph also contains a theoretical three line prediction (dotted line with rectangular markers) of the expected behavior during testing as well as a dashed line that corresponds to the design capacity from Table 30. All unstrengthened beams exhibited traditional RC beam behavior that can be described in in three ascending phases: concrete cracking, steel yielding, and concrete crushing. Accordingly, the three phases observed in beams strengthened with FRCM consisted of concrete cracking, steel yielding, and ultimate FRCM failure. It is noteworthy to mention that all steel strain gauges performed satisfactory until the onset of concrete cracking. In almost all cases, the steel strain gauges recorded abnormal strain values post-concrete cracking. This is possibly due to the friction between the strain gauge and the concrete at the steel-concrete interface that caused the strain gauge to "strip off" during loading. Due to this unfortunate occurrence, the corresponding yield loads were determined by performing a cross sectional analysis using known concrete compressive strain, FRCM tensile strain, and deflection values.

**S-CONa and S-CONb**

Two unsrengthened RC beams, S-CONa and S-CONb were tested statically to failure. Figure 84 and Figure 85 illustrate the theoretical, experimental, and design behavior where

a description of each loading phase corresponds to the experimental curve. Due to the similarity in behavior, the average load values of the two tests will be discussed. The first (flexural) crack occurred when the stress in the bottom of the soffit reached the concrete

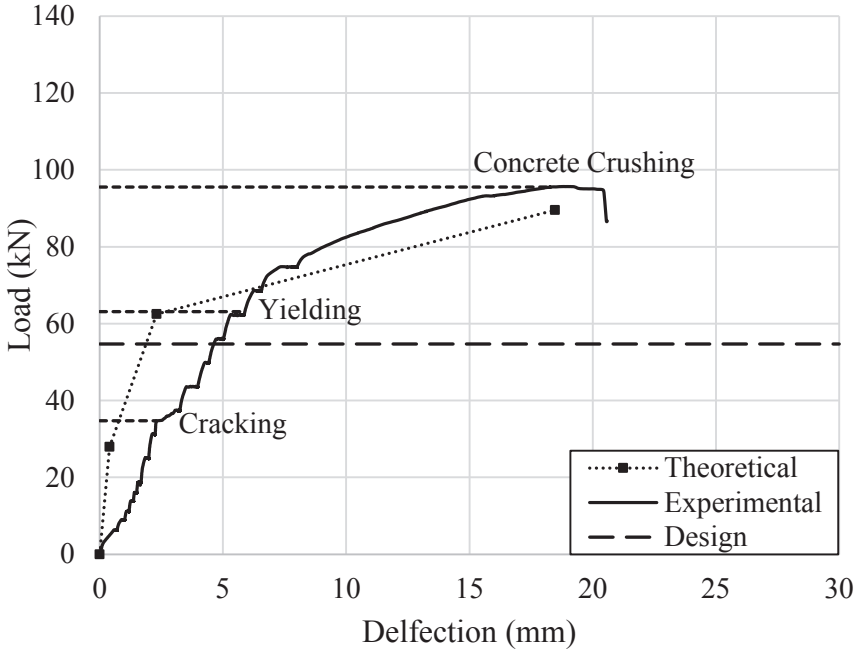


**Figure 84 – Load vs. Deflection for S-CONa**

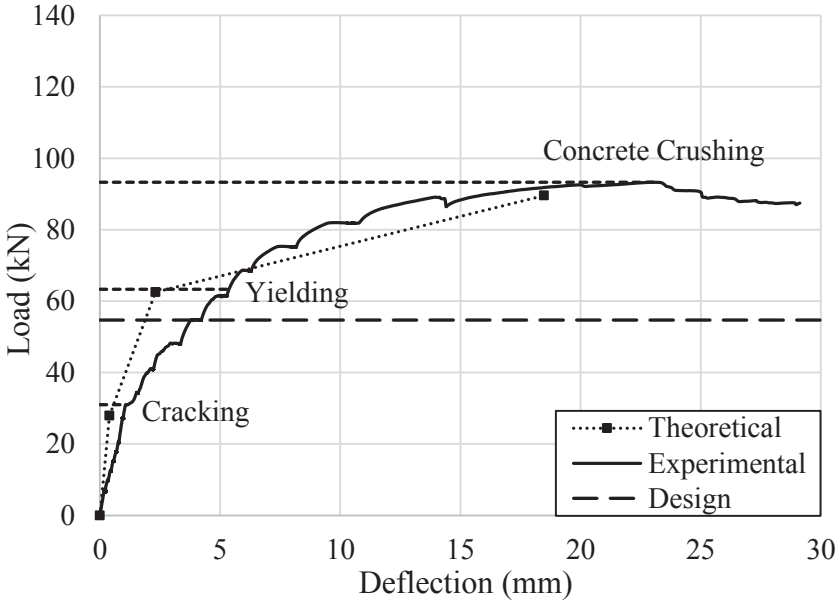


**Figure 85 – Load vs. Deflection for S-CONb**

modulus of rupture. This occurred at an average load of 32.9 kN at the location of maximum moment, under the load point. As more cracks formed, the stiffness of the system decreased and the load approached the yield load at an average value of 63.1 kN. Post-yielding, the system exhibited an increasing rate of stiffness degradation and showed significant deflection. The average maximum load occurred at 97.1 kN at which point the beam failed due to concrete crushing. The theoretical curves proved to be conservative in predicting the load-deflection values for each load phase.

**S-FRCM-1P**

Specimen S-FRCM-1P strengthened with 1 layer of FRCM was tested statically to failure. In the load-deflection curve for S-FRCM-1P given in Figure 86, the first crack occured at 34.2 kN. Further cracking was observed as the stiffness decreased and approached a yield load of 66.6 kN. The post-yield stiffness of system began to deteriorate as fabric slippage intiates at the location of a flexural crack in the area of maximum moment

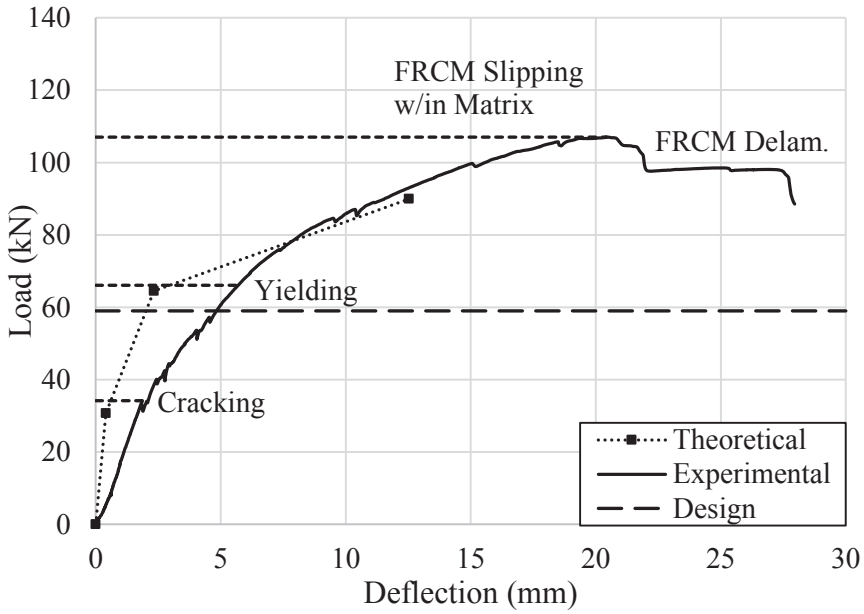


**Figure 86 – Load vs. Deflection for S-FRCM-1P**

which is at midspan. The fabric-matrix slip gradually propagated outward towards the support as the curve reached a maximum load of 107 kN. As slippage continued, eventually the FRCM could no longer carry the applied load and FRCM delamination suddnely occured at the midspan. This mechanism can be confirmed by the sudden drop of the load-deflection curve (Figure 86). Following delamination, the FRCM contribution is lost and the beam behaviour falls back to that of a RC beam. Ultimately, the failure mode of specimen was initially due to slipping of the fabric in the matrix followed by a secondary failure mode of FRCM delamination.

**S-FRCM-3P**

The load-deflection curve for specimen S-FRCM-3P strengthened with three layers of FRCM is shown in Figure 87. Similar to S-FRCM-1P, the first crack was observed at 34.2 kN. After reaching a yield load of 68.9 kN, the system exhibited a stiffness greater than S-FRCM-1P. The load reached a maximum value of 125.7 kN, when a sudden FRCM

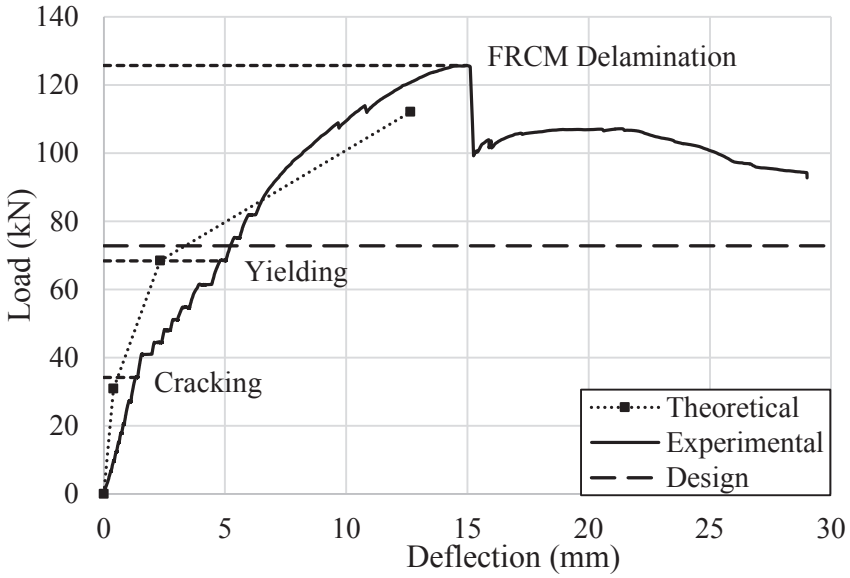


**Figure 87 – Load vs. Deflection for S-FRCM-3P**

delamination occurred, which initiated at the mouth of a wide flexural crack in the area of maximum moment (midspan) and propagated outward towards the support. Following delamination, the specimen behaved similar to the benchmark specimens containing no FRCM strengthening.

**S-FRCM-5P**

Beam S-FRCM-5P with five layers of FRCM exhibited a similar behavior to S-FRCM-3P up to a cracking load of 37.2 kN and subsequently to a yield load of 72.5 kN (Figure 88). The post-yield stiffness was significantly high and as the load-deflection curve began to lose stiffness, a sudden pre-mature FRCM delamination occurred. The resulted maximum load was 96.9 kN which was less than both S-FRCM-1P and S-FRCM-3P specimens. In fact, the load was almost exactly equal to the ultimate load observed for the control specimens S-CONa and S-CONb.

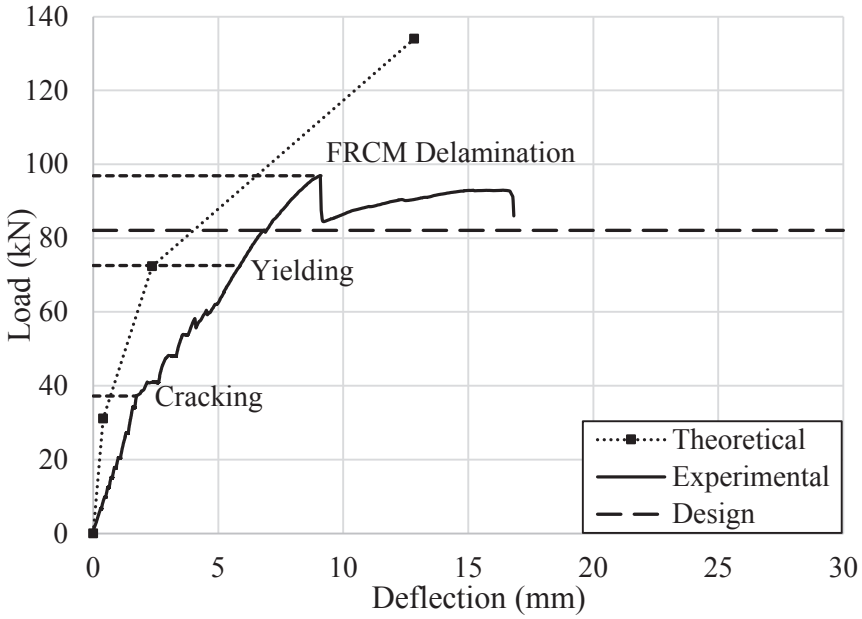


**Figure 88 – Load vs. Deflection for S-FRCM-5P**

**Discussion of Phase I Tests**

A comparison of all load-deflection curves for the Phase I tests is given in Figure 89. Similarly, a summary of all experimental and theoretical yield and ultimate load values are given in Table 35 and Table 36, where S-CON* denotes the average of specimen S-CONa and S-CONb. The theoretical values are determined using the experimental material properties. The strength enhancement is the ratio of FRCM strengthened member to the average benchmark value and all experimental results were compared to theoretical values.

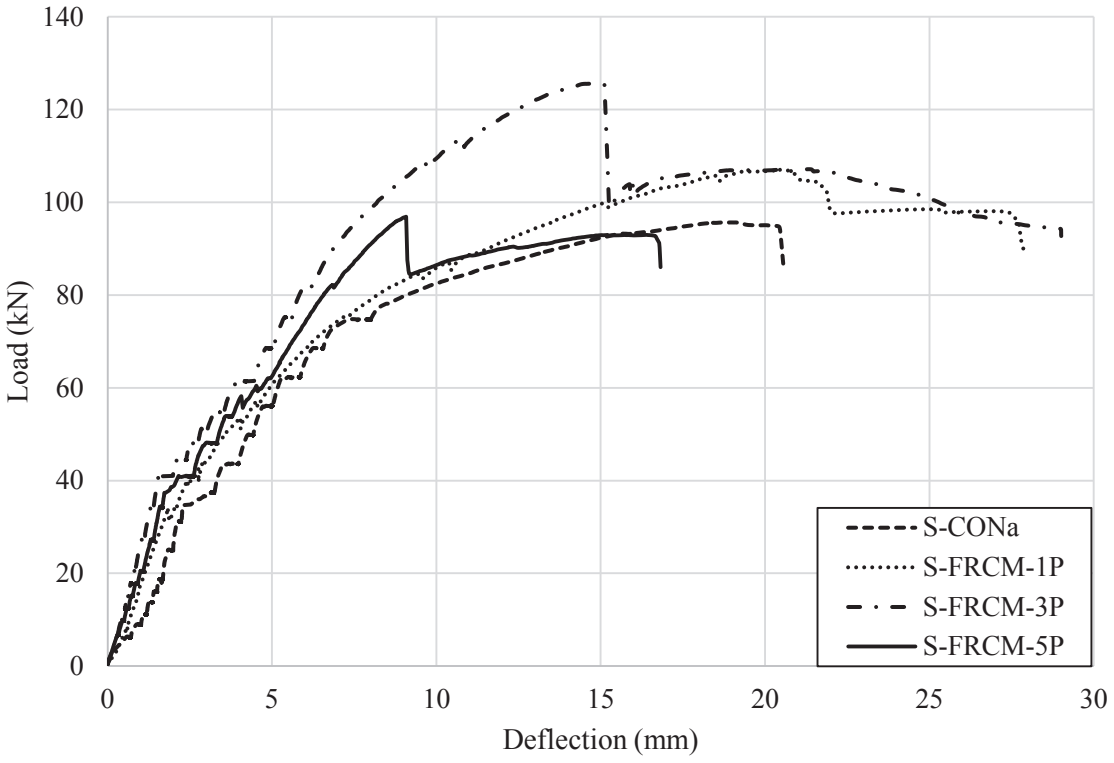


**Figure 89 – Load vs. Deflection for Phase I Specimens**

All five beams exhibited similar behavior up to cracking where the cracking load was not significantly affected by the FRCM application. All FRCM strengthened specimens displayed a greater post cracking stiffness than the benchmark specimens up to steel yielding, with S-FRCM-3P showing the greatest stiffness increase followed by S-FRCM-

5P and S-FRCM-1P. All FRCM strengthened specimens exhibited an increase in static yield relative to the benchmark specimens. The greatest static yield value was observed in S-FRCM-3P followed by S-FRCM-5P, and S-FRCM-1P.

**Table 35 – Static Tests Results: Yield Load ($P_y$)**

| Specimen ID | $\beta^f$ (%) | Theoretical | Experimental | | Experimental/Theoretical |
|---|---|---|---|---|---|
| | | $P_{y,Th}$ (kN) | $P_{y,avg}$ (kN) | Enhancement $P_{y,strengthened}/P_{y,control}$ | $P_{y,avg}$ / $P_{y,Th}$ |
| S-CON* | - | 62.5 | 63.7 | 1.00 | 1.02 |
| S-FRCM-1P | 1.7% | 64.5 | 66.6 | 1.05 | 1.03 |
| S-FRCM-3P | 5.1% | 68.4 | 68.9 | 1.08 | 1.01 |
| S-FRCM-5P | 8.5% | 72.3 | 73.1 | 1.15 | 1.01 |

*Represents the average of S-CONa and S-CONb control beams

**Table 36 – Static Tests Results: Ultimate Load ($P_u$)**

| Specimen ID | $\beta^f$ (%) | Theoretical | Experimental | | Experimental/Theoretical |
|---|---|---|---|---|---|
| | | $P_{y,Th}$ (kN) | $P_{u,avg}$ (kN) | Enhancement $P_{u,strengthened}/P_{u,control}$ | $P_{u,avg}/P_{u,Th}$ |
| S-CON* | - | 89.5 | 97.1 | 1.00 | 1.08 |
| S-FRCM-1P | 1.7% | 90 | 107.02 | 1.10 | 1.19 |
| S-FRCM-3P | 5.1% | 112 | 125.7 | 1.29 | 1.12 |
| S-FRCM-5P | 8.5% | 134 | 96.9 | 1.00 | 0.72 |

*Represents the average of S-CONa and S-CONb control beams

Additionally, the failure modes respective to each test are shown in Figure 90. The term delamination is used to describe a failure mechanism that involves the debonding of one material from another. The observed mechanisms consisted of two types of delamination which include: surface delamination and interlaminar delamination. Surface delamination is described as the sudden detaching of the FRCM from the concrete substrate, where the fracture surface ocurs within the concrete-mortar interface. While interlaminar delamination occurs within the net's layer. This mechanism consists of FRCM fabric debonding from the matrix mortar with a fracture surface at the fabric-matrix interface.

Interlaminar delamination tyically occurs at the interface of the first layer of mortar and the first layer of fabric and can then propagate further into other reinforcing layers. A combination of both surface and interlaminar delamination was observed in all tests

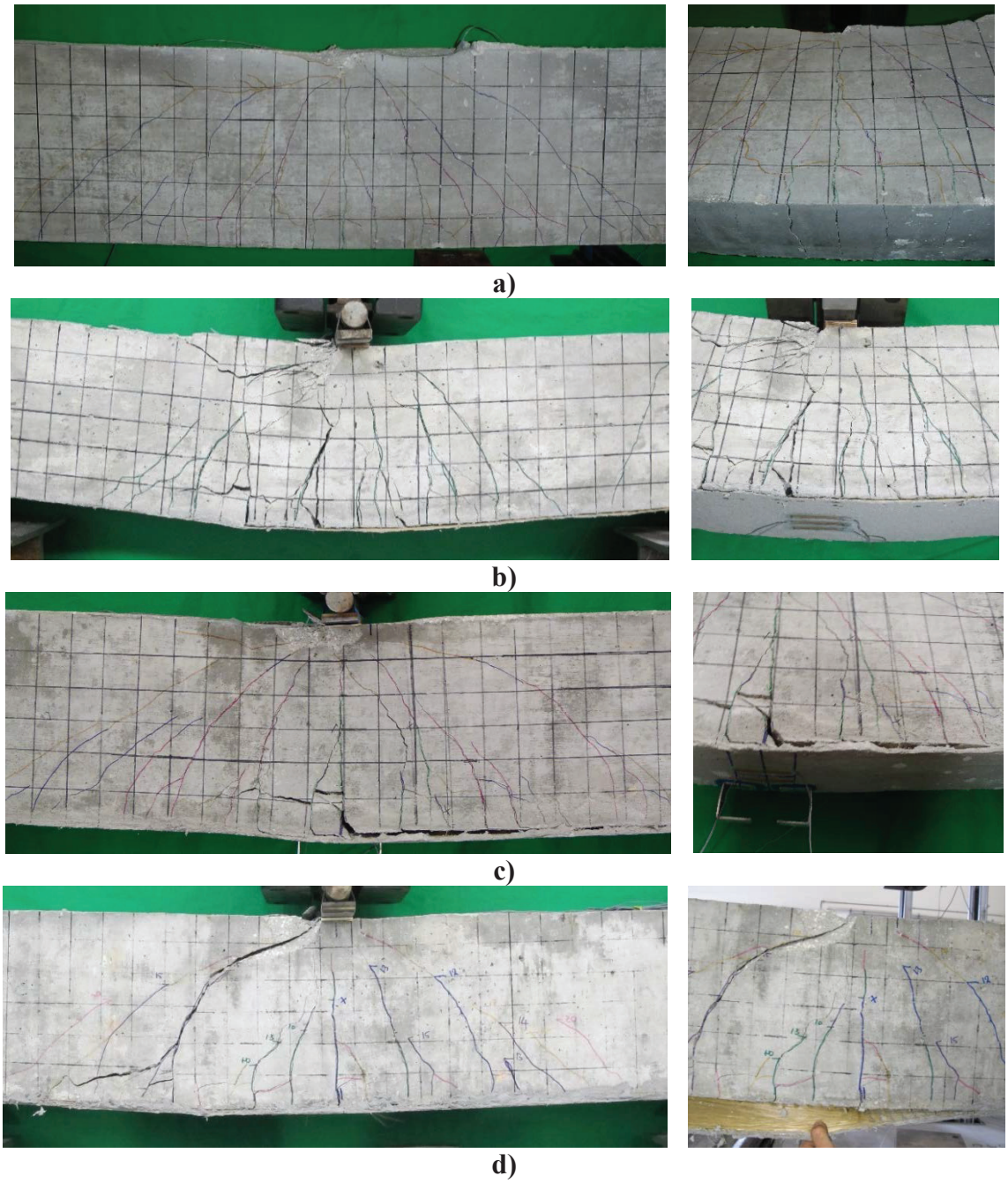

**Figure 90 – Typical Failure Modes for Phase I Static Test Specimens: a) S-CONa b) S-FRCM-1P c) S-FRCM-3P d) S-FRCM 5P**

exhibiting failure due to FRCM delamination. A similar trend was observed in study 1 where the direct tension tests showed a different mode of failure depending on the number of fabric layers. RC beams strengthened with one FRCM layer exhibited a failure mode consistent with one layer direct tension tests of fabric slipping within the matrix. Similarly, RC beams with three and FRCM layers exhibited failure modes in accordance with the observed three and five ply direct tension failures, respectively, which consisted of interlaminar delamination with little to no fabric-matrix slippage. The flexural cracks observed during testing and are also shown in Figure 90 as the benchmark specimens (S-CONa) showed larger crack openings with respect to those strengthened with FRCM. It was visually noted that the FRCM bridges cracks located at the soffit, which delayed cracking during loading and also reduced crack opening and propagation.

Experimental results indicate that S-FRCM-1P attained an increased ultimate load of 10% in comparison to the benchmark specimens. Similarly, S-FRCM-3P has a $\beta^f$ factor equal to three times that of S-FRCM-1P and showed an increase in strength of 29%, which is roughly three times the increase in strength of specimen S-FRCM-1. S-FRCM-5P strengthened with five layers of FRCM behaved quite differently, having no increase in strength compared to the benchmark value. Based on the observed failure mode and negligible increase in ultimate strength, this behavior suggests that the beam was over reinforced due to the excessive amount of material and added stiffness to the system, thus impairing the effectiveness of the FRCM. A similar behavior has been observed with steel reinforcement. There is a threshold for reinforced concrete members beyond which any increase in steel reinforcement provides a negligible strength enhancement. Similarly, for FRCM there is a threshold for which additional reinforcement does not provide increase in

strength. The addition of too many FRCM layers notably increases stiffness and the material then carries a larger portion of the applied load. This load is transmitted as a shear stress at the concrete-FRCM interface. The load is then distributed within the FRCM through an adhesive bond between fabric and matrix. If the applied shear force approaches the maximum adhesive bond strength at the concrete-FRCM interface and/or the matrix-fabric interface, FRCM delamination will occur. Therefore a member with a large amount of FRCM material will reach the maximum allowable bond strengths at a lower load. This concept is demonstrated in the load versus FRCM strain diagram for all FRCM strengthened specimens shown in Figure 91 showing that S-FRCM-1P exhibits a larger

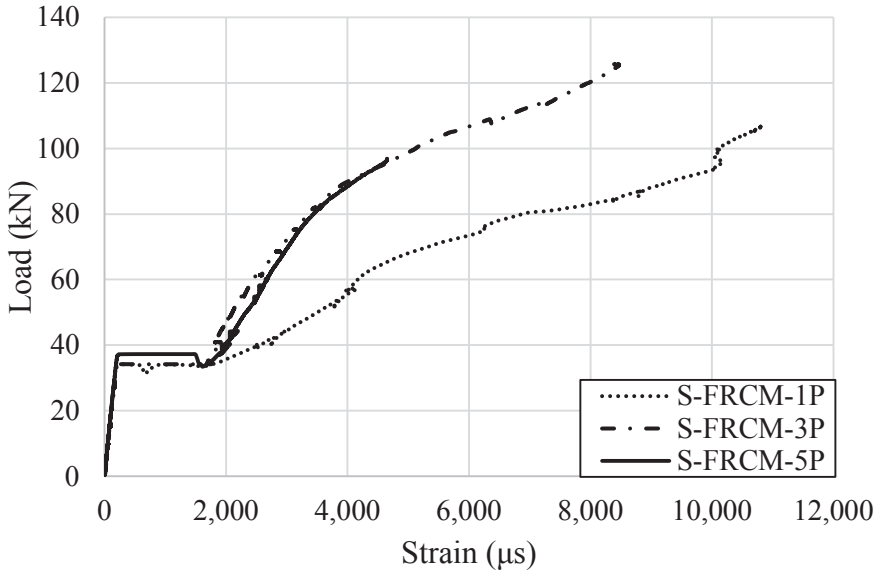


**Figure 91 – Load vs. FRCM Strain Relationship for Phase I Specimens**

maximum strain in the FRCM due to a lower stiffness contribution. In contrast, S-FRCM-5P experienced a lower maximum FRCM strain value due to the larger stiffness contribution. More FRCM reinforcement does not always ensure an increase in strength.S-FRCM-3P exhibited the same failure mode as S-FRCM-5P, and provided a significant

increase in strength while the latter did not. It is evident that for $\beta^f$ up to 5.1%, there is a (nearly linear) positive increasing trend in ultimate flexural capacity. While for $\beta^f$ equal to 8.1%, the FRCM has no strengthening effect whatsoever. This phenomenom was observed in study 1 where the bond strength exhibited a dramatic degradation due to the increased number of fabric layers. It is evident that for $\beta^f$ equal to 8.1% the bond behavior provides affects the structural performance more significantly than the tensile behavior. Accordingly, all theoretical values were conservative in predicting both the yield and ultimate load values with the exception of ultimate load for S-FRCM-5P. A similar study performed by Babaeidarabad et al. 2014 evaluates the flexural strength of RC beams with the same beam cross section, load configuration, and externally applied PBO-FRCM system. However, the beams consisted of different steel rebar sizes and concrete compressive strengths. RC beams were strengthened with one layer and four layers of FRCM which were then statically tested to failure. Because the βf factor is a function of the nominal material properties and beam geometry, the βf factors were also determined for the RC beams tested by Babaeidarabad et al. 2014. These factors along with the experimental values and corresponding enhancement are shown in Table 37 where the $\beta^f$ and enhancement can be added to the values from Table 36. As a result, the theoretical design and theoretical experimental vs. $\beta^f$ previously shown in Figure 14 are compared with the actual experimental enhancement results from this study along with the four layer

**Table 37 – Static Test Results ($P_u$) from Babaeidarabad et al. 2014**

| Beam | $\beta^f$ (%) | Maximum Load $P_u$ (kN) | Enhancement $P_{u,strengthened}/P_{u,control}$ |
|---|---|---|---|
| Control | - | 55.8 | 1 |
| 1 Layer FRCM | 1.70% | 63 | 1.13 |
| 4 Layers FRCM | 6.80% | 96.8 | 1.73 |

values to develop a third experimental curve shown in Figure 92. The grey area represents the region where a safe FRCM system can be designed for RC strengthening. In addition, Ebead et al. 2016 conducted experimental tests on using the same PBO-FRCM system applied to RC beams with a different beam cross section and steel reinfrocement. $\beta^f$ and enhancement values were determined for each beam, which are also included in Figure 92. This figure can be used by engineers in practice to select a FRCM configuration that is suitable for a desired level of enhancement.

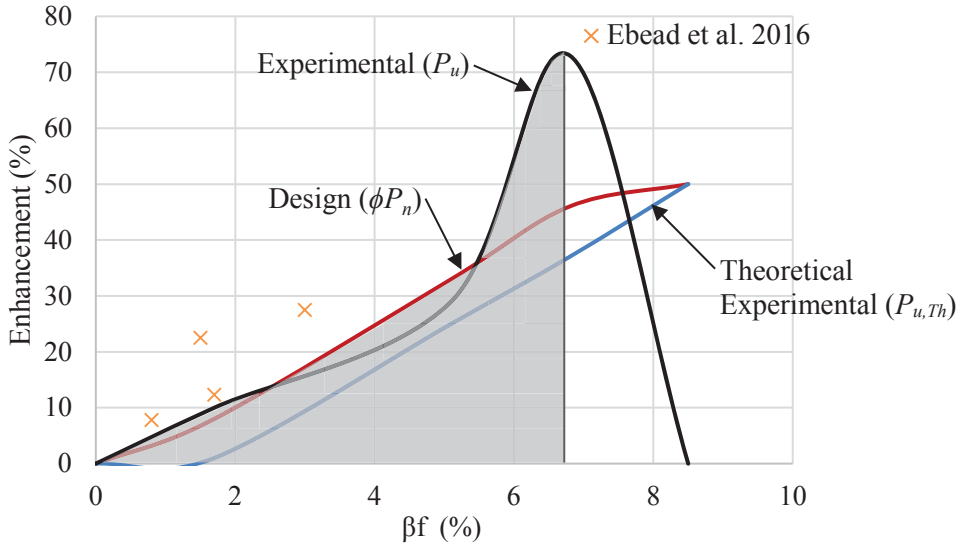


**Figure 92 – Enhancement vs. $\beta^f$**

**Phase II Test Results**

All beams in Phase II were subjected to cyclic loading. RC beams strengthened with three layers of FRCM were tested with descending maximum load values, in an attempt to determine an endurance limit based on the level of stress in the reinforcing steel. Once the endurance limit was determined, unstrengthened RC beams were tested at this limit for comparison. In addition, beams strengthened with one and five layers of FRCM were tested

at the endurance limit to determine whether this limit was applicable to all values of $\beta^f$. The failure type, number of cycles to failure (fatigue life), and residual maximum load values are summarized in Table 38. The residual to experimental ratio is defined as the ratio of residual maximum load ($P_{u.R}$) to the average maximum load ($P_{u.avg}$) for the statically tested S-FRCM-3P given in Table 36. All results and observations including: fatigue life, fatigue behavior, failure modes, and residual strength are discussed where a S-N curve is then presented. Similar to the results from Phase I, the strain gauges applied to the steel reinforcing bars recorded abnormal strain values post-concrete cracking and unfortunately are not reported herein.

**Table 38 – Summary of Phase II Fatigue Results**

| Specimen | Max % static yield (PSY) | Failure Type | Number of Cycles at failure $\times 10^6$ | Residual Max Load $P_{u.R}$ (kN) | Residual/ Experimental $P_{u.R}/P_{u.avg}$ |
|---|---|---|---|---|---|
| F-CON-0-75a | 75 | Steel Fracture | 0.919 | - | - |
| F-CON-0-75b | | Steel Fracture | 1.46 | - | - |
| F-FRCM-3P-90 | 90 | Steel Fracture | 0.492 | - | - |
| F-FRCM-3P-85 | 85 | Steel Fracture | 0.562 | - | - |
| F-FRCM-3P-80a | 80 | None* | 2 | 131.7* | 1.05 |
| F-FRCM-3P-80b | | Steel Fracture | 1.89 | - | - |
| F-FRCM-3P-75a | 75 | None* | 2 | 124.5* | 0.99 |
| F-FRCM-3P-75b | | None* | 2 | 119.8* | 0.95 |
| F-FRCM-1P-75 | | Fabric Slippage w/in Matrix | 0.962 | - | - |
| F-FRCM-5P-75 | | None* | 2 | 102.4* | 1.06 |

**Maximum load from monotonic load test performed after 2M cycles of fatigue loading*

**Fatigue Life**

Results show that beams strengthened with three layers of FRCM subjected to a higher load range experienced shorter fatigue lives. The shortest fatigue life of $0.492\times10^6$ cycles

was observed for F-FRCM-3P-90, $0.562\times10^6$ cycles for F-FRCM-3P-85, and $1.89\times10^6$ cycles for F-FRCM-3P-80b, reaching close to the 2M-cycle threshold. F-FRCM-3P-80a reached 2 million cycles without failure, reflecting the neighborhood of the fatigue endurance. Similarly, Beams F-FRCM-3P-75a and F-FRCM-3P-75b reached 2 million cycles without failure. The un-strengthened (benchmark) cyclically loaded RC beams F-CON-0-75a and F-CON-0-75a were tested for comparison purposes and have fatigue lives equivalent to $0.919\times10^6$ and $1.46\times10^6$, respectively.

**Fatigue Behavior**

The fatigue behavior of specimens F-FRCM-3P-90, F-FRCM-3P-85, and F-FRCM-3P-80b that exhibited failure prior to 2 million cycles can be describe in three stages throughout the life of the beam: considerable damage in the first stage, steady and gradually increasing damage in the second stage, followed by the final stage where significant loss in strength occurs prior to sudden failure (Figure 93). During the first stage, numerous cracks formed and propagated along the height of the beam. Local FRCM debonding occurred at crack locations along the soffit and (Figure 93b). In the second stage, concrete cracks continued to grow at a more gradual rate with one primary flexural crack that steadily propagated towards the compressive zone (Figure 93c). Gradual but minimal local FRCM delamination occurred in the form of cracks along the concrete-FRCM interface which propagated into the matrix-fabric interface (Figure 93d). Also, cracks initiated in the rebars at areas of high-stress concentration (rib root) possibly within first stage or early second stage. During the second stage, fatigue cracks gradually propagated along the rebar cross section. In the final stage, the stress in the steel reinforcement reached high levels due to the reduced effective cross section which caused the rate of stiffness degradation

and deflection to increase significantly (Figure 93e). Eventually, a brittle fracture occurred in the steel followed by sudden FRCM delamination as the ram (in load control) attempted to reach the preset maximum load (Figure 93f). Similar to the delamination observed in Phase I, the observed FRCM delamination consists of a combined surface delamination and interlaminar delamination.F-FRCM-1P-75 exhibited similar behavior with an identical first stage, whereas the gradual slipping of the fabric combined with minimal delamination was observed in the second stage, and combined slipping and delamination was observed in the final stage. Similarly, fatigue behavior for benchmark specimens F-CON-75a and

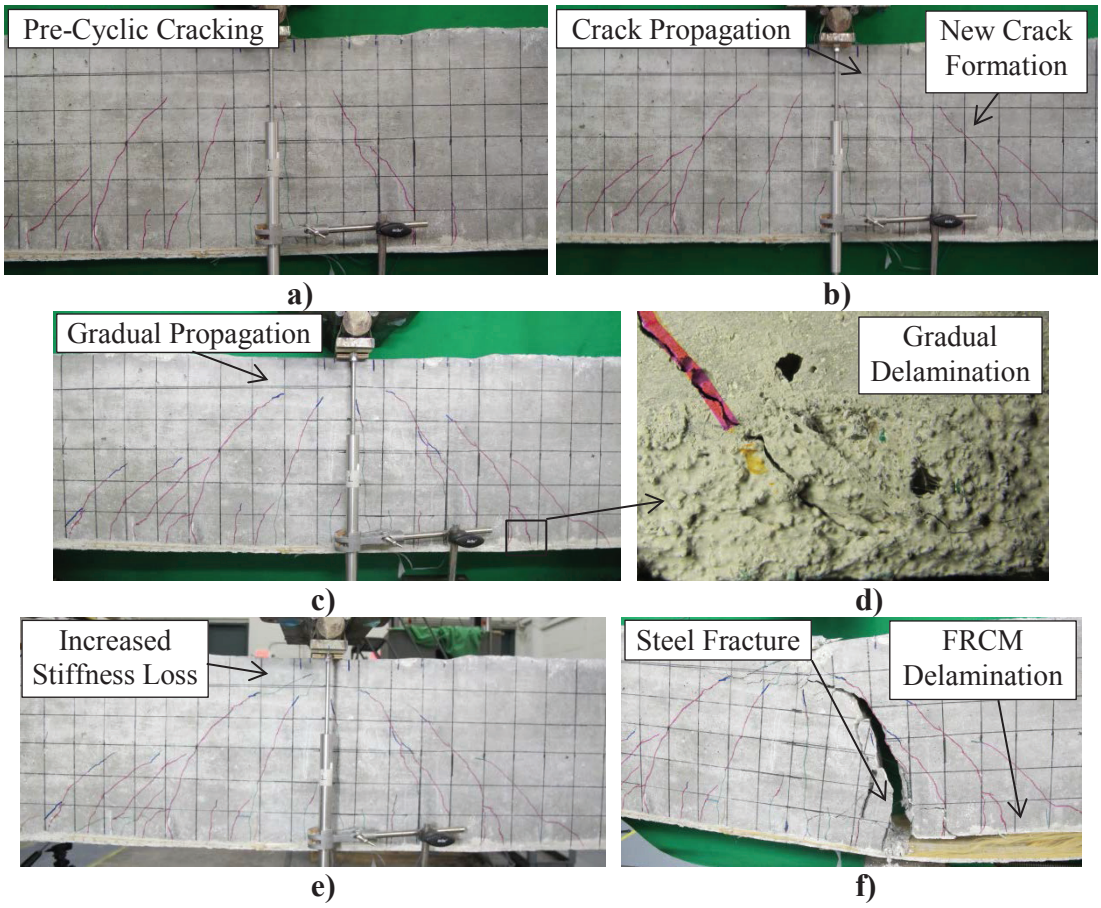


**Figure 93 – Fatigue Behavior for F-FRCM-80a during: a) Pre-Cyclic Cracking b) Stage One c) Stage Two d) Stage Two Gradual Delamination e) Stage Three f) Fatigue Failure**

F-CON-75b experienced all three phases apart from the observed FRCM mechanisms. While beams F-FRCM-80a, F-FRCM-75a and F-FRCM-75b that did not experience failure only exhibited the first two stages of damage and no final sudden loss in stiffness was observed. All behaviors are summarized in Figure 94. For all beams strengthened with While beams F-FRCM-80a, F-FRCM-75a and F-FRCM-75b that did not experience failure only exhibited the first two stages of damage and no final sudden loss in stiffness was observed. All behaviors are summarized in Figure 94. For all beams strengthened with

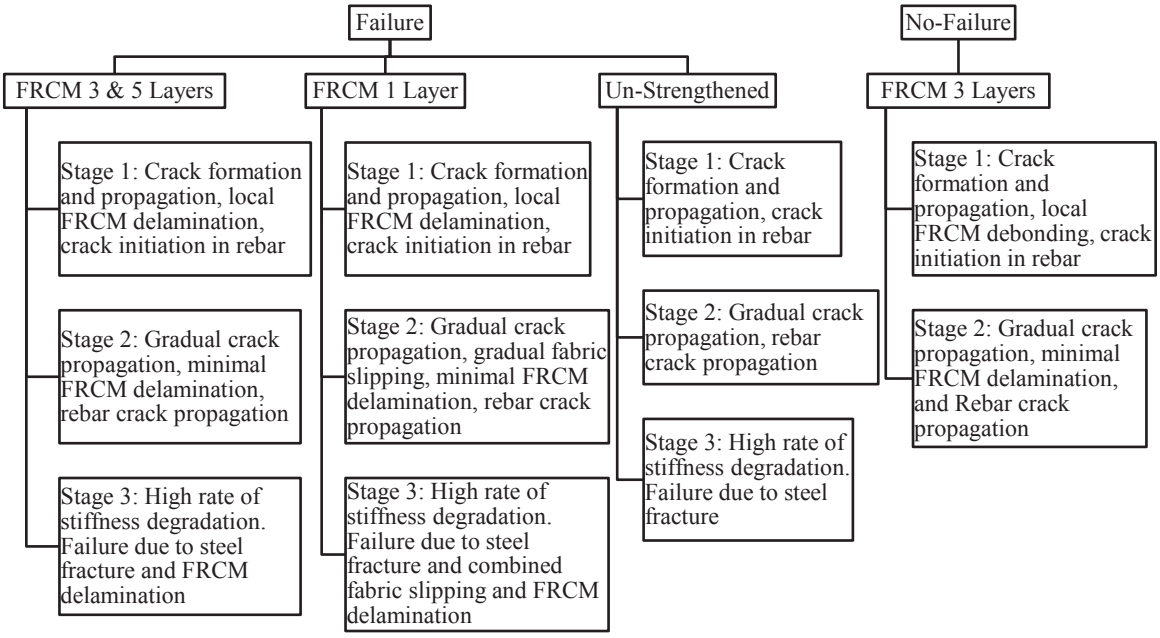


**Figure 94 – Stages of Fatigue Behavior**

FRCM, it was observed that the FRCM mitigated crack opening on the flexural surface which potentially slowed crack propagation compared to an un-strengthened RC beam. Figure 95 illustrates this concept by comparing the crack configuration for un-strengthened F-CONb and strengthened F-FRCM-3P-75a at 0.6 million cycles.

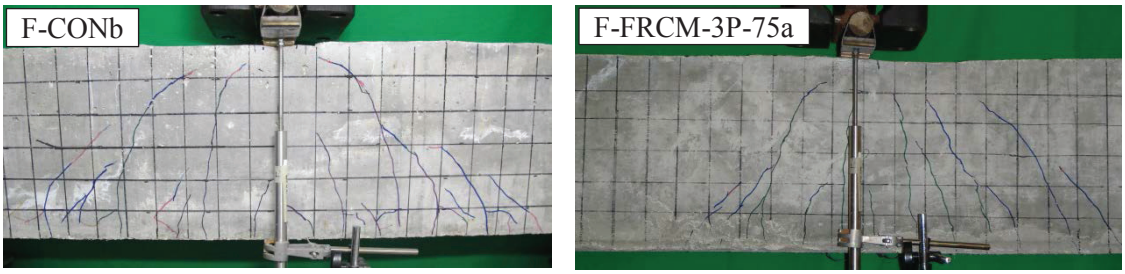


**Figure 95 – Crack Configuration for F-CONb (left) and F-FRCM-3P-75a (right) at 0.6 Million Cycles**

**Stiffness and Deflection**

The stages of progressive damage are best represented in terms of beam stiffness and maximum deflection at midspan. Figure 96 shows the normalized stiffness and maximum deflection versus number of cycles curves, for all three layer FRCM specimens and benchmarks. Figure 97 shows the same respective curves for benchmark, one layer, three layer, and five layer configurations of FRCM strengthening. Each curve was normalized

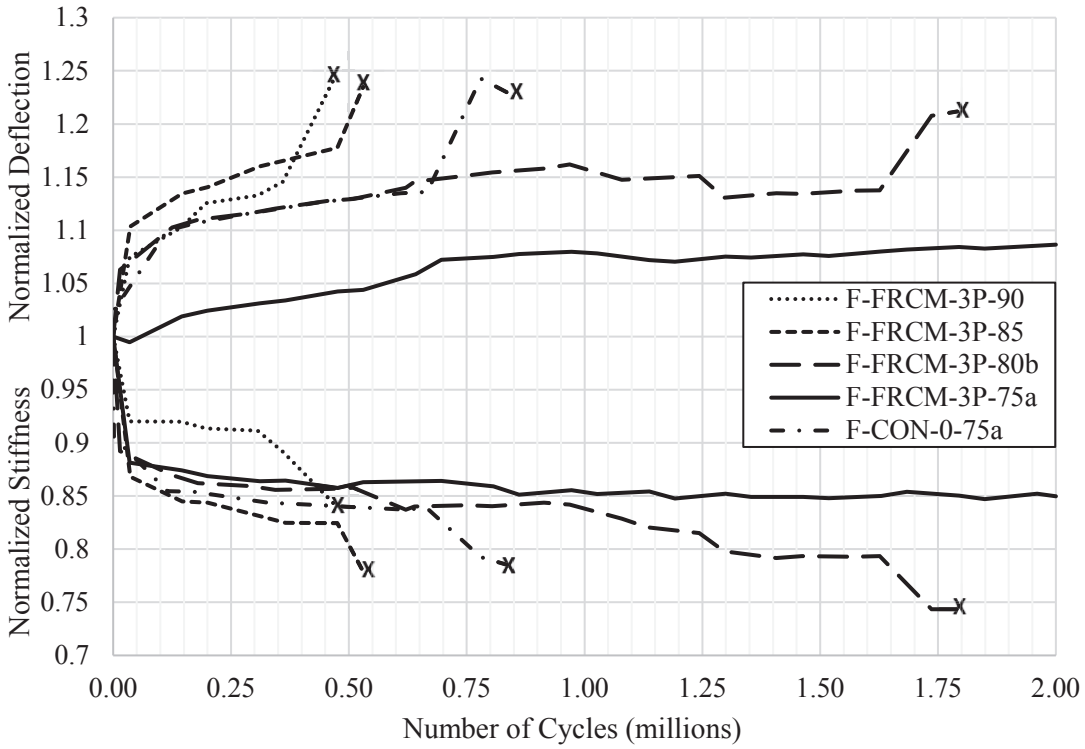


**Figure 96 – Degradation of Stiffness and Deflection for $\beta^f$ = 5.1%**

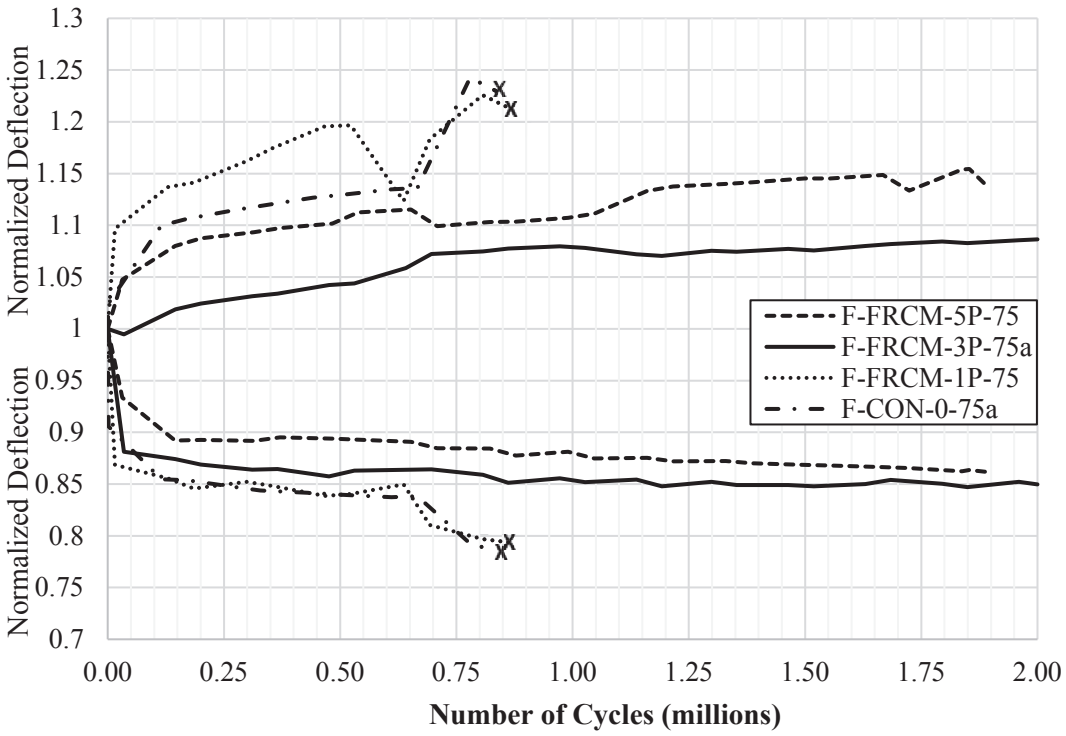


**Figure 97 – Degradation of Stiffness and Deflection for Various $\beta^f$**

with respect to the initially measured stiffness and deflection values at 0 cycles. It was observed that all beams showed a significant loss of stiffness up to 0.1 million cycles. Tests with higher values of maximum load exhibited a greater rate of intermediate damage during the second stage than those with lower loads. F-FRCM-1P-75 with one layer of FRCM exhibited a stiffness and deflection degradation behavior similar to the benchmark specimens. In contrast, FRCM-3P-75a/b and FRCM-5P-75 demonstrated a more gradual and steady degradation. The normalized deflection curves closely resemble the typical damage progression for FRP Strengthened RC beams previously discussed in Figure 70.

**Strain Measurements**

The maximum compressive strain in the concrete and tensile strain in the FRCM were measured over the fatigue life for each beam (Figure 98 and Figure 99). In general, the strain behavior exhibited a constant positively increasing trend, where larger maximum

loads induced a higher rate of strain increase, while lower maximum loads exhibited a gradual increase. It was more difficult to differentiate between the three fatigue stages due to the fact that the strain gauges measure local material behavior rather than the global behavior which is measured by deflection. In some cases, the compressive concrete strain

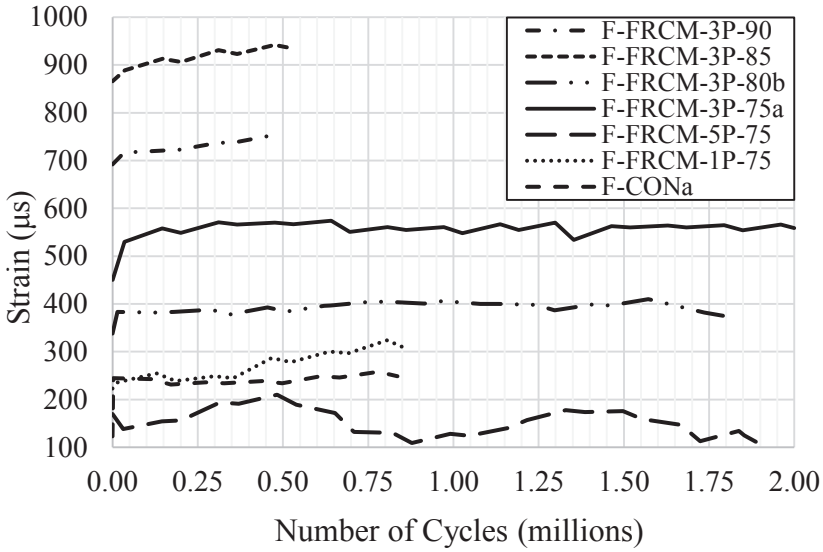


**Figure 98 – Concrete Strain vs. Number of Cycles**

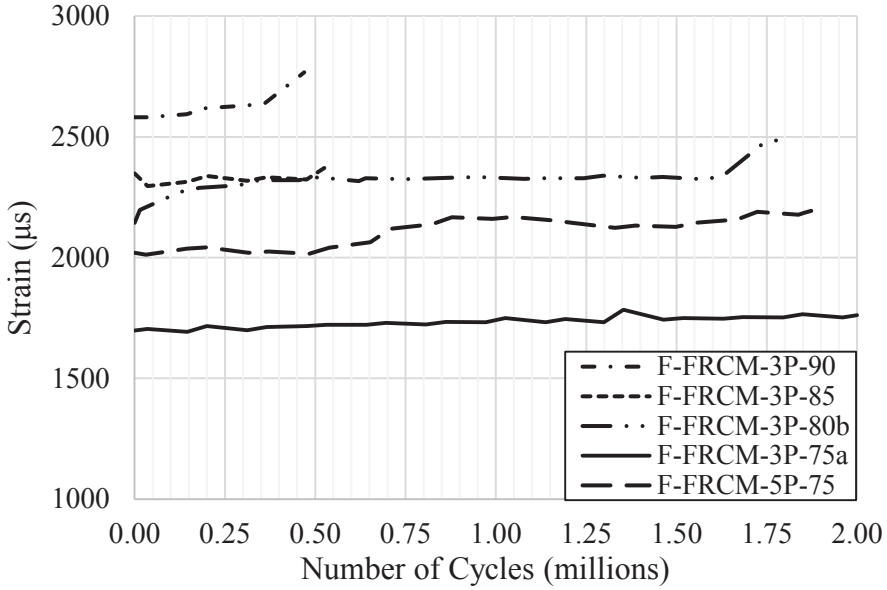


**Figure 99 – FRCM Strain vs. Number of Cycles**

showed a decreasing trend over time, which occurred as a result of: crack formation at the location of the strain gauge, formation of a horizontal crack in the cross section under the strain gauge, or gauge malfunctioning. There were no through transverse cracks observed in the FRCM along the beam width for specimens with three and five layers, while F-FRCM-1P with one FRCM layer showed transverse cracks through the entire beam width which resulted in strain gauge malfunction. Crack formation in the FRCM varies depending on the amount of supplemental FRCM reinforcement. This concept was similarly observed in Study 1 of this dissertation for direct tension behavior.

**Failure Mode**

For FRCM specimens subjected to cyclic loading, the primary failure mode was due to fatigue rupture of steel reinforcement and the secondary failure mode was due to slipping of the fabric within the matrix and/or FRCM delamination, where the secondary failure mode is a function of the amount of FRCM reinforcement provided. Specimens F-FRCM-3P-90, and F-FRCM-3P-85, F-FRCM-3P-80 corresponding to a maximum loading of 90, 85, and 80 PSY, respectively, failed due to fatigue rupture of the steel followed by FRCM delamination and then concrete crushing as shown in Figure 100. Specimens F-FRCM-3P-75a, F-FRCM-3P-75b, F-FRCM-5P-75 subjected to a maximum load of 75 PSY successfully reached 2M cycles without failure, while F-CON-0-75a and F-CON-0-75b

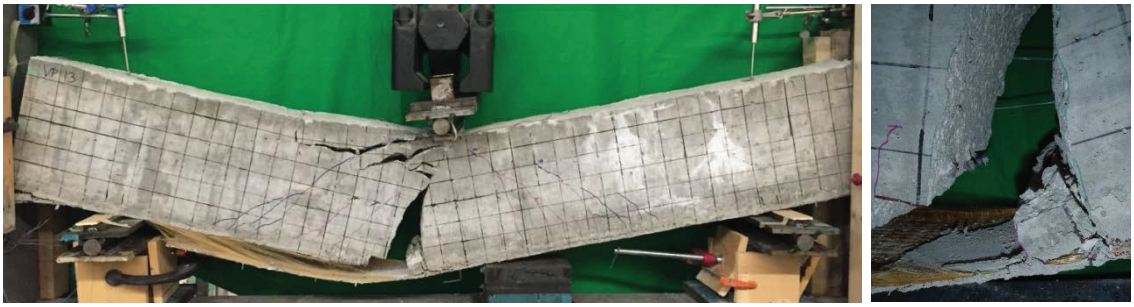

**Figure 100 – Typical Fatigue Failure Mode for Beams ($\beta^f$=5.1%)**

without FRCM reinforcement exhibited fatigue failure prior to 2 million cycles due to rupture of the steel followed by concrete crushing as shown in Figure 101. This indicates that FRCM strengthening improves the fatigue life of RC beams by lowering stress levels in the reinforcing steel. But F-FRCM-1P-75 with one layer of FRCM experienced a slightly

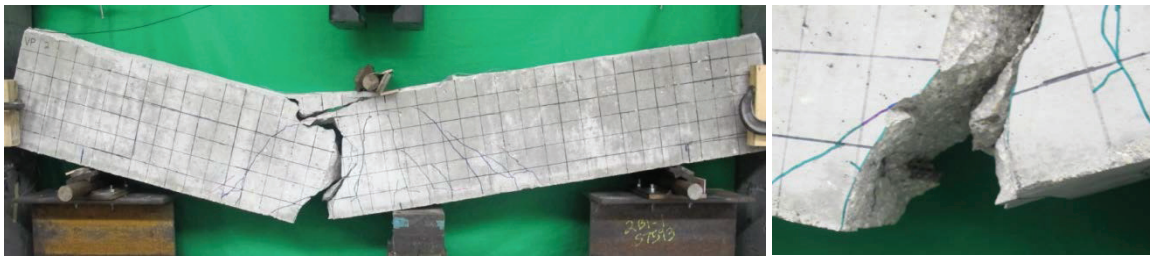

**Figure 101 – Typical Fatigue Failure Mode for Unstrengthened RC Beam**

different failure due to steel rupture followed by a combination of fabric slippage and FRCM delamination (Figure 102) prior to 2M cycles, which indicates that the level of fatigue improvement is dependent on the amount of supplemental FRCM reinforcement. Overall, the results show that for $\beta^f \geq 5.1\%$, FRCM strengthening improves the fatigue life

**Figure 102 – Typical Fatigue Failure Mode for F-FRCM-1P-75 ($\beta^f$=1.7%)**

of RC beams by lowering stress levels in the reinforcing steel. In addition, a steel rebar was extracted from F-FRCM-3P-80b and was compared to the fatigue fracture cross section reported in NCHRP 1976. Figure 103 shows a distinct similarity of fatigue surface and fracture surface between the two rebars. This further confirms that the primary failure mode was due to fatigue fracture.

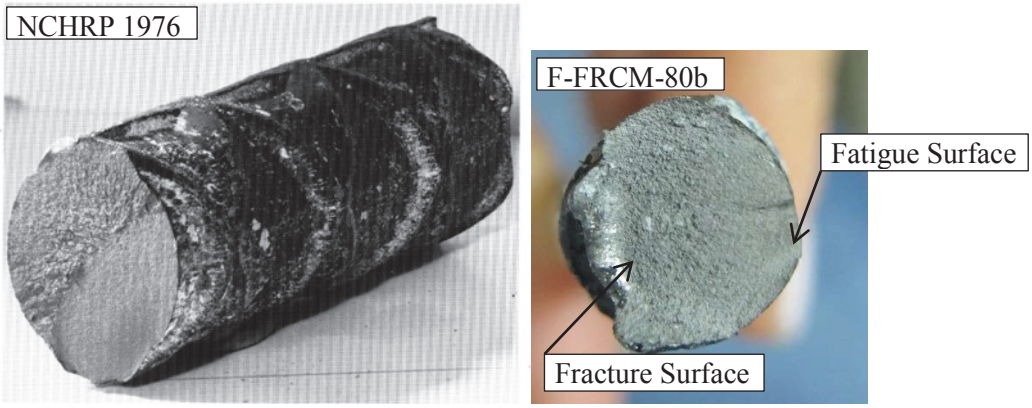


**Figure 103 –Fatigue Fracture Comparison**

**Residual Strength**

Specimens that successfully reached 2 million cycles without fatigue failure include: F-FRCM-3P-80a, F-FRCM-3P-75a, F-FRCM-3P-75b, and F-FRCM-5P-75. Each beam was tested statically to failure where maximum load values are listed in Table 38. The load-deflection curves for 3 layer and 5 layer FRCM specimens are presented in Figure 104 and Figure 105, respectively, and were compared to the static test from Phase I with equivalent

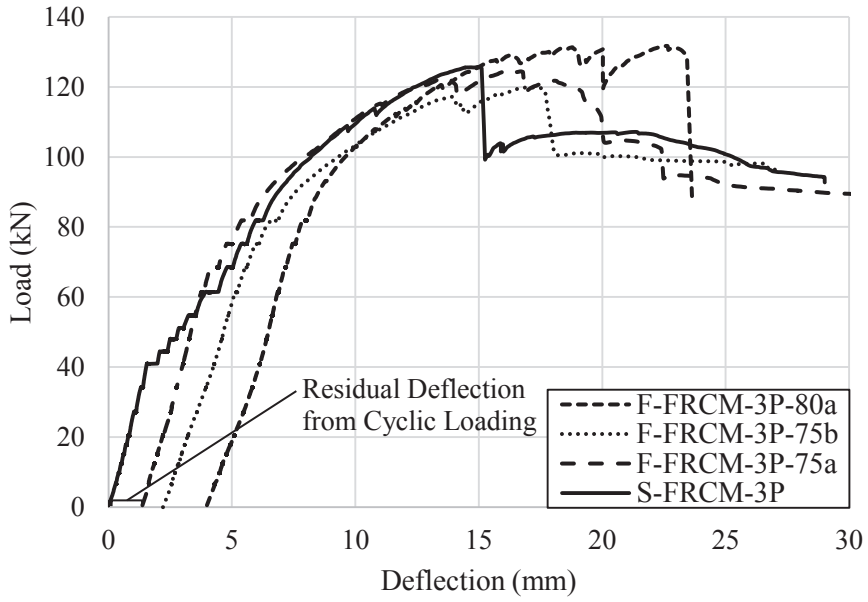


**Figure 104 – Load vs. Deflection Curves for Residual Static Tests ($\beta^f$=5.1%)**

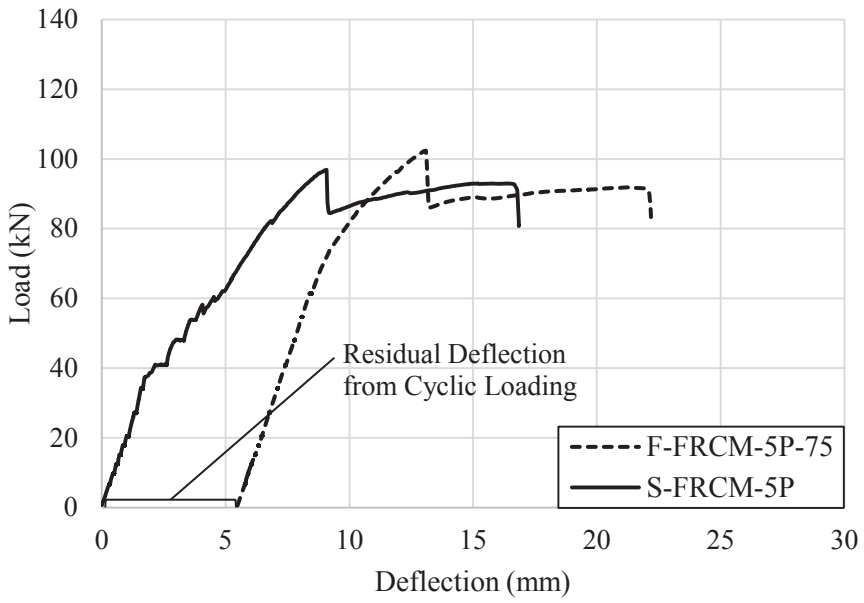


**Figure 105 – Load vs. Deflection Curves for Residual Static Tests ($\beta^f$=8.5%)**

FRCM reinforcement. All specimens behaved similarly and exhibited initial residual deflections as well as initial reduced stiffnesses from the cracks developed during fatigue conditioning. When loaded beyond the maximum applied fatigue load, each beam stiffness was similar to that of the static beam from Phase I. The measured maximum loads were at least 95% of the static ultimate loads given in Table 36, and the corresponding deflections at ultimate conditions were noticeably greater by an amount almost equal to the initial residual deflection. Observed failure modes were due to FRCM delamination which initiated at midspan and propagated outward to the supports followed by the formation of a flexural-shear crack resulting in concrete crushing as shown in Figure 106 and Figure 107. For specimens with 3 layers of FRCM (F-FRCM-3P-80a, F-FRCM-3P-75a, and F-FRCM-3P-75b), delamination occurred more gradually in comparison to the static beam S-FRCM-3P that exhibited a more sudden delamination as can be seen as by the abrupt

decrease in load shown in Figure 104. Gradual delamination occurred as a result of the slow debonding that ensued during the second phase of fatigue loading. In contrast,

**Figure 106 – Typical Failure Mode for Residual Static Tests $\beta^f$=5.1%**

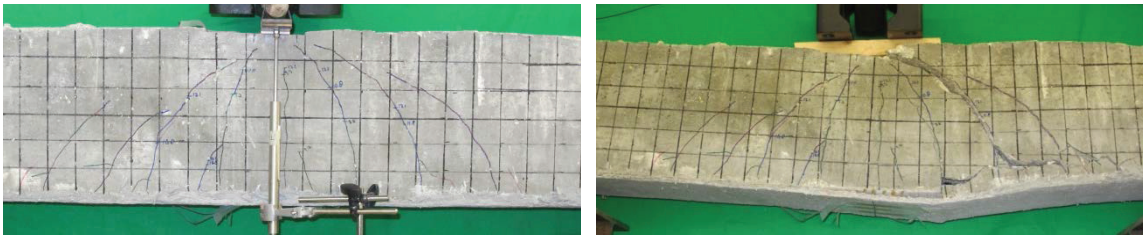

**Figure 107 – Typical Failure Mode for Residual Static Tests $\beta^f$=8.5%**

specimen F-FRCM-5P-75 with 5 FRCM layers exhibited a sudden delamination failure mode similar to the statically loaded S-FRCM-5P (Figure 105).

**S-N Curve**

Based on the data collected, a *stress ratio* versus the number of cycles (S-N) curve is shown in Figure 108. Note that the stress ratio is plotted rather than the traditionally used stress range. A solid marker denotes a failure that occurred before 2 million cycles while a hollow marker with an arrow depicts a beam that did not experience failure at 2 million cycles. A comparison is also made with specimens containing one and five layers of FRCM reinforcement tested at 75 PSY. In addition, the experimental results indicate that F-FRCM-1P-75 had a fatigue life less than 2 million cycles ($0.919\times10^6$) and F-FRCM-5P-75 reached 2 million cycles without failure. This suggests that the fatigue endurance is largely dependent on the amount of FRCM reinforcement provided.

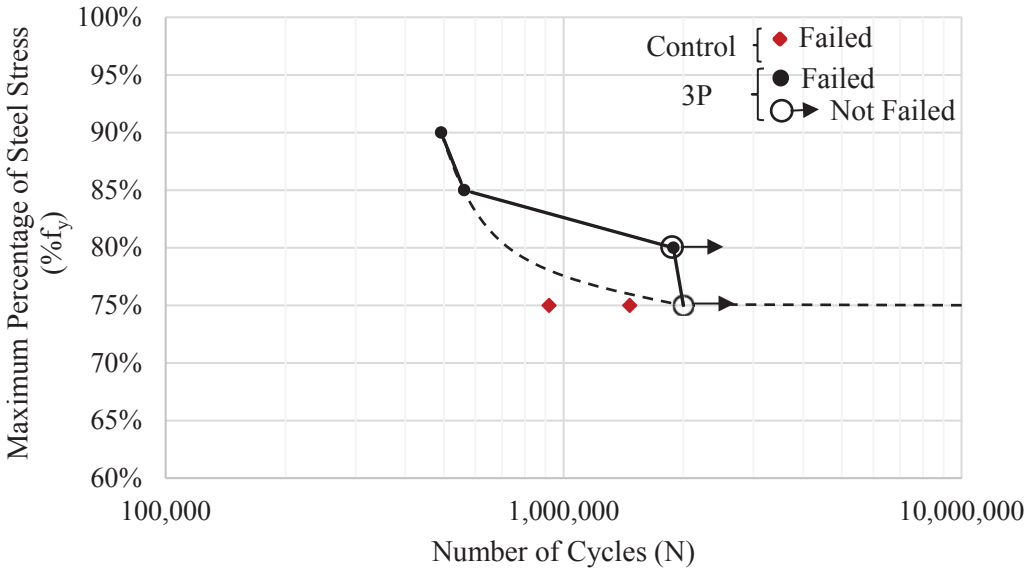


**Figure 108 – S-N Diagram for 3-Layers PBO FRCM ($\beta^f$=5.1%)**

**Recommendations to ACI 549.4R**

Based on the provisions given in ACI 549.4R-92, it was predicted that for tests less than or equal to 80 PSY no fatigue failure should occur prior to 2 million cycles. For all specimens tested at 75 PSY, beams with three and five layers of FRCM reached 2 million cycles and satisfy ACI 549.4R-13. While the un-strengthened and one layer specimens experienced failure prior to 2 million cycles, and do not satisfy ACI 549.4R-13. Similar to FRP strengthened RC beams, the addition of FRCM improves the fatigue performance by lowering stress levels in the reinforcing steel, but the level of improvement is largely dependent on the amount of FRCM provided. Test results indicate that for $\beta_f \geq 5.1\%$, the FRCM significantly contributes to this stress redistribution, while for $\beta_f < 5.1\%$ there is no significant contribution. Based on these results, it is clear that the provisions given in Section 11.1.2 of ACI 549.4R-13 stating "*The tensile stress in the steel reinforcement under service load, $f_{ss}$, should be limited to 80 percent of the steel yield strength, $f_y$,* are

under-conservative and should be re-evaluated based on the appropriate value of $\beta_f$ which is dependent on the amount of supplemental FRCM reinforcement. There is no experimental evidence of the 80% threshold and as such, this limitation should be experimentally verified. In addition, there were no observed fatigue failures due to the FRCM material. The maximum FRCM strain measured for specimen F-FRCM-3P-90 was 0.00277 which corresponds to a stress level of 24% of the FRCM design tensile strength, $f_{fd}$. And while this value satisfies the fatigue design provisions limiting the stress to be 30% of $f_{fd}$ specified in ACI 549.4R-13, it also suggests that 30% may be an overly conservative limitation. It is recommended for the fatigue stress limitations to be evaluated and experimentally verified specifically for PBO reinforcement.

**Concluding Remarks**

The fatigue performance of PBO-FRCM strengthening technology was evaluated. To account for differences in reinforcing material properties a stiffness-dependent factor, $\beta^f$, was used to compare the FRCM to steel reinforcement contribution. Based on the experimental results, the following concluding remarks can be inferred:

Phase I – Monotonic Tests

- The application of FRCM mitigates crack opening and delays crack propagation.
- The application of PBO-FRCM to RC beams provides an increase in stiffness, yield point, and strength compared to benchmark specimens with the exception of $\beta^f$ equal to 8.1% (5 layers) where no increase in strength was observed.
- FRCM failure modes vary as a function of the amount of FRCM strengthening and consist of fabric slippage within the matrix and/or FRCM delamination.

- There is a threshold for which additional FRCM reinforcement does not provide increase in strength. This threshold is dependent on the bond capacity at the FRCM-concrete interface as well as the fabric-matrix interface.
- A similar trend was observed in study 1 where the direct tension tests for one and three plies tests showed failure modes consistent with RC beams strengthened with the same respective number of fabric layers. While the failure mode observed in the RC beam strengthened with five layers ($\beta^f = 8.1\%$) was influenced more from the degradation of bond strength with increasing number of fabric layers, rather than the tensile behavior.

Phase II – Fatigue Tests

- All observed fatigue failure mechanisms for FRCM strengthened specimens were due to steel fracture followed by FRCM failure.
- FRCM improves the fatigue performance by lowering stress levels in the reinforcing steel, but the level of improvement is largely dependent on the amount of FRCM provided.
- Fatigue life decreases with increase in peak load up to an endurance limit of 75 PSY for $\beta^f$ equal to 5.1%.
- When the stress in steel is below 75 PSY for an RC beam strengthened with $\beta^f \geq 5.1\%$, no failure due to fatigue occurs up to 2M cycles.
- All specimens statically tested for residual strength sustained at least 95% of the non-conditioned static ultimate load.
- It is recommended that the design limitations for stress levels in the reinforcing steel and the FRCM material specified by ACI 549.4R to be re-evaluated and experimentally verified.

# CHAPTER 4

## Conclusions

FRCM is considered a relatively "young" material in the repair industry where its full potential as a strengthening system has yet to be completely understood. However, a growing amount of research conducted on externally bonded FRCM systems indicate proven mechanical, structural, and durability performance which deems it a viable alternative to current repair methods used specifically for RC in transportation structures. The studies conducted herein expand on the current knowledge and confirm FRCM's ability to optimize the performance of RC through its mechanical behavior, validated structural application, and effective design methodology. Each study is intended to uncover a different aspect of FRCM technology, where each study is also captivatingly interdependent with one another. FRCM as a repair system for bridge-type structures cannot be validated without extensive mechanical characterization, accurate design guidelines, and proven long-term fatigue performance. Similarly, FRCM fatigue performance cannot be investigated without knowing the systems material properties and behavior as well as demonstrated structural performance. A summary of the findings for each study is presented along with additional recommendations for future work that is still needed to fully validate FRCM as a repair system.

### Study 1 – FRCM MATERIAL CHARACTERIZATION: INVESTIGATION OF MULTI-PLY BEHAVIOR

In this study the effect of number of fabric layers on the direct tension and bond strength performance of a PBO-FRCM system was investigated. Results indicate that

increasing fabric plies causes a shift in crack propagation as well as a change in failure mode. One ply failure is defined by fabric-matrix slipping and four ply failure is caused by interlaminar delamination, while two and three plies exhibit a hybrid combination of both failure types. The increased number of layers also results in a decreased crack modulus of elasticity, and decreased bond strength. The largest values of ultimate stress and ultimate strain were observed in the two and three ply direct tension specimens followed by one and four plies. Overall, optimum performance of FRCM applied to RC is dependent on the tensile and bond characteristics where a two or two or three layer strengthening configuration is considered ideal for this PBO-FRCM system.

Theoretical ultimate capacities were computed using FRCM material properties determined from direct tension tests. RC beams strengthened with one and three FRCM layers were analyzed. Material properties for one ply direct tension tests were used for the RC beam strengthened with one FRCM layer. While the RC beam with three layers was analyzed twice using one and three ply direct tension properties. The analysis performed using one ply material properties resulted in a more realistic prediction with a larger theoretical load that was closest in value to the experimental results. Thus, one ply direct tension results were used for all theoretical and design analyses using the PBO-FRCM system for study 2 and study 3.

In addition, the early age bond strength was investigated as an additional tool to be used by DOT's in order to minimize traffic closure time to allow for FRCM installation and an appropriate curing time. Early age bond and matrix compression tests show that significant strength is developed within 3 days and full strength is nearly developed after 7 days of FRCM installation. All bond tests meet and exceed AC343 standards after 7 days of FRCM

installation, and the matrix mortar compressive strength exceeds the 7-day and 28-day strength criteria designated by AC434.

**Study 2 – REPAIR OF DAMAGED PRESTRESSED CONCRETE GIRDERS WITH FRCM AND FRP COMPOSITES**

The effectiveness of FRP and FRCM systems for the strengthening and repair of damaged PC girders is evaluated in this study. Three PC girders were tested: one girder served as the control girder (girder A) and the other two girders were strengthened with FRP (girder C) and FRCM (girder D), respectively. The material properties given in Study 1 were used in combination with AASHTO (2010), ACI 440.2R (2008), and ACI 549.4R (2013) to predict the experimental nominal flexural capacities. Experimental tests indicate that girder A sustained a maximum load equal to 95% of the theoretical ultimate capacity. The test was stopped upon reaching the actuator's maximum load. Although failure was not attained, the girder exhibited crack patterns that were representative of a forthcoming flexural failure. For the FRP strengthened girder C, the experimental capacity reached and exceed the theoretical ultimate value and demonstrated that FRP as a strengthening technology can successfully restore flexural strength to damaged PC girders. Accordingly, during the testing of girder D strengthened with FRCM, premature damage occurred in the form of horizontal and vertical shear cracking as a result of deck defects from bridge demolition. Without the presence of accidental saw cuts in the deck, it is likely the girder would have reached its predicted capacity. Finally, the design nominal capacities were determined and compared using AASHTO 2010, ACI 440.2R, FRPS-1, and ACI 549.4R design literature. ACI 440.2R proved to have the most conservative estimate of design strengthened capacity. Recommendations were made to adjust the strength reduction factor

equation that is dependent on the level of strain in the prestressing steel. A design approach based on AASHTO and ACI 440.2R ACI 549.4R methodology was proposed for ACI 549.4R to incorporate design provisions for the strengthening of PC girders. In addition, the design examples provided in Appenix _ can be used by engineers in practice to effectively design FRP and FRCM strengthened PC girders.

**Study 3 – FATIGUE PERFORMANCE OF RC BEAMS STRENGTHENED WITH FRCM**

The same PBO-FRCM system used in the previous two studies is evaluated for its strength and fatigue performance when applied to RC beams. This study was divided into two phases, Phase I comprising of statically loading beams and Phase II consisting of beams subjected to cyclic (fatigue) loading. The following parameters were investigated: amount of supplemental reinforcement (fabric layers), ultimate strength, static failure mode, applied stress range, fatigue life, fatigue failure mode and residual strength. A stiffness-dependent $\beta^f$ was developed to generally describe the amount of FRCM and steel reinforcement used. A design aid based on $\beta^f$ versus the design, theoretical, and experimental enhancement is presented to provide guidance to engineers in practice for the selection of a suitable FRCM configuration given a desired level of strengthening.

Results from Phase I tests indicate that FRCM mitigates crack opening and delays crack propagation for statically loaded beams. In addition, FRCM successfully provides an increase in stiffness, yield point, and strength compared to benchmark specimens with the exception of $\beta^f$ equal to 8.1% (5 layers) where no increase in strength was observed. The beam failure modes consisted of fabric slippage within the matrix and/or FRCM delamination and varied depending on the amount of fabric used FRCM strengthening. A

similar trend was observed in study 1 where the direct tension tests for one and three plies tests showed failure modes consistent with RC beams strengthened with the same respective number of fabric layers. Similar to study 1, the failure mode observed in the RC beam strengthened with five layers ($\beta^f = 8.1\%$) was influenced more by the degraded bond strength rather than the tensile behavior. This further validates the fact that there is a threshold for which additional FRCM reinforcement does not provide increase in strength. This threshold is dependent on the bond capacity at the FRCM-concrete interface as well as the fabric-matrix interface.

Phase II RC beams were subjected to fatigue loading and all observed failure mechanisms occurred due to steel fracture followed by FRCM failure. FRCM failure modes varied as a function of the amount of strengthening and were consistent with the modes observed in Phase I and Study 1, which consisted of fabric slippage within the matrix and/or FRCM delamination. The application of FRCM improved RC beam fatigue performance by lowering stress levels in the reinforcing steel but the level of improvement was largely dependent on the amount of FRCM provided. It was observed that the fatigue life decreases with increase in peak load up to an endurance limit of 75 PSY (percent of static yield) for $\beta^f$ equal to 5.1% (3 FRCM layers). When the level of stress in the steel reinforcement is below 75 PSY for $\beta^f \geq 5.1\%$, there was no observed fatigue failure up to 2M cycles. Specimens that reached the 2M cycle threshold were tested statically for residual strength. All fatigue-conditioned specimens sustained at least 95% of the non-conditioned static ultimate load. Based on the experimental results and observations, it was recommended for the design guidelines provided in ACI 549.4R for stress levels in the FRCM and steel reinforcement to be re-evaluated and experimentally verified.

**Recommendations for Future Work**

The number of FRCM systems used for repair is rapidly growing as a result of the favorable mechanical, structural, and durability performance reported in both literature and field applications. However, due to the many combinations of fabric materials, fabric orientation, fabric geometry, fabric layers, and mortar types available to formulate FRCM systems, it is critical to conduct extensive material characterization specific to each type of material system. Material characterization should be conducted per AC434 and meet the respective acceptance criteria. The effect of multi-ply behavior for all FRCM systems should also be evaluated for all FRCM systems following the test procedures specified in AC434, given that a multiple fabric configuration is a more likely to be used for design. Study 2 reported that girder D was not successfully tested to its full flexural capacity. There was no observed failure due in the FRCM system which suggests that the FRCM could have provided an increase in strength, however it was not experimentally verified. Thus, further investigation of the PBO-FRCM system as well as other FRCM systems to be used for the PC girder strengthening should be conducted. In addition, study 3 reports on the fatigue behavior of a specific PBO-FRCM system. And while FRCM systems exhibit different structural behavior, it is critical for the fatigue performance of other FRCM systems to be investigated. Particular focus should be given to the upper stress limitations for both the FRCM and steel reinforcement. The fatigue performance of FRCM applied to PC elements should also be investigated as well as the fatigue behavior of FRCM subjected to aggressive environmental exposure.

## REFERENCES


Abel, A. A., & Zheng, H. (1999). Fatigue Properties of Reinforcing Steel Produced by TEMPCORE Process. *Journal of Materials in Civil Engineering, 11*(2), 158-165.

AC434 (2013), "Acceptance Criteria for Masonry and Concrete Strengthening Using Fabric-reinforced Cementitious Matrix (FRCM) Composite Systems," Whittier, CA: ICC-Evaluation Service.

AC125 (2014). "Acceptance Criteria for Concrete and Reinforced and Unreinforced Masonry Strengthening Using Externally Bonded Fiber-Reinforced Polymer (FRP) Composite Systems," Whittier, CA: ICC-Evaluation Service.

ACI Committee 215R (1997). *Considerations for Design of Concrete Structures Subjected to Fatigue Loading (ACI 215R-97),* American Concrete Institute, Farmington Hills, Mich.

ACI Committee 318 (2014). *Building Code Requirements for Structural Concrete (ACI 318-14) and Commentary (ACI 318R-14),* American Concrete Institute, Farmington Hills, Mich.

ACI Committee 549.4R (2013). *Guide to Design and Construction of Externally Bonded Fabric-Reinforced Cementitious Matrix Systems for Repair and Strengthening Concrete and Masonry Structures (ACI 549.4R-13),* American Concrete Institute, Farmington Hills, Mich.

ACI Committee 440.2R (2008). *Guide for the Design and Construction of Externally Bonded FRP Systems for Strengthening Concrete Structures (ACI 440.2R-08),* American Concrete Institute, Farmington Hills, Mich.

ASTM D3039/D3039M-14 (2014). "Standard Test Method for Tensile Properties of Polymer Matrix Composite Materials." ASTM International, West Conshohocken, PA 2014, www.astm.org

ASTM C109/C109M (2013). "Standard Test Method for Compressive Strength of Hydraulic Cement Mortars" ASTM International, West Conshohocken, PA 2014, www.astm.org

ASTM C1583/C1583M (2013). "Standard Test Method for Tensile Strength of Concrete Surfaces and the Bond Strength or Tensile Strength of Concrete Repair and Overlay Materials by Direct Tension (Pull-off Method)" ASTM International, West Conshohocken, PA 2014, www.astm.org

Al-Salloum, Y. A.; Siddiqui, N.; Elsanadedy, H. M.; Abadel, A. A.; and Aqel, M. A., 2011, "Textile-Reinforced Mortar versus FRP as Strengthening Material for Seismically Deficient RC Beam-Column Joints," *Journal of Composites for Construction*, 15 (6), 920-933.

American Association of State Highway and Transportation Officials (2010). *AASHTO LRFD Bridge Design Specifications (AASHTO LRFD 2010),* 5th edn, American Association of State Highway and Transportation Officials, Washington, D.C.

American Association of State Highway and Transportation Officials (AASHTO). (2012). Guide Specifications for Design of bonded FRP systems for repair and strengthening of concrete bridge elements (FRPS-1). Washington, D.C: American Association of State Highway and Transportation Officials.

Arboleda, D. (2014). "Fabric Reinforced Cementitious Matrix (FRCM) Composites for Infrastructure Strengthening and Rehabilitation: Characterization methods." Ph.D Thesis, Univ. of Miami, Coral Gables, FL.

Babaeidarabad, S., Arboleda, D., Loreto, G. & Nanni, A. (2014). "Flexural Strengthening of RC Beams with an Externally Bonded Fabric-Reinforced Cementitious Matrix", *Journal of Composites for Construction,* 18(5), 4014009.

Barnes, R.A. & Mays, G.C. (1999). "Fatigue Performance of Concrete Beams Strengthened with CFRP Plates", *Journal of Composites for Construction,* 3 (2), 63-72.

Belarbi, A., Bae, S., & Brancaccio, A. (2012). Behavior of Full-Scale RC T-beams Strengthened in Shear with Externally Bonded FRP Sheets. *Construction and Building Materials,* 32, 27-40.

Bizindavyi, L., Neale, K.W. & Erki, M.A. (2003). "Experimental Investigation of Bonded Fiber Reinforced Polymer-Concrete Joints under Cyclic Loading", *Journal of Composites for Construction,* 7(2), 127-134.

Brameshuber, W. (2006). *Report 36: Textile Reinforced Concrete-State-of-the-Art Report of RILEM TC 201-TRC* RILEM publications.

Carozzi, F. G., & Poggi, C. (2015). Mechanical Properties and Debonding Strength of Rabric Reinforced Cementitious Matrix (FRCM) Systems for Masonry strengthening.*Composites Part B: Engineering,* 70, 215-230.

Čavojcová, A., Moravčík, M., Bahleda, F., & Jošt, J. (2014). Experimental Verification of Reinforced Concrete Member Under Cyclic Loading. *Procedia Engineering,* 91, 262-267.

D'Ambrisi, A., Feo, L. & Focacci, F. (2012). Experimental Analysis on Bond Between PBO-FRCM Strenghtening Materials and Concrete. *Composites: Part B,* 44(1), 524-532.

D'Ambrisi, A., & Focacci, F. (2011). Flexural Strengthening of RC Beams with Cementbased Composites. *Journal of Composites for Construction,* 15(5), 707-720.

Dawood, M., Rizkalla, S., & Sumner, E. (2007). "Fatigue and Overloading Behavior of Steel–Concrete Composite Flexural Members Strengthened with High Modulus CFRP Materials", *Journal of Composites for Construction,* 11(6), 659-669.

De Caso y Basalo, F.; Matta, F.; and Nanni, A., 2012, "Fiber Reinforced Cement-Based Composite System for Concrete Confinement," *Construction & Building Materials*, 32, 55-65.

Di Ludovico, M.; Prota, A.; and Manfredi, G., 2010, "Structural Upgrade Using Basalt Fibers for Concrete Confinement," *Journal of Composites for Construction*, 14 (5), 541-552.

Di Ludovico, M., Nanni, A., Prota, A., & Cosenza, E. (2005). Repair of Bridge Girders with Composites: Experimental and Analytical Validation. *ACI Structural Journal,* 102(5), 639-648.

Dong, J., Wang, Q., & Guan, Z. (2013). Structural Behaviour of RC beams with External Flexural and Flexural-Shear Strengthening by FRP sheets. *Composites Part B,* 44(1), 604.

Ekenel, M., Rizzo, A., Myers, J. J., & Nanni, A. (2006). "Flexural Fatigue Behavior of Reinforced Concrete Beams Strengthened with FRP Fabric and Precured Laminate Systems", *Journal of Composites for Construction,* 10(5), 433-442.

ElSafty, A., Graeff, M. K., & Fallaha, S. (2014). Behavior of Laterally Damaged Prestressed Concrete Bridge Girders Repaired with CFRP Laminates Under Static and Fatigue Loading. *International Journal of Concrete Structures and Materials*, 8(1), 43-59.

Helgason, T., Hanson, J. M., Somes, N. F., Corley, W. G., and Hognestad, E. (1976). "Fatigue Strength of High-yield Reinforcing Bars", NCHRP Report 164, Transportation Research Board, Washington, DC.

Heffernan, P.J. & Erki, M.A. (2004). "Fatigue Behavior of Reinforced Concrete Beams Strengthened with Carbon Fiber Reinforced Plastic Laminates", *Journal of Composites for Construction,* 8(2), 132-140.

Hilsdorf, H. & Kesler, C. E. (1960). "The Behavior of Concrete in Flexure Under VaryingRepeated Loads", T. & A. M. Report No.172, University of Illinois.

International Code Council, & International Conference of Building Officials. (2000). *International Building Code*.

Jones, M., Gangi, M., Leisen, J., Pino, V., Wollmann, C., Cousins, T., Koutromanos, I., Nanni, A., (2015). "Evaluation of Repair Techniques for Impact Damaged Prestressed Girders," FHWA/VTRC Report, June 2015.

Kim, Y. J., & Heffernan, P. J. (2008). "Fatigue Behavior of Externally Strengthened Concrete Beams with Fiber-Reinforced Polymers: State of the art", *Journal of Composites for Construction,* 12(3), 246-256.

Kokubu, M., & Okamura, H. (1965). "Fundamental Study on Fatigue Behaviour of Reinforced Concrete Beams Using High Strength Deformed Bars", *Transactions of the Japan Society of Civil Engineers,* (122), 29-41.

Kotynia, R., Abdel Baky, H., Neale, K. W., & Ebead, U. A. (2008). Flexural Strengthening of RC Beams with Externally Bonded CFRP systems: Test Results and 3D Nonlinear FE analysis. *Journal of Composites for Construction,* 12(2), 190-201.

Loreto, G., Leardini, L., Arboleda, D., & Nanni, A. (2014). Performance of RC slab-type Elements Strengthened with Fabric-Reinforced Cementitious-Matrix Composites. *Journal of Composites for Construction,* 18(3), A4013003.

MaCGregor, J., Jhamb, I., & Nuttall, N. (1971). "Fatigue Strength of Hot Rolled Deformed Reinforcing Bars", *J Amer Concr Inst, Proc,* 68(3), 169-179.

Mechtcherine, V. (2013). Novel Cement-Based Composites for the Strengthening and Repair of Concrete Structures. *Construction and Building Materials,* 41, 365-373.

Moore, H. F., & Kommers, J. B. (1927). *The Fatigue of Metals* (1st ed.). New York: McGraw-Hill Book Company, Inc.

Murdock, J. W. & Kesler C. E. (1958). "Effect of Range of Stress on Fatigue Strength of Plain Concrete Beams," *Journal of the American Concrete Institute*, 30(2), 221-233.17.

Namaan, A.E. (2012). "Evolution in Ferrocement and Thin Reinforced Cementitious Composites," *Arabian Journal for Science and Engineering*, 37 (2), 421-441.

Nanni, A. (1995), "Concrete Repair with Externally Bonded FRP Reinforcement: Examples from Japan," *Concrete International: Design and Construction*, 17(6), June, 22-25.

Nanni, A. (1997), "Carbon FRP Strengthening: New Technology Becomes Mainstream," *Concrete International: Design and Construction*, 19(6), June, 19-23.

Nanni, A., & Arduini, M. (1997). Behavior of Precracked RC Beams Strengthened with Carbon FRP Sheets. *Journal of Composites for Construction,* 1(2), 63-70.

Neville, A. (1996). *Properties of Concrete* (4th ed.). New York: J. Wiley.

McCall, John T. (1958), "Probability of Fatigue Failure of Plain Concrete," *Journal of the American Concrete Institute*, 30(2), 233-245.18.

NDT James Instruments, Inc., (2016). James Bond Test™ MK III For Testing Tensile Strength of Overlays, and Overlayments. http://www.ndtjames.com/James-Bond-Tester-p/p-c-7300.htm (May 23, 2016).

Ombres, L. (2010). "Structural Performances of PBO FRCM-Strengthened RC Beams." Proceedings of the ICE - Structures and Buildings, 164, 7-15.

Ombres, L. (2015). Analysis of the Bond Between Fabric Reinforced Cementitious Mortar (FRCM) Strengthening Systems and Concrete. *Composites Part B: Engineering,* 69, 418-426.

Ombres, L. (2012). Debonding Analysis of Reinforced Concrete Beams Strengthened with Fibre Reinforced Cementitious Mortar. *Engineering Fracture Mechanics,* 81, 94-109.

Pellegrino, C., & D'Antino, T. (2013). Experimental Behaviour of Existing Precast Prestressed Reinforced Concrete Elements Strengthened with Cementitious Composites. *Composites Part B,* 55, 31.

Pino, V., and Nanni, A. (2015). "Repair of Damaged PC Girder with FRCM and FRP Composites," Publication No. 00042134-04, Grant No. DTRT13-G-UTC45, USDOT RE-CAST University Transportation Center, 88.

Schläfli, M., & Brühwiler, E. (1998). "Fatigue of Existing Reinforced Concrete Bridge Deck Slabs", *Engineering Structures,* 20(11), 991-998.

Shahawy, M. and Beitelman, T. (1999). "Static and Fatigue Performance of RC Beams Strengthened with CFRP Laminates." Journal of Structural Engingeering, 125(6), 613–621.

Soltani, A., Miller, R. A., Harries, K. A., Russell, H. G., & Shahrooz, B. M. (2012). "Fatigue Performance of High-Strength Reinforcing Steel", *Journal of Bridge Engineering,* 17(3), 454-461.

Rabinovitch, O., & Frostig, Y. (2003). Experiments and Analytical Comparison of RC Beams Strengthened with CFRP Composites. *Composites Part B,* 34(8), 663-677.

Rosenboom, O., Walter, C., & Rizkalla, S. (2009). Strengthening of Prestressed Concrete Girders with Composites: Installation, Design and Inspection. Construction and Building Materials, 23(4), 1495-1507.

Tilly, G. P. (1979). "Fatigue of Steel Reinforcement Bars in Concrete: A Review", *Fatigue of Engineering Materials and Structures,* 2(3), 251-268.

Triantafillou, T. C., 2007, "Textile-Reinforced Mortars (TRM) versus Fibre-Reinforced Polymers (FRP) as Strengthening and Seismic Retrofitting Materials for Reinforced Concrete and Masonry Structures," *International Conference on Advanced Composites in Construction (ACIC07),* University of Bath.

Triantafillou, T. C., and Papanicolaou, C. G., 2006, "Shear Strengthening of Reinforced Concrete Members with Textile Reinforced Mortar (TRM)," *Materials and Structures*, 39(1), 93-103.

Zobel, R. S., Carrasquillo, R., & Fowler, D. (1997). Repair of Impact Damaged Prestressed Bridge Girder Using a Variety of Materials and Placement Methods. Construction and Building Materials, 11(5), 319-326.

## APPENDIX A

## Material Properties Provided by Manufacturer for PBO-FRCM System

### PBO fibres properties

| | |
|---|---|
| Density (g/cm³) | 1,56 |
| Tensile strength (GPa) | 5,8 |
| Modulus of elasticity (GPa) | 270 |
| Ultimate deformation (%) | 2,15 |
| Breakdown temperature (°C) | 650 |
| Coefficient of thermal dilation ($10^{-6}$ °C$^{-1}$) | -6 |

### Mesh properties

| | |
|---|---|
| Weight of PBO fibres in the mesh | 88 g/m² |
| Equivalent dry fabric thickness in the direction of the warp | 0,0455 mm |
| Equivalent dry fabric thickness in the direction of the weft | 0,0115 mm |
| Ultimate tensile stress of the warp per unit of width | 264,0 kN/m |
| Ultimate tensile stress of the weft per unit of width | 66,5 kN/m |
| Mesh weight (Substrate + PBOfiber) | 110 to 126 g/m² |

### Inorganic matrix properties

| | |
|---|---|
| Consistency (UNI EN 13395-1) | 175 |
| Specific weight of fresh mortar | 1,80 ± 0,05 g/cc |
| Litres of $H_2O$ for 100 kg of Ruredil X MORTAR | 25 - 27 |
| Yield kg/m²/mm (dry product) | 1,400 |
| Compressive strength (UNI EN 196-1) | ≥ 30.0 MPa (at 28 days) |
| Bending strength (UNI EN 196-1) | ≥ 4.0 MPa (at 28 days) |
| Secant modulus of elasticity (UNI EN 13412) | ≥ 7000 MPa (at 28 days) |

# APPENDIX B

## AC434 Annex A (2013): Tensile Testing of Fabric-Reinforced Cementitious Matrix (FRCM) Composite Systems

### A1.0 Summary of Test Method

A thin flat strip of material having a near-constant rectangular cross section is mounted in the grips of a mechanical testing machine and loaded with monotonically increasing load in tension while recording load and movement. The ultimate strength of the material can be determined from a maximum load carried before failure. The coupon strain or elongation is monitored with displacement transducers to determine the nominal stress-strain response of the material, and from that the cracking stress and strain, ultimate tensile strain, tensile modulus of elasticity before and after cracking of cement-based matrix can be derived.

This test procedure is designed to produce tensile property data for material specifications, quality assurance, and structural design and analysis. Factors that influence the tensile response and shall therefore be reported include the following: material, methods of material preparation and lay-up, specimen preparation, specimen conditioning, environment of testing, specimen alignment and gripping, and speed of testing. Properties, in the test direction, which may be obtained from this test include:

1. Ultimate tensile strength

2. Ultimate tensile strain

3. Tensile modulus of elasticity of uncracked specimen

4. Tensile modulus of elasticity of cracked specimen

5. Transition point

Attention shall be paid to material and specimen preparation, gripping, and test system alignment. Poor material fabrication practices, lack of control in alignment of fiber grid, and damage induced by improper cutting and machining the coupons are known causes of high material data scatter. Specimen gripping problems can also cause a high percentage of grip-influenced failures and therefore more scatter in data. Every effort shall be made to eliminate excess bending due to system misalignment and out-of-tolerance conditions caused by poor specimen preparation.

**A2.0 Apparatus**

**A2.1 Dimension Measurements:** The accuracy of instruments used for measuring dimensions of the test specimens shall be suitable for reading to within 1 percent of the sample dimensions.

**A2.2 Testing Machine:** The testing machine shall be in conformance with Practices ASTM E4. The testing machine shall have both an essentially stationary head and a movable head. The drive mechanism shall be capable of imparting to the movable head a controlled velocity with respect to the stationary head. The testing machine load sensing device shall be able to indicate the applied load to the specimen within 1 percent of the indicated value. Each head of the testing machine shall carry one grip for holding the test specimen in coincident with the longitudinal axis of the specimen. It is desirable to use grips that are rotationally self-aligning to minimize bending stresses in the coupon.

**A2.3 Gripping mechanism**: Clevis-type grips shall be used to transfer the load from the testing machine to the specimen. At least one of the two grips (preferably the top one)

shall allow for rotation in two perpendicular planes. No clamping force (i.e., pressure exerted on the tabs) should be applied to the specimen during testing. An illustration depicting the gripping mechanism with typical specimen dimensions is shown in Figure A1.

**A.2.4 Strain Indicating Device:** An extensometer satisfying Practice ASTM E83, Class B-1 requirements can be used for strain/elongation measurement. A minimum gage length of 2 inches (50 mm) shall be used. Since the coupon undergoes cracking in the early stages of loading, the gage length shall be adequate to at least include within itself one transverse crack. The bearing points of the extensometer on the coupon shall not be disturbed by cracking. If cracking occurs at the bearing points, the specimen shall be unloaded and extensometer moved. The discontinuity in elongation reading can be removed in data reduction process by matching the stop and restart point or similar means. The weight of extensometer shall not cause significant bending in the specimen.

**A3.0 Test Specimens**

At least five specimens shall be tested per test condition. Specimens can be cut from larger panels laid up in special molds. Control of fiber grid alignment is critical in lay-up procedure. Effective cutting tools and methods need to used, and precautions shall be taken to avoid notches, undercuts, uneven surfaces, or delaminations. The specimen preparation method shall be reported. Specimens shall be labeled properly to be distinct from each other and traceable to the raw material.

The test specimens shall be rectangular coupons. The thickness of coupons shall be as required and be a function of number of layers and thickness of matrix for each layer. The width of the coupon shall be adequate to include a minimum number of strands (e.g., three

(3) strands in each layer) and shall not be less than four times the thickness of the specimen. The width shall also be kept as a multiple of the grid spacing. Also, in case the strands in different layers are staggered with respect to each other, it is preferable to have the same number of strands in each layer along the width of the coupon. The minimum length of the coupon shall include gripping distance, plus twice the width plus gage length. Longer lengths are preferred to minimize the bending effects on the specimen.

Metallic tabs (e.g., steel, aluminum) are recommended to avoid damage to the specimen by the clevis-type grips. The tabs can be glued to the specimen ends (two at each end, one at each face). The tabs shall have the same width as the coupon. The tab length can be calculated based on the maximum expected tensile load, glue and tab bond strength to the matrix, and development length of the fiber strands within matrix. A minimum of 3 inches (75 mm) tab length is recommended. The thickness of the tabs shall be adequate to distribute uniformly the gripping force to the overall width of the coupons. A minimum thickness of 1/16 inch (2 mm) is recommended.

**A4.0 Calibration**

The accuracy of all measuring equipment shall have certified calibrations that are current at the time of use of the equipment.

**A5.0 Conditioning**

Unless a different environment is specified as part of the experiment, test specimens shall be moist cured at least for seven days after lay-up, and another seven days at laboratory environment before testing. Tests can be conducted at 14-day age and later. Storage after curing and testing shall be at standard laboratory atmospheric conditions.

**A6.0 Procedure**

After conditioning and before testing, coupon type and geometry and environmental conditioning test parameters are specified. The overall cross-sectional area of the specimen is calculated as follows:

$$A = w_s \, h_s \tag{A1}$$

where *ws* is the nominal width and $h_s$ is the nominal thickness of the coupon. The width and thickness are measured at three locations along the specimen and averaged. This value is determined for reporting purposes only. For computation of FRCM mechanical properties, the area of grid reinforcement by unit width, *Af* measured in.$^2$/in (mm$^2$/mm), as reported by the manufacturer, is used.

Special tabs prepared for installation are glued to the specimen. The glue shall be permitted to cure per applicant instruction. The specimen placed in the clevis-type grips of testing machine, taking care to align the axis of the gripped specimen with the test direction. An initial minimal tension, less than 5 percent of the anticipated failure load, is applied to straighten potential bow in the specimen. The displacement transducer is attached to the specimen, preferably symmetrically about the mid-span, mid-width location. The load is applied under displacement control. The loading rate can be adjusted by the velocity of the machine head. A standard rate of 0.01 in./min (0.2 mm/min) is recommended.

The load versus displacement shall be recorded continuously or at frequent regular intervals. The load, displacement, and mode of cracking (or any other damage) during testing that would cause transition region in otherwise a linear response are recorded. Cracks may occur at regular spacing along the specimen. If the cracks intercept the transducer bearing points, the specimen shall be unloaded to the level of the initial loading.

The displacement transducer shall then be slightly moved and reinstalled to bear at uncracked region of the matrix. Reload the specimen with the same rate of loading and continue data recording. The displacement transducer shall be removed before anticipated failure to avoid damage to the sensor, but load readings shall continue until failure. The maximum load, the failure load, and corresponding displacements at, or as near as possible to, the moment of rupture shall be recorded, along with the failure mode and location.

**A7.0 Calculation**

The recorded data shall be reduced to reflect the initial tensile loading and reading discontinuity if the transducer were to be moved during the test. This will likely result in a near bilinear response curve (Figure A2) with an initial line for uncracked specimen, a secondary line for cracked specimen, and possibly a curved transition segment in between.

**A7.1 Expected Tensile Stress – Strain Curve:** The expected tensile stress, *ff*, versus tensile strain, ε*f*, curve of an FRCM coupon specimen is shown in Figure A2. If a curved segment exist in between two linear portions of the response curve, the two lines to initial and secondary segments of the response curve shall be continued until they intersect. The displacement and load corresponding to the intersection are calculated as the transition point data, named T in Figure A2.

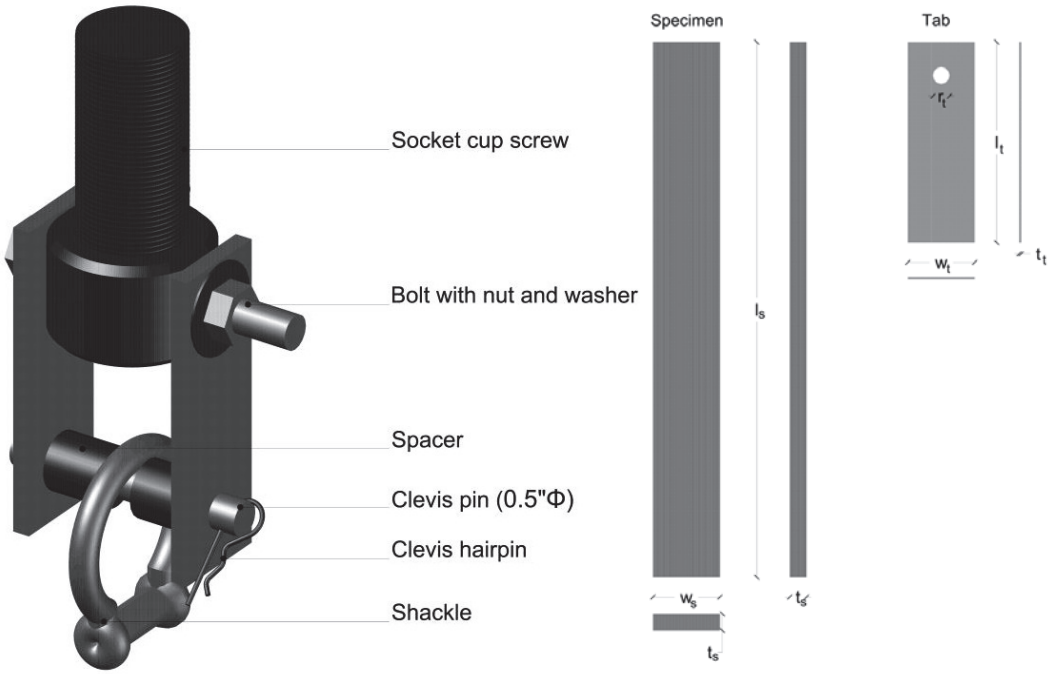


**FIGURE A1—GRIPPING MECHANISM AND TYPICAL SPECIMEN DIMENSIONS**

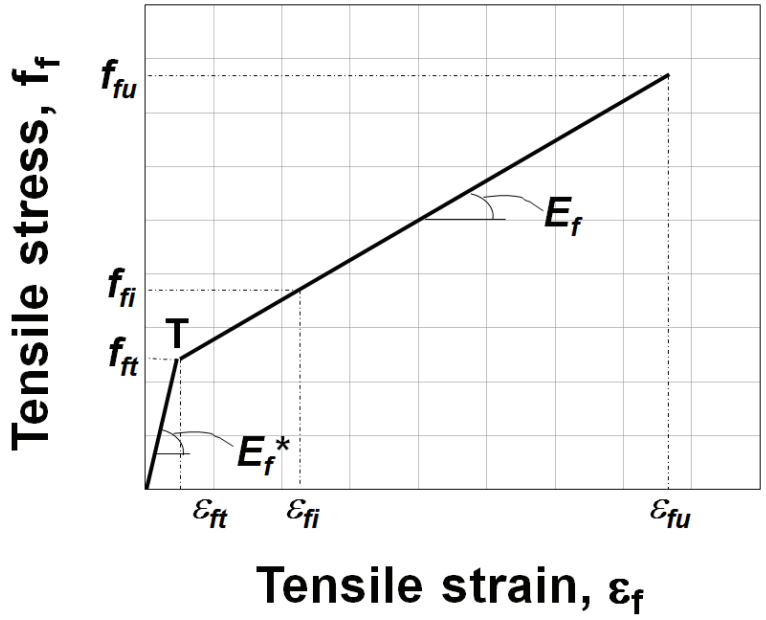


**FIGURE A2—EXPECTED TENSILE STRESS VERSUS TENSILE STRAIN CURVE OF AN FRCM COUPON SPECIMEN. THE TRANSITION POINT T IS INDICATED**

In Figure A2 the following quantities are shown:

$E_f$ = tensile modulus of elasticity of the cracked specimen, psi (MPa)

$E_f$* = tensile modulus of elasticity of the uncracked specimen, psi (MPa)

$f_{fi}$ = tensile stress at *i*th data point, psi (MPa)

$f_{fu}$ = ultimate tensile strength, psi (MPa)

$f_{ft}$ = tensile stress corresponding to the transition point, psi (MPa)

$\varepsilon_{fi}$ = tensile strain at *i*th data point, in./in. (mm/mm)

$\varepsilon_{fu}$ = ultimate tensile strain, in./in. (mm/mm)

$\varepsilon_{ft}$ = tensile strain corresponding to the transition point, in./in. (mm/mm)

**A7.2 Transition Point (T):** If a curved segment exist in between two linear portions of the response curve, the two lines to initial and secondary segments of the response curve shall be continued until they intersect. The displacement and load corresponding to the intersection are calculated as the transition point data.

**A7.3 Tensile Stress/Tensile Strength:** The ultimate tensile strength and, if needed, the tensile stress at a specific data point are calculated using the following equations:

$$f_{fu} = P_{max} / (A_f w_s) \quad \text{(A2)}$$

$$f_{fi} = P_i / (A_f w_s) \quad \text{(A3)}$$

where:

$P_{max}$ = maximum load before failure, lbf (N).

$P_i$ = load at *i*th data point, lbf (N).

$A_f$ = area of grid reinforcement by unit width, in.2/in (mm2/mm)

$w_s$ = nominal width of the specimen , in. (mm)

**A7.4 Tensile Strain:** Tensile strain at a specific data point is calculated using the following equation:

$$\varepsilon_{fi} = \delta_i / L_g \quad \text{(A4)}$$

where:

$\delta_i$ = extensometer displacement at $i$th data point, in. (mm).

$L_g$ = extensometer gage length, in. (mm).

**A7.5 Tensile Modulus of Elasticity of Uncracked Specimen:** On the linear segment of the initial line of the response bilinear curve corresponding to uncracked behavior of the specimen two points connecting the results in a line that closely follows the trend and slope of the response curve at that region are selected. The tensile modulus of elasticity of the uncracked specimen is calculated using:

$$E_f^* = \Delta f / \Delta \varepsilon \quad \text{(A5)}$$

where:

$\Delta f$ = difference in tensile stress between two selected points, MPa.

$\Delta \varepsilon$ = difference in tensile strain between two selected points, mm/mm.

Alternatively, the slope of the initial line passing through the origin and drawn to obtain the transition point on the response curve can be calculated as the modulus of elasticity of uncracked specimen.

**A7.6 Tensile Modulus of Elasticity of Cracked Specimen:** On the segment of the response curve corresponding to cracked behavior after the transition as defined in Section A7.2, two points are selected on the experimental curve at a stress level equal to $0.90f_{fu}$

and $0.60f_{fu}$[1]. The slope of the line that connects these two points represents the tensile modulus of elasticity at that region:

$$E_f = \Delta f / \Delta \varepsilon = (0.90f_{fu} - 0.60f_{fu}) / (\varepsilon_{f@0.90ffu} - \varepsilon_{f@0.60ffu}) \quad \text{(A6)}$$

**A7.7 Ultimate Tensile Strain:** Ultimate tensile strain, $\varepsilon_{fu}$, is by obtaining the y-intercept of the line used to compute Ef as defined in A7.6 (i.e., yintercept = $0.60f_{fu}$ - $E_f$ $\varepsilon_{f@0.60ffu}$) and the following equation:

$$\varepsilon_{fu} = (f_{fu} - y_{intercept}) / E_f \quad \text{(A7)}$$

[1] The experimental stress-strain curve is typically jagged and the intersects with horizontal lines at values of $0.90f_{fu}$ and $0.60f_{fu}$ may occur more than once. In this instance, the first $0.90\,f_{fu}$ and the last $0.60\,f_{fu}$ intersects are the ones selected for the computation of $E_f$.

[1] The experimental stress-strain curve is typically jagged and the intersects with horizontal lines at values of $0.90f_{fu}$ and $0.60f_{fu}$ may occur more than once. In this instance, the first $0.90\,f_{fu}$ and the last $0.60\,f_{fu}$ intersects are the ones selected for the computation of $E_f$.

## APPENDIX C: Direct Tension Test Results for Study 1

### Table C1 – Individual Tensile Strength Results for One Ply Specimen Tests

| Specimen ID | $f_{fu}$ MPa | $0.6f_{fu}$ MPa | $0.9f_{fu}$ MPa | $\varepsilon_{f@0.6ffu}$ mm/mm | $\varepsilon_{f@0.9ffu}$ mm/mm | $E_f$* MPa | Y int MPa | $\varepsilon_{f@ffu}$ mm/mm | $f_{ft}$ MPa | $\varepsilon_{f@fft}$ mm/mm | $E_f$ MPa |
|---|---|---|---|---|---|---|---|---|---|---|---|
| FRCM_DT_1Ply_01 | 1,678 | 1,006 | 1,510 | 0.0117 | 0.0155 | 135,406 | -584 | 0.0167 | 389 | 0.00012 | 1,675,102 |
| FRCM_DT_1Ply_02 | 1,674 | 1,004 | 1,423 | 0.0132 | 0.0172 | 102,578 | -346 | 0.0197 | 300 | 0.0002 | 1,437,540 |
| FRCM_DT_1Ply_03 | 1,572 | 943 | 1,415 | 0.0112 | 0.0154 | 114,146 | -338 | 0.0167 | 358 | 0.00013 | 2,470,015 |
| FRCM_DT_1Ply_04 | 1,773 | 1,064 | 1,596 | 0.0138 | 0.0175 | 142,211 | -901 | 0.0188 | 324 | 0.00016 | 1,361,781 |
| FRCM_DT_1Ply_05 | 1,560 | 936 | 1,404 | 0.0108 | 0.0145 | 125,926 | -425 | 0.0158 | 330 | 0.00025 | 1,500,000 |
| FRCM_DT_1Ply_06 | 1,728 | 1,036 | 1,555 | 0.013 | 0.0165 | 145,613 | -850 | 0.0177 | 546 | 0.00017 | 2,388,623 |
| Average | 1,664 | 998 | 1,448 | 0.0123 | 0.0161 | 127,647 | -574 | 0.0176 | 374.5 | 0.00017 | 1,805,510 |
| Stand. Dev. | 77 | 46 | 74 | 0.0011 | 0.0011 | 15,323 | 228 | 0.0013 | 81.62 | 0.00004 | 451,706 |
| C.O.V. (%) | 5 | | | | | 0.12 | | 8 | | | |

### Table C2 – Individual Tensile Strength Results for Two Ply Specimen Tests

| Specimen ID | $f_{fu}$ MPa | $0.6f_{fu}$ MPa | $0.9f_{fu}$ MPa | $\varepsilon_{f@0.6ffu}$ mm/mm | $\varepsilon_{f@0.9ffu}$ mm/mm | $E_f$* MPa | Y int MPa | $\varepsilon_{f@ffu}$ mm/mm | $f_{ft}$ MPa | $\varepsilon_{f@fft}$ mm/mm | $E_f$ MPa |
|---|---|---|---|---|---|---|---|---|---|---|---|
| FRCM_DT_2Ply_01 | 2,050 | 1,230 | 1,845 | 0.0104 | 0.0231 | 48,500 | 725 | 0.0273 | 768 | 0.0009 | 863,667 |
| FRCM_DT_2Ply_02 | 1,711 | 1,027 | 1,540 | 0.0111 | 0.0195 | 61,129 | 347 | 0.0223 | 384 | 0.0006 | 630,595 |
| FRCM_DT_2Ply_03 | 1,750 | 1,050 | 1,575 | 0.0118 | 0.0250 | 39,742 | 581 | 0.0294 | 654 | 0.0018 | 354,462 |
| FRCM_DT_2Ply_04 | 1,923 | 1,154 | 1,730 | 0.0119 | 0.0228 | 53,108 | 519 | 0.0264 | 991 | 0.0089 | 111,620 |
| FRCM_DT_2Ply_05 | 2,229 | 1,338 | 2,007 | 0.0128 | 0.0278 | 44,533 | 772 | 0.0329 | 830 | 0.0013 | 634,510 |
| Average | 1,933 | 1,187 | 1,739 | 0.0116 | 0.0237 | 49,402 | 589 | 0.0277 | 726 | 0.0027 | 518,971 |
| Stand. Dev. | 215 | 131 | 193 | 0.0009 | 0.0031 | 8,202 | 170 | 0.0039 | 226 | 0.0035 | 290,526 |
| C.O.V. (%) | 11 | | | | | 17 | | 14 | | | |

**Table C3 – Individual Tensile Strength Results for Three Ply Specimen Tests**

| Specimen ID | $f_{fu}$ MPa | $0.6f_{fu}$ MPa | $0.9f_{fu}$ MPa | $\varepsilon_{f@0.6ffu}$ mm/mm | $\varepsilon_{f@0.9ffu}$ mm/mm | $E_f$* MPa | Y int MPa | $\varepsilon_{f@ffu}$ mm/mm | $f_{ft}$ MPa | $\varepsilon_{f@fft}$ mm/mm | $E_f$ MPa |
|---|---|---|---|---|---|---|---|---|---|---|---|
| FRCM_DT_3Ply_01 | 1,967 | 1,180 | 1,770 | 0.01226 | 0.02985 | 33,534 | 769 | 0.0357 | 782 | 0.00040 | 1,974,723 |
| FRCM_DT_3Ply_02 | 1,973 | 1,184 | 1,776 | 0.01010 | 0.02095 | 54,560 | 633 | 0.0246 | 659 | 0.00047 | 1,391,323 |
| FRCM_DT_3Ply_03 | 2,019 | 1,211 | 1,817 | 0.01442 | 0.03225 | 33,969 | 722 | 0.0382 | 750 | 0.00083 | 898,088 |
| FRCM_DT_3Ply_04 | 1,893 | 1,136 | 1,704 | 0.00819 | 0.01913 | 51,906 | 711 | 0.0228 | 724 | 0.00026 | 2,770,340 |
| FRCM_DT_3Ply_05 | 1,752 | 1,051 | 1,577 | 0.00761 | 0.01725 | 54,520 | 636 | 0.0205 | 672 | 0.00065 | 1,029,080 |
| Average | 1,921 | 1,152 | 1,729 | 0.01052 | 0.02389 | 45,698 | 694 | 0.0283 | 717 | 0.00052 | 1,612,711 |
| Stand. Dev. | 105 | 63 | 94 | 0.00284 | 0.00672 | 10,959 | 59 | 0.0080 | 52 | 0.00022 | 769,981 |
| C.O.V. (%) | 5 | | | | | 5 | | 28 | | | |

**Table C4 – Individual Tensile Strength Results for Four Ply Specimen Tests**

| Specimen ID | $f_{fu}$ MPa | $0.6f_{fu}$ MPa | $0.9f_{fu}$ MPa | $\varepsilon_{f@0.6ffu}$ mm/mm | $\varepsilon_{f@0.9ffu}$ mm/mm | $E_f$* MPa | Y int MPa | $\varepsilon_{f@ffu}$ mm/mm | $f_{ft}$ MPa | $\varepsilon_{f@fft}$ mm/mm | $E_f$ MPa |
|---|---|---|---|---|---|---|---|---|---|---|---|
| FRCM_DT_4Ply_01 | 1,224 | 734 | 1,102 | 0.00873 | 0.01751 | 41,819 | 369 | 0.0204 | 420 | 0.00121 | 346,490 |
| FRCM_DT_4Ply_02 | 1,338 | 803 | 1,204 | 0.00809 | 0.01997 | 33,778 | 529 | 0.0239 | 544 | 0.00044 | 1,229,288 |
| FRCM_DT_4Ply_03 | 1,278 | 767 | 1,150 | 0.00558 | 0.01627 | 35,871 | 567 | 0.0198 | 571 | 0.00013 | 4,560,172 |
| FRCM_DT_4Ply_04 | 1,371 | 822 | 1,234 | 0.00670 | 0.01886 | 33,819 | 596 | 0.0229 | 853 | 0.00759 | 69,756 |
| FRCM_DT_4Ply_05 | 1,456 | 873 | 1,310 | 0.01145 | 0.02534 | 31,434 | 513 | 0.0300 | 531 | 0.00055 | 965,486 |
| FRCM_DT_4Ply_06 | 1,226 | 735 | 1,103 | 0.00724 | 0.01672 | 38,790 | 455 | 0.0199 | 491 | 0.00094 | 522,117 |
| Average | 1,315 | 789 | 1,184 | 0.00796 | 0.01911 | 35,918 | 505 | 0.0228 | 568 | 0.00181 | 1,282,218 |
| Stand. Dev. | 91 | 54 | 81 | 0.00203 | 0.00335 | 3,799 | 82 | 0.0039 | 149 | 0.00286 | 1,659,609 |
| C.O.V. (%) | 7 | | | | | 11 | | 17 | | | |

## APPENDIX D: Theoretical Analysis of Girder D Strengthened with FRCM

This program is designed to analyze the strength of an AASHTO Type III girder using AASHTO LRFD Bridge Design Specifications (2010) and ACI 549.4R-13 Guide for the Design and Construction of Externally Bonded FRCM Systems for Repair and Strengthening Concrete and Masonry Structures. The design calculations are organized as follows:

Section 1 - Material and Geometric Properties of Virgin and Damaged Girder
Section 2 - Prestress Losses
Section 3 - Initial Stresses
Section 4 - Damaged Strands
Section 5 - Strength of Damaged Girder with Externally Bonded FRCM

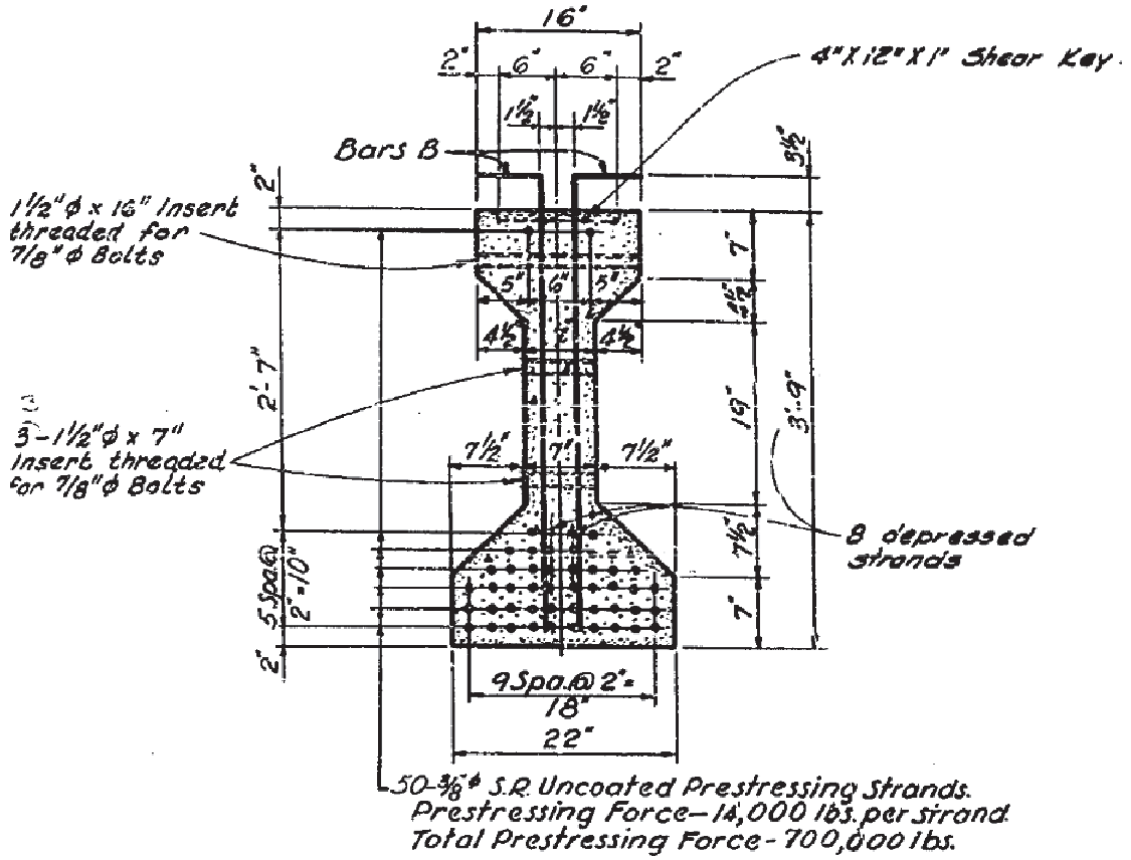


***Figure 1 - AASHTO Type III Girder***

Note:
1. All highlighted variables indicate a user input value
2. All values of ultimate strength are calculated at a specified location "x" along the span of the girder. For the estimation of prestressing losses, the girder properties at midspan were used.

# Section 1

## Material Properties

Deck concrete strength $f_{c.slab} := 6.02ksi$

$\beta_{1.deck} = 0.749$

$E_{c.deck} = 4704 \cdot ksi$

Girder concrete strength $f_{ci.girder} := 4.2ksi$

$f_{c.girder} := 6.65ksi$

$\beta_{1.girder} = 0.7175$

Modulusof elasticity of Girder $E_{c.girder} = 4943.808628 \cdot ksi$

$E_{ci.girder} = 3928.9406969 \cdot ksi$

Modular Ratio between deck and girder $n = 0.9514532$

Maximum Compressive Strain $\varepsilon_{cu} := .003$

Ultimate prestressing stress $f_{pu} := 262ksi$

Yield stress in prestressing steel $f_{py} := 214ksi$

Modulus of elasticity of prestressing steel $E_s := 27000ksi$

Minimum modulus of elasticity $E_{s.min} := 25500ksi$

## Girder Geometric Properties

| | |
|---|---|
| Girder Span Length | $Span := 60ft$ |
| At what point along the span do you want to evaluate the properties | $x := 20ft = 20 \cdot ft$ |
| Girder Depth | $h_{nc} := 45in$ |
| Top flange width | $b_{tf} := 16in$ |
| Top flange depth | $h_{tf} := 7in$ |
| Top flange sloped section thickness | $h_{tsf} := 4.5in$ |
| Bottom flange width | $b_{bf} := 22in$ |
| Bottom flange depth | $h_{bf} := 7in$ |
| Bottom flange sloped section thickness | $h_{bsf} := 7.5in$ |
| Width of web | $b_{web} := 7in$ |
| Section Area | $A_c := 560in^2$ |
| Neutral Axis to bottom of beam | $y_b := 20.27in$ |
| Neutral Axis to top of beam | $y_t := 24.73in$ |
| Moment of Inertia | $I_g := 125390in^4$ |
| Section Modulus Top | $S_t = 5070.36 \cdot in^3$ |
| Section Modulus Bottom | $S_b = 6185.99 \cdot in^3$ |

## Slab Geometric Properties

Slab thickness $t_{slab} := 9.5in$

Slab width (same as flange width) $b_{slab} := 15in$

Effective slab width $b_{slab.tr} = 14.27 \cdot in$

Slab area transformed $A_{slab.tr} = 135.58 \cdot in^2$

## Reinforcing Steel Properties

Area of non-prestressed tension steel reinforcement $A_s := 0in^2$

yield stress of steel $f_y := 60ksi$

## Prestressing Steel Properties

Steel Strands

Strand Type $strand_{type} := 2$ Enter: 1 -- Low Lax; 2 -- Stress Relieved

Tendons $Bond := 1$ Enter: 1 -- Bonded Tendons; 2 -- Unbonded Tendons

Nominal Diameter $\phi_s := \frac{3}{8}in$

Area of strand $A_{strand} := .0799in^2$

Harped Strands Slope $strand_{slope} := \frac{3ft + 9in - 17in}{23ft + 10.5in} = 0.0977312$

## *Virgin Girder*

| | |
|---|---|
| Number of strands total | $strands_{total} := 50$ |
| Area of strands Total | $A_{ps.total} = 3.995 \cdot in^2$ |
| Straight strands | $n_{ps.straight} := 40$ |
| Area of straight strands | $A_{ps.straight} = 3.196 \cdot in^2$ |
| Number of straight strands in top flange | $n_{ps.straight.top} := 2$ |
| Area of straight strands in the top flange | $A_{ps.straight.top} = 0.1598 \cdot in^2$ |
| Harped Strands | $n_{ps.harped} := 8$ |
| Area of harped strands | $A_{ps.harped} = 0.6392 \cdot in^2$ |

## *Damaged Girder*

| | |
|---|---|
| Number of strands total | $strands_{total.d} := 46$ |
| Area of strands Total | $A_{ps.total.d} = 3.6754 \cdot in^2$ |
| Straight strands | $n_{ps.straight.d} := 36$ |
| Area of straight strands | $A_{ps.straight.d} = 2.8764 \cdot in^2$ |
| Number of straight strands in top flange | $n_{ps.straight.top.d} := 2$ |
| Area of straight strands in the top flange | $A_{ps.straight.top.d} = 0.1598 \cdot in^2$ |
| Harped Strands | $n_{ps.harped.d} := 8$ |
| Area of harped strands | $A_{ps.harped.d} = 0.6392 \cdot in^2$ |
| Modular ratio between the prestressing strand and beam | $n_p = 5.4613764$ |

## Composite Section Properties

Composite Area (beam area plus transformed slab area)

$A_{composite} = 695.5820785 \cdot in^2$

Height of the composite section

$h_{composite} = 54.5 \cdot in$

Distance from centroid of beam to extreme fiber in tension (composite)

$y_{b.composite} = 26.0162085 \cdot in$

Distance from centroid of beam to extreme fiber in compression

$y_{t.composite} = 28.4837915 \cdot in$

Moment of Inertia of slab

$I_{slab} = 77392.11 \cdot in^4$

Moment of Inertia of Beam

$I_{girder} = 143880.5909878 \cdot in^4$

Moment of Inertia of composite section

$I_{composite} = 221272.7 \cdot in^4$

Section modulus top

$S_{t.composite} = 7768.3723336 \cdot in^3$

Section modulus bottom

$S_{b.composite} = 8505.1861937 \cdot in^3$

Eccentricity of pretressed strands

$e_c = 17.7290881 \cdot in$

Depth to centroid of prestressing strands

$d_{p.c} = 46.2128796 \cdot in$

Section modulus at level of prestressing steel

$S_{b.ps.composite} = 12480.7714988 \cdot in^3$

## Virgin Girder - Composite Section Transformed Properties

Center of gravity of harped strands at "x"

$y_{cg.harped} = 13.54\,in$ from bottom of girder

Center of gravity of harped strands at midspan

$y_{cg.harped.midspan} = 9\,in$ from bottom of girder

Centroid of prestressing strands at "x"

$y_{p} = 8.29\,in$ from bottom of girder

Centroid of prestressing strands at midspan

$y_{p.midspan} = 7.36\,in$ from bottom of girder

Composite area transformed

$A_{c.tr} = 713.4052774 \cdot in^2$

Neutral Axis to Bottom of Beam
Composite neutral axis transformed

$y_{b.tr} = 25.5732779 \cdot in$

Neutral Axis to Top of Beam
Composite neutral axis transformed

$y_{t.tr} = 28.9267221 \cdot in$

Composite inertia transformed

$I_{tr} = 226598.4697683 \cdot in^4$

Composite section modulus, top of slab

$S_{slab.tr} = 7833.5342949 \cdot in^3$

Composite section modulus, top of beam

$S_{top.tr} = 11664.2667953 \cdot in^3$

Composite section modulus, bottom of beam

$S_{bot.tr} = 8860.7518689 \cdot in^3$

Eccentricity of strands for composite section

$e_{cg.tr} = 17.2861575 \cdot in$

Section modulus at level of prestressing steel

$S_{ps.tr} = 13108.6663002 \cdot in^3$

Distance between neutral axis of composite section to level of prestressing steel)

$y_{p.c.tr} = 17.2861575\,in$

Section modulus at level of prestressing steel

$S_{b.ps.tr} = 13108.6663002 \cdot in^3$

## Virgin Girder - Non-Composite Section Transformed Properties

Modular ratio between the prestressing strand and beam

$n_p = 5.4613764$

Non - composite area transformed

$A_{nc.tr} = 577.8231989 \cdot in^2$

Non - composite area transformed at midspan

$A_{nc.tr.midspan} = 577.8231989 \cdot in^2$

non composite neutral axis transformed

$y_{b.nc.tr} = 19.9003831 \cdot in$ from bottom of girder

non composite neutral axis transformed at midspan

$y_{b.nc.tr.midspan} = 19.8717856 \cdot in$ from bottom of girder

Non composite inertia transformed

$I_{nc.tr} = 127793.7768558 \cdot in^4$

$I_{nc.tr.midspan} = 128180.128748 \cdot in^4$

Radius of gyration of Non composite transformed section

$r_{nc.tr} = 14.8715887 \cdot in$

Non composite transformed section modulus top at "x"

$S_{topnc.tr} = 5091.4632335 \cdot in^3$

Non composite transformed section modulus top at midspan

$S_{topnc.tr.midspan} = 5101.044065 \cdot in^3$

Non composite transformed section modulus bottom at "x"

$S_{botnc.tr} = 6421.6742216 \cdot in^3$

Non composite transformed section modulus bottom at midspan

$S_{botnc.tr.midspan} = 6450.3578641 \cdot in^3$

Non composite transformed section modulus at level of prestressing

$S_{ps.nc.tr} = 11004.1235502 \cdot in^3$

Non composite transformed section modulus at level of prestressing at midspan

$S_{ps.nc.tr.midspan} = 10244.7510276 \cdot in^3$

eccentricity of pretressed strands in non-composite transformed section

$e_{cg.nc.tr} = 11.6132626 \cdot in$

$e_{cg.nc.tr.midspan} = 12.5117856 \cdot in$

Depth to prestressing steel in non-composite section

$d_{p.nc} = 36.7128796 \cdot in$

Eeccentricity in prestressing steel in non-composite section

$e_{nc} = 11.9828796 \cdot in$

## Damaged Girder - Composite Section Transformed Properties

### Prestressing Geometric Properties

Total area of prestress

$A_{ps.d} = 3.6754 \cdot in^2$

Center of gravity of harped strands at "x"

$y_{cg.harped.d} = 13.54 \cdot in$ from bottom of girder

Centroid of prestressing strands at "x"

$y_{p.d} = 8.7 \cdot in$ from bottom of girder

Composite area transformed

$A_{c.tr.d} = 711.9794215 \cdot in^2$

Composite neutral axis transformed

$y_{b.tr.d} = 25.6174832 \cdot in$ from bottom of girder

Composite inertia transformed

$I_{tr.d} = 225963.7559244 \cdot in^4$

Composite section modulus, top of slab at "x"

$S_{slab.tr.d} = 7823.547992 \cdot in^3$

Composite section modulus, top of beam at "x"

$S_{top.tr.d} = 11658.1225667 \cdot in^3$

Composite section modulus, bottom of beam at "x"

$S_{bot.tr.d} = 8820.6852219 \cdot in^3$

Eccentricity of strands for composite section

$e_{cg.tr.d} = 16.9140915 \cdot in$

Section modulus at level of prestressing steel

$S_{ps.tr.d} = 13359.497083 \cdot in^3$

Depth to prestressed of composite_section

$d_{p.c.d} = 45.7966082 \cdot in$

Eccentricity of pretressed strands in composite section

$e_{c.d} = 17.3128168 \cdot in$

Section modulus at level of prestressing steel in composite secion

$S_{b.ps.composite.d} = 12780.860592 \cdot in^3$

Radius of Gyration of composite section transformed

$r_{tr.d} := \sqrt{\frac{I_{tr.d}}{A_{c.tr.d}}} = 17.8149936\ in$

## Damaged Girder - Non-Composite Section Transformed Properties

Depth to prestressing strands from top of girder

$d_{p.nc.d} = 36.3 \cdot in$

Eccentricity of pretressed strands in girder

$e_{nc.d} = 11.5666082 \cdot in$

Modular ratio between the prestressing strand and beam

$n_p = 5.4613764$

Non - composite area transformed

$A_{nc.tr.d} = 576.397343 \cdot in^2$

Non - composite neutral axis transformed

$y_{b.nc.tr.d} = 19.9409533 \cdot in$ from bottom of girder

Non - composite inertia transformed

$I_{nc.tr.d} = 127460.7022122 \cdot in^4$

Radius of gyration of non - composite transformed section

$r_{nc.tr.d} = 14.8705547 \cdot in$

Non - composite transformed section modulus top

$S_{topnc.tr.d} = 5086.4146489 \cdot in^3$

Non - composite transformed section modulus top

$S_{botnc.tr.d} = 6391.9061583 \cdot in^3$

Section modulus at level of prestressing steel in composite transformed secion

$S_{ps.nc.tr.d} = 11342.3807945 \cdot in^3$

Eccentricity of pretressed strands in non-composite transformed section

$e_{cg.nc.tr.d} := y_{b.nc.tr.d} - y_{p.d} = 11.2375615 \cdot in$

## Loads

Self weight of girder

$w_o := 583plf$

Weight of Deck

$w_{deck} := t_{slab} \cdot b_{slab} \cdot 150pcf = 148.4375 \cdot plf$

Total DL Weight

$w := w_o + w_{deck} = 0.7314375 \cdot klf$

$l := 60ft$

$b := 52ft$

$a := 1ft$

$c := 7ft$

$$R_{1.g} := \frac{w_o \cdot l \cdot (1 - 2 \cdot c)}{2 \cdot b}$$

Moment Due to self weight of girder

$$M_{dl}(x) := R_{1.g} \cdot x - \frac{w_o \cdot (a + x)^2}{2}$$

Moment due to self weight at "x"

$M_{dlx} = 177.3665385 \cdot kip \cdot ft$

Moment due to self weight at midspan

$M_{dl.midspan} = 186.3357692 \cdot kip \cdot ft$

$$R_{1.d} := \frac{w_{deck} \cdot l \cdot (1 - 2 \cdot c)}{2 \cdot b}$$

Moment due to weight of deck

$$M_{deck}(x) := R_{1.d} \cdot x - \frac{w_{deck} \cdot (a + x)^2}{2}$$

Moment due to weight of deck at "x"

$M_{deckx} = 45.1592548 \cdot kip \cdot ft$

Virgin Girder Prestressing Force

$F_{ps} := 14kip \cdot strands_{total} = 700 \cdot kip$

Damaged Girder Prestressing Force

$F_{ps.d} := 14kip \cdot strands_{total.d} = 644 \cdot kip$

Initial Prestressing Stress

$$f_{pi} := \frac{\frac{F_{ps}}{strands_{total}}}{A_{strand}} = 175.2190238 \cdot ksi$$

## Strand Damage

Four strands were damaged as shown in the following figure at location L/3

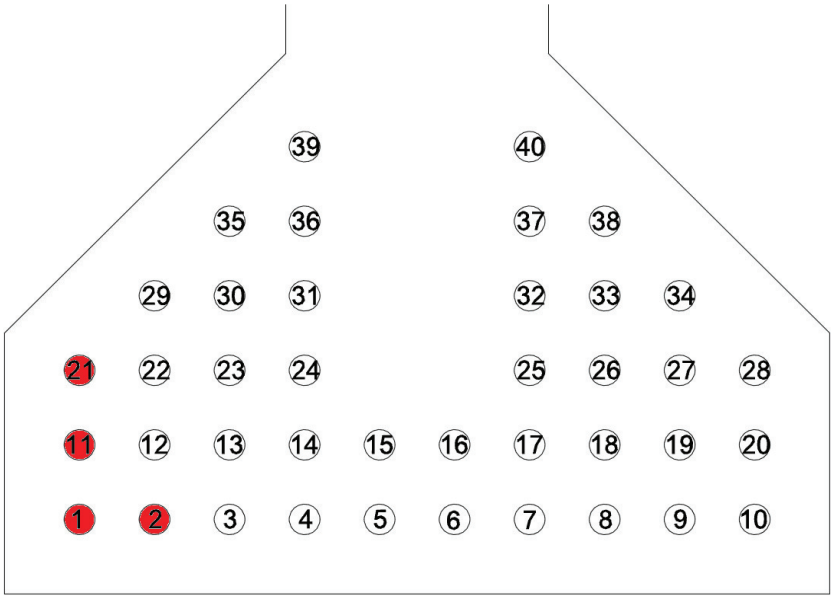


# Section 2

## Prestress Losses

Approximate method LRFD

Define Strand Type

$$strand_{Type} := \begin{cases} \text{"Low Lax"} & \text{if } strand_{type} = 1 \\ \text{"Stress Relieved"} & \text{if } strand_{type} = 2 \end{cases}$$

$strand_{Type} = \text{"Stress Relieved"}$

Initial Stress in Strands

yield stress

$f_{py} = 214 \cdot ksi$

jacking stress

$$f_{pj} := \begin{cases} .75 \cdot f_{pu} & \text{if } strand_{type} = 1 \\ .7 \cdot f_{pu} & \text{otherwise} \end{cases}$$

LRFD 5.9.3

$f_{pj} = 183.4 \cdot ksi$

$E_{ci.girder} = 3928.9406969 \cdot ksi$

$E_s = 27000 \cdot ksi$

$F_{ps} := A_{ps.total} \cdot f_{pj} = 732.683 \cdot kip$

$F_{ps} = 732.683 \cdot kip$

Eccentricity of prestressed strands at midspan

$e_{cg.nc.tr.midspan} = 12.5117856 \cdot in$

Moment of Inertia Non Composite Transformed at Midspan

$I_{nc.tr.midspan} = 128180.128748 \cdot in^4$

Area Non-Composite Transformed at Midspan

$A_{nc.tr.midspan} = 577.8231989 \cdot in^2$

Dead Load at Midspan

$M_{dl.midspan} = 186.3357692 \cdot kip \cdot ft$

Stress in the concrete at level of prestressing force at transfer and the self weight of the beam at maximum moment location (midspan)

$$f_{cgp.midspan} := \frac{F_{ps}}{A_{nc.tr.midspan}} + \frac{F_{ps} \cdot e_{cg.nc.tr.midspan}^2}{I_{nc.tr.midspan}} - \frac{M_{dl.midspan} \cdot e_{cg.nc.tr.midspan}}{I_{nc.tr.midspan}}$$

$f_{cgp.midspan} = 1.9445611 \cdot ksi$

$$force := \begin{cases} \text{"Compression"} & \text{if } f_{cgp.midspan} > 0 \\ \text{"Tension"} & \text{if } f_{cgp.midspan} < 0 \end{cases}$$

Define type of force

$force = \text{"Compression"}$

Elastic Shortening

$$\Delta f_{pES} := \frac{E_s}{E_{ci.girder}} \cdot f_{cgp.midspan}$$

$\Delta f_{pES} = 13.3631819 \cdot ksi$

Prestressing stress at transfer

$f_{pt} := if\left(f_{pj} - \Delta f_{pES} \geq .55 \cdot f_{py}, f_{pj} - \Delta f_{pES}, .55 \cdot f_{py}\right)$

$$f_{pt} = 170.0368181 \cdot ksi$$

Time Dependent Losses (Approximate Estimate) LRFD 5.9.5.3

$$H := 70$$

$$\gamma_h := 1.7 - .01 \cdot H = 1$$

$$\gamma_{st} := \frac{5}{1 + \frac{f_{ci.girder}}{ksi}} = 0.9615385$$

$$\Delta f_{pR} := \begin{cases} (2.4ksi) & \text{if } strand_{Type} = \text{"Low Lax"} \\ (10ksi) & \text{if } strand_{Type} = \text{"Stress Relieved"} \end{cases}$$

$$\Delta f_{pR} = 10 \cdot ksi$$

Long term prestress loss due to creep of concrete, shrinkage of conrete, and relaxation of steel

$$\Delta f_{pLT} := 10 \cdot \frac{f_{pj} \cdot A_{ps.total}}{A_{nc.tr}} \cdot (\gamma_h \cdot \gamma_{st}) + 12ksi \cdot \gamma_h \cdot \gamma_{st} + \Delta f_{pR} = 33.7308222 \cdot ksi$$

$$\Delta f_{pLT} = 33.7308222 \cdot ksi$$

Total Prestress Loss (Approximate Estimate)

$$\Delta f_{pT} := \Delta f_{pES} + \Delta f_{pLT}$$

$$\Delta f_{pT} = 47.0940041 \cdot ksi$$

Final prestressing stress after losses

$$f_{pe} := f_{pj} - \Delta f_{pT}$$

$$f_{pe} = 136.3059959 \cdot ksi$$

If effective presstressing is known

$$f_{pe} := 132ksi$$

Final prestress force after losses

$$P_{ps.final} := f_{pe} \cdot A_{ps.total}$$

$$P_{ps.final} = 527.34 \cdot kip$$

Final prestress force after losses (damaged girder)

$$P_{ps.final.d} := f_{pe} \cdot A_{ps.total.d}$$

$$P_{ps.final.d} = 485.1528 \cdot kip$$

# Section 3

## Calculate initial stresses at the top of the beam and bottom of beam and at level of prestressing steel

Initial stress at top of beam due to prestressing force, dead load of beam and dead load of deck

$$f_{tg.i.virgin} := \frac{P_{ps.final}}{A_{nc.tr}} - \frac{P_{ps.final} \cdot e_{cg.nc.tr}}{S_{topnc.tr}} + \frac{M_{dlx} + M_{deckx}}{S_{topnc.tr}}$$

$f_{tg.i.virgin} = 0.23428 \cdot ksi$

$$force_{tg.virgin} := \begin{cases} \text{"Compression"} & \text{if } f_{tg.i.virgin} > 0 \\ \text{"Tension"} & \text{if } f_{tg.i.virgin} < 0 \end{cases}$$

$force_{tg.virgin} = \text{"Compression"}$

Initial stress at bottom of beam due to prestressing force, dead load of beam and dead load of deck

$$f_{bg.i.virgin} := \frac{P_{ps.final}}{A_{nc.tr}} + \frac{P_{ps.final} \cdot e_{cg.nc.tr}}{S_{botnc.tr}} - \frac{M_{dlx} + M_{deckx}}{S_{botnc.tr}}$$

$f_{bg.i.virgin} = 1.4504713 \cdot ksi$

$$force_{bg.virgin} := \begin{cases} \text{"Compression"} & \text{if } f_{bg.i.virgin} > 0 \\ \text{"Tension"} & \text{if } f_{bg.i.virgin} < 0 \end{cases}$$

$force_{bg.virgin} = \text{"Compression"}$

initial stress at level of prestressing steel due to prestressing force, dead load of beam, and dead load of deck

$$f_{ps.i.virgin} := \frac{P_{ps.final}}{A_{nc.tr}} + \frac{P_{ps.final} \cdot e_{cg.nc.tr}}{S_{ps.nc.tr}} - \frac{M_{dlx} + M_{deckx}}{S_{ps.nc.tr}}$$

$f_{ps.i.virgin} = 1.2264988 \cdot ksi$

$$force_{ps.virgin} := \begin{cases} \text{"Compression"} & \text{if } f_{ps.i.virgin} > 0 \\ \text{"Tension"} & \text{if } f_{ps.i.virgin} < 0 \end{cases}$$

$force_{ps.virgin} = \text{"Compression"}$

Strain in the top of section

$$\varepsilon_{tg.i.ud} := \frac{f_{tg.i.virgin}}{E_{c.girder}}$$

$$\boxed{\varepsilon_{tg.i.ud} = 0.00005 \cdot \frac{in}{in}}$$ Compression

$$\varepsilon_{ps.i.d} := \frac{f_{pe}}{E_s} + \left( \frac{P_{ps.final}}{A_{nc.tr}} + \frac{P_{ps.final} \cdot e_{cg.nc.tr}}{S_{ps.nc.tr}} + \frac{M_{dlx} + M_{deckx}}{S_{ps.nc.tr}} \right) \cdot \frac{1}{E_{c.girder}}$$

$$\boxed{\varepsilon_{ps.i.d} = 0.0052351}$$

$$\varepsilon_{bg.i.ud} := \frac{f_{bg.i.virgin}}{E_{c.girder}}$$

$$\boxed{\varepsilon_{bg.i.ud} = 0.000293 \cdot \frac{in}{in}}$$ Compression

## Variable Definition for Girder Cross Section

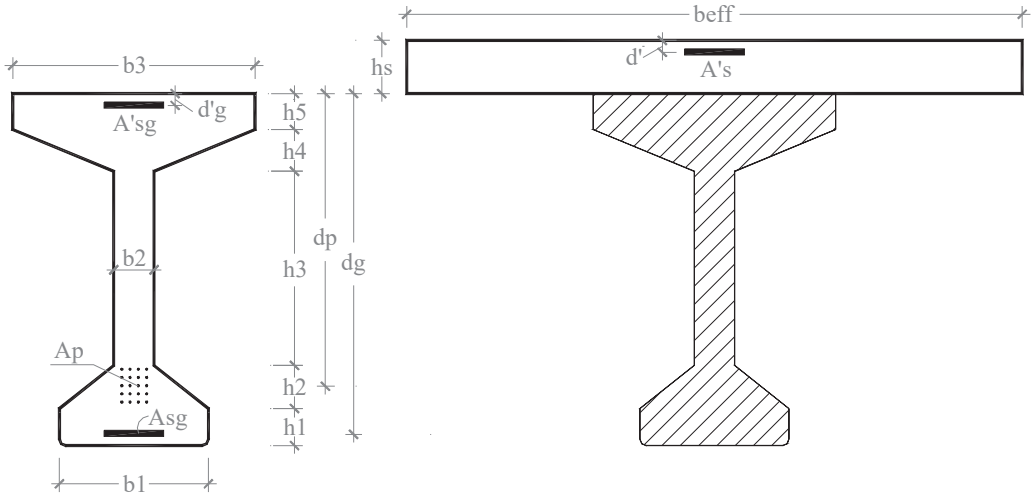


**Input Properties**

$h1 := h_{bf} = 7\ in$

$b2 := b_{web} = 7\ in$

$h2 := h_{bsf} = 7.5\ in$

$b3 := b_{tf} = 16\ in$

$h3 := h_{nc} - h_{tf} - h_{tsf} - h_{bf} - h_{bsf} = 19\ in$

$beff := b_{slab.tr} = 14.2717977\ in$

$h4 := h_{tsf} = 4.5\ in$

$Ap := A_{ps.total.d} = 3.6754\ in^2$

$h5 := h_{tf} = 7\ in$

$\varepsilon cu := .003$

$hs := t_{slab} = 9.5\ in$

$f'c := f_{c.girder} = 6650\ psi$

$h := h1 + h2 + h3 + h4 + h5 + hs$

$h = 54.5\ in$

$dg := 0$

$dp := d_{p.c.d} = 45.7966082\ in$

$z := \frac{h}{50}, \frac{2 \cdot h}{50} .. h$

$A'sg := 0$

$fy := 60000$

$A's := 0$

$d'g := 0$

$Es := 29000000$

$d' := 0$

$c(z) := z$

$\varepsilon_y := \frac{fy}{Es} = 0.002069$

$Asg := 0$

$fpy := f_{py} = 214000\ psi$

$Ln := Span = 720\ in$

$fpu := f_{pu} = 262000\ psi$

$Pf := P_{ps.final.d} = 485152.8\ lbf$

## Analytical Approximations to the Compressive Stress-Strain Curve

### *Todeschini's Model*

$f'_c := f_{c.girder} = 6650\,psi$

$E_c := E_{c.girder}$

Compressive strain at peak

$$\varepsilon_{c0} := \frac{1.71 \cdot f'_c}{E_c} = 0.0023$$

Compressive stress at peak

$$\sigma''_c := 0.9 \cdot f'_c = 5985 \cdot psi$$

Stress-strain curve equation

$$\sigma_c(\varepsilon_c) := \frac{2 \cdot \sigma''_c \cdot \left(\frac{\varepsilon_c}{\varepsilon_{c0}}\right)}{1 + \left(\frac{\varepsilon_c}{\varepsilon_{c0}}\right)^2}$$

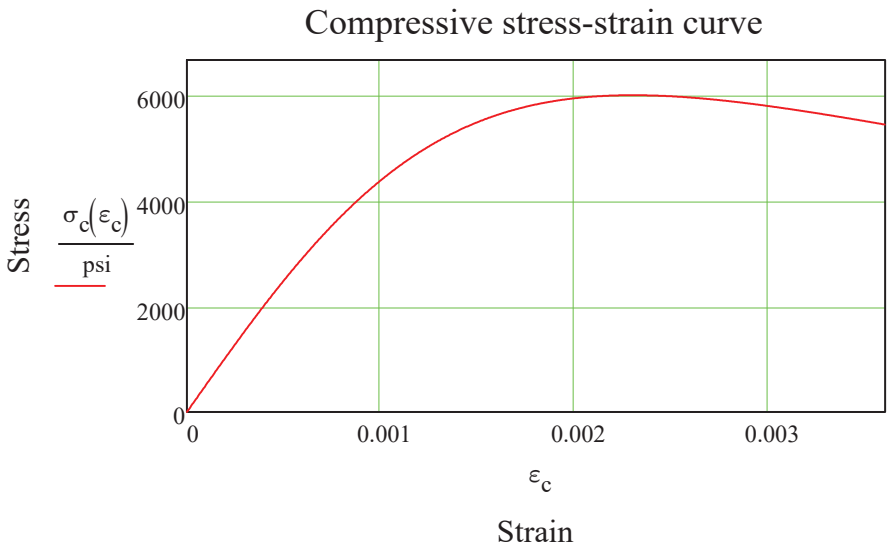

# Section 4

## Damaged Strands Analysis Approach

Due to the loss of 4 prestressing strands, there is a reduction in prestressing force. So, there will be a tensile force equal to and opposite to the the prestressing force of 4 strands. This force will occur at the centroid of the 4 damaged strands. This tensile force will be applied as a result of strand damage. Accordingly, there will be an added strain distribution in the cross section as follows.

Centroid of lost force in prestressing strands (from bottom of beam)

$$y_{p.d4s} := \frac{2in\cdot 2 + 4in\cdot 1 + 6in\cdot 1}{4} = 3.5\,in$$

Centroid of lost prestressing strands from top of beam

$$y_{t.tr.d4s} := h_{composite} - y_{p.d4s} = 51\,in$$

Centroid of lost prestressing strands From neutral axis

$$e_{cg.tr.d4s} := y_{b.tr.d} - y_{p.d4s} = 22.1174832\,in$$

Force due to damaged 4 tendons

$$P_{ps.4ds} := 4\cdot A_{strand}\cdot f_{pe} = 42187.2\,lbf$$

Stress in the top of the slab due to the damaged 4 tendons

$$f_{td.4ds1} := -\frac{P_{ps.4ds}}{A_{c.tr.d}} + \frac{P_{ps.4ds}\cdot e_{cg.tr.d4s}}{S_{slab.tr.d}} = 60.0115047\,psi$$

Stress in the top of the beam due to the damaged 4 tendons

$$f_{td.4ds2} := -\frac{P_{ps.4ds}}{A_{c.tr.d}} + \frac{P_{ps.4ds}\cdot e_{cg.tr.d4s}}{S_{top.tr}} = 20.7408876\,psi$$

Stress in the bottom of the beam due to the damaged 4 tendons

$$f_{bd.4ds} := -\frac{P_{ps.4ds}}{A_{c.tr.d}} - \frac{P_{ps.4ds}\cdot e_{cg.tr.d4s}}{S_{bot.tr.d}} = -165.0359609\,psi$$

### Stress in the Concrete at Top of Deck, Top of Girder Girder, Level of Prestressing, and at Bottom of Girder

Initial stress at top of slab due to prestressing force, dead load of beam and dead load of deck

$$f_{td.i.d} := f_{td.4ds1} = 60.0115047\,psi$$

Initial stress at top of beam due to prestressing force, dead load of beam and dead load of deck

$$f_{tg.i.d} := \frac{P_{ps.final}}{A_{nc.tr}} - \frac{P_{ps.final}\cdot e_{cg.nc.tr}}{S_{topnc.tr}} + \frac{M_{deckx} + M_{dlx}}{S_{topnc.tr}} + f_{td.4ds2} \qquad f_{tg.i.d} = 0.25502\cdot ksi$$

$$force_{tg.d} := \begin{cases} \text{"Compression"} & \text{if } f_{tg.i.d} > 0 \\ \text{"Tension"} & \text{if } f_{tg.i.d} < 0 \end{cases}$$

$force_{tg.d} = \text{"Compression"}$

Initial stress at bottom of beam due to prestressing force, dead load of beam and dead load of deck

$$f_{bg.i.d} := \frac{P_{ps.final}}{A_{nc.tr}} + \frac{P_{ps.final} \cdot e_{cg.nc.tr}}{S_{botnc.tr}} + f_{bd.4ds} - \frac{M_{dlx} + M_{deckx}}{S_{botnc.tr}}$$

$f_{bg.i.d} = 1.2854354 \cdot ksi$

$$force_{bg.d} := \begin{cases} \text{"Compression"} & \text{if } f_{bg.i.d} > 0 \\ \text{"Tension"} & \text{if } f_{bg.i.d} < 0 \end{cases}$$

$force_{bg.d} = \text{"Compression"}$

initial stress in the concrete at level of prestressing steel due to prestressing force, dead load of beam, and dead load of deck

$$f_{ps.i.d} := \frac{P_{ps.final}}{A_{nc.tr}} + \frac{P_{ps.final} \cdot e_{cg.nc.tr}}{S_{ps.nc.tr}} - \frac{P_{ps.4ds}}{A_{c.tr.d}} - \frac{P_{ps.4ds} \cdot e_{cg.tr.d4s}}{S_{ps.tr.d}} - \frac{M_{dlx} + M_{deckx}}{S_{ps.nc.tr}}$$

$f_{ps.i.d} = 1.0974019 \cdot ksi$

$$force_{ps.d} := \begin{cases} \text{"Compression"} & \text{if } f_{ps.i.d} > 0 \\ \text{"Tension"} & \text{if } f_{ps.i.d} < 0 \end{cases}$$

$force_{ps.d} = \text{"Compression"}$

**Corresponding Strain in the Concrete at Top of Deck, Top of Girder Girder, Level of Prestressing, and at Bottom of Girder**

Change in Strain in the top of the slab due to 4 damaged tendons (compressive strain)

$$\varepsilon_{td.i.d} := \frac{f_{td.4ds1}}{E_{c.girder}} = 0.0000121$$

Change in strain in the top of the beam due to 4 damaged tendons (tensile strain)

$$\varepsilon_{tg.i.d1} := \frac{f_{td.4ds2}}{E_{c.girder}} = 0.0000042$$

Change in strain in the bottom of the beam due to 4 damaged tendons (tensile strain)

$$\varepsilon_{bd.i.d} := \frac{f_{bd.4ds}}{E_{c.girder}} = -0.0000334$$

Strain in the top of the girder due to 4 damaged tendons

$$\varepsilon_{tg.i.d} := \frac{f_{tg.i.d}}{E_{c.girder}}$$

$$\varepsilon_{tg.i.d} = 0.00005 \cdot \frac{in}{in} \quad \text{Tension}$$

Strain in the concrete at level of prestresing due to 4 damaged tendons

$$\varepsilon_{ps.i.net.d} := \frac{f_{ps.i.d}}{E_{c.girder}}$$

$$\varepsilon_{ps.i.net.d} = 0.000222 \cdot \frac{in}{in} \quad \text{Compression}$$

Strain in the prestressing steel due to 4 damaged tendons

$$\varepsilon_{ps.i.d} := \frac{f_{pe}}{E_s} + \left( \frac{P_{ps.final}}{A_{nc.tr}} + \frac{P_{ps.final} \cdot e_{cg.nc.tr}}{S_{ps.nc.tr}} + \frac{P_{ps.4ds}}{A_{c.tr.d}} + \frac{P_{ps.4ds} \cdot e_{cg.tr.d4s}}{S_{ps.tr.d}} + \frac{M_{dlx} + M_{deckx}}{S_{ps.nc.tr}} \right) \cdot \frac{}{E}$$

$$\varepsilon_{ps.i.d} = 0.0052613$$

Strain in the bottom of the girder due to 4 damaged tendons

$$\varepsilon_{bg.i.d} := \frac{f_{bg.i.d}}{E_{c.girder}}$$

$$\varepsilon_{bg.i.d} = 0.00026 \cdot \frac{in}{in} \quad \text{Compression}$$

# Section 5

## Ultimate Strength of Damaged Girder with Externally Bonded FRCM

**FRCM Material Properties:**

Modulus of Elasticity from characterization

$E_f := 18000\text{ksi} = 124.1056313\cdot\text{GPa}$

Ultimate Strain from characterization

$\varepsilon_{fu} := .017565$

Standard Deviation of Ultimate Strain

$\sigma_{\varepsilon fu} := .001338$

Number of plies

$n := 4$

Area of FRCM mesh by unit weight

$A_{f.unit} := 0.0018\,\frac{\text{in}^2}{\text{in}}$

Area1 of FRCM

$A_{f1} := b_{bf}\cdot A_{f.unit}\cdot n = 0.1584\,\text{in}^2$

Distance to center of Area 1 of FRCM

$d_{f1} := h_{composite} = 54.5\,\text{in}$

Area 2 of FRCM

$A_{f2} := 2\cdot h_{bf}\cdot A_{f.unit}\cdot n = 0.1008\,\text{in}^2$

Distance to center of Area 2 of FRCM

$d_{f2} := h_{composite} - \frac{1}{2}\cdot h_{bf} = 51\,\text{in}$

Area 3 of FRCM

$A_{f3} := 2\left(\sqrt{h_{bsf}^{\,2} + h_{bsf}^{\,2}}\right)\cdot A_{f.unit}\cdot n = 0.1527351\,\text{in}^2$

Distance to center of Area 3 of FRCM

$d_{f3} := h_{composite} - h_{bf} - \frac{h_{bsf}}{2} = 43.75\,\text{in}$

Total area of FRCM

$$\boxed{A_f := A_{f1} + A_{f2} + A_{f3} = 0.4119351\,\text{in}^2}$$

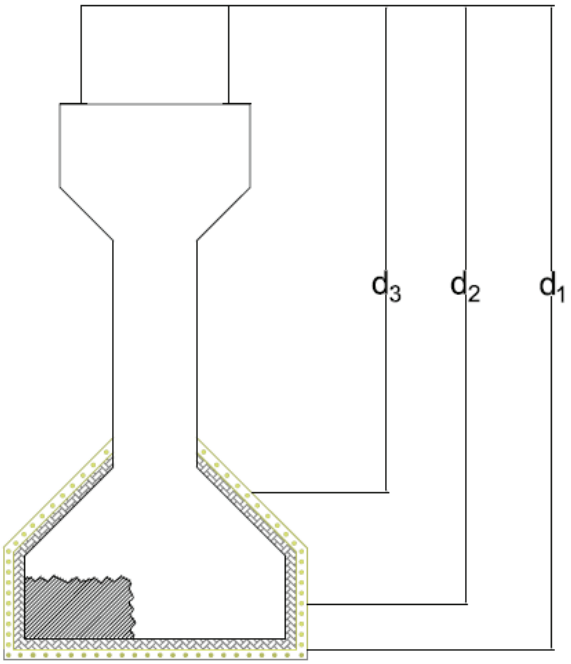


Ultimate Stress from characterization tests $F_{tu} := 241ksi$

Standard deviation of ultimate stress from characterization tests $\sigma_{Ftu} := 11ksi$

Ultimate stress $f_{fu} := F_{tu} = 241 \cdot ksi$

$\frac{f_{fu}}{E_f} = 0.0133889$

Ultimate tensile strain $(\varepsilon_{fu}$ - 1 STD) $\varepsilon_{fd} := \min\left[\left(\varepsilon_{fu}\right), \frac{f_{fu}}{E_f}\right] = 0.0133889$

**FRCM Design Using ACI 549.4R-13**

Estimate c.trial and iterate until c.trial matches c $c_{trial} := 14.92091\ in$

1. Calculate FRCM Design Tensile Strain

$\varepsilon_{fe} := \varepsilon_{fd} = 0.0133889$

2. Initial Strain in the Bottom of the Girder

$\varepsilon_{bi} := -\varepsilon_{bg.i.d} = -0.00026$

3. Compute the Strain in the Concrete if failure is controlled by Concrete Crushing

$\varepsilon_{c1} := .003 = 0.003$

4. Compute the strain in the concrete if failure is controlled by tendon rupture

$$\varepsilon_{pe} := \frac{f_{pe}}{E_s} = 0.0048889$$

$$\varepsilon_{p1} := \varepsilon_{pe} + \left( \frac{P_{ps.final}}{A_{nc.tr}} + \frac{P_{ps.final} \cdot e_{cg.nc.tr}}{S_{ps.nc.tr}} + \frac{P_{ps.4ds}}{A_{c.tr.d}} + \frac{P_{ps.4ds} \cdot e_{cg.tr.d4s}}{S_{ps.tr.d}} \right) \cdot \frac{1}{E_{c.girder}} \ldots + \frac{M_{dlx} + M_{deckx}}{S_{ps.nc.tr} \cdot E_{c.girder}}$$

$$\varepsilon_{p1} = 0.0052613$$

$$\varepsilon_{c2} := \left(.035 - \varepsilon_{p1}\right) \cdot \frac{c_{trial}}{d_{p.c.d} - c_{trial}}$$

$$\varepsilon_{c2} = 0.0143715$$

5. Compute the strain in the concrete if failure is controlled by FRCM failure

$$\varepsilon_{c3} := \left(\varepsilon_{fe} + \varepsilon_{bi}\right) \cdot \left( \frac{c_{trial}}{h_{composite} - c_{trial}} \right)$$

$$\varepsilon_{c3} = 0.0049495$$

6. Compute the strain in the concrete based on which mode of failure governs

$$\varepsilon_c := \min\left(\varepsilon_{c1}, \varepsilon_{c2}, \varepsilon_{c3}\right)$$

$$\varepsilon_c = 0.003$$

$$Failure_{Mode} := \begin{cases} \text{"Concrete Crushing"} & \text{if } \varepsilon_{c1} < \varepsilon_{c2} \wedge \varepsilon_{c1} < \varepsilon_{c3} \\ \text{"Tendon Rupture"} & \text{if } \varepsilon_{c2} < \varepsilon_{c1} \wedge \varepsilon_{c2} < \varepsilon_{c3} \\ \text{"FRCM Failure"} & \text{otherwise} \end{cases}$$

$$Failure_{Mode} = \text{"Concrete Crushing"}$$

$$\boxed{\varepsilon cu := \varepsilon_c = 0.003}$$

5. Calculate the strain in the existing PS Steel

net strain in the prestressing steel

$$\varepsilon_{pnet}(z) := \varepsilon cu \cdot \left[ \frac{\left(d_{p.c.d}\right) - c(z)}{c(z)} \right]$$

total strain in prestressing steel

$$\varepsilon_p(z) := \begin{cases} \left(\frac{f_{pe}}{E_s} + \varepsilon_{pnet}(z) + \varepsilon_{p1}\right) & \text{if } \frac{f_{pe}}{E_s} + \varepsilon_{pnet}(z) + \varepsilon_{p1} \le .035 \\ .035 & \text{otherwise} \end{cases}$$

coefficient for concrete compression block

$$\beta_1 := \begin{cases} 0.85 & \text{if } f_{c.girder} \le 4000psi \\ 1.05 - 0.05 \cdot \frac{f_{c.girder}}{1000psi} & \text{if } 4000psi < f'c < 8000psi \\ 0.65 & \text{if } f_{c.girder} \ge 8000psi \end{cases}$$

$$\beta_1 = 0.718$$

distance from extreme compression fiber to center of compression block

$$a(z) := \beta_1 \cdot c(z)$$

$$k := 2 \cdot \left(1.04 - \frac{f_{py}}{f_{pu}}\right)$$

$$f_{p\_bonded}(z) := fpu \cdot \left(1 - \frac{k \cdot c(z)}{d_{p.c.d}}\right)$$

$$f_p(z) := f_{p\_bonded}(z)$$

**FORCE EQUILIBRIUM:**

Force in prestressing steel

$$F_p(z) := Ap \cdot f_p(z)$$

Coefficient for compression block

$$\alpha_1 := .85$$

Compression force based on neutral axis location

$$C1(z) := \alpha_1 \cdot f'c \cdot beff \cdot a(z)$$

$$C2(z) := \alpha_1 \cdot f'c \cdot [beff \cdot hs + b3 \cdot (a(z) - hs)]$$

$$C3(z) := \alpha_1 \cdot f'c \cdot \left[ \begin{array}{l} beff \cdot hs + b3 \cdot h5 \ ... \\ + \left[ \frac{b3 - b2}{2} + \frac{(b3 - b2) \cdot (h4 + h5 + hs - a(z))}{2 \cdot h4} \right] \cdot [a(z) - (hs + h5)] \ ... \\ + b2 \cdot [a(z) - (hs + h5)] \end{array} \right]$$

$$C4(z) := \alpha_1 \cdot f'c \cdot \left[ beff \cdot hs + b3 \cdot h5 + \frac{b3 - b2}{2} \cdot h4 + b2 \cdot h4 + b2 \cdot [a(z) - (h4 + h5 + hs)] \right]$$

$$C_c(z) := \begin{cases} C1(z) & \text{if } a(z) \le hs \\ C2(z) & \text{if } hs < a(z) \le hs + h5 \\ C3(z) & \text{if } hs + h5 < a(z) \le hs + h5 + h4 \\ C4(z) & \text{if } a(z) > hs + h5 + h4 \end{cases}$$

8. Calculate the strain in the FRCM

$$\varepsilon_{frcm1}(z) := \varepsilon cu \cdot \frac{d_{f1} - c(z)}{c(z)} + \left| \varepsilon_{bi} \right|$$

$$\varepsilon_{frcm2}(z) := \varepsilon cu \cdot \frac{d_{f2} - c(z)}{c(z)}$$

$$\varepsilon_{frcm3}(z) := \varepsilon cu \cdot \frac{d_{f3} - c(z)}{c(z)}$$

9. Calculate the stress level in PS steel and FRCM

Stress in prestressing steel $f_p(z)$ Equation 10-24b ACI 440.2R-08

Force in Prestressing Steel $F_p(z) := Ap \cdot f_p(z)$

Stress in FRCM Area 1 $f_{frcm1}(z) := E_f \cdot \varepsilon_{frcm1}(z)$

Stress in FRCM Area 2 $f_{frcm2}(z) := E_f \cdot \varepsilon_{frcm2}(z)$

Stress in FRCM Area 3 $f_{frcm3}(z) := E_f \cdot \varepsilon_{frcm3}(z)$

Force in FRCM Area 1 $F_{frcm1}(z) := \left( f_{frcm1}(z) \cdot A_{f1} \right)$

Force in FRCM Area 2 $F_{frcm2}(z) := \left( f_{frcm2}(z) \cdot A_{f2} \right)$

Force in FRCM Area 3 $F_{frcm3}(z) := \left( f_{frcm3}(z) \cdot A_{f3} \right)$

Force in FRCM $F_{frcm}(z) := F_{frcm1}(z) + F_{frcm2}(z) + F_{frcm3}(z)$

**EQUILIBRIUM:** Given

$z := h_{composite}$

Equilibrium equation $F_p(z) + F_{frcm}(z) - C_c(z) = 0$

distance to neutral axis $c := \text{Find}(z) = 14.92091 \cdot \text{in}$

$\text{Equilibrium} := \text{if}\left(-.01\text{kip} \le C_c(c) - F_p(c) - F_{frcm}(c) \le .01\text{kip}, \text{"Satisfied"}, \text{"Re-Calculate c"}\right)$

Equilibrium = "Satisfied"

**DETERMINE THE CENTER OF GRAVITY OF THE CONCRETE COMPRESSION FORCE**
(based on the depth of the cross section)

$$y_{b1}(z) := \frac{a(z)}{2}$$

$$y_{b2}(z) := \frac{b_{slab.tr} \cdot t_{slab}^2 + b_{tf} \cdot \left(a(z)^2 - t_{slab}^2\right)}{2 \cdot \left[b_{slab.tr} \cdot t_{slab} + b_{tf} \cdot \left(a(z) - t_{slab}\right)\right]}$$

$$yb3(z) := \frac{\begin{aligned} &0.5 b_{slab.tr} \cdot t_{slab}^2 + b_{tf} \cdot h_{tf} \cdot \left(t_{slab} + 0.5 \cdot h_{tf}\right) \ldots \\ &+ \left[\frac{b_{tf} - b_{web}}{2} + \frac{\left(b_{tf} - b_{web}\right) \cdot \left(h_{tsf} + h_{tf} + t_{slab} - a(z)\right)}{2 \cdot h_{tsf}}\right] \cdot \left[a(z) - \left(t_{slab} + h_{tf}\right)\right] \cdot \frac{a(z) + 2 \cdot (t}{3} \\ &+ b_{web} \cdot \left[a(z) - \left(t_{slab} + h_{tf}\right)\right] \cdot \left(\frac{a(z) + t_{slab} + h_{tf}}{2}\right) \end{aligned}}{\begin{aligned} &b_{slab.tr} \cdot t_{slab} + b_{tf} \cdot h_{tf} + \left[\frac{b_{tf} - b_{web}}{2} + \frac{\left(b_{tf} - b_{web}\right) \cdot \left(h_{tsf} + h_{tf} + t_{slab} - a(z)\right)}{2 \cdot h_{tsf}}\right] \cdot \left[a(z) - \left(t_{slab}\right.\right. \\ &+ b_{web} \cdot \left[a(z) - \left(t_{slab} + h_{tf}\right)\right] \end{aligned}}$$

$$y_{b4}(z) := \frac{0.5\cdot b_{slab.tr}\cdot t_{slab}^{2} + b_{tf}\cdot h_{tf}\cdot\left(0.5\cdot h_{tf} + t_{slab}\right) + \frac{b_{tf} - b_{web}}{2}\cdot h_{tsf}\cdot\left(h_{tf} + t_{slab} + \frac{h_{tsf}}{3}\right) \ldots + b_{web}\cdot h_{bsf}\cdot\left(0.5\cdot h_{tsf} + h_{tf} + t_{slab}\right) + b_{web}\cdot\left[a(z) - \left(t_{slab} + h_{tf} + h_{tsf}\right)\right]\cdot\left(\frac{a(z) + t_{slab} + h_{tf}}{2}\right)}{b_{slab.tr}\cdot t_{slab} + b_{tf}\cdot h_{tf} + \frac{b_{tf} - b_{web}}{2}\cdot h_{tsf} + b_{web}\cdot h_{tsf} + b_{web}\cdot\left[a(z) - \left(t_{slab} + h_{tf} + h\right.\right.}$$

$$y(z) := \begin{cases} y_{b1}(z) & \text{if } a(z) \le t_{slab} \\ y_{b2}(z) & \text{if } t_{slab} < a(z) \le t_{slab} + h_{tf} \\ yb3(z) & \text{if } t_{slab} + h_{tf} < a(z) \le t_{slab} + h_{tf} + h_{tsf} \\ y_{b4}(z) & \text{if } a(z) > t_{slab} + h_{tf} + h_{tsf} \end{cases}$$

$y := y(c) = 5.4167863\cdot in$

10. Recalculate c and check if equilibrium is satisfied

$c = 14.92091\cdot in$

$Check_c := if\left(\left|c - c_{trial}\right| < .05in, "OK", "Adjust c.trial to match c"\right)$

$Check_c = "OK"$

Compressive Force in Concrete $C_c(c) = 875.4259934\cdot kip$

AASHTO factor accounting for the fact that were using the equivalent prestressing steel centroid

Force in prestressing steel $F_{ps} = 732.683\cdot kip$

Force in FRCM $F_{frcm}(c) = 52.5279184\cdot kip$

$F_p(c) + F_{frcm}(c) - C_c(c) = -0\cdot lbf$ Equilibrium = "Satisfied"

**Flexural Capacity of Strengthened System**

$$Mn_{frcm} := \left[A_{f1}\cdot f_{frcm1}(c)\cdot\left(d_{f1} - y\right) + A_{f2}\cdot f_{frcm2}(c)\cdot\left(d_{f2} - y\right) + A_{f3}\cdot f_{frcm3}(c)\cdot\left(d_{f3} - y\right)\right] \ldots + A_{ps.total.d}\cdot f_p(c)\cdot\left(d_{p.c.d} - y\right)$$

$Mn_{frcm} = 2966\cdot kip\cdot ft$

Failure Mode $Failure_{Mode} = \text{"Concrete Crushing"}$

$c = 14.92091 \cdot in$

$Check_c = \text{"OK"}$

$\varepsilon_{pnet}(c) = 0.0062079$

$Mn_{frcm} = 2966 \cdot kip \cdot ft$ 2966 kip·ft = 4021.3560348·kN·m

**APPENDIX E: Design Analysis of PBO-FRCM Strengthened RC Beam**

## *Define beam geometry and concrete properties*

### *Geometry*

$b := 6in$ — Beam width

$h := 12in$ — Beam height

$L_0 := 5ft$ — Beam length

$c_c := 1.46in$ — Clear concrete cover at bottom

$c'_c := 1.25in$ — Clear concrete cover at top

### *Concrete properties*

Select concrete class: 0 = 4,000 psi
1 = 6,200 psi

$\varepsilon_{cu} := 0.003$ — Ultimate compressive strain

$\rho_c := 145 \frac{lbf}{ft^3}$ — Density

$w_{dl} := \rho_c \cdot b \cdot h = 72.5 \cdot plf$ — Dead load per foot of concrete

$M_0 := \frac{w_{dl} \cdot L_0^2}{8} = 2.719 \cdot kip \cdot in$ — Dead Load Moment

$f'_c := 7000psi$ — Compressive strength

$E_c := 33psi^{0.5} \left( \frac{\rho_c}{lbf \cdot ft^{-3}} \right)^{1.5} \cdot \sqrt{f'_c}$ — Compressive modulus of elasticity (ACI 318-11)

$E_c = 4821\,ksi$

$f'_{ct} := 7.5 \cdot \sqrt{f'_c \cdot psi} = 0.63 \cdot ksi$ — Tensile strength (ACI 318-11)

## Analytical Approximations to the Compressive Stress-Strain Curve

### *Todeschini's Model*

$\varepsilon_{c0} := \frac{1.71 \cdot f'_c}{E_c} = 0.0025$ Compressive strain at peak

$\sigma''_c := 0.9 \cdot f'_c = 6300 \cdot psi$ Compressive stress at peak

$\sigma_c(\varepsilon_c) := \frac{2 \cdot \sigma''_c \cdot \left(\frac{\varepsilon_c}{\varepsilon_{c0}}\right)}{1 + \left(\frac{\varepsilon_c}{\varepsilon_{c0}}\right)^2}$ Stress-strain curve equation

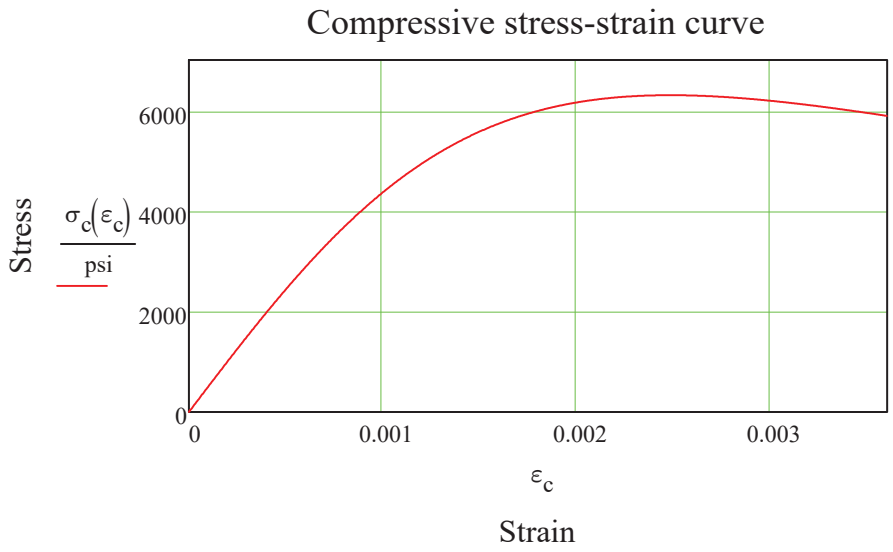


## *Define Internal and External Reinforcement Properties*

US steel reinforcement

Legend

| |
|---|
| Area ($in^2$) |
| Weight (lbf/ft) |
| Diameter (in) |

$cb := 0..2$ $rb := 0..11$ $Bar_{rb,cb} := 0.0$ Counters definition

$Bar_{3,cb} := Bar_{4,cb} := Bar_{5,cb} := Bar_{6,cb} := Bar_{7,cb} := Bar_{8,cb} := Bar_{9,cb} := Bar_{10,cb} := Bar_{11,cb}$

| | | | | | | | | |
|---|---|---|---|---|---|---|---|---|
| 0.11 | 0.2 | 0.31 | 0.44 | 0.6 | 0.79 | 1.00 | 1.27 | 1.56 |
| 0.376 | 0.668 | 1.043 | 1.502 | 2.044 | 2.67 | 3.4 | 4.303 | 5.313 |
| 0.375 | 0.5 | 0.625 | 0.75 | 0.875 | 1.0 | 1.128 | 1.27 | 1.41 |

## *Secondary Shear Reinforcement Properties*

$\Phi_v := 0.252in$ Stirrup diameter

$s_v := 5in$ Stirrup spacing

$f_{yt} := 60ksi$ Yield strength

$A_v := 2 \cdot \pi \cdot \frac{\Phi_v^2}{4} = 0.1\ in^2$ Area of transversal steel reinforcement

$$A_{vmin} := \max\left(0.75 \cdot \sqrt{\frac{f'_c \cdot 1000}{ksi}} \cdot b \cdot \frac{s_v}{\frac{f_{yt} \cdot 1000}{ksi}},\ 50 \cdot b \cdot \frac{s_v}{\frac{f_{yt} \cdot 1000}{ksi}}\right) = 0.03\ in^2$$

## *Internal Steel Reinforcement Properties*

$BarSize := 3$ i.e. #3 bar

$n_{bar} := 3$ Number of bars

$f_y := 60ksi$ Specified yield strength of reinforcement steel

$E_s := 29000ksi$ Tensile modulus of elasticity of reinforcement stee

$\Phi_s := Bar_{BarSize,2}\ in = 0.375\ in$ Bar diameter

$A_s := n_{bar}\, Bar_{BarSize,0} \cdot in^2 = 0.33\ in^2$ Area of longitudinal steel reinforcement

$d := h - c_c - \Phi_v - \frac{\Phi_s}{2} = 10.1\ in$ Distance from extreme compression fiber to centroid of tension reinforcement

$\varepsilon_{sy} := \frac{f_y}{E_s} = 0.00207$ Yield tensile strenght of the reinforcement steel

$\varepsilon_{sh} := 0.0058$ Hardening strain

$\varepsilon_{sd} := \varepsilon_{sy}$ Design Strain (I used a larger value than yield)

$n_s := \frac{E_s}{E_c} = 6$ Ratio of steel to concrete modulus

### *Internal Compressed Steel Reinforcement Properties*

$BarSize' := 3$

$n'_{bar} := 2$

$\Phi' := Bar_{BarSize',2}\,in = 0.375\,in$ Bar diameter

$A'_s := n'_{bar}\,Bar_{BarSize',0}\cdot in^2 = 0.22\,in^2$ Area of longitudinal steel reinforcement

$d' := c'_c + \Phi_v + \frac{\Phi'}{2} = 1.7\,in$ Distance from extreme compression fiber to centroid of tension reinforcement

**Analytical approximations to the tensile stress-strain curve**

$$f_s(\varepsilon_s) := \begin{cases} E_s\cdot\varepsilon_s & \text{if } \varepsilon_s < \varepsilon_{sy} \\ f_y & \text{if } \varepsilon_{sy} \le \varepsilon_s \le \varepsilon_{sh} \\ f_y & \text{if } \varepsilon_{sh} < \varepsilon_s \end{cases}$$

Stress-strain curve equation

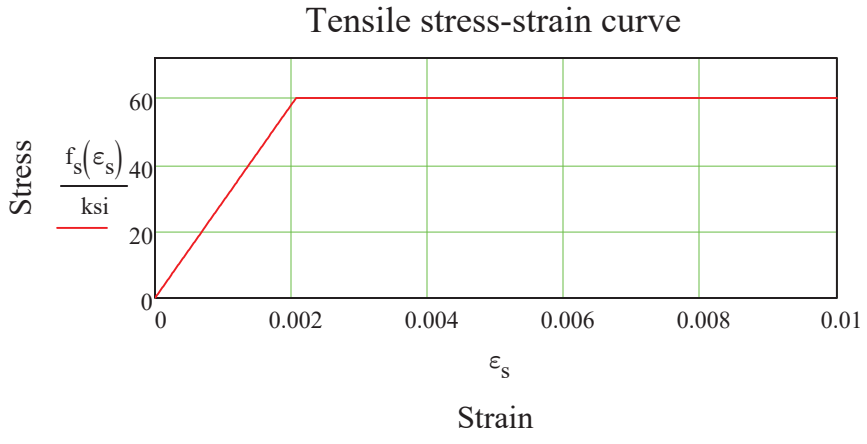

**FRCM Material Properties:**

| | |
|---|---|
| Modulus of Elasticity from characterization | $E_f := 18000ksi = 124.106 \cdot GPa$ |
| Ultimate Strain from characterization | $\varepsilon_{fu} := .017565$ |
| Standard Deviation of Ultimate Strain | $\sigma_{\varepsilon fu} := .001338$ |
| Number of plies | $n := 3$ |
| Area of FRCM mesh by unit length | $A_{f.unit} := 0.0018 \frac{in^2}{in}$ |
| Ply Width | $b_f := b = 6\,in$ |
| Area1 of FRCM | $A_f := b_f \cdot A_{f.unit} \cdot n = 0.032\,in^2$ |
| Distance to center of Area 1 of FRCM | $d_f := h = 12\,in$ |
| Ultimate Stress from characterization tests | $F_{tu} := 241ksi$ |
| Standard deviation of ultimate stress from characterization tests | $\sigma_{Ftu} := 11ksi$ |
| Ultimate stress | $f_{fu} := F_{tu} = 241 \cdot ksi$ |
| Ultimate tensile strain $(\varepsilon_{fu}$ - 1 STD) | $\varepsilon_{fd} := \varepsilon_{fu} - \sigma_{\varepsilon fu} = 0.016$ |
| | $\varepsilon_{fe1} := \min(\varepsilon_{fd}, .012) = 0.012$ |

**Analytical approximations to the tensile stress-strain curve**

$f_{fi}(\varepsilon_{fi}) := E_f \cdot \varepsilon_{fi}$ Stress-strain curve equation

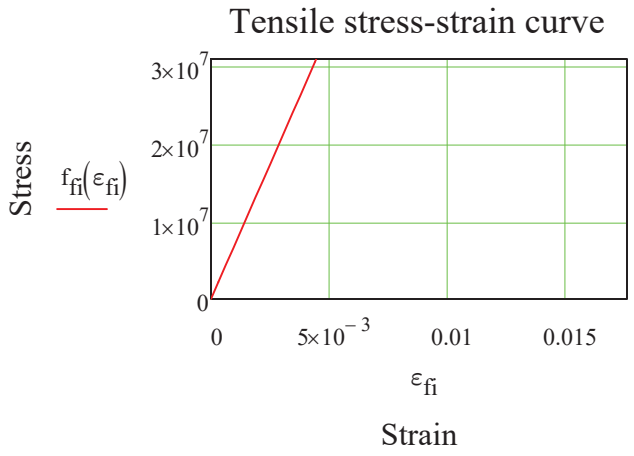

$$n_f := \frac{E_f}{E_c} = 3.7$$ Ratio of modulus of elasticity of FRP Reinforcement to modulus of elasticity of concrete

## ***Calculate Strain in Each Material to Determine the Neutral Axis Location and Failure Mode***

Effective level of strain in the FRCM reinforcement

$$\varepsilon_c(x) := \begin{cases} .003 & \text{if } \left[.003 < \frac{\varepsilon_{fe1} \cdot x}{(h - x)}\right] \\ \frac{\varepsilon_{fe1} \cdot x}{h - x} & \text{if } \left[\frac{\varepsilon_{fe1} \cdot x}{(h - x)} < .003\right] \end{cases}$$

$d' = 1.69\,in$

$$\varepsilon_{fe}(x) := \frac{(h - x)}{x} \cdot \varepsilon_c(x)$$

$$\varepsilon_s(x) := \varepsilon_c(x) \cdot \left(\frac{d - x}{x}\right)$$ Strain in concrete

$$\varepsilon'_s(x) := \varepsilon_c(x) \cdot \left(\frac{d' - x}{x}\right)$$ Strain in the reinforcing steel

Strain in the compressed steel

$$\sigma_s(x) := \begin{cases} E_s \cdot \varepsilon_s(x) & \text{if } \varepsilon_s(x) < \varepsilon_{sy} \\ f_y & \text{otherwise} \end{cases}$$ Stress level in the reinforcing steel

$$\sigma'_s(x) := \begin{cases} E_s \cdot \varepsilon'_s(x) & \text{if } \left|\varepsilon'_s(x)\right| < \varepsilon_{sy} \\ f_y & \text{if } \left|\varepsilon'_s(x)\right| \geq \varepsilon_{sy} \end{cases}$$

Stress level in the compressed steel

$$\sigma_f(x) := E_f \cdot \varepsilon_{fe}(x)$$

Stress level in the FRCM

## ***Calculate the Internal Force Resultants and Check Equilibrium***

$$\varepsilon_{c1}(x, y) := \frac{\varepsilon_c(x)}{\frac{x}{in}} y$$

Strain in concrete

$$C_c(x) := b \cdot \int_0^{\frac{x}{in}} \frac{2 \cdot \sigma''_c \cdot \left(\frac{\varepsilon_{c1}(x,y)}{\varepsilon_{c0}}\right)}{1 + \left(\frac{\varepsilon_{c1}(x,y)}{\varepsilon_{c0}}\right)^2} dy \cdot in$$

Compressive force in the concrete

$$T_{tot}(x) := A_s \cdot \sigma_s(x) + A_f \cdot \sigma_f(x) + A'_s \cdot \sigma'_s(x)$$

Tension force in the reinforcement

$$C_{tot}(x) := C_c(x)$$

**Neutral Axis Location**

Static equilibrium

$$f_1(x) := C_{tot}(x) - T_{tot}(x)$$

Input an anticipated value of neutral axis depth

$$x_{01} := 0.2 \cdot d$$

$d' = 1.69\,in$

$$x_u := root\left(f_1\left(x_{01}\right), x_{01}\right)$$

Neutral axis depth

$$x_u = 1.4128\,in$$

Verify Neutral Axis Location

$T_{tot}(x_u) = 28.8 \cdot kip$

$C_{tot}(x_u) = 28.8 \cdot kip$

$Neutral_{Axis.Location} := if(|T_{tot}(x_u) - C_{tot}(x_u)| \leq .0000001 lbf, "OK", "Re-Evaluate")$

$Neutral_{Axis.Location} = "OK"$

$\varepsilon_c(x_u) = 1.601 \times 10^{-3}$

$\varepsilon_s(x_u) = 0.01$

$\varepsilon_{fe}(x_u) = 0.012$

## Determine Failure Type

$$Failure_{Type} := \begin{cases} "Failure\ by\ Concrete\ Crusing" & if\ \varepsilon_c(x_u) = \varepsilon_{cu} \\ "Failure\ of\ Steel" & if\ \varepsilon_s(x_u) = \varepsilon_{sy} \\ "Failure\ of\ FRCM" & otherwise \end{cases}$$

$Failure_{Type} = "Failure\ of\ FRCM"$

$\varepsilon_{fe}(x_u) = 0.012$

## Check yielding of steel

$Yielding_{steel} := if(\varepsilon_s(x_u) \geq \varepsilon_{sy}, "YES", "NO")$

$Yielding_{steel} = "YES"$

$\varepsilon_t := \varepsilon_s(x_u) = 0.009847$

$\varepsilon'_s(x_u) = 0.0003$

$\varepsilon_c(x_u) = 0.001601$

$\varepsilon_{fe}(x_u) = 0.012$

## ***Determine Flexural Strength***

$$M_n := A_s \cdot \sigma_s(x_u) \cdot (d - x_u) + A'_s \cdot \sigma'_s(x_u) \cdot (d' - x_u) + A_f \cdot \sigma_f(x_u) \cdot (h - x_u) \ldots$$
$$+ b \cdot \int_0^{\frac{x_u}{in}} y \frac{2 \cdot \sigma''_c \cdot \left( \frac{\varepsilon_{c1}(x_u, y)}{\varepsilon_{c0}} \right)}{1 + \left( \frac{\varepsilon_{c1}(x_u, y)}{\varepsilon_{c0}} \right)^2} dy \cdot in^2$$

$$P_n := 4 \cdot \frac{M_n}{L_0} = 80.91 \cdot kN$$

$$\chi_n := \frac{\varepsilon_s(x_u)}{d - x_u} = 0.00113 \frac{1}{in}$$

$$\Delta_n := \frac{\left( \chi_n \cdot L_0^{\,2} \right)}{12} = 8.64 \cdot mm$$

$$\phi := \begin{cases} .9 & \text{if } \varepsilon_t \geq .005 \\ .65 + \frac{.25 \cdot (\varepsilon_t - \varepsilon_{sy})}{.005 - \varepsilon_{sy}} & \text{if } \varepsilon_{sy} < \varepsilon_t < .005 \\ .65 & \text{otherwise} \end{cases}$$

$$\phi = 0.9$$

$$\phi \cdot P_n = 72.817 \cdot kN$$

## ***Check the Shear Strength***

$V_u := \frac{P_n}{2} = 9.09 \cdot kip$ Maximum shear load

$\lambda := 1$ for normal weigth concrete

$V_c := 2 \cdot \lambda \cdot \sqrt{\left(\frac{f'_c \cdot 1000}{ksi}\right)} \cdot b \cdot d \cdot psi = 10.14 \cdot kip$

$Minimum_{Shear.Reinforcement} := if\left(V_u \leq \frac{V_c}{2}, "Not\ Required", "Required"\right)$ ACI 318-11 11.4.6.1

$Minimum_{Shear.Reinforcement} = "Required"$

$V_s := \frac{A_v \cdot f_{yt} \cdot d}{s_v} = 12.09 \cdot kip$

$\phi := 1$

$V_n := \phi \cdot \left(V_c + V_s\right) = 22.23 \cdot kip$

$Check_{Shear} := if\left(V_u \geq V_n, "NOT\ GOOD", "OK"\right)$ In design of beams we consider also the contribution of stirrups

$Check_{Shear} = "OK"$

# APPENDIX F: Theoretical Analysis of PBO-FRCM Strengthened Beam

## *Define beam geometry and concrete properties*

### *Geometry*

$b := 6in$ Beam width

$h := 12in$ Beam height

$L_0 := 5ft$ Beam length

$c_c := 1.46in$ Clear concrete cover at bottom

$c'_c := 1.25in$ Clear concrete cover at top

### *Concrete properties*

Select concrete class: 0 = 4,000 psi
1 = 6,200 psi

$\varepsilon_{cu} := 0.003$ Ultimate compressive strain

$\rho_c := 145 \frac{lbf}{ft^3}$ Density

$w_{dl} := \rho_c \cdot b \cdot h = 72.5 \cdot plf$ Dead load per foot of concrete

$M_0 := \frac{w_{dl} \cdot L_0^2}{8} = 2.7187 \cdot kip \cdot in$ Dead Load Moment

$f'_c := 7610psi$ Compressive strength

$E_c := 33psi^{0.5} \left( \frac{\rho_c}{lbf \cdot ft^{-3}} \right)^{1.5} \cdot \sqrt{f'_c}$ Compressive modulus of elasticity (ACI 318-

$E_c = 5026\,ksi$

$f'_{ct} := 7.5 \cdot \sqrt{f'_c \cdot psi} = 0.65 \cdot ksi$ Tensile strength (ACI 318-11)

## Analytical Approximations to the Compressive Stress-Strain Curve

### *Todeschini's Model*

$\varepsilon_{c0} := \frac{1.71 \cdot f'_c}{E_c} = 0.0026$ Compressive strain at peak

$\sigma''_c := 0.9 \cdot f'_c = 6849 \cdot psi$ Compressive stress at peak

$\sigma_c(\varepsilon_c) := \frac{2 \cdot \sigma''_c \cdot \left(\frac{\varepsilon_c}{\varepsilon_{c0}}\right)}{1 + \left(\frac{\varepsilon_c}{\varepsilon_{c0}}\right)^2}$ Stress-strain curve equation

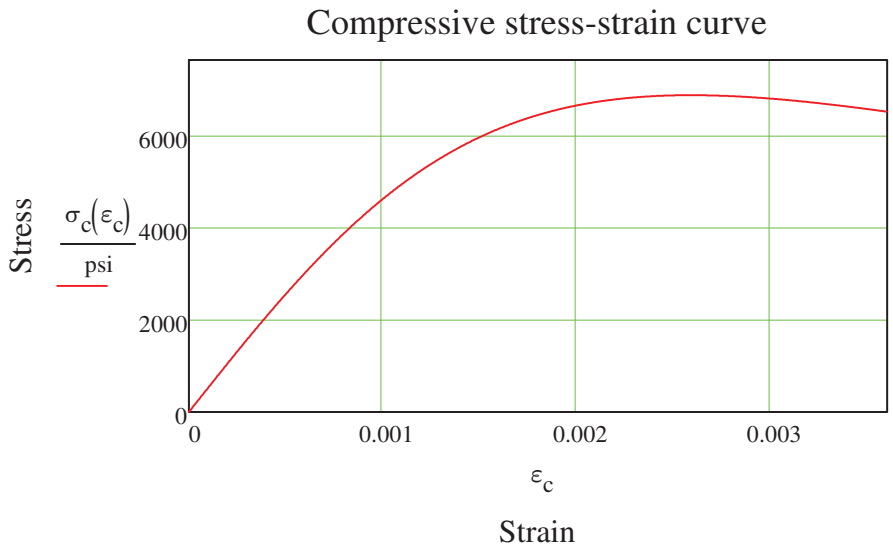


## *Define Internal and External Reinforcement Properties*

US steel reinforcement

Legend

| |
|---|
| Area ($in^2$) |
| Weight (lbf/ft) |
| Diameter (in) |

$cb := 0..2$ $rb := 0..11$ $Bar_{rb,cb} := 0.0$ Counters definition

$Bar_{3,cb} := Bar_{4,cb} := Bar_{5,cb} := Bar_{6,cb} := Bar_{7,cb} := Bar_{8,cb} := Bar_{9,cb} := Bar_{10,cb} := Bar_{11,cb}$

| | | | | | | | | |
|---|---|---|---|---|---|---|---|---|
| 0.11 | 0.2 | 0.31 | 0.44 | 0.6 | 0.79 | 1.00 | 1.27 | 1.56 |
| 0.376 | 0.668 | 1.043 | 1.502 | 2.044 | 2.67 | 3.4 | 4.303 | 5.313 |
| 0.375 | 0.5 | 0.625 | 0.75 | 0.875 | 1.0 | 1.128 | 1.27 | 1.41 |

## *Secondary Shear Reinforcement Properties*

$\Phi_v := 0.252in$ Stirrup diameter

$s_v := 5in$ Stirrup spacing

$f_{yt} := 68.38ksi$ Yield strength

$A_v := 2 \cdot \pi \cdot \frac{\Phi_v^2}{4} = 0.0998\,in^2$ Area of transversal steel reinforcement

$$A_{vmin} := \max\left(0.75 \cdot \sqrt{\frac{f'_c \cdot 1000}{ksi}} \cdot b \cdot \frac{s_v}{\frac{f_{yt} \cdot 1000}{ksi}}, 50 \cdot b \cdot \frac{s_v}{\frac{f_{yt} \cdot 1000}{ksi}}\right) = 0.03\,in^2$$

## *Internal Steel Reinforcement Properties*

$BarSize := 3$ i.e. #3 bar

$n_{bar} := 3$ Number of bars

$f_y := 68.38ksi$ Specified yield strength of reinforcement steel

$E_s := 28321.4\,ksi$ Tensile modulus of elasticity of reinforcement stee

$\Phi_s := Bar_{BarSize,2}\,in = 0.375\,in$ Bar diameter

$A_s := n_{bar}\,Bar_{BarSize,0} \cdot in^2 = 0.33\,in^2$ Area of longitudinal steel reinforcement

$d := h - c_c - \Phi_v - \frac{\Phi_s}{2} = 10.1\,in$ Distance from extreme compression fiber to centroid of tension reinforcement

$\varepsilon_{sy} := \frac{f_y}{E_s} = 0.00241$ Yield tensile strenght of the reinforcement steel

$\varepsilon_{sh} := 0.0058$ Hardening strain

$\varepsilon_{sd} := .018$ Design Strain (I used a larger value than yield)

$n_s := \frac{E_s}{E_c} = 5.6$ Ratio of steel to concrete modulus

### *Internal Compressed Steel Reinforcement Properties*

$BarSize' := 3$

$n'_{bar} := 2$

$\Phi' := Bar_{BarSize',2}\,in = 0.375\,in$ Bar diameter

$A'_s := n'_{bar}\,Bar_{BarSize',0}\cdot in^2 = 0.22\,in^2$ Area of longitudinal steel reinforcement

$d' := c'_c + \Phi_v + \frac{\Phi'}{2} = 1.7\,in$ Distance from extreme compression fiber to centroid of tension reinforcement

**Analytical approximations to the tensile stress-strain curve**

$$f_s(\varepsilon_s) := \begin{cases} E_s\cdot\varepsilon_s & \text{if } \varepsilon_s < \varepsilon_{sy} \\ f_y & \text{if } \varepsilon_{sy} \le \varepsilon_s \le \varepsilon_{sh} \\ \frac{90.31ksi - f_y}{0.020 - \varepsilon_{sh}}\cdot(\varepsilon_s - \varepsilon_{sh}) + f_y & \text{if } \varepsilon_{sh} < \varepsilon_s \end{cases}$$ Stress-strain curve equation

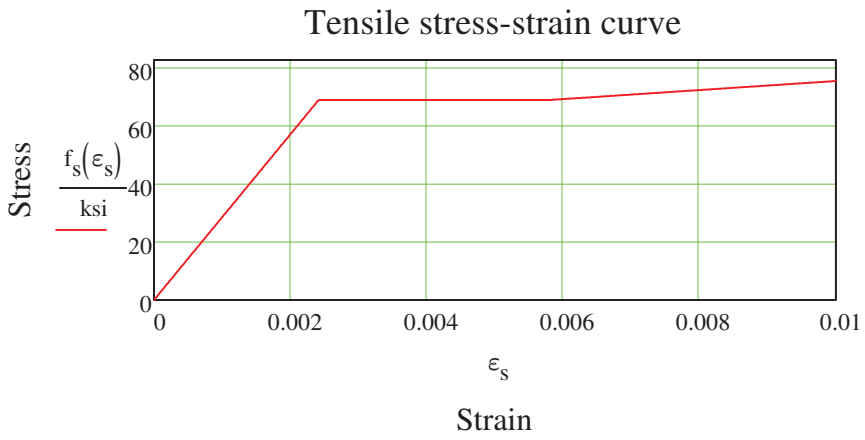

**FRCM Material Properties:**

| | |
|---|---|
| Modulus of Elasticity from characterization | $E_f := 18000ksi = 124.1056 \cdot GPa$ |
| Ultimate Strain from characterization | $\varepsilon_{fu} := .017565$ |
| Standard Deviation of Ultimate Strain | $\sigma_{\varepsilon fu} := .001338$ |
| Number of plies | $n := 3$ |
| Area of FRCM mesh by unit length | $A_{f.unit} := 0.0018 \frac{in^2}{in}$ |
| Ply Width | $b_f := b = 6\,in$ |
| Area1 of FRCM | $A_f := b_f \cdot A_{f.unit} \cdot n = 0.0324\,in^2$ |
| Distance to center of Area 1 of FRCM | $d_f := h = 12\,in$ |
| Ultimate Stress from characterization tests | $F_{tu} := 241ksi$ |
| Standard deviation of ultimate stress from characterization tests | $\sigma_{Ftu} := 11ksi$ |
| Ultimate stress | $f_{fu} := F_{tu} = 241 \cdot ksi$ |
| Ultimate tensile strain $(\varepsilon_{fu}$ - 1 STD) | $\varepsilon_{fd} := \varepsilon_{fu} - \sigma_{\varepsilon fu} = 0.0162$ |
| | $\varepsilon_{fe1} := \varepsilon_{fu} = 0.0176$ |

**Analytical approximations to the tensile stress-strain curve**

$f_{fi}(\varepsilon_{fi}) := E_f \cdot \varepsilon_{fi}$ Stress-strain curve equation

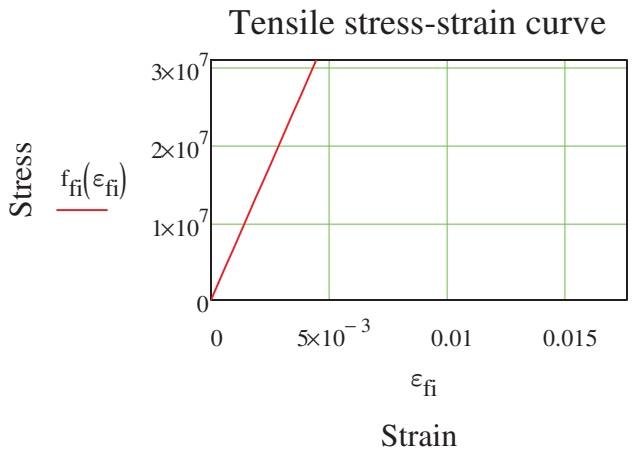


$n_f := \frac{E_f}{E_c} = 3.6$ Ratio of modulus of elasticity of FRP Reinforcement to modulus elasticity of concrete

## ***Calculate Strain in Each Material to Determine the Neutral Axis Location and Failure Mode***

Effective level of strain in the FRCM reinforcement

$$\varepsilon_c(x) := \begin{cases} \varepsilon_{cu} & \text{if } \varepsilon_{cu} < \frac{\varepsilon_{fe1} \cdot x}{(h - x)} \\ \frac{\varepsilon_{fe1} \cdot x}{h - x} & \text{if } \left[\frac{\varepsilon_{fe1} \cdot x}{(h - x)} < \varepsilon_{cu}\right] \end{cases}$$

Strain in concrete

$\varepsilon_{fe}(x) := \frac{(h - x)}{x} \cdot \varepsilon_c(x)$ Strain in the reinforcing steel

$\varepsilon_s(x) := \varepsilon_c(x) \cdot \left(\frac{d - x}{x}\right)$ Strain in the compressed steel

$d' = 1.6895\,in$

$\varepsilon'_s(x) := \varepsilon_c(x) \cdot \left(\frac{d' - x}{x}\right)$

$$\sigma_s(x) := \begin{cases} E_s \cdot \varepsilon_s(x) & \text{if } \varepsilon_s(x) < \varepsilon_{sy} \\ f_y & \text{if } \varepsilon_{sy} \le \varepsilon_s(x) \le \varepsilon_{sh} \\ \frac{90.31\text{ksi} - f_y}{0.020 - \varepsilon_{sh}} \cdot \left(\varepsilon_s(x) - \varepsilon_{sh}\right) + f_y & \text{if } \varepsilon_{sh} < \varepsilon_s(x) \end{cases}$$

Stress level in the reinforcing steel

$$\sigma'_s(x) := \begin{cases} E_s \cdot \varepsilon'_s(x) & \text{if } \left|\varepsilon'_s(x)\right| < \varepsilon_{sy} \\ f_y & \text{if } \left|\varepsilon'_s(x)\right| \ge \varepsilon_{sy} \end{cases}$$

Stress level in the compressed steel

$$\sigma_f(x) := E_f \cdot \varepsilon_{fe}(x)$$

Stress level in the FRCM

## ***Calculate the Internal Force Resultants and Check Equilibrium***

$$\varepsilon_{c1}(x, y) := \frac{\varepsilon_c(x)}{\frac{x}{\text{in}}} y$$

Strain in concrete

$$C_c(x) := b \cdot \int_0^{\frac{x}{\text{in}}} \frac{2 \cdot \sigma''_c \cdot \left(\frac{\varepsilon_{c1}(x, y)}{\varepsilon_{c0}}\right)}{1 + \left(\frac{\varepsilon_{c1}(x, y)}{\varepsilon_{c0}}\right)^2} dy \cdot \text{in}$$

Compressive force in the concrete

$$T_{tot}(x) := A_s \cdot \sigma_s(x) + A_f \cdot \sigma_f(x) + A'_s \cdot \sigma'_s(x)$$

Tension force in the reinforcement

$$C_{tot}(x) := C_c(x)$$

**Neutral Axis Location**

Static equilibrium

$$f_1(x) := C_{tot}(x) - T_{tot}(x)$$

Input an anticipated value of neutral axis depth

$$x_{01} := 0.2 \cdot d$$

$$x_u := \text{root}\left(f_1\left(x_{01}\right), x_{01}\right)$$

$x_u = 1.4443\,\text{in}$ $\quad d' = 1.6895\,\text{in}$

Neutral axis depth

Verify Neutral Axis Location

$T_{tot}(x_u) = 39.7 \cdot kip$

$C_{tot}(x_u) = 39.7 \cdot kip$

$Neutral_{Axis.Location} := if\left(\left|T_{tot}(x_u) - C_{tot}(x_u)\right| \le .0000001lbf, "OK", "Re\text{-}Evaluate"\right)$

$Neutral_{Axis.Location} = "OK"$

## Determine Failure Type

$$Failure_{Type} := \begin{cases} "Failure\ by\ Concrete\ Crusing" & if\ \varepsilon_{cu}\cdot\left(\frac{h - x_u}{x_u}\right) < \varepsilon_{fe1} \wedge \varepsilon_{cu}\cdot\left(\frac{h - x_u}{x_u}\right) < \varepsilon_{sd}\cdot\left(\frac{h - x_u}{d - x_u}\right. \\ "Failure\ of\ Steel" & if\ \varepsilon_{sd}\cdot\left(\frac{h - x_u}{d - x_u}\right) < \varepsilon_{fe1} \wedge \varepsilon_{sd}\cdot\left(\frac{h - x_u}{d - x_u}\right) < \varepsilon_{cu}\cdot\left(\frac{h - x_u}{x_u}\right) \\ "Failure\ of\ FRCM" & otherwise \end{cases}$$

$Failure_{Type} = "Failure\ of\ FRCM"$

$\varepsilon_{fe}(x_u) = 0.0176$

## Check yielding of steel

$Yielding_{steel} := if\left(\varepsilon_s(x_u) \ge \varepsilon_{sy}, "YES", "NO"\right)$

$Yielding_{steel} = "YES"$

$\varepsilon_t := \varepsilon_s(x_u) = 0.014404$

$\varepsilon'_s(x_u) = 0.0004$

$\varepsilon_c(x_u) = 0.002403$

## ***Determine Flexural Strength***

$$M_n := A_s \cdot \sigma_s(x_u) \cdot (d - x_u) + A'_s \cdot \sigma'_s(x_u) \cdot (d' - x_u) + A_f \cdot \sigma_f(x_u) \cdot (h - x_u) \ldots$$
$$+ b \cdot \int_0^{\frac{x_u}{in}} y \frac{2 \cdot \sigma''_c \cdot \left( \frac{\varepsilon_{c1}(x_u, y)}{\varepsilon_{c0}} \right)}{1 + \left( \frac{\varepsilon_{c1}(x_u, y)}{\varepsilon_{c0}} \right)^2} dy \cdot in^2$$

$$P_n := 4 \cdot \frac{M_n}{L_0} = 112.06 \cdot kN$$

$$\chi_n := \frac{\varepsilon_s(x_u)}{d - x_u} = 0.00166 \frac{1}{in}$$

$$\Delta_n := \frac{\left( \chi_n \cdot L_0^{\,2} \right)}{12} = 12.68 \cdot mm$$

## ***Cracking Moment***

$$N_A := \frac{b \cdot h \cdot \frac{h}{2} + \frac{E_f}{E_c} \cdot A_f \cdot (h) + \frac{E_s}{E_c} \cdot A'_s \cdot (d') + \frac{E_s}{E_c} \cdot A_s \cdot (d)}{b \cdot h + A_f + A'_s + A_s} = 6.2586 \, in$$

$$I_g := \frac{\left( b \cdot h^3 \right)}{12} + b \cdot h \cdot \left( \frac{h}{2} - N_A \right)^2 + \left( \frac{E_f}{E_c} - 1 \right) \cdot A_f \cdot (h - N_A)^2 + \left( \frac{E_s}{E_c} - 1 \right) \cdot A'_s \cdot (d' - N_A)^2 \ldots$$
$$+ \left( \frac{E_s}{E_c} - 1 \right) \cdot A_s \cdot (d - N_A)^2$$

$$M_{cr} := f'_{ct} \cdot \frac{I_g}{(h - N_A)}$$ Cracking moment

$$P_{cr} := 4 \cdot \frac{M_{cr}}{L_0} = 30.94 \cdot kN$$

$$\Delta_{cr} := \frac{\left[ P_{cr} \cdot (L_0)^3 \right]}{48 \cdot E_c \cdot I_g} = 0.173 \cdot mm$$

***Yielding Moment***

$\varepsilon_{sy} = 0.0024$ Strain in the reinforcing steel

$\varepsilon_{cy}(x_y) := \left[\varepsilon_{sy}\cdot\left(\frac{x_y}{d - x_y}\right)\right]$ Strain in concrete

$\varepsilon'_{sy}(x_y) := \varepsilon_{sy}\cdot\left(\frac{x_y - d'}{d - x_y}\right)$ Strain in the compressed steel

$\varepsilon_{fy}(x_y) := \varepsilon_{sy}\cdot\left(\frac{h - x_y}{d - x_y}\right)$ Strain in the FRCM reinforcement

$\sigma_{sy} := E_s\cdot\varepsilon_{sy}$ Stress level in the reinforcing steel

$\sigma'_{sy}(x_y) := E_s\cdot\varepsilon'_{sy}(x_y)$ Stress level in the compressed steel

$\sigma_f(x_y) := E_f\cdot\varepsilon_{fy}(x_y)$ Stress level in the FRCM

***Calculate the Internal Force Resultants and Check Equilibrium***

$\varepsilon_{c1y}(x_y, y) := \frac{\varepsilon_{cy}(x_y)}{\frac{x_y}{in}}y$ Strain in concrete

$C_{cy}(x_y) := b\cdot\int_0^{\frac{x_y}{in}} \frac{2\cdot\sigma''_c\cdot\left(\frac{\varepsilon_{c1y}(x_y, y)}{\varepsilon_{c0}}\right)}{1 + \left(\frac{\varepsilon_{c1y}(x_y, y)}{\varepsilon_{c0}}\right)^2}\,dy\cdot in$ Compressive force in the concrete

$T_{toty}(x_y) := A_s\cdot\sigma_{sy} + A_f\cdot\sigma_f(x_y)$ Total tension force in the reinforcement

$C_{toty}(x_y) := C_{cy}(x_y) + A'_s\cdot\sigma'_{sy}(x_y)$ Total compression force

**Neutral Axis Location**

$f_{1y}(x_y) := C_{toty}(x_y) - T_{toty}(x_y)$ Static equilibrium

Input an anticipated value of neutral axis depth

$x_{0y} := 0.2d$

$x_y := root(f_{1y}(x_{0y}), x_{0y})$

$x_y = 2.22\,in$ Neutral axis depth

Verify Neutral Axis Location

$T_{toty}(x_y) = 24.3 \cdot kip$

$C_{toty}(x_y) = 24.3 \cdot kip$

$Neutral_{Axis.Locationy} := if(|T_{toty}(x_y) - C_{toty}(x_y)| \le .0000001kip, "OK", "Re-Evaluate")$

$Neutral_{Axis.Location} = "OK"$

$$M_y := A_s \cdot \sigma_{sy} \cdot (d - x_y) + A'_s \cdot \sigma'_{sy}(x_y) \cdot (x_y - d') + A_f \cdot \sigma_f(x_u) \cdot (h - x_u) \ldots + b \cdot \int_0^{\frac{x_y}{in}} y \frac{2 \cdot \sigma''_c \cdot \left(\frac{\varepsilon_{c1y}(x_y, y)}{\varepsilon_{c0}}\right)}{1 + \left(\frac{\varepsilon_{c1y}(x_y, y)}{\varepsilon_{c0}}\right)^2} dy \cdot in^2$$

$P_y := 4 \cdot \frac{M_y}{L_0} = 68.4 \cdot kN$

$\frac{P_y}{P_n} = 0.6105$

## APPENDIX G

### RC Slab Bridge Simulation based on FDOT Example #2

The objective of this appendix is to determine the minimum loads that a typical reinforced concrete slab bridge structure will experience under service conditions. In order to take a realistic approach to the justification for the minimum loads applied, a simulation of a typical reinforced concrete slab bridge will be performed. The bridge will be analyzed and design according to AASHTO LRFD 2010 specifications for an HL-93 truck load configuration. The flexural response will be determined and the minimum loads will be converted to equivalent levels of stress in the reinforcing steel. The dimensions and characteristics of the concrete slab bridge under investigation will be taken from FDOT Design Example #2: Cast-in-Place Flat Slab Bridge Design. The design parameters will be as follows:

**Bridge Geometery and Material Properties**

Design Method: AASHTO LRFD 2010

Design Loading: HL-93 Truck

Bridge Type: 3 Span Continuous

Concrete Compressive Strength: $f'_c$ = 4,500 psi (Class II Bridge Deck)

Environmental Classification: Slightly Aggressive

Reinforcing Steel: ASTM A615, Grade 60

Concrete Cover: 2” All surfaces (superstructure)

Bridge Geometry:

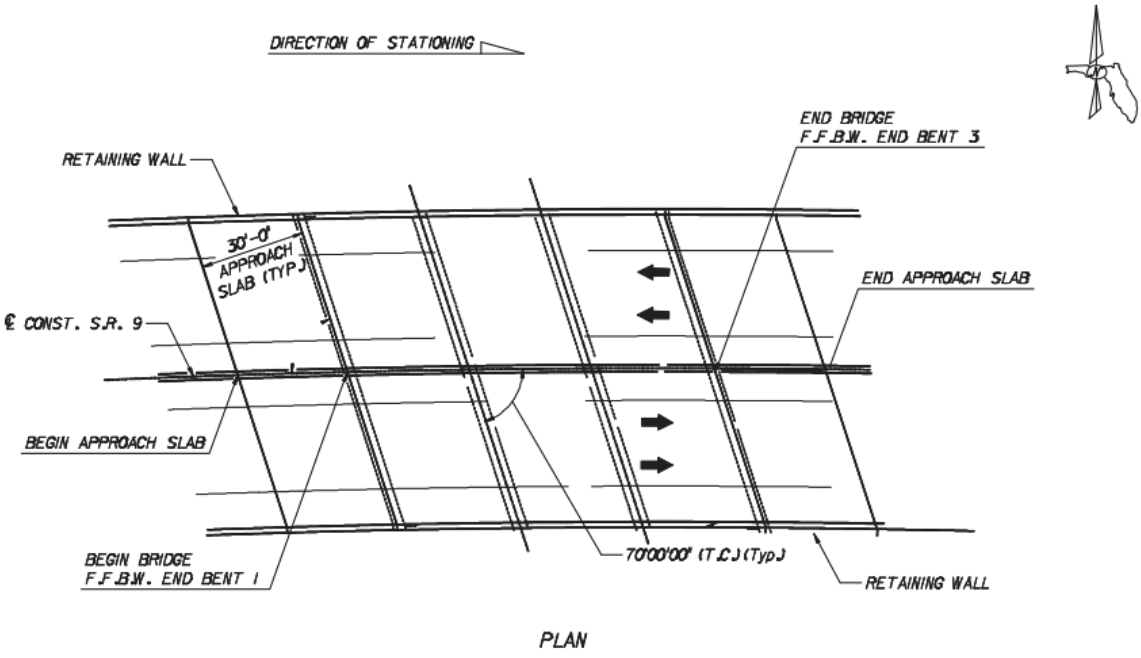


**Figure 1 - Horizontal Profile**

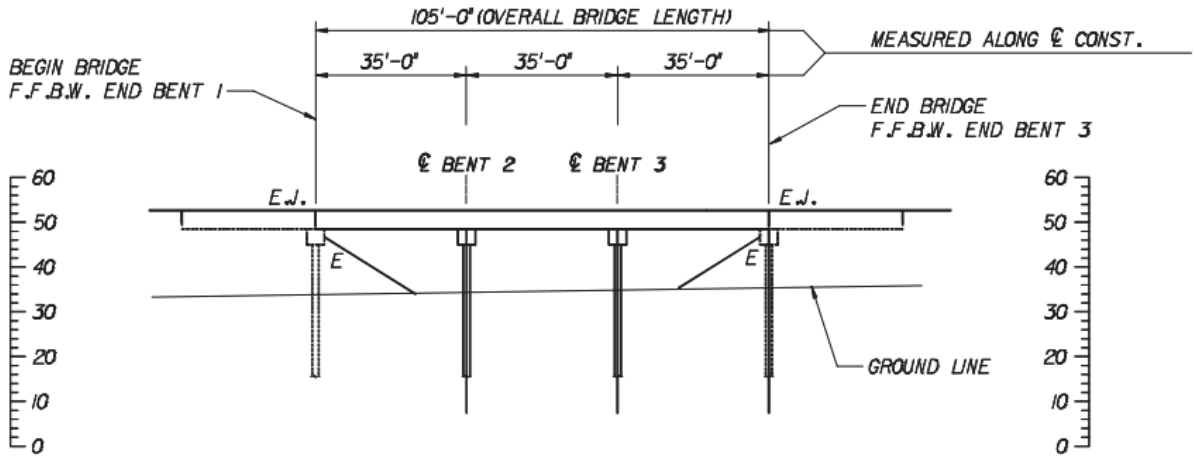


**Figure 2 - Vertical Profile**

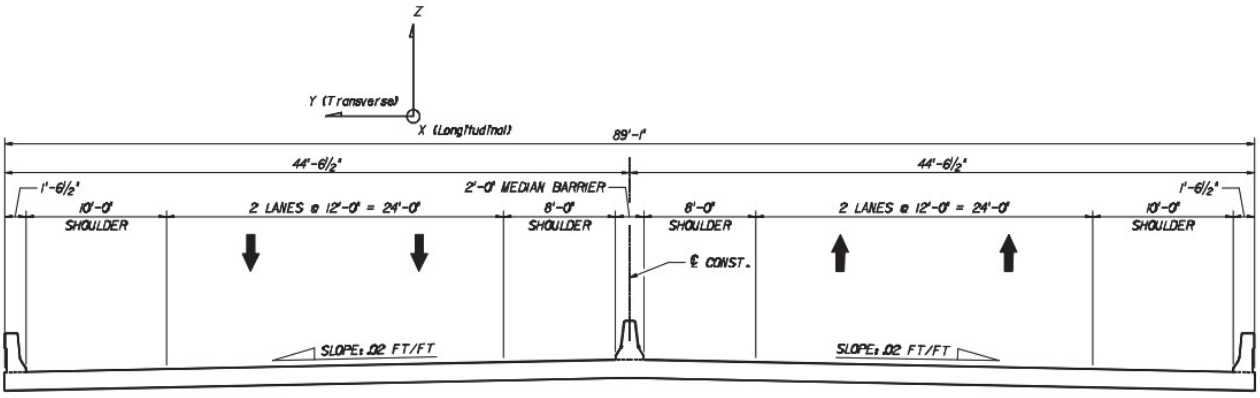


**Figure 3 – Typical Cross Section**

Overall Bridge Length: 105 ft

Design Span Length: 35 ft

Bridge Width: 89 ft - 1 in.

Number of Design Lanes: 3

**Material Properties**

Unit weight of Concrete: $\rho_c$ = 145 lb/ft$^3$

Reinforcing Steel: $E_s$ = 29,000 ksi

Resistance Factor for Tension and Flexure: $\phi$ = 0.9

Determine Deck Thickness: For continuous reinforced slabs with main reinforcement parallel to traffic: $t_{min} = \max(\frac{L_{span}+10ft}{30}, 0.54ft)$

$$t_{slab} = 18\ in$$

Design Life: 75 years

## Dead Load Analysis

Results are taken from FDOT Design Example #2 as shown in Figure 3.

| | | | | |
|---|---|---|---|---|
| | | Bridge Length = | 105 | ft |
| | | Bridge Width = | 89.0833 | ft |
| | | # of Traffic Barriers = | 2 | each |
| | | # of Median Barriers = | 1 | each |
| | | No. of spans = | 3 | each |
| | | End Span Lengths = | 35.000 | ft |
| | | Interior Span Lengths = | 35.000 | |
| | | Concrete Weight (DC) = | 0.150 | kcf |
| | | Traffic Railing Barrier (DC) = | 0.418 | klf |
| | | Median Barrier (DC) = | 0.483 | klf |
| | | Wearing Surface and/or fw s (DW) = | 0.015 | ksf |
| | | Barriers & Median (DC) = | 0.0148 | ksf = [(2 x 0.418 klf) + (1 x 0.483 klf) ] / 89.0833 ft = 0.0148 ksf |
| 18 | in = Thickness | Bridge Slab (DC) = | 0.225 | ksf = 18 in. / 12) x 0.15 kcf = 0.225 ksf |
| | | Additional Misc Loads (DC) | 0.000 | |
| | | Components & Attachments (DC) = | 0.240 | ksf = 0.0148 ksf + 0.225 ksf+ 0 ksf = 0.24 ksf |

span ratio = 1.00

Use tables 1.0 and 1.1

(From "Moments, Shears and Reactions for Continuous Highw ay Bridges" published by AISC, 1966)

| | | Influence Line Coordinates | | DC MOMENTS | DW MOMENTS | DC SHEARS | DW SHEARS |
|---|---|---|---|---|---|---|---|
| Pt. | AISC Table | 1.0 | 1.1 | (FT-KIP/FT) | (FT-KIP/FT) | (KIP/FT) | (KIP/FT) |
| 0 | **A** | 0.0000 | 0.0000 | 0.0 | 0.0 | 3.4 | 0.2 |
| 1 | **0.1** | 0.0350 | 0.0340 | 10.3 | 0.6 | 2.5 | 0.2 |
| 2 | **0.2** | 0.0600 | 0.0580 | 17.6 | 1.1 | 1.7 | 0.1 |
| 3 | **0.3** | 0.0750 | 0.0720 | 22.0 | 1.4 | 0.8 | 0.1 |
| 4 | **0.4** | 0.0800 | 0.0760 | 23.5 | 1.5 | 0.0 | 0.0 |
| 5 | **0.5** | 0.0750 | 0.0700 | 22.0 | 1.4 | -0.8 | -0.1 |
| 6 | **0.6** | 0.0600 | 0.0540 | 17.6 | 1.1 | -1.7 | -0.1 |
| 7 | **0.7** | 0.0350 | 0.0280 | 10.3 | 0.6 | -2.5 | -0.2 |
| 8 | **0.8** | 0.0000 | -0.0080 | 0.0 | 0.0 | -3.4 | -0.2 |
| 9 | **0.9** | -0.0450 | -0.0540 | -13.2 | -0.8 | -4.2 | -0.3 |
| 10 | **B** | -0.1000 | -0.1100 | -29.4 | -1.8 | -5.0 | -0.3 |
| | **B** | -0.1000 | -0.1100 | -29.4 | -1.8 | 4.2 | 0.3 |
| 11 | **1.1** | -0.0550 | -0.0555 | -16.2 | -1.0 | 3.1 | 0.2 |
| 12 | **1.2** | -0.0200 | -0.0132 | -5.9 | -0.4 | 2.1 | 0.1 |
| 13 | **1.3** | 0.0050 | 0.0171 | 1.5 | 0.1 | 1.0 | 0.1 |
| 14 | **1.4** | 0.0200 | 0.0352 | 5.9 | 0.4 | 0.0 | 0.0 |
| 15 | **1.5** | 0.0250 | 0.0413 | 7.3 | 0.5 | 0.0 | 0.0 |
| 16 | **1.6** | 0.0200 | 0.0352 | 5.9 | 0.4 | -0.7 | 0.0 |
| 17 | **1.7** | 0.0050 | 0.0171 | 1.5 | 0.1 | -1.4 | -0.1 |
| 18 | **1.8** | -0.0200 | -0.0132 | -5.9 | -0.4 | -2.1 | -0.1 |
| 19 | **1.9** | -0.0550 | -0.0555 | -16.2 | -1.0 | -2.8 | -0.2 |
| | **C** | -0.1000 | -0.1100 | -29.4 | -1.8 | -4.2 | -0.3 |
| 20 | **C** | -0.1000 | -0.1100 | -29.4 | -1.8 | 5.0 | 0.3 |
| 21 | **2.1** | -0.0450 | -0.0540 | -13.2 | -0.8 | 4.2 | 0.3 |
| 22 | **2.2** | 0.0000 | -0.0080 | 0.0 | 0.0 | 3.4 | 0.2 |
| 23 | **2.3** | 0.0350 | 0.0280 | 10.3 | 0.6 | 2.5 | 0.2 |
| 24 | **2.4** | 0.0600 | 0.0540 | 17.6 | 1.1 | 1.7 | 0.1 |
| 25 | **2.5** | 0.0750 | 0.0700 | 22.0 | 1.4 | 0.8 | 0.1 |
| 26 | **2.6** | 0.0800 | 0.0760 | 23.5 | 1.5 | 0.0 | 0.0 |
| 27 | **2.7** | 0.0750 | 0.0720 | 22.0 | 1.4 | -0.8 | -0.1 |
| 28 | **2.8** | 0.0600 | 0.0580 | 17.6 | 1.1 | -1.7 | -0.1 |
| 29 | **2.9** | 0.0350 | 0.0340 | 10.3 | 0.6 | -2.5 | -0.2 |
| 30 | **D** | 0.0000 | 0.0000 | 0.0 | 0.0 | -3.4 | -0.2 |

**Figure 3 – Dead Load Analysis**

**Equivalent Strip Widths**

The superstructure is designed on a per foot basis longitudinally. However, in order to distribute the live loads, equivalent strips of flat slab deck widths are calculated. The moment and shear effects of a single HL-93 vehicle or multiple vehicles are divided by the appropriate equivalent strip width. The equivalent strips account for the transverse distribution of LRFD wheel loads. This section is only applicable for spans greater than 15 feet.

For One Design Lane:

$E_{OneLane} = 10 + 5\sqrt{L_1 W_1}$

Modified Length $L_1 = \min(L_{span}, 60\text{ft}) = 35$ ft

Modified Width: $W_1 = \min(W_{bridge}, 30\text{ft}) = 30$ft

Equivalent width for one lane load $E_{OneLane}$= 14.3ft

For Two or More Design Lane:

$E_{OneLane} = 84 + 1.44\sqrt{L_1 W_1} \leq \frac{12W}{N_L}$

Modified Length $L_1 = \min(L_{span}, 60\text{ft}) = 35$ ft

Modified Width: $W_1 = \min(W_{bridge}, 60\text{ft}) = 60$ ft

Number of Lanes: $N_L = 2N_L$

Equivalent width for one lane load $E_{TwoLane}$= 12.5ft

The equivalent strip is the smaller of the two values: E = 12.5ft

**Live Load Analysis**

Determine the live load moments and shears due to HL-93 live load on the continuous flat slab structure. The design live loads will consists of the HL-93 vehicle moments, divided by the appropriate equivalent strip widths. This will result in a design live load per foot width of flat slab.

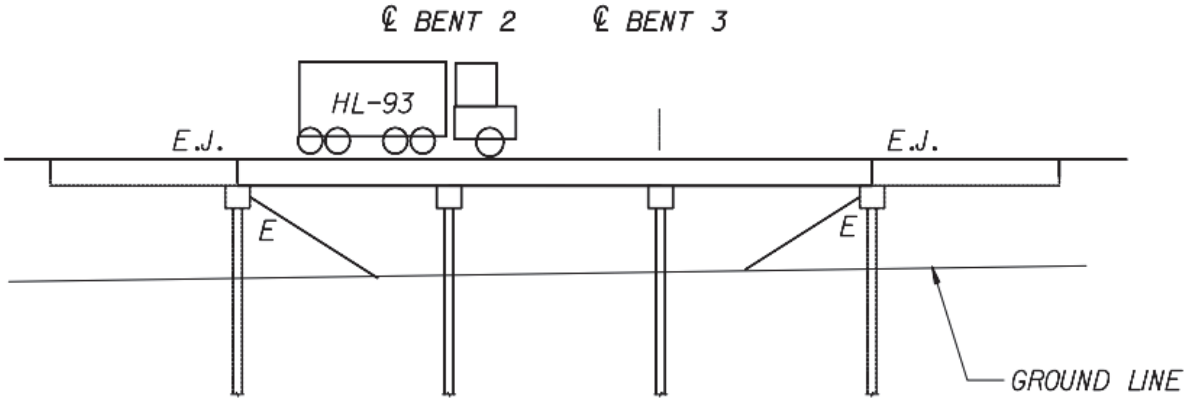


**Figure 4 – HL-93 Loading**

The HL-93 loading is the maximum of the combined design tandem and lane load or design truck and lane load, where the lane load is not considered for the fatigue limit state. A live load analysis was performed using the a Mathcad program "FDOT Live Load Generator." For the design truck, the axle spacing is taken as 14ft from the front to middle axle and 30ft from the middle to rear axle. The design tandem is taken as two 25-kip axles spaced at 4 ft. Both the design truck and design tandem load configurations are shown in Figure 5.

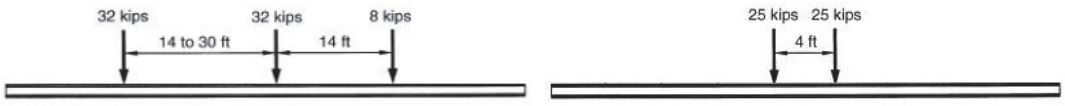


**Figure 5 – HL-93 Design Truck (Left) and Design Tandem (Right)**

Results from LRFD Example #2 for the HL-93 live load envelopes are shown in Figure 6.

| HL-93 Live Load Envelopes | | | | | | | | |
|---|---|---|---|---|---|---|---|---|
| | (10th points) | Service I | | Strength I | | Fatigue | | |
| Pt. | "X" distance | +M | -M | +M | -M | +M | -M | $M_{Range}$ |
| 0 | 0 | 0.0 | 0.0 | 0.0 | 0.0 | 0.0 | 0.0 | 0.0 |
| 1 | 3.5 | 220.9 | -23.0 | 386.6 | -40.2 | 92.7 | -5.8 | 98.5 |
| 2 | 7 | 369.4 | -46.0 | 646.5 | -80.4 | 156.0 | -11.6 | 167.5 |
| 3 | 10.5 | 460.8 | -69.0 | 806.4 | -120.7 | 195.5 | -17.3 | 212.8 |
| 4 | 14 | 495.0 | -92.1 | 866.3 | -161.1 | 209.2 | -23.1 | 232.3 |
| 5 | 17.5 | 482.8 | -115.0 | 844.9 | -201.3 | 198.4 | -28.9 | 227.3 |
| 6 | 21 | 433.1 | -137.7 | 757.9 | -241.0 | 171.1 | -34.7 | 205.8 |
| 7 | 24.5 | 340.6 | -161.5 | 596.1 | -282.6 | 138.0 | -40.5 | 178.5 |
| 8 | 28 | 213.3 | -184.5 | 373.3 | -322.9 | 94.9 | -59.1 | 154.0 |
| 9 | 31.5 | 88.1 | -232.9 | 154.2 | -407.6 | 39.8 | -117.9 | 157.7 |
| 10 | 35 | 76.1 | -383.5 | 133.2 | -671.1 | 27.0 | -186.9 | 213.8 |
| 11 | 38.5 | 89.5 | -275.7 | 156.7 | -482.5 | 48.7 | -122.2 | 170.8 |
| 12 | 42 | 215.3 | -228.7 | 376.8 | -400.2 | 95.6 | -81.2 | 176.8 |
| 13 | 45.5 | 322.4 | -196.6 | 564.2 | -344.1 | 124.3 | -67.5 | 191.8 |
| 14 | 49 | 386.1 | -165.5 | 675.7 | -289.6 | 136.6 | -54.0 | 190.5 |
| 15 | 52.5 | 403.4 | -133.9 | 706.0 | -234.3 | 134.4 | -40.5 | 174.9 |
| 16 | 56 | 386.1 | -165.5 | 675.7 | -289.6 | 136.6 | -54.0 | 190.5 |
| 17 | 59.5 | 322.4 | -196.6 | 564.2 | -344.1 | 124.3 | -67.5 | 191.8 |
| 18 | 63 | 215.3 | -228.7 | 376.8 | -400.2 | 95.6 | -81.2 | 176.8 |
| 19 | 66.5 | 90.1 | -275.7 | 157.6 | -482.5 | 48.7 | -122.2 | 170.8 |
| 20 | 70 | 76.1 | -383.0 | 133.2 | -670.3 | 27.0 | -186.9 | 213.8 |
| 21 | 73.5 | 87.5 | -232.9 | 153.1 | -407.6 | 39.8 | -117.9 | 157.7 |
| 22 | 77 | 213.3 | -184.5 | 373.3 | -322.9 | 94.9 | -59.1 | 154.0 |
| 23 | 80.5 | 340.6 | -161.5 | 596.1 | -282.6 | 138.0 | -40.5 | 178.5 |
| 24 | 84 | 433.1 | -137.7 | 757.9 | -241.0 | 171.1 | -34.7 | 205.8 |
| 25 | 87.5 | 482.8 | -115.0 | 844.9 | -201.3 | 198.4 | -28.9 | 227.3 |
| 26 | 91 | 495.0 | -92.1 | 866.3 | -161.1 | 209.2 | -23.1 | 232.3 |
| 27 | 94.5 | 460.8 | -69.0 | 806.4 | -120.7 | 195.5 | -17.3 | 212.8 |
| 28 | 98 | 369.4 | -46.0 | 646.5 | -80.4 | 156.0 | -11.6 | 167.5 |
| 29 | 101.5 | 220.9 | -23.0 | 386.6 | -40.2 | 92.7 | -5.8 | 98.5 |
| 30 | 105 | 0.0 | 0.0 | 0.0 | 0.0 | 0.0 | 0.0 | 0.0 |

**Figure 6 – HL-93 Live Load Envelopes**

The design values can be obtained by dividing the moments by the distribution width, E = 12.5ft and for fatigue, $E_{OneLane}$= 14.3ft as shown in Figure 7.

**Design Live Load Envelopes**

E = 12.5 ft

$E_{fatigue}$ = 14.3 ft

| Joint | (10th points) "X" distance | Service I +M | Service I -M | Strength I +M | Strength I -M | Fatigue +M | Fatigue -M | $M_{Range}$ |
|---|---|---|---|---|---|---|---|---|
| 0 | 0 | 0.0 | 0.0 | 0.0 | 0.0 | 0.0 | 0.0 | 0.0 |
| 1 | 3.5 | 17.7 | -1.8 | 30.9 | -3.2 | 6.4 | -0.4 | 6.8 |
| 2 | 7 | 29.6 | -3.7 | 51.7 | -6.4 | 10.8 | -0.8 | 11.6 |
| 3 | 10.5 | 36.9 | -5.5 | 64.5 | -9.7 | 13.6 | -1.2 | 14.8 |
| 4 | 14 | 39.6 | -7.4 | 69.3 | -12.9 | 14.5 | -1.6 | 16.1 |
| 5 | 17.5 | 38.6 | -9.2 | 67.6 | -16.1 | 13.8 | -2.0 | 15.8 |
| 6 | 21 | 34.6 | -11.0 | 60.6 | -19.3 | 11.9 | -2.4 | 14.3 |
| 7 | 24.5 | 27.2 | -12.9 | 47.7 | -22.6 | 9.6 | -2.8 | 12.4 |
| 8 | 28 | 17.1 | -14.8 | 29.9 | -25.8 | 6.6 | -4.1 | 10.7 |
| 9 | 31.5 | 7.1 | -18.6 | 12.3 | -32.6 | 2.8 | -8.2 | 10.9 |
| 10 | 35 | 6.1 | -30.7 | 10.7 | -53.7 | 1.9 | -13.0 | 14.8 |
| 11 | 38.5 | 7.2 | -22.1 | 12.5 | -38.6 | 3.4 | -8.5 | 11.8 |
| 12 | 42 | 17.2 | -18.3 | 30.1 | -32.0 | 6.6 | -5.6 | 12.3 |
| 13 | 45.5 | 25.8 | -15.7 | 45.1 | -27.5 | 8.6 | -4.7 | 13.3 |
| 14 | 49 | 30.9 | -13.2 | 54.1 | -23.2 | 9.5 | -3.7 | 13.2 |
| 15 | 52.5 | 32.3 | -10.7 | 56.5 | -18.7 | 9.3 | -2.8 | 12.1 |
| 16 | 56 | 30.9 | -13.2 | 54.1 | -23.2 | 9.5 | -3.7 | 13.2 |
| 17 | 59.5 | 25.8 | -15.7 | 45.1 | -27.5 | 8.6 | -4.7 | 13.3 |
| 18 | 63 | 17.2 | -18.3 | 30.1 | -32.0 | 6.6 | -5.6 | 12.3 |
| 19 | 66.5 | 7.2 | -22.1 | 12.6 | -38.6 | 3.4 | -8.5 | 11.8 |
| 20 | 70 | 6.1 | -30.6 | 10.7 | -53.6 | 1.9 | -13.0 | 14.8 |
| 21 | 73.5 | 7.0 | -18.6 | 12.2 | -32.6 | 2.8 | -8.2 | 10.9 |
| 22 | 77 | 17.1 | -14.8 | 29.9 | -25.8 | 6.6 | -4.1 | 10.7 |
| 23 | 80.5 | 27.2 | -12.9 | 47.7 | -22.6 | 9.6 | -2.8 | 12.4 |
| 24 | 84 | 34.6 | -11.0 | 60.6 | -19.3 | 11.9 | -2.4 | 14.3 |
| 25 | 87.5 | 38.6 | -9.2 | 67.6 | -16.1 | 13.8 | -2.0 | 15.8 |
| 26 | 91 | 39.6 | -7.4 | 69.3 | -12.9 | 14.5 | -1.6 | 16.1 |
| 27 | 94.5 | 36.9 | -5.5 | 64.5 | -9.7 | 13.6 | -1.2 | 14.8 |
| 28 | 98 | 29.6 | -3.7 | 51.7 | -6.4 | 10.8 | -0.8 | 11.6 |
| 29 | 101.5 | 17.7 | -1.8 | 30.9 | -3.2 | 6.4 | -0.4 | 6.8 |
| 30 | 105 | 0.0 | 0.0 | 0.0 | 0.0 | 0.0 | 0.0 | 0.0 |

**Figure 7 – HL-93 Design Load Envelopes**

The service, strength, and fatigue limit states used to design the bridge section are calculated and shown in Figure 8.

**Limit State Design Loads**

| | | Service I | | Strength I | | Fatigue | | | |
|---|---|---|---|---|---|---|---|---|---|
| | (10th points) | 1.0DC + 1.0DW + 1.0LL | | 1.25DC + 1.50DW + 1.75LL | | 1.0DC + 1.0DW + 1.5LL MRange = 0.75LL ; $-M_{min}$ = 0.75LL | | | |
| Pt. | "X" dist | +M | -M | +M | -M | +M | -M | $M_{Range}$ | $-M_{min}$ |
| 0 | 0 | 0.0 | 0.0 | 0.0 | 0.0 | 0.0 | 0.0 | 0.0 | 0.0 |
| 1 | 3.5 | 28.6 | 9.1 | 44.7 | 10.6 | 20.6 | 10.3 | 6.8 | -0.4 |
| 2 | 7 | 48.3 | 15.1 | 75.4 | 17.3 | 35.0 | 17.5 | 11.6 | -0.8 |
| 3 | 10.5 | 60.3 | 17.9 | 94.1 | 20.0 | 43.8 | 21.6 | 14.8 | -1.2 |
| 4 | 14 | 64.6 | 17.6 | 100.9 | 18.7 | 46.7 | 22.6 | 16.1 | -1.6 |
| 5 | 17.5 | 62.0 | 14.2 | 97.2 | 13.5 | 44.1 | 20.4 | 15.8 | -2.0 |
| 6 | 21 | 53.4 | 7.7 | 84.3 | 4.4 | 36.5 | 15.1 | 14.3 | -2.4 |
| 7 | 24.5 | 38.2 | -2.0 | 61.5 | -8.8 | 25.3 | 6.7 | 12.4 | -2.8 |
| 8 | 28 | 17.1 | -14.8 | 29.9 | -25.8 | 9.9 | -6.1 | 10.7 | -4.1 |
| 9 | 31.5 | -7.0 | -32.7 | -5.4 | -50.4 | -9.9 | -26.3 | 10.9 | -8.2 |
| 10 | 35 | -25.1 | -61.9 | -28.8 | -93.2 | -28.4 | -50.7 | 14.8 | -13.0 |
| 11 | 38.5 | -10.0 | -39.2 | -9.2 | -60.3 | -12.1 | -29.9 | 11.8 | -8.5 |
| 12 | 42 | 11.0 | -24.5 | 22.2 | -39.9 | 3.7 | -14.7 | 12.3 | -5.6 |
| 13 | 45.5 | 27.4 | -14.2 | 47.1 | -25.6 | 14.5 | -5.5 | 13.3 | -4.7 |
| 14 | 49 | 37.1 | -7.0 | 61.9 | -15.3 | 20.5 | 0.6 | 13.2 | -3.7 |
| 15 | 52.5 | 40.1 | -2.9 | 66.3 | -8.9 | 21.8 | 3.6 | 12.1 | -2.8 |
| 16 | 56 | 37.1 | -7.0 | 61.9 | -15.3 | 20.5 | 0.6 | 13.2 | -3.7 |
| 17 | 59.5 | 27.4 | -14.2 | 47.1 | -25.6 | 14.5 | -5.5 | 13.3 | -4.7 |
| 18 | 63 | 11.0 | -24.5 | 22.2 | -39.9 | 3.7 | -14.7 | 12.3 | -5.6 |
| 19 | 66.5 | -10.0 | -39.2 | -9.1 | -60.3 | -12.1 | -29.9 | 11.8 | -8.5 |
| 20 | 70 | -25.1 | -61.9 | -28.8 | -93.1 | -28.4 | -50.7 | 14.8 | -13.0 |
| 21 | 73.5 | -7.0 | -32.7 | -5.5 | -50.4 | -9.9 | -26.3 | 10.9 | -8.2 |
| 22 | 77 | 17.1 | -14.8 | 29.9 | -25.8 | 9.9 | -6.1 | 10.7 | -4.1 |
| 23 | 80.5 | 38.2 | -2.0 | 61.5 | -8.8 | 25.3 | 6.7 | 12.4 | -2.8 |
| 24 | 84 | 53.4 | 7.7 | 84.3 | 4.4 | 36.5 | 15.1 | 14.3 | -2.4 |
| 25 | 87.5 | 62.0 | 14.2 | 97.2 | 13.5 | 44.1 | 20.4 | 15.8 | -2.0 |
| 26 | 91 | 64.6 | 17.6 | 100.9 | 18.7 | 46.7 | 22.6 | 16.1 | -1.6 |
| 27 | 94.5 | 60.3 | 17.9 | 94.1 | 20.0 | 43.8 | 21.6 | 14.8 | -1.2 |
| 28 | 98 | 48.3 | 15.1 | 75.4 | 17.3 | 35.0 | 17.5 | 11.6 | -0.8 |
| 29 | 101.5 | 28.6 | 9.1 | 44.7 | 10.6 | 20.6 | 10.3 | 6.8 | -0.4 |
| 30 | 105 | 0.0 | 0.0 | 0.0 | 0.0 | 0.0 | 0.0 | 0.0 | 0.0 |

**Figure 8 – Limit State Design Loads**

The moment values for fatigue were plotted along the longitudinal axis of the beam for the entire span as shown in Figure 9. The maximum peak moments were recorded for each span. All moment diagrams indicate that the lowest maximum moment occurred in span #2. This value is determined to be 21.8 kip-ft (261.6 kip-in).

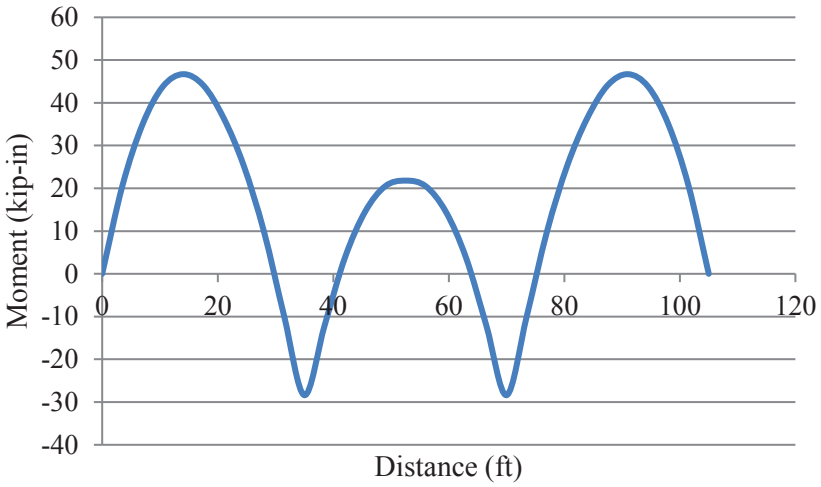


**Figure 9 – Moment vs. Distance along Bridge Length**

**Flat Slab Design**

LRFD Example #2 designed the slab section to resist the maximum shear and moment force effects calculated in Figure 8. The factored resistance was determined as $M_r = \phi M_n$ where $\phi$=0.9. The slab is designed with #8 bars spaced at 8" O.C.

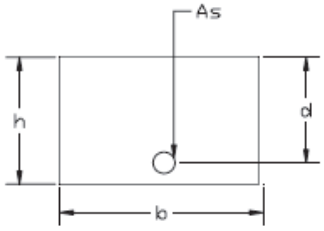


The nominal flexural resistance was determined as $M_n = A_s f_y \left(d - \frac{a}{2}\right)$ where $a = \frac{A_s f_y}{0.85 f`_c b}$.

The equation for $M_n$ indicates that the yield strength of the steel controls the flexural capacity. This value is determined to be $M_n$ = 114.3 kip-ft. The fatigue moment calculated previously (21.8 kip-ft) was divided by $M_n$ to determine a percentage. This percentage reperesents a fraction of the yield capacity of the system and is equal to 19%. Based on this value, the minimum percentage used in the fatigue loading configuration for study 3 is chosen to be 20% of the static yield capacity.